NEW APPLICATIONS OF EXCIMER LAMPS TO THE LOW TEMPERATURE PHOTO-DEPOSITION OF THIN FILMS

A thesis submitted to the
University of London
for the degree of Doctor of Philosophy

PHILIPPE BERGONZO

Department of Electronic and Electrical Engineering
UNIVERSITY COLLEGE LONDON

ProQuest Number: 10055371

All rights reserved

INFORMATION TO ALL USERS
The quality of this reproduction is dependent upon the quality of the copy submitted.

In the unlikely event that the author did not send a complete manuscript
and there are missing pages, these will be noted. Also, if material had to be removed,
a note will indicate the deletion.

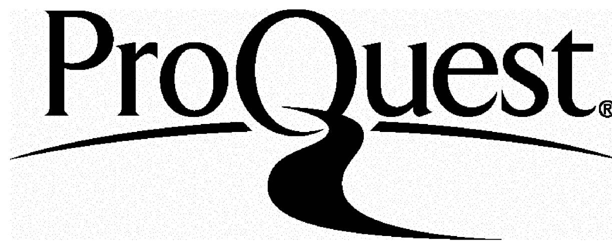

ProQuest 10055371

Published by ProQuest LLC(2016). Copyright of the Dissertation is held by the Author.

All rights reserved.
This work is protected against unauthorized copying under Title 17, United States Code.
Microform Edition © ProQuest LLC.

ProQuest LLC
789 East Eisenhower Parkway
P.O. Box 1346
Ann Arbor, MI 48106-1346

à Karine,
à mes parents,

Abstract

Over the last decade, the requirement for low temperature processing in the semiconductor industry has become apparent due to the continued reduction in device geometry and the emergence of temperature sensitive materials. Of the low temperature techniques available, photo-enhanced processing of materials is very promising since the growing films are not subject to damaging ionic bombardment which is present in plasma assisted systems. Here is presented the development of a flexible large area, low temperature photo enhanced chemical vapour deposition reactor (photo-CVD) for applications to low temperature thin films processing.

The development of novel excimer lamps has opened up the field of direct photo-CVD. Such lamps are a cheap and intense source of visible, UV and vacuum ultraviolet radiation (VUV: below 200nm). The major breakthrough with the development of these lamps is that they offer a large number of wavelengths that can be used for selective photo-CVD. The fabrication and characterisation of those light sources were conducted, and various devices generating up to a few watts are presented. Applications of the available radiation are also presented such as for the direct VUV enhanced generation of ozone and various metal-organic depositions (MOD).

For the first time, the 172nm radiation of a xenon excimer lamp has been used to deposit silicon dioxide (SiO_2), silicon nitride (Si_3N_4), and silicon oxynitride films from the photo-CVD of gas mixtures of silane with nitrous oxide and ammonia, and at temperatures as low as 300°C. Fast deposition (up to 500Å/min) of SiO_2 was also achieved by irradiating silane and oxygen gas mixtures. Investigations into the deposition photochemistry are reported, together with the characterisation of the deposited material properties. Good SiO_2 and Si_3N_4 film quality was obtained, as well as a very good control of the stoichiometry in the case of silicon oxynitride film deposition, therefore providing interesting perspectives for electronic and optical applications.

Acknowledgements

The completion of this project would not have been possible without the help and assistance from a number of people, all of whom contributed in their own special way, and rightly deserve their mention here.

I am grateful to all the persons who allowed me to use their equipment, such as Prof. M. Green for the ellipsometry measurements, Dr. S. Best and Miss E. Lloyd for the FTIR analyses, and Dr. S.J.B. Corrigan who lent me a vacuum ultraviolet monochromator without expecting it back. I would also like to acknowledge Dr. M. Dubois for the SIMS analysis, and Dr. V. Craciun and his Romanian compatriots who did the XPS measurements.

I am deeply indebted to Dr Frank Beech and Dr. Glenn C. Tyrrell for proof-reading the manuscripts of this thesis, and dealing with my written French accent. Their constructive suggestions and advices were invaluable in the making of this dissertation, as well as their help on many occasions during this research, in spite of the numerous arguments I had with Glenn.

I shall also recognise the support of the Service Science and Technology of the French Embassy, and namely of Mrs. V. Fleurette, who managed to make possible my military service as a researcher at UCL. I am also indirectly very thankful to Parthiv Patel, who let me take over his project. Many thanks are also due to all the people from room 919, and in particular to the great colleagues and friends who are R. Duncan Marshall and Tim H. York, for having shared so many technical problems, as well as so many late night discussions and social events. Since they had to cope with my French arrogance, I forgive Duncan for cycling faster than I, and Tim for smoking all my cigarettes.

I am also deeply grateful to Dr U. Kogelschatz, from ABB, who, further to sponsor this work, also let me learn all the necessary knowledge involved with excimer lamps technologies in his laboratory. I greatly appreciate how he often solved my problems at the other end of the fax machine. I am also indebted to Prof. P. Pinard, who further to recommending me for this PhD and always trying his best for my grant applications, was indeed like a second supervisor, especially in terms of motivation and moral support.

Finally, I would like to thank my supervisor Ian W. Boyd, for accepting me as a research student in his laboratory. I recognise that I owe him very much, for his understanding and encouragement, his scientific advice, his moral support, and his financial contribution. In fact, in spite of tremendous efforts to find a grant for this project, no success was ever gained from almost 12 applications for an EEC studentship over the last three years. Ian managed to sort out my financial difficulties by juggling with contracts, other grants, and arranging financed periods during the completion of this project.

January 1994 *UCL, London*

Table of Contents

Abstract
Preface and Acknowledgements
Table of Contents 1

Introduction 4

Chapter 1 .... **Photo-CVD, Apparatus and Methods** 8
1- ....**Introduction to photo-CVD processing** 9
1.1- ....The need for low temperature techniques 9
1.2- ....A brief outline on other techniques 9
1.3- .... Photo-enhanced Chemical Vapour Deposition 10
1.4- ....Sources of Vacuum Ultraviolet light 13
2.- ....**Design of a photo-CVD reactor** 17
2.1- ....Stipulations 17
2.2- ....General diagram of the photo-CVD reactor 18
2.3- ....Safety requirements 25
2.4- ....Maintenance 26
3.- ....**Characterisation of the deposited films** 27
3.1-... Ellipsometry 27
3.2- ....Infra-red spectrometry 31
4.- ....**Conclusion** 34
References to chapter 1 35

Chapter 2 ....**Excimer Lamps** 38
1.- ....**Silent discharges for excimer generation** 39
1.1- ....Electrical discharges for UV generation 39
1.2- ....The silent discharge or dielectric barrier discharge 42
1.3- ....Application to rare gas molecules 49
2.- ....**Excimer lamps ($\lambda \geq$ 160nm)** 54
2.1- ....Construction of excimer lamps 54
2.2- ....Power measurements 58
3.- ....**VUV excimer lamps** 64
3.1- ....Introduction 64
3.2 ....Initial VUV excimer lamp design 64
3.3- ....Improvements 66
3.4- ....Incorporation to a CVD reactor 69
4.- ....**Conclusion** 70
References to chapter 2 71

Chapter 3 ....**Initial Applications of Excimer Lamps** 74
1.- ....**Photochemical generation of ozone** 75
1.1- ....Fundamentals of ozone generation 75
1.2- ....Ozone generation with UV radiation 79
1.3- ....The VUV enhanced ozone reactor 82
1.4- ....Conclusion 90
2.- ....**Application of excimer lamps to MOD** 91
2.1- ....Experimental set-up 91
2.2- ....UV induced metal depositions 93
2.3- ....UV induced dielectric material depositions 96
2.4- ....Conclusion 100
References to chapter 3 101

Chapter 4 ....**The Photochemical Deposition and Characterisation of Silicon Dioxide Layers** 103

1.- ....**The photo-CVD of silicon dioxide from silane and nitrous oxide gas mixtures** 104
1.1- ....Experimental conditions 104
1.2- ....Results and discussion 110
1.3- ....Conclusion 118
2- ....**The photo-CVD of silicon dioxide from silane and oxygen gas mixtures** 120
2.1- ....Introduction 120
2.2- ....Experimental details and sample preparation 121
2.3- ....Results and discussion 125
2.4- ....Conclusion 135
References to chapter 4 137

Chapter 5 ....**The Photochemical Deposition and Characterisation of Silicon Nitride and Oxynitride Layers** 140

1.- ....**The photo-CVD of silicon nitride from silane and ammonia gas mixtures** 141
1.1- ....Introduction 141
1.2- ....Experimental details 142
1.3- ....The window fogging problem 146
1.4- ....Growth kinetics 154
1.5- ....Thin film characterisation 158
1.6- ....Conclusion 167

2.- ....The *in-situ* photo-CVD of silicon oxide-nitride-oxide multilayers 169

2.1- ....Interest 169

2.2- ....Experimental Conditions 169

2.3- ....SIMS analysis 169

3.- ....The photo-CVD of silicon oxynitride SiO_xN_y 171

3.1- ....Interests in silicon oxynitride 171

3.2- ....Thin SiO_xN_y film deposition 171

3.3- ....Conclusion 175

References to chapter 5 176

Conclusions 180

Appendix 1 ....**The photochemical deposition of a-Si:H using an argon excimer lamp** 183

1.- ....Hydrogenated amorphous silicon (a-Si:H) 183

2.- ....Photo-CVD of a-Si:H 188

3- ....Thin Film deposition 192

4.- ....Conclusions and improvements 201

References to appendix 1 202

Appendix 2........**Colours presented by silicon dioxide films (in perpendicular white light)** 204

Appendix 3 ....**Assignments of the principal infra-red features for the study of thin silicon dielectric films** 205

Appendix 4 ....**Estimation of the error on V_0** 207

Appendix 5 ....**List of publications based on this work** 209

Introduction

The level of world-wide research linked with the densification of integrated circuits down to ultra large scale integration (ULSI) has burgeoned in recent years indicating without any doubt the enormous potential of this proposed research field. Because of the inherent problems associated with high temperature processing for thin film deposition, low temperature processing is extremely important for a multitude of future generation devices in related technologies. Among the numerous techniques which have been brought out to reduce this "thermal budget", photo-CVD has many advantages because of its properties (spatial resolution, chemical specificity, and absence of ion damage to the film).

These photo assisted processes have attracted strong interest in recent years by enabling the possibility of producing many types of high quality dielectric and semiconducting film compounds at low temperature. This is appealing for many technologies such as micro-electronics, opto-electronics, magnetic films and other multilayer film systems. During this work at UCL, a new kind of excimer lamp has been developed, capable of producing at high power very energetic photons (up to 9.8eV). This project involves the design and the use of these lamps to initiate photo-deposition of various materials. The principle of light emission from *exc*ited d*imer* systems has already been exploited for excimer laser technology. In our case, the lamp dispenses with the need for standing wave oscillations within an optical cavity, since for photo-deposition there is no need of purely monochromatic light. This enables the use of low wavelength photons at much cheaper prices than excimer lasers. Furthermore, the relatively low energies involved allows pure rare gases to be excited, hence shorter wavelengths. Finally, being pseudo-continuous, the total photon power can easily reach that of a powerful excimer laser.

The interest in photo assisted techniques stems from the ability of optical radiation to induce specific chemical reactions in the gas phase or at a surface. The selective, optical production of atoms, molecular radical species in the vicinity of a surface, and the ability to do so independently of the substrate temperature, largely decouples temperature effects from the production of the species of interest. In other words, the introduction of photons into a thin film deposition reactor allows one to drive the chemical environment far from equilibrium by selectively producing species that are not normally present in significant concentrations in conventional CVD, MBE or MOCVD reactors. This flexibility inherent with the photo-deposition of films permits operation at lower temperatures. The variety of materials that can be deposited by photo-CVD processes is truly remarkable: to date, some 24 elements, in addition to at least 20 insulator and semiconductor compound films have been deposited in this way [Eden], using various optical radiation from lasers or lamps. However, the use of excimer lamps for photo-CVD is exceptionally new. Excimer lamps, with their capability of emitting tunable wavelengths in the vacuum ultraviolet range (VUV: below 200nm) could potentially enable better quality films and devices to be made at lower temperatures than with conventional photo-CVD reactors. Since most precursor gas molecules exhibit an appreciable absorption spectrum in the vacuum UV range, a wide range of compounds can be deposited. For silicon dioxide (SiO_2) and silicon nitride (Si_3N_4), mixtures of silane, nitrous oxide, ammonia, and oxygen (SiH_4, N_2O, NH_3, O_2) were studied.

This project concentrates on novel applications of excimer lamps to the photo-enhanced deposition of thin films. At first the deposition of SiO_2 using SiH_4 and N_2O as precursors has been performed. This work constituted the first application of an excimer lamp to the deposition of silicon dielectric films. A xenon excimer lamp, which radiates at 172nm, was used to photochemically activate the nitrous oxide precursor. The properties of the layers obtained on our prototype system gives evidence of promising new domains of application for these light sources. The technique is expanded to the deposition of silicon nitride (Si_3N_4) layers using ammonia and silane as precursors, as well as that of silicon oxynitride and oxide-nitride-oxide stacked layers. Fast deposition (up to 500Å/min) of SiO_2 was also achieved by irradiating silane and oxygen gas mixtures. Investigations into the

deposition photochemistry are reported, together with the characterisation of the deposited material properties. Good SiO_2 and Si_3N_4 film quality was obtained, as well as a very good control of the stoichiometry in the case of silicon oxynitride film deposition, therefore providing interesting perspectives for electronic and optical applications.

This thesis is divided into 5 parts. In **chapter 1**, the photo-chemical vapour deposition is presented, as a technique allowing films to be deposited at low temperatures for semiconductor applications. The description of the photo-CVD reactor developed at UCL is given, together with a short review on the characterisation techniques used. The importance of well understanding the theory of excimers as the main precursor in this technique leads to **chapter 2**. In particular, the wide range of radiations that can be emitted with such lamps is presented. Various devices are described, enabling the generation of excimer continua from 308nm (xenon chloride), down to 126nm (pur argon). The possibilities offered by the excimer lamps available at UCL are reviewed, in terms of geometry and power output, and a few techniques allowing the measurement of VUV radiations are presented. **Chapter 3** concentrates on two direct applications of the ultraviolet radiation. In fact, since a new type of vacuum ultraviolet source became available during this project, new areas of application were investigated, namely the direct VUV enhanced generation of ozone, as well as various other applications of the UV enhanced organometallic technique (MOD). In fact, at the time of writing this thesis, a new project is about to begin at UCL to further extend those MOD experiments.

The photo-CVD of silicon dioxide films from gaseous precursors is presented in **chapter 4**. The technique involves the use of a xenon excimer lamp, radiating at 172nm, and two cases are studied, whether the gaseous mixture uses nitrous oxide or oxygen in combination with silane. All details concerning the experimental procedures and the film properties are given. In **chapter 5**, using the same light precursor, the 172nm enhanced deposition of silicon nitride thin films is presented, as well as that of silicon oxide-nitride-oxide (ONO) multilayers, and eventually that of silicon oxynitride thin films (SiO_xN_y). The thesis ends with a **conclusion** used to note the significant implications arising from this study and also future directions for study.

Further to this work, the recent use of devices generating shorter wavelengths, namely the 126nm continuum of argon, has been studied in order to enhance the direct photo-dissociation of silane to deposit hydrogenated amorphous silicon (a-Si:H) layers. Since those results showed some interests, they are presented in **appendix 1**.

Reference: J.G. Eden, in Photochemical vapour deposition, *Vol. 122 of "Chemical analysis", John Wiley & Sons, Inc., New york (1992).*

Photo-CVD, Apparatus and Methods

The aim of the first chapter of this thesis is to describe the reactor which has been developed to deposit under vacuum thin films of various materials at low temperatures with the photo-chemical vapour deposition method (photo-CVD). Initially is presented the context into which enters the chemical vapour deposition technique and in particular when ultraviolet light is used as a precursor. The specifications to fulfil in order to achieve the realisation of a reactor are given, and particularly to satisfy the experiment requirements and offer a wide degree of flexibility to its user. A full description of the reactor follows. Finally, the chapter terminates by a review of the usual diagnosis techniques used during the completion of this project.

1- Introduction to photo-chemical vapour deposition processing (photo-CVD)

1.1- The need for low temperature techniques

Thin dielectric films are of importance in their use as passivating and insulating layers on integrated devices and protecting the active parts of devices from dust and moisture. Over the last decade many different techniques of growth and deposition have been developed to produce these thin films. However, current trends to reduced device geometries and the growing importance of temperature sensitive materials such as III-V semiconductors means that high temperatures cannot be applied to semiconductor processing if all these materials are to be used in a single integrated circuit. One of the problems is that the group V elements from these materials can hardly be processed at temperatures higher than 300°C [Chang]. Clearly, in order to accommodate this step into current device fabrication procedures, the deposition of dielectric materials has to be processed at low temperature. Various techniques have been developed, according to the fact that suppressing the temperature means bringing energy in a different form.

1.2- A brief outline on other techniques

1.2.1 Physical Vapour Deposition (PVD)

This technique relies on the condensation of vapour phase molecules onto a nearest substrate. Evaporation and sputtering are two well known forms of PVD. Conventional resistive evaporation is not useful because at the elevated temperature used the deposited films can be contaminated by the metal from the filament. In case of sputtering, however, ions are directly generated from a plasma, e.g., in Argon. The target and the substrate are located on each of the electrodes, and three types of plasma can be generated: DC sputtering, RF sputtering and magnetron sputtering. The DC sputtering is generally not used for dielectric materials because of its tendency to implant charged particles. For RF sputtering, this effect is compensated on each alternate cycle and hence is more suitable. In magnetron sputtering, plasma

electrons are created by a magnetic field and accelerated to the target. This method gives higher deposition rates. Generally, PVD does not produce good quality dielectric films due to poor stoichiometry and adhesion. They also have poor electrical characteristics.

1.2.2- Chemical Vapour Deposition (CVD)

In CVD, the formation of thin films depends on the surface reaction that occurs between the surface atoms of the substrate and the chemical species that arrive on it from the gas phase. High temperature CVD (for SiO_2: 700 to 1100°C) gives very good quality films. These dielectrics are stoichiometric and do not contain hydrogen [Pliskin].

The tendency to reduce the temperature has developed a technique where electrical energy is provided to dissociate gas phase molecules. This form is called Plasma-Enhanced-Chemical Vapour Deposition (PECVD). The sample is located on one grounded electrode, and a high voltage RF signal (typically 13.56 MHz) is applied to the other electrode facing the substrate. This causes electrical discharges between the plates producing a plasma which breaks up the source gas molecules into radicals, ions, and other energetic species. The substrate temperature used can consequently be reduced (from 400°C to room temperature), but charged or high kinetic energy species can be the cause of bombardment of the sample which is detrimental to interface sensitive devices [Vinckier] [Buchanan].

1.3- Photo-enhanced Chemical Vapour Deposition

1.3.1- Generalities

An alternative to PECVD has led to the development of the photo-CVD technique where the energy is provided from photons from infra-red, visible or ultraviolet radiation. Although the deposition of films by gas phase photochemical reactions was reported in the scientific literature more than 50 years ago [Romeyn] [Emeléus], only since the late 1970s has the application of laser and lamp radiation to the growth of high quality films been pursued vigorously [Boyd] [Eden]. There are many ways

of photochemically dissociating a gas for thin film material deposition. Many light sources have been used from powerful lasers to lamps. The energy provided from the photons can be used in various ways for the deposition of thin films, the most frequent way being the photolytic dissociation of reactant gases. This direct photolysis is defined from the interaction of one photon with one gas phase molecule. The excited molecule liberates its energy by breaking into different molecules or radicals which may be used in the film growth process. Generally only ultraviolet (UV) photons can provide enough energy for direct photolysis.

The dissociation of the molecule can also be caused by the collision with an excited species which required less energy than that necessary for direct photolysis. This is called photo-sensitisation and has been extensively used with mercury lamps [Peters] [Saitoh] [Tarui-1983]. Powerful lasers can also enhance multiphoton photolysis or pyrolytic dissociation [Boyer-1982, -1984] [Fogarassy]. Figure 1.1 shows a variety of configurations used for photo-CVD reactors.

1.3.2- Photo-deposition of dielectric materials.

Photo-CVD techniques are low temperature techniques (from 350°C to room temperature) which do not present the drawback effect of surface bombardment with high energetic species. These techniques have been applied in various ways to the deposition of dielectric materials on substrates. In the case of silicon dioxide (SiO_2), the most frequently used dielectric material for gate oxides and passivating layers, two reaction schemes are possible:

- Oxidation, allowing growth of SiO_2 by the oxidation of the surface layer of silicon,
- Deposition, achieved when both silicon and oxygen radicals are brought together and allowed to react on the substrate surface.

Generally, the oxidation route gives better quality Si-SiO_2 interfaces due to its inner volume characteristic, but it is obviously restricted to silicon substrates. The deposition technique is preferred for the deposition of thick passivating layers on various materials.

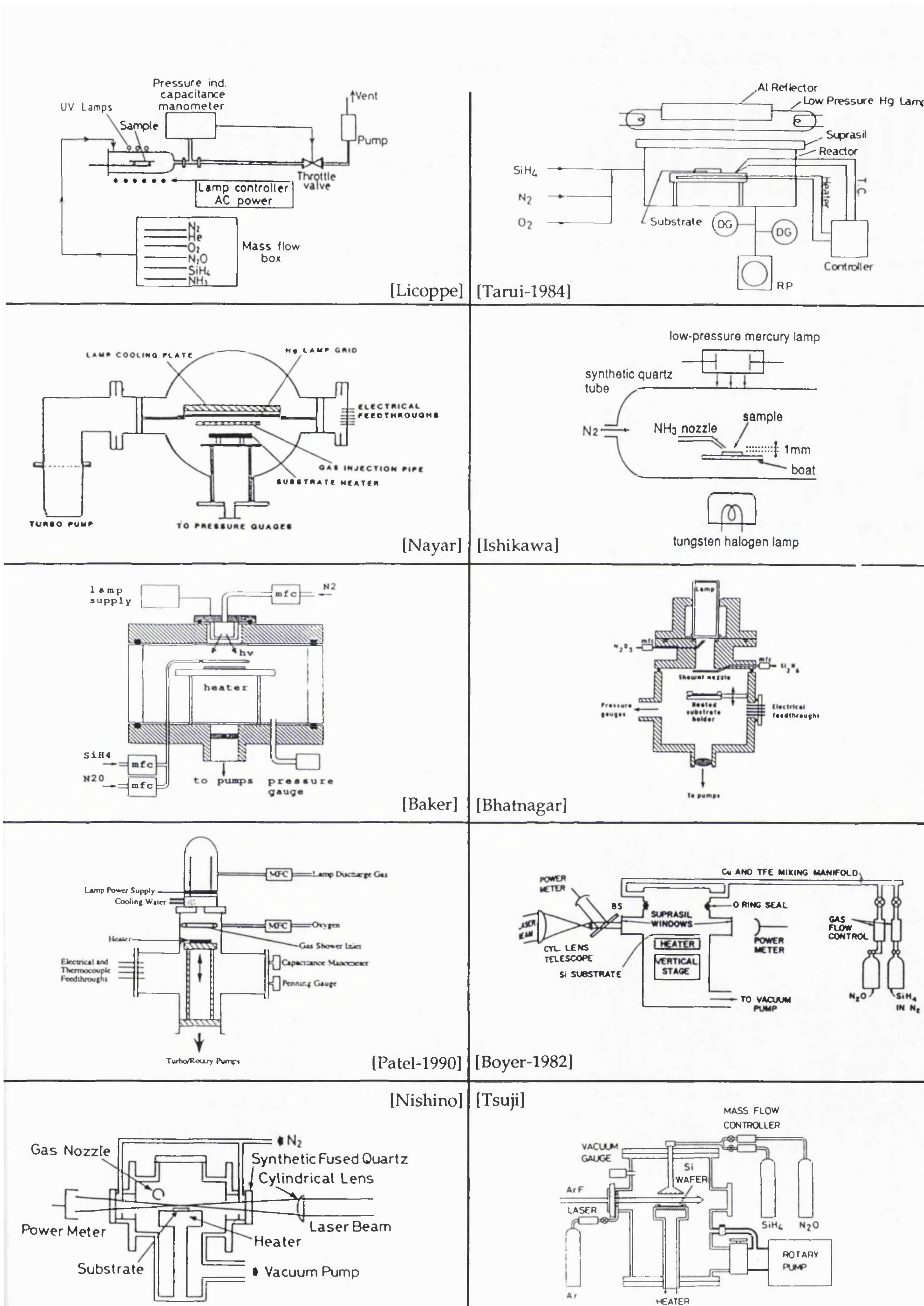

Figure 1.1 : A review of photo-CVD reactor configurations

The principle of the deposition technique is to have a gas phase reaction between Si and oxygen radicals. The commonly used precursors for these reactions are silicon hydrides such as silane (SiH_4), disilane (Si_2H_6) or trisilane (Si_3H_8), and for the oxygen radicals molecular oxygen (O_2), nitrous oxide (N_2O) or nitrogen dioxide (NO_2) can be used. The photon source used has to dissociate these precursors. A look at absorption cross section data [Itoh] [Okabe] [Calvert] [Baulch], showed that radiations below 200nm are suitable. This domain of ultra-violet is called Vacuum Ultra-Violet (VUV) according to its absorption in oxygen, and hence in air.

The sources of photons to be used for direct photo-CVD techniques on various substrates for dielectric materials have then to provide high energy photons close to, or in the Vacuum Ultra-Violet range (Table 1.1).

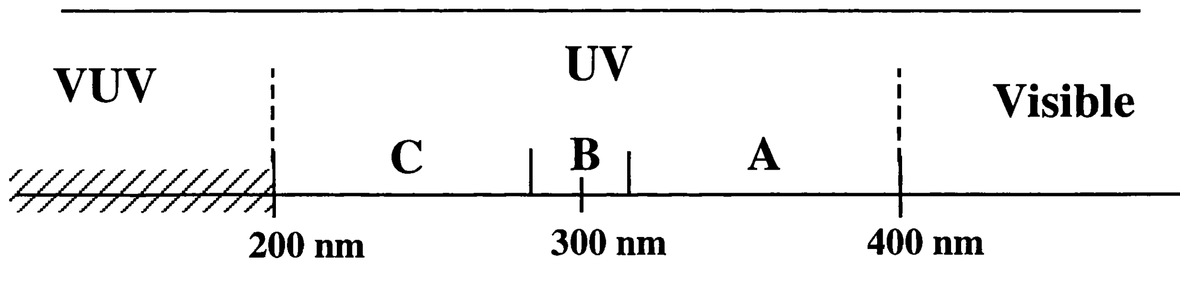

Table 1.1 : Wavelength location of the UV ranges

1.4- Sources of Vacuum Ultraviolet light

1.4.1- Lamps

Owing to the high absorbance of air, early spectroscopic studies in the ultraviolet region of the spectrum were limited to wavelengths longer than about 2000Å. In 1893, Viktor Schumann built the first vacuum spectrograph and made the first investigation of vacuum ultraviolet radiation. In 1906, Theodore Lyman, using a vacuum spectrograph equipped with a concave diffraction grating, was the first to measure wavelengths in this region. He found that the Schumann's spectrum had a

short wavelength limit of about 125nm, the limit due to the transmission characteristics of the fluorite material used. The region 200 to 125Å is since known as the Schumann region [Samson]. This is our wavelength range of interest.

Several gas discharge sources can emit in the vacuum ultraviolet range (cf. table 1.2). The low pressure mercury lamp (germicidal lamp) is by far the most widely used UV lamp [Phillips]. In the short wavelength range, its spectrum consists of 2 lines centred at 254nm and 185nm. The total UV efficiency can reach 50%; a very high value for such an energetic radiation. However, the 185nm line efficiency hardly reaches 10 % of the 254nm line, and implies the use of expensive window materials. When shorter wavelengths are required, low pressure discharge lamps and internal lamps have been used [Tarui-1984] [Robertson] [Marks] [Patel]. The conversion efficiency of these sources is however very low as can be seen in table 1.2. This point is discussed in detail in chapter 2.

Discharge medium	Wavelength (nm)	Efficiency (%)
Mercury (Low Pressure)	185, 254	50
Hydrogen, Deuterium	100- 300	0.33, 0.05
Nitrogen	120- 130	0.08
Glow discharge in Argon Krypton Xenon	 105- 135 125- 170 150- 180	 ≈ 0.01 ≈ 0.01 ≈ 0.01

Table 1.2 : VUV sources

The lamp window may also be a source of UV attenuation. There are very few materials transparent to far UV radiations that are stable under intense UV exposure. The price of these materials has also to be taken into account, according to the fact that commercially available VUV discharge lamps are far more expensive when enclosed in VUV transparent materials (table 1.3). The lifetime of the window material when subjected to radiation damage may also limit the lifetime of the entire device (e.g., colour centres) [Escher].

Materials	Cut off Wavelength (nm)	Cost (£/cm^2)	Comments
LiF	105	10	hydroscopic
MgF_2	115	30	hardly soluble in HF
Sapphire	142	15	
Crystalline quartz	160	1	
fused quartz (Suprasil®)	160	1	non crystalline (!)

Table 1.3 : Vacuum ultraviolet materials

1.4.2- Lasers

Lasers have also been used as VUV sources of photons. Excimer lasers are powerful coherent sources of short wavelength UV photons [Rhodes]. Generally pulsed, they can provide energies of 100mJ per pulse at frequencies up to 100Hz. The most commonly used excimer lasers commercially available are using rare gas-halogen mixtures with limited photon energy radiation (KrF, 248nm or ArF, 193nm). Shorter wavelengths may be obtained with pure rare gas excimer lasers, but these are, so far, only used as laboratory devices, because of the very high energy necessary for pumping these gases to inversion and the very high gas purity required. We can quote however the recent pure Argon laser emitting 80mJ at 126nm developed by Kurosawa *et al.* [Kurosawa].

The price of excimer lasers is by no mean comparable with those of lamps (e.g., typical number for capital cost: ≈£30k). The costs to safely operate (e.g., gases, power, mirrors & protective coatings) and handle these powerful low wavelength radiations are high.

1.4.3- Excimer Lamps

Recently, a new kind of UV lamp has been reported [Kogelschatz]. Experimentally developed in a Swiss Company, Asea Brown Boveri (ABB), this new generation of ultraviolet lamps work on the principle of excimer discharge generation. To date, they are not commercially available and have never been used experimentally for the photo-CVD of dielectric materials. As for the previously described UV lamps, the principle relies on an electrical discharge of a plasma gas. However, and this is the distinctive feature of these lamps, the efficiency of light generation can theoretically reach 40%. Experimental efficiencies as high as 10% have been reported [Gellert]. They cover a wide range of wavelengths from visible to VUV. These sources are therefore very attractive for photo-enhanced CVD (table 1.4).

The aim of this project, which was sponsored primarily by ABB, is to develop new prototypes of those light emitting devices, and then to exploit their potential for the photo-chemical vapour deposition of thin films. The whole of Chapter 2 will be dedicated to the presentation of these new lamp features.

Discharge medium	Wavelength (nm)	Efficiency (%)
Excimer discharge in		
Argon	126	
Krypton	146	≈10%
Xenon	172	

Table 1.4 : VUV Excimer sources

2.- Design of a photo-Chemical Vapour Deposition reactor

At the time of the first drawings for the construction of this vacuum system, there was no precise idea on the shapes, sizes and powers to be available from the light sources. The main objectives were to build a very flexible system to host very different photon sources. Here is presented in detail the deposition reactor, in terms of geometry and incorporated features, namely the substrate holder/heater, the precursor gas feeding control and the pumping apparatus. Also, since the next chapter will be concentrating on the UV source, only a minimum description of the parts incorporating the light source is given here.

2.1- Stipulations

A photo-CVD plant is generally composed of a combination of a light source, gas distribution equipment, a processing chamber, various in-situ diagnosis apparatus, and a pumping unit. According to the geometry of the processing chamber and to the size of the samples required, various configurations are possible for the light handling. Two main families of reactors can be denoted depending on whether the process uses focused light or not. Generally lamps are used in perpendicular illumination mode which allows the deposition of thin films on large areas with a very good homogeneity [Su] [Petitjean]. Lasers have been used for silicon dioxide growth either under parallel [Boyer-1982] [Szorényi] or perpendicular modes [Nayar], the former allowing the exposition of a gas phase to the photon flux without bombarding the sample surface, the latter being more appropriate with writing, etching or ablating techniques. The laser light beams can moreover be focused to offer on smaller size coverage much higher energies.

For direct photolysis, lamps providing very short wavelengths ($\lambda<300$nm) are used, and only the photolytic power hν of the photons is used. In our case, where the light source emits high energy photons ($\lambda<200$nm) and over a uniform surface, there is no need for focusing the light beam. The configuration which was chosen allows parallel illumination of the sample surface, on sizes up to one inch in diameter.

To allow further flexibility in the material to be deposited, the design of the reactor offers different processing gas lines, including silane (SiH_4), nitrous oxide (N_2O), ammonia (NH_3) and oxygen (O_2). The pumping system provides a high vacuum for sample preparation, as well as a high pumping speed during processing when high precursor fluxes are used.

2.2- General diagram of the photo-CVD reactor

Figure 1.2 shows a view of the entire system. The vacuum chamber is located on the left, whether the electrical apparatus including readout and control equipments are incorporated on a vertical rack on the right handside of the system. The gas handling is located outside the room for safety requirements, and one of the four gas feeding mass flow controllers appears in the background of the system on the right hand side. The vacuum system is built from stainless steel vacuum components (figure 1.3). It consists of the superposition of two chambers separated by a window transparent to the light radiation. The top chamber hosts the light source, whether the bottom chamber is the deposition reactor. According to the fact that light radiations well below the air cut-off are to be used, the top chamber has to be kept under vacuum. The processing chamber offers an ultraclean environment for sample preparation prior to deposition with background pressures of 10^{-6} mbar. Access to the sample stage implies the removal of the lamp chamber and the breaking of the vacuum.

To the lamp chamber is connected a vacuum ultraviolet grating monochromator which records the spectrum of the lamp. This spectrometer is isolated from the lamp chamber by a magnesium fluoride window transparent to the light radiation. It is also equipped with its separated pumping unit for spectra measurements below 200nm.

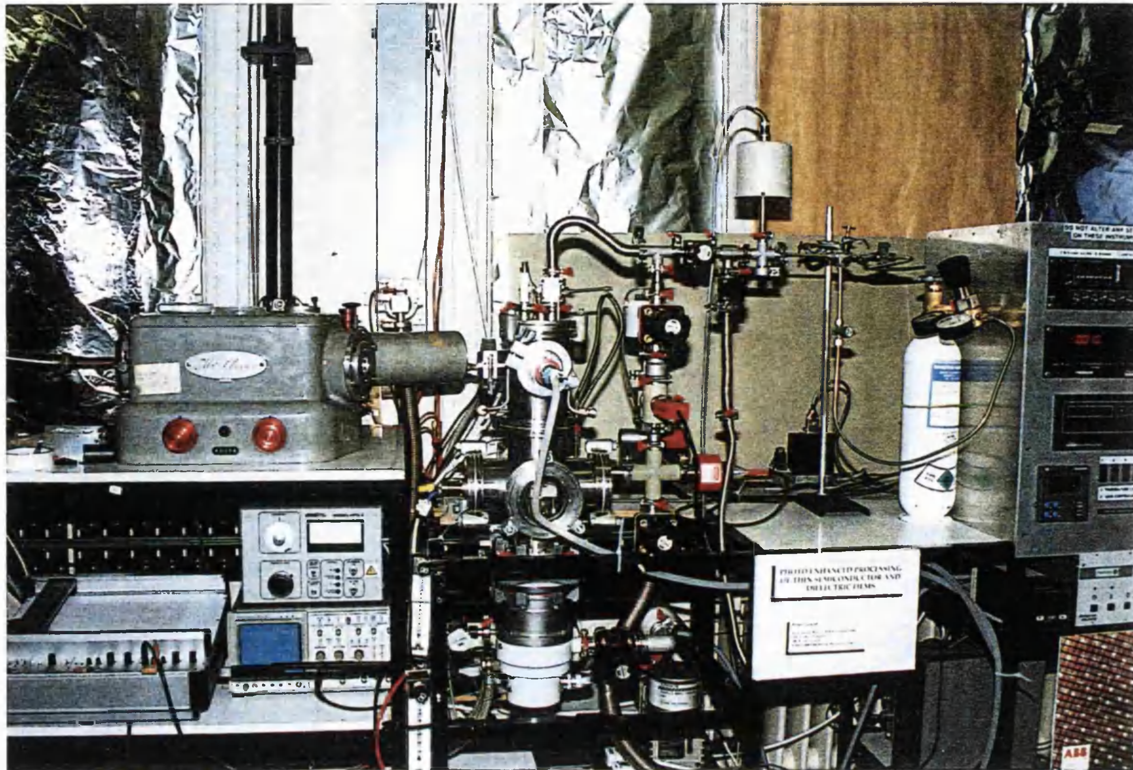

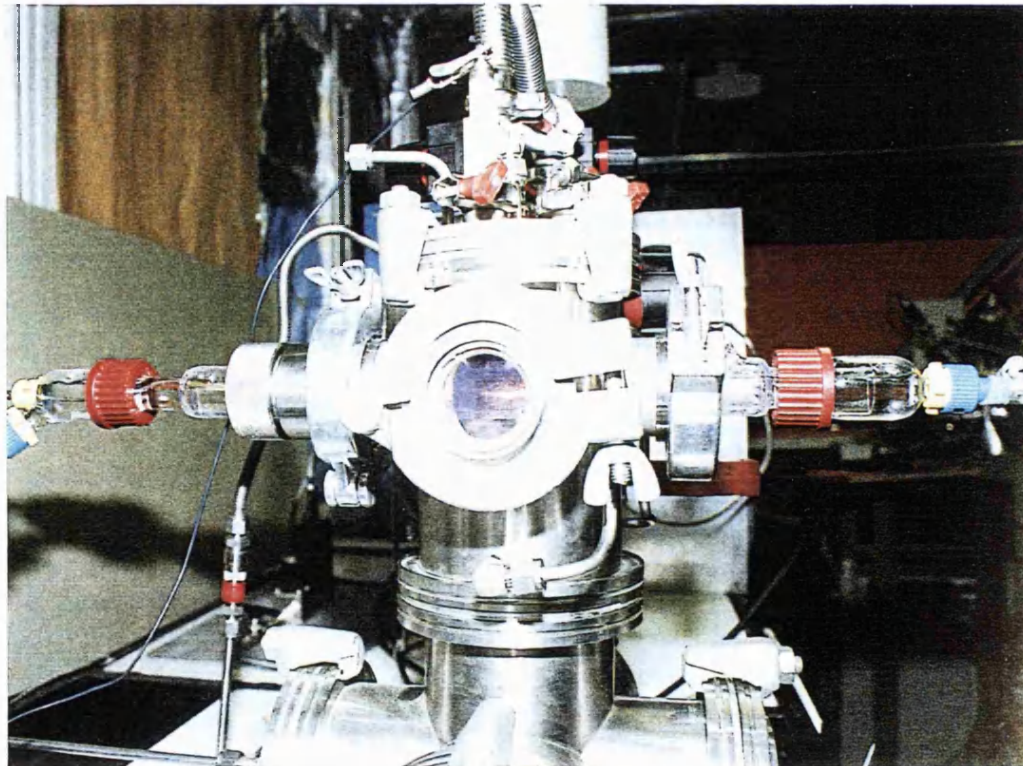

Figure 1.2 : Views of the photo-CVD system at UCL
(Entire system (top), Deposition reactor (bottom))

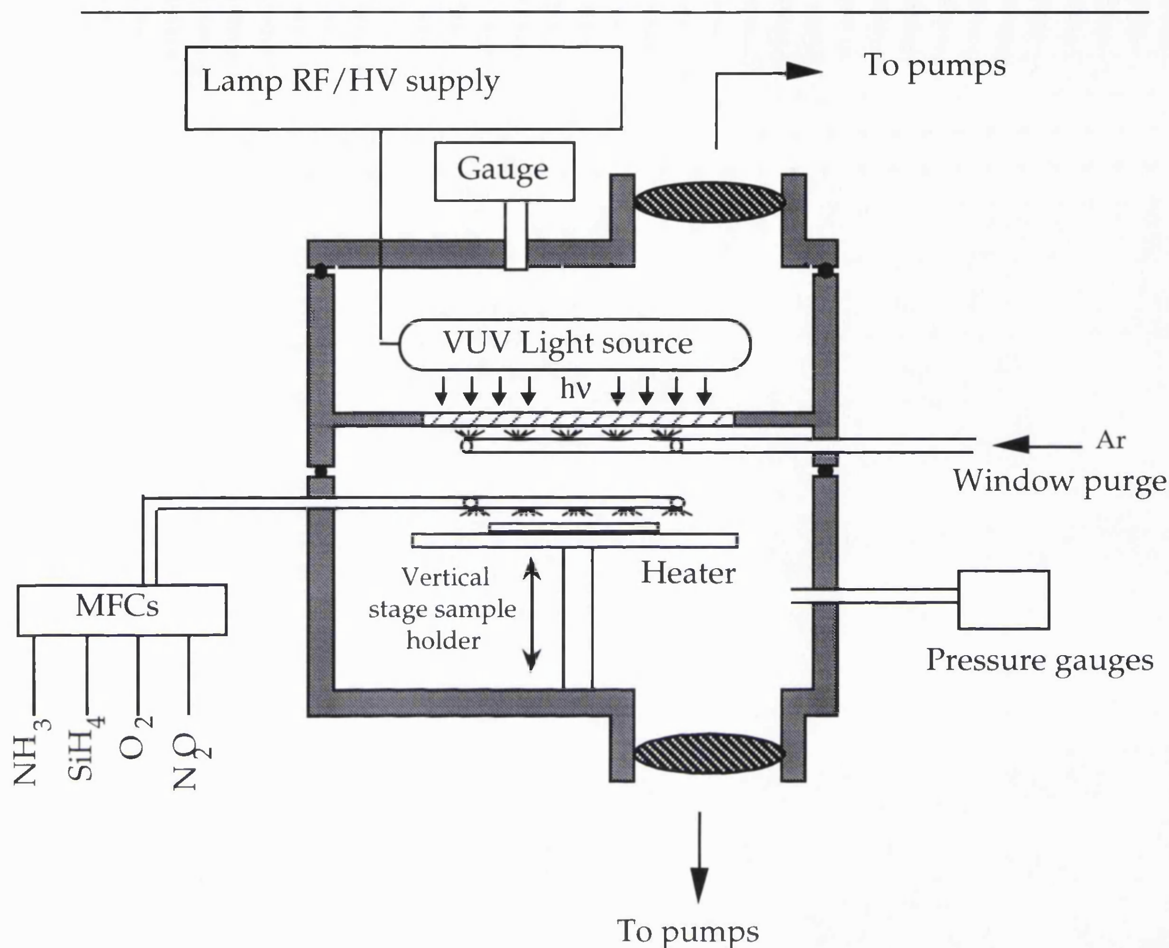

Figure 1.3 : Diagram of the photo-Chemical Vapour Deposition system

2.2.1- The deposition reactor

The deposition reactor hosts a vertical stage holder for the sample. The window-to-substrate distance can be varied from 10 mm to about 10 cm. In practice, maximum distances of 50mm were used in the present film growth process. On top of this vertical stage is attached the sample. The MINCO® substrate heater used provides very uniform heating ($\Delta<10^{\circ}C$ at 500°C) over the entire surface (ø 30mm) of the sample holder. The temperature is probed using a K-type thermocouple and gauged on an external controller. Working temperatures achieved with this heating set-up are in the range of 20°C to 550°C. Precursor gases are fed above the substrate through a toric-shaped shower. The distance shower-substrate was typically 5 to 7mm. The

flows of the precursor gases entering the chamber are controlled by a set of 4 thermal mass flow controllers (MFC). The nitrogen ranges of the flow controllers are of 20, 200, 200 and 200 sccm (Standard Cubic Centimetre per Minute (25°C, 760 torr)) for silane, nitrous oxide, ammonia and oxygen respectively. The MFCs are controlled using a MKS remote unit allowing 4 channel power supply/readout with gas correction potentiometers and set point signal for each channel. From those, the gas precursors are directly fed to the in-situ shower through a 1/4 inch pipe, the latter has the potential of being heated up to about 100°C to study the effect of warming the precursors.

A gas purge shower is placed facing the window separating the two chambers. This enables the use of a transparent gas such as argon during deposition to flush any precursor away from the window. The shower consists of a very thin perforated stainless steel straw (ø2mm). This apparatus is required for the deposition of materials that show a high cross section to the radiation used during their deposition. It is of particular use in the cases of silicon nitride and amorphous silicon. In some cases, however, (in particular for silicon dioxide which hardly absorbs radiations above 165nm), a good control of the pressure and the flow of the gas precursors can be sufficient to limit the deposition on the window. Window purging is therefore not recommended in these cases as it can cause flow perturbations which alter the experimental conditions. This problem will be discussed in detail in chapter 4 and 5 when depositions are presented.

2.2.2- The lamp chamber

Depending on the required lamp configuration, this chamber has to offer a wide range of possibilities for holding a lamp device. As the chamber configuration is in turn dependent on the type of lamp used, it is appropriate to describe it after the discussion of the lamps which is presented in chapter 2. Here is only mentioned that this vacuum chamber offers electrical feedthrough features, viewports and pressure gauges.

2.2.3- VUV transparent window.

The window separating the two chambers has to offer a very low photon cut-off, as well as mechanical resistance to the possible pressure difference between the chambers. As presented in table 1.3, some quartz materials fit applications using wavelengths as low as 160nm. However, as lower radiations may have to be used, the window will have to be crystalline magnesium fluoride (MgF_2) or lithium fluoride (LiF). Furthermore, the use of a fluorinated saturated compound allows eventual cleaning with fluoridric acid, good remover of materials such as silicon dioxide that are to be deposited. MgF_2 was chosen, although more expensive than LiF, since it has the advantages of being for being not hygroscopic and therefore more stable to successive cleanings.

At the early stages of this project we bought a magnesium fluoride viewport supplied by a vacuum company. Despite the high cost of these windows mainly due to UHV sealing requirements, they unfortunately do not offer mechanical resistance to an inverted pressure gradient. In fact, a pressure difference of 1 atmosphere in the "wrong" direction was sufficient to unseal it. I therefore recommend buying the window from a crystal growing company and to assemble it to any home made flange ensuring vacuum with a compressed seal (figure 1.4).

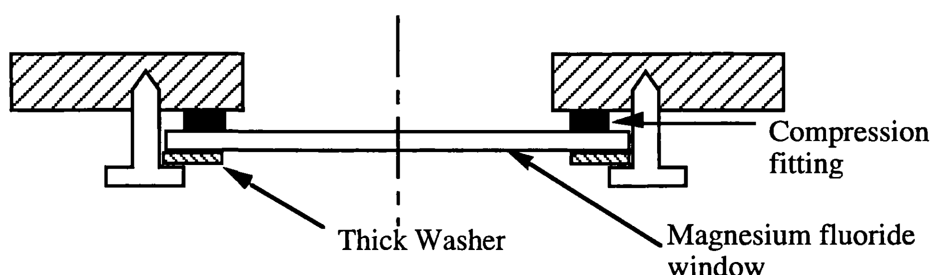

Figure 1.4: scheme of the window holder arrangement

The minimum thickness of the window is calculated with

$$Thick_{min} = \sqrt{\frac{K P D}{S}} \qquad (1.1)$$

where S is the apparent elastic limit of the material, D the unsupported diameter, P the differential pressure, and K a coefficient that incorporates a minimum safety factor.

2.2.4- Vacuum apparatus

The pumping set-up offers high vacuum background pressures (10^{-6} mbar) from a water cooled turbomol ecular pump (170 l/s), backed up with a miniature double stage rotary pump (30 l/min). In parallel to this stage is a high pumping speed fomblinised rotary pump (540 l/min). This pump is used during deposition to maintain the chamber pressure constant when the precursor gases are fed into the reactor. Also, due to the very small pumping speed of the miniature backing pump, the 540l/min rotary pump is also used to provide primary vacuum before turbomollecular pumping. Figure 1.5 gives a schematic diagram of the pumping set-up. The entire unit complies with any of the following scenario:

- it allows permanent high vacuum pumping of both the reactor and the lamp chamber between deposition experiments
- it allows during processing the pumping at high speed of the gas precursors fed into the deposition reactor while the lamp chamber is maintained at a constant pressure
- it allows the purge of the lamp discharge gas in the top chamber without stopping high vacuum pumping in the reactor
- it ensures insulation of the turbomollecular pump during deposition to avoid its contamination with the precursor chemicals.

The pressures are measured with 3 gauges. In order to achieve high accuracy in the measurement of the medium pressure lamp discharge and the use of corrosive precursor chemicals in the reactor, the system is equipped with two capacitance manometers ranging 1000 to 10^{-1} mbar and 10 to 10^{-3} mbar respectively. A third pressure device consisting of a Penning gauge combined with a pirani is finally used to monitor the high vacuum background pressure in the reactor.

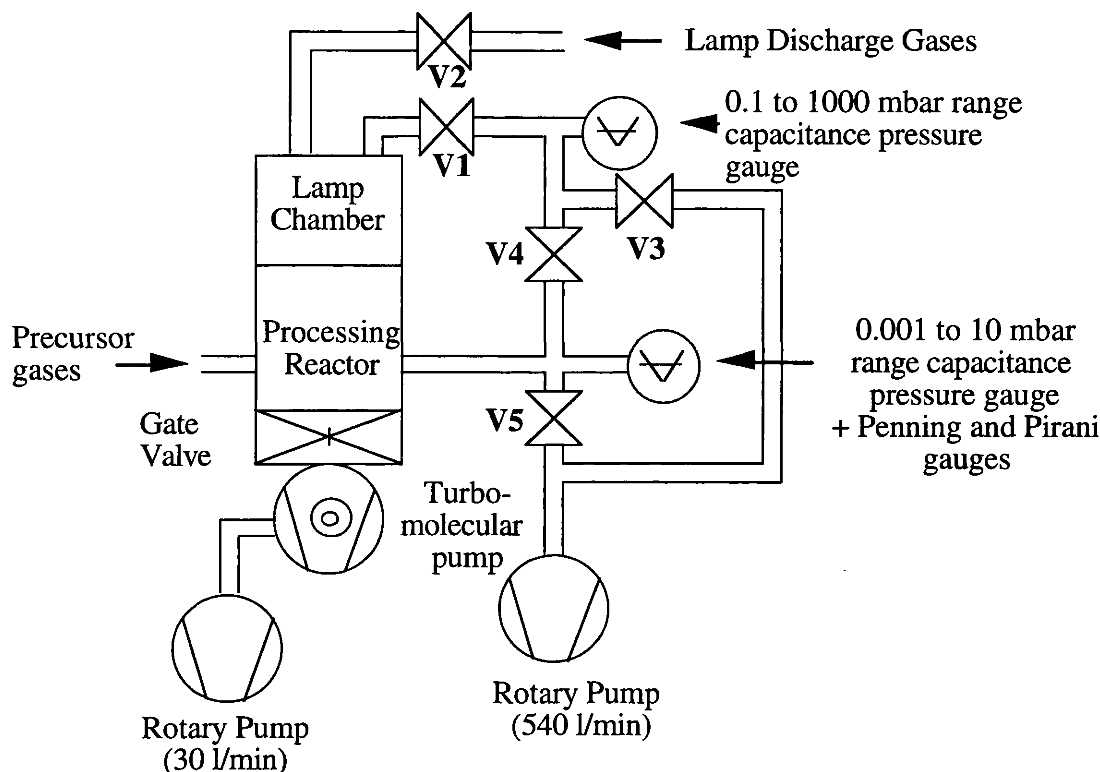

Figure 1.5 : Pumping setup

2.2.5- VUV and UV monochromator

The radiations emitted from the lamp devices are probed using a MacPherson monochromator. The grating is aluminium coated with 2400 grooves /mm, enabling a wavelength range from 1050Å to 5000Å under a resolution of a few Å. The readout of the monochromator was calibrated using several lines from an argon ion laser, as well as that of a low pressure mercury lamp. The instrument volume was evacuated to pressures below 10^{-1} mbar for *vacuum* UV measurement. The spectrum scanning is mechanical and requires the rotation of the grating mirror. The output measuring unit consists of a photomultiplier tube with a sodium salicylate fluorescent coating (§ 3.1 of chapter 2 for further information on sodium salicylate). When biased at voltages around 700V DC, the photomultiplier gives measurable voltages (a few 100s of mV) which are recorded on a X/Y chart recorder. All spectra shown in this thesis are obtained using this apparatus, unless otherwise stated.

2.3- Safety requirements

The use of toxic and dangerous chemicals such as ammonia and silane has required the use of various safety apparatus to prevent any experimental mishandling. In particular, the silane is pyrophoric and therefore has to be handled with particular care. In the pure gas phase, it is thermally stable up to 200°C, but small leaks of the gas into air will spontaneously ignite to give clouds of white amorphous silica particles. Large leaks can lead to an unstable cloud of gas which will suddenly explode with no preflame [Tucker]. Pure silane was used, in order to avoid any eventual diluting gas experimental artefact. Also, when pure silane is used, the risks are reduced by the much lower pressures of silane involved and the considerable reduction in the amounts of gas required for each individual experiment. In fact, the very low silane flows employed often made possible the work on a closed silane cylinder after having filled only the feeding line.

In terms of safety, the gas handling has to be contemplated separately whether the presence of silane is considered at high pressures *before* the reactor, or at atmospheric pressures getting in contact with air *after* the pumps.

2.3.1- From cylinder to reactor

In most of the pipes and fittings of the supply lines, the pressures used are higher than atmospheric. It is essential to prevent any faulty action of a valve that could leak hazardous gas into the laboratory or to another apparatus. As such, an automatic shut off valve is located on the silane cylinder, to act as a flow limiting device to cut the gas supply if the flow happens to exceed a critical value of 7 LPM (Standard Litre per Minute (21°C, 17 PSI N_2)). A set of three other normally closed air actuated valves, locked with key-actuated switches, is used from the cylinder to the mass flow controllers and finally to the reactor (figure 1.6).

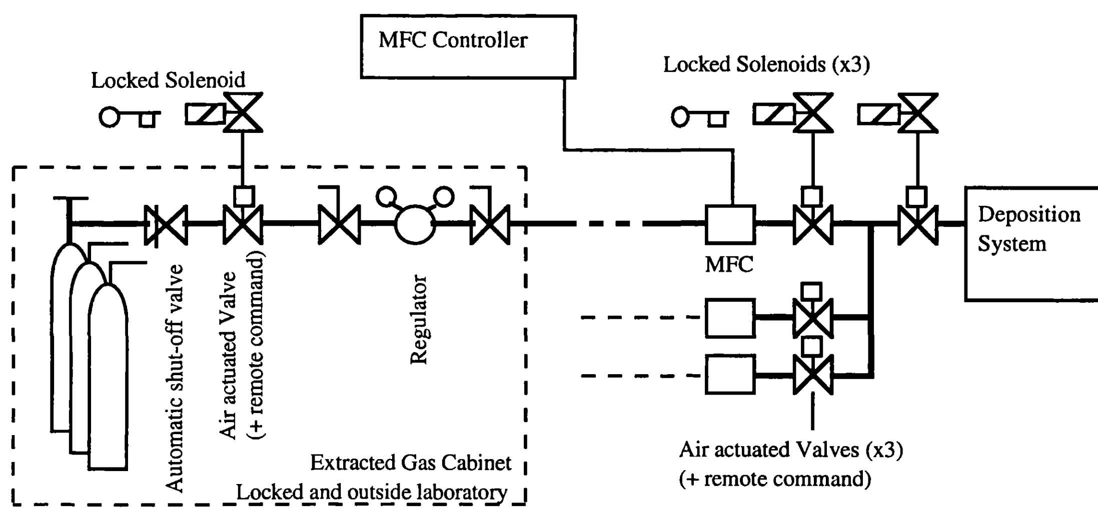

Figure 1.6 : Gas Handling system (Only the case of silane is drawn)

2.3.2- Exhaust gas handling

Because the reactant gases are pumped away from the system, toxic and hazardous residual gases will be present in the pumps at possibly high temperatures and released into the atmosphere after the pump. In fact, unreacted silane in the exhaust system, particularly if H_2 is present, can lead to exhaust fires [Hammond]. To prevent such a problem, the exhaust system of the pump is connected to an extractor, and during use the pump is heavily purged (about 1000 times the incoming silane flow) with an inert gas. This inert gas purge is introduced into the ballast of the two stage rotary pump in order to dilute the actual content of the gas in the pump without affecting its pumping speed.

2.4- Maintenance

A regular maintenance regime consists of regular checkups of pump oil and water cooling circuitry. The actual use, this reactor showed a good reliability and very low level of failures. The reproducibility of the deposition experiments was very good, as long as regular cleaning of the reactor and of the window was carried out. Before each deposition experiment, the MgF_2 window was systematically cleaned from any deposited product, using a cotton bud wetted in a highly diluted HF solution.

3.- Characterisation of the deposited thin films

In this section are presented the experimental characterisation techniques used during this project to analyse the photo-deposited thin film layers. The thicknesses (a few hundred Ångströms) and refractive indices were measured using ellipsometry. The background principles of the technique are presented, and the level of accuracy obtained in these measurements is discussed. To further study the physical characteristics of the deposited films, Infra-Red spectroscopy was used. This technique offers a way to analyse the concentration of the species present in the film from their binding vibration modes. In particular, Fourier Transformed Infra Red Spectroscopy (FTIR) will be discussed.

3.1- Ellipsometry

Ellipsometry is a non-destructive optical analysis method, based on the measurement of a change in the polarisation state of an incident light when refracted on a surface.

The measure of this change in polarisation gives:

- either optical parameters of a reflecting surface if the latter is not covered by any film,
- or the thickness and optical properties of a layer covering a reflecting surface,
- or in the case of spectroscopic ellipsometry (wavelength variation of the incident beam), the optical characteristics of the transient region between substrate and thin film.

In the case of ellipsometry measurements, the parameters concerned are:

- The refractive index, n, refraction parameter of the incident radiation,
- The absorption coefficient, k, optical attenuation of a beam while traversing a medium.

n and k are directly dependent on the wavelength of the light beam used, e.g., a Helium-Neon laser source radiating at 632.8nm. Thin dielectric films generally show a very low reflectivity, and most of them are transparent (k=0) in a broad region of the spectrum.

3.1.1- Fundamental equation of ellipsometry

For this discussion, the incident and reflected beams are invoked by their electrical components $E_{//}$, $E_{\perp}$ and $E''_{//}$, $E''_{\perp}$ projected in the incident (//) and the perpendicular ($\perp$) plane respectively (see figure 1.7). Ellipsometry enables the measurement of the difference in polarisation of the light beam after reflection. These measures give the phase shift (Δ) and the ratio ($\tan\psi$) between the peak values of the // and $\perp$ components of the reflected beam.

It comes:

$$\tan\psi = \frac{\dfrac{|E''_{//}|}{|E_{//}|}}{\dfrac{|E''_{\perp}|}{|E_{\perp}|}} \qquad (1.2)$$

The reflection on the surface causes a different phase shift in the // and $\perp$ waves which are designated by $\Delta_{//}$ and $\Delta_{\perp}$ respectively, and:

$$\Delta = \Delta_{//} - \Delta_{\perp} \qquad (1.3)$$

The ratio $\rho = \dfrac{\dfrac{E''_{//}}{E_{//}}}{\dfrac{E''_{\perp}}{E_{\perp}}}$ can then be expressed with:

$$\rho = \tan\Psi\, e^{i\Delta} \qquad (1.4)$$

with $0^\circ \le \Psi \le 90^\circ$ and $0 \le \Delta \le 360^\circ$.

Equation (1.4) is the basic equation of ellipsometry

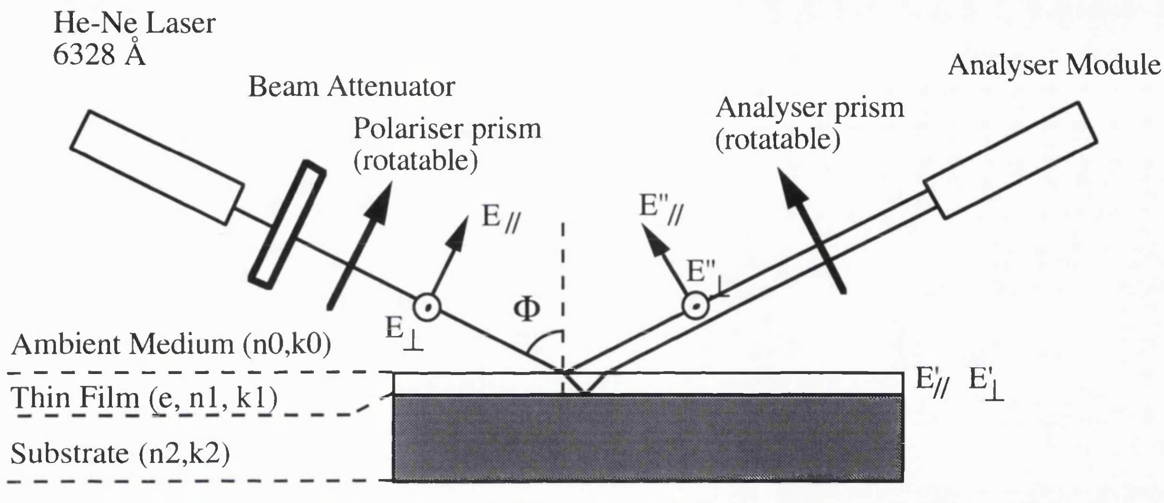

Figure 1.7 : Schematic diagram of ellipsometry

3.1.2- Characterisation of a thin film with ellipsometry

An ellipsometric measurement involves irradiating the surface of a sample at a known angle of incidence Φ with a collimated beam of monochromatic light having a known, controllable state of polarisation, and determining the differences between the states of polarisation of the incident and reflected beams caused by the sample. Δ and Ψ are directly obtained from the measure of the angular azimuths of the polariser and the analyser respectively when the light extinction condition is obtained. Δ and Ψ are cyclic functions of the film thickness, and the cyclic function reaches the starting point when the optical path is a multiple of the light wavelength.

In the last century, Fresnel derived equations for the reflection of light from a film-free surface, establishing that Δ and Ψ are each functions of the angle of incidence Φ, the wavelength of the light, the refractive index n_0 of the ambient medium, as well as the real part n_2 and the imaginary part k_2 of the substrate refractive index. Drude extended the Fresnel reflection equations to a single-film model where Δ and Ψ depend on the real part n_1 and the imaginary part k_1 of the film refractive index and on the film thickness e. Namely:

$$\Delta = f_2 (\Phi, \lambda, n_0, n_2, k_2, n_1, k_1, e) \quad (1.5)$$

$$\Psi = g_2 (\Phi, \lambda, n_0, n_2, k_2, n_1, k_1, e) \quad (1.6)$$

The angle of incidence $\Phi = 70°$, and the medium refractive index n_0 are constant, and in the case of thin films on silicon, n_2, k_2 are also constants at λ=632.8nm. From the measure of Δ and Ψ, and as the optical constants of the substrate are known, it is possible to determine the values of the thickness and the refractive index of the film, within the limits of a periodic constant. Practically, either graphical methods or computerised calculations can be used. In the case of silicon oxide or nitride thin films on silicon, the cycle thickness is 2815Å and 1792Å respectively. For most of the experiments, the deposited layers have thicknesses well below these values. However, if the deposited films were sufficiently thick to reach these values, the colour of the sample gives a good idea of the thickness (see Appendix 2), enabling the determination of the cycle.

3.1.3- Precision and accuracy

Ellipsometry can measure film thicknesses of at least an order of magnitude smaller than can be measured by other methods. For thin films from 20 to 200Å, the reproducibility of measurements remained within the boundaries of a maximum of 10Å error, most probably resulting from power drift of the He-Ne laser used. This error was compensated by always measuring the thickness of the same reference sample prior to the measurement. The ellipsometer used was a Rudolf AutoEl II model, which showed very good reliability.

3.2- Infra-red spectrometry

3.2.1- Interest

Infra-red spectroscopy is a well known technique for structural analysis of materials. In the case of silicon and silicon dielectrics, the optical absorption measurements in the infra-red region can yield important information about the film such as thickness, chemical composition, density and impurity concentrations. The measurements were performed on films deposited on single crystal silicon wafer substrates, which are transparent over the spectral range of interest (25µm to 2.5µm, corresponding to 400 to 4000cm^{-1}). Absorption in the near infra-red region is due to vibrational mode resonance of the inter-atomic bonds in the material. Different vibrational modes and bonds between different elements, give rise to a range of characteristic absorption frequencies associated with each bond type. Appendix 3 gives a review of the usual infra-red vibrational mode for several silicon bonded light elements, which are of interest in this work.

3.2.2- Instruments

3.2.2.1- Dual beam spectrophotometers

At the early stages of this project, a Perkin Elmer 380 dual beam spectrophotometer, which scans over the range 200 cm^{-1} to 4000 cm^{-1} was used. The infra-red radiation source in this instrument is a red hot silicon carbide rod, which illuminates both the coated sample and the bare silicon substrate reference. The transmitted radiation through each sample is alternately reflected, via a diffraction grating, onto a pyroelectric sensor by a rotating mirror. The ratio of the two signals at a given wavenumber then defines the transmission through the coated sample relative to the reference. The diffraction grating slowly sweeps the detected infra-red radiation over the desired wavenumber range and a chart recorder plots out the transmission spectrum during the scan. However, those instruments are far from being as convenient as modern instruments using Fourier Transform Infra-Red spectroscopy (FTIR).

3.2.2.2- Fourier Transform Infrared Spectroscopy (FTIR)

FTIR spectroscopy offers potential advantages compared with conventional dispersion infra-red spectroscopy, namely:

- Higher signal to noise ratios for spectra obtained under conditions of equal measurement time, (only a few seconds per scan),
- Higher accuracy in frequency for spectra taken over a wide range of frequencies,
- Fewer difficulties with insufficient sample size.

An FTIR spectrometer basically consists of two parts: an optical system which uses an interferometer, and a dedicated computer. The computer controls optical components, collects and stores data, performs computation on data, and displays spectra. The use of a dedicated computer with *any* spectrometer has advantages. However, the real advantages of an FTIR spectrometer result in the use of an interferometer rather than a grating or prism. Figure 1.8 shows a simplified diagram of the optical system.

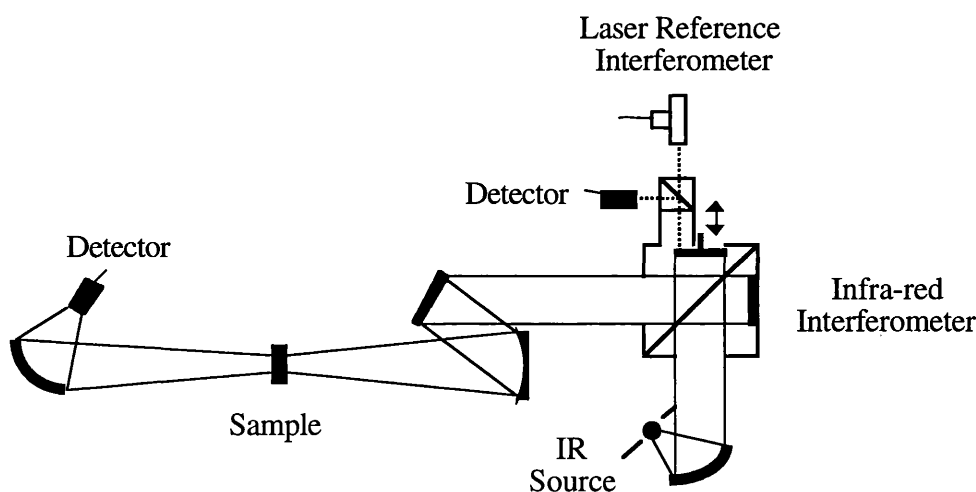

Figure 1.8 : Simplified diagram of the optical system of a Fourier Transform Infra-Red spectrometer [Green]

The light from an infra-red source is collimated and sent to the beam splitter of a Michelson interferometer. The beam is divided, part going to the moving mirror and part to the fixed mirror. The return beams recombine at the beam splitter undergoing interference. The reconstructed beam is then directed through the sample and focused onto the detector. A laser beam, undergoing the same change of optical path as the infrared beam, serves to reference the position of the mirror during the scan, and initiates the collection of data points from the signal of the infrared detector at uniform intervals of mirror travel. The data points are digitized by an analog-to-digital converter and stored in a computer memory. The result is an interferogram, i.e., a record of the signal of the infra-red detector as a function of the difference in path (retardation) for the two beams in the interferometer. The interferometer scans are generally taken quite rapidly (a few seconds each) to avoid extensive signal averaging before digitalisation. Data from additional scans can be coadded to the data stored in computer memory to improve the signal to noise ratio of the interferogram. A Fourier transformation is performed on the interferogram using a fast Fourier transform algorithm, to convert the signal as a function of retardation to a signal as a function of frequency. Two different FTIR spectrometers have been used during this project. Part of the results in Chapter 4 and 5 are either computed from a Nicolet 200 spectrometer, or from a Perkin-Elmer 7000 model.

4.- Conclusion

The context into which enters the photo-CVD technique has been presented. The inherent necessity associated with the use of low temperatures during thin film processing make these processes good candidates towards future industrial applications. The interest in photo-CVD techniques stems from the ability of optical radiation to induce specific chemical reactions in the gas phase or at a surface. The development of a new kind of lamps, namely the excimer lamps, capable of producing high fluxes of photons in the VUV region, opens up new applications towards the direct photo-initiated deposition of thin films.

The photo-CVD reactor, which has been developed at UCL during this project has been presented. It offers, with a very high flexibility, the possibility to expose substrates and/or gas phases (SiH_4, N_2O, NH_3 or O_2), in a high vacuum environment (10^{-6}mbar), to the radiations emitted from such excimer lamps. Using this reactor, the deposition of thin films is proposed, namely that of silicon dioxide and silicon nitride materials. The main techniques used to characterise the deposited thin films during this project have also been reviewed, namely the ellipsometry and the fourier transform infra-red spectrometry.

References to chapter 1

[Baulch] D.L. Baulch, R.A. Cox, P.J. Crutzen, R.F. Hampson, J.A. Kerr, J. Troe, R.T. Watson, J. Phys. Chem. Ref. Data, **11** (1982) 359

[Boyd] I.W. Boyd, *Laser Processing of Thin Films and Microstructures*, (Springer, New York, 1987)

[Boyer-1982] P.K. Boyer, G.A. Roche, W,H Ritchie and G.J. Collins Appl. Phys. Lett., **40** (1982) 716

[Boyer-1984] P.K. Boyer, K.A. Emery , H. Zarnani and G.J. Collins Appl. Phys. Lett., **45** (1984) 979

[Buchanan] D.A. Buchanan Appl. Phys. Lett., **56** (1990), 1037

[Calvert] J.G. Calvert & J.N. Pitts, *Photochemistry*, J. Wiley & Sons, New york (1966)

[Chang] R.R.Chang, R. Iyer, D.L. Lile J. Appl. Phys., **61** (1987) 1995

[Eden] J.G. Eden, in *Thin film process II*, ed. by J.L. Vossen & W. Kern, Academic press, San Diego, CA (1991)

[Emeléus] H.J. Emeléus and K Stewart, Trans. Faraday Soc., **32** (1936) 1577

[Escher] G.C. Escher, SPIE Vol. 998 *Excimer Beam Applications* (1988) 30

[Fogarassy] E. Fogarassy, A. Slaoui, C. Fuchs & J.P. Stoquert Appl. Surf. Sci., **54** (1992) 180

[Gellert] B. Gellert and U. Kogelschatz, Appl. Phys. B, **53** (1991) 14

[Green] D.W. Green and G.T Reedy, in *Fourier Transform Infrared Spectroscopy*, ed. by J.R. Ferraro, L.J. Basile, Academic Press, New York, (1978)

[Hammond] M.L. Hammond, Solid State Technology, (Dec. 1980) 104

[Itoh] U. Itoh, Y. Toyoshima, H. Onuki, N. Washida, T. Ibuki, J. Chem. Phys., **85** (1986), 4867

[Kogelschatz] U. Kogelschatz, Appl. Surf. Sci., **54** (1992) 410

[Kurosawa] K.Kurosawa, Y. Takigawa, W. Sasaki, M. Katto, Y. Inoue Jap. J. Appl. Phys., **30** (1991) 3219

[Lefevre] H. Lefevre, M.Schulz, in *The Si-SiO2 system*, ed. by P. Balk, ch.6 (1988)

[Marks] J. Marks and R.E. Robertson Appl. Phys. Lett. **52** (1988)810

[Nayar] V. Nayar, I.W. Boyd, F.N. Goodall, G. Arthur, Appl. Surf. Sci., **36** (1989) 134

[Okabe] H. Okabe *Photochemistry of small molecules*, John Wiley & Sons (1978) New York

[Patel] P.Patel and I.W. Boyd, Appl. Surf. Sci., **46** (1990) 352

[Peters] J.W. Peters Tech. Dig. IEEE Int. Electron. Dev. Meet., New York, (1981) 240

[Petitjean] M. Petitjean, N. Proust, J-F. Chapeaublanc, J. Perrin, Appl. Surf. Sci., **46** (1990) 189

[Phillips] R. Phillips, in "Sources and Applications of Ultraviolet Radiation", Academic Press, London (1983)

[Pliskin] W.A. Pliskin J. Vac. Sci. Technol., **14** (1977) 1064

[Rhodes] Ch.K. Rhodes, *Excimer Lasers*, Vol. 30 of *Topics of Applied Physics* , Springer, Berlin (1984)

[Robertson] P.A. Robertson, *The photo-enhanced deposition of amorphous silicon and silicon oxide thin films*, PhD thesis, University of Cambridge, UK (1987)

[Romeyn] H. Romeyn, Jr., and W.A. Noyes, Jr. J. Am. Chem. Soc., **54** (1932) 4143

[Saitoh] T. Saitoh, T. Shimada, M. Migitaka, and Y. Tarui J. Non-Cryst. Solids, **59** (1983) 715

[Samson] J.A.R. Samson in *Techniques of Vacuum Ultraviolet spectroscopy*, John Wiley & Sons, New York (1967)

[Su] Y.K. Su, C.R. Huang, Y.C. Chou, Jpn. J. Appl. Phys., **28** (1989) 1664

[Szorényi] T. Szorényi, P. González, M.D. Fernández, J. Pou, B. León, M. Pérez-Amor, Thin Sol. Films., **193/194** (1990) 619

[Tarui-1983] Y. Tarui, K. Sorimachi, K. Fujii, K. Aota, T Saitoh J. Non-Cryst. Solids, **59/60** (1983) 711

[Tarui-1984] Y. Tarui, K. Aota, K. Kamisako, S. Suzuki, T. Hiramoto Ext. Abs. XVI Int. Conf. Sol. State Devices and Materials, Kobe, Japan (1984) 429

[Tucker] E.A. Tucker, Eur. Semicond. Design and Prod., (July 1985) 27

[Vinckier] C. Vinkier, S. de Jaegere J. Electrochem. Soc., **137** (1990) 628

Chapter 2

Excimer Lamps

The lamp devices used during this project are not commercially available and part of the reported work consists of the fabrication of prototype sources. In order to put this work into context, the current understanding of the theory of the excimer effect and its application to light emitting devices are reviewed. In particular, this chapter addresses the excimer lamps, also found in the recent literature under the names of dielectric barrier discharge (DBD) sources, silent discharge lamps, or excimer light sources.

1.- Silent discharges for excimer generation

1.1- Electrical discharges for UV generation

1.1.1- History

The luminous emission observed when an electrical current passes through a gas has fascinated observers since their discovery at the very beginning of the study of electricity. Initial investigations of this phenomenon was limited by the low deliverable current initiated by electrostatic machines, and the area of study centred on atmospheric pressure low current breakdown experiments. Also, due to the very dangerous electrical equipment used, the study of the high pressure electrical discharge of lightning proved fatal to far more physicists than it enlightened.

In 1879, long before the concepts of mobility, diffusion, attachment or recombination had been born, Sir William Crookes had already studied the rays emitted from discharges in low pressure glass tubes whilst submitted to DC voltages from voltaic piles. After his long series of experiments, and the design of his many Crookes tubes, he championed the theory that these emitted rays were due to charged particles. With the improvement of vacuum and glass blowing techniques and electricity handling, the behaviour of the glow discharge as a function of pressure, electrode geometry, and type of gas, filled the literature for many years till the discovery of X-rays (1895) and the electron (1896).

It is only by 1911, with the work of J.J. Thomson and J.S. Townsend, that we can really consider the beginning of the historical development of the field of study of the electrical discharge in gases, with the clear recognition of the nature of the elementary charged particles, especially the electron, as well as the concept of positive and negative ions. J.S. Townsend became the acknowledged leader in discharge research of his time. He and his students dominated the field for a generation, amassing an impressive volume of data, coefficients, and parameters to characterise the "passage of electricity through gases". The knowledge of the electrical discharge in gases considerably advanced during this time to the point where experimentation could not be improved with the equipment of the time.

With the great classification of atomic theory together with the remarkable improvements in laboratory techniques through the use of Pyrex glass, better pumps, induction furnaces, electron tubes, and oscillographs, the mid-twentieth century accelerated many types of discharge tubes and plasma research. Engineers introduced these phenomena into everyday life in the form of domestic fluorescent light and neon signs. In the last decade, interest in this field has rapidly increased because of increased activity in atmospheric research and plasma physics.

1.1.2- Electrical discharges

Electrical discharges are transitions of charges through a gas, generating light by radiative decomposition of excited states [Hirsh]. Today intense UV radiations from medium and high pressure glow discharge xenon and mercury/rare gases lamps are generated by the application of a high electric field between two electrodes. In such a way, low wavelengths can be obtained from low pressure rare gas resonance line sources, e.g., the argon line at 106nm [Patel-1990], the Krypton line at 124nm and the Xenon line at 147nm.

However these glow discharges are only accessible at low pressures, which implies that few light-generating excited species exist, and furthermore low pressure often shows self absorption of the emitted light (see details in § 1.2.2). Only low efficiency photon fluxes will therefore be obtained with such devices. For higher fluxes, the gas pressure has to be increased and the type of the discharge changes from glow discharge to arc discharge. For arc discharges, the light generation is caused by a charge transition between the electrodes. Increasing the electric field between two plates to a critical field or breakdown voltage results in the appearance of an arc. The breakdown voltage is directly correlated with the dielectric strength of the gas mixture and is therefore lower for rare gases and it increases with the pressure.

The breakdown is reached when the induced field in the gap exceeds the corresponding Paschen field. This is obtained by dividing the Paschen voltage of the gas by the product *nd,* concentration per electrode gap spacing (figure 2.1).

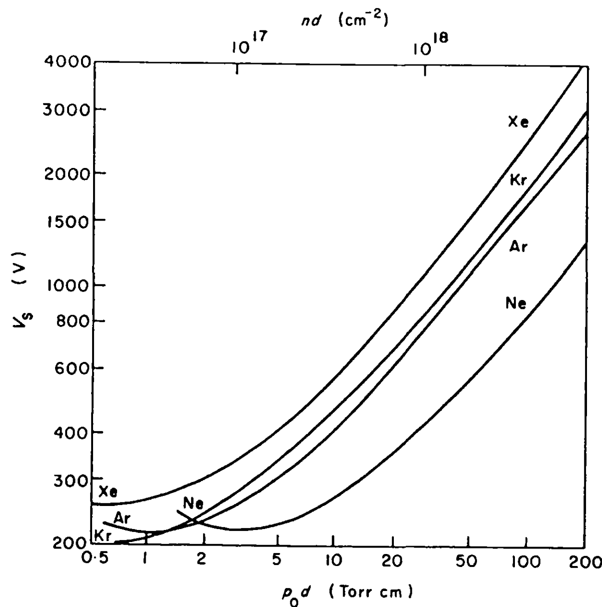

Figure 2.1 : Paschen breakdown voltages for rare gases [Meek]

The discharge is a filament within which electrons and ions can migrate from one electrode to the other, in a single channel of excited states. However, when an arc appears in the gap separating the electrodes, the local dielectric strength drops. The arc is thus self-sustained and a very high current passes through the discharge. Heavy bombardment of the electrodes with excited species during an arc discharge results in their gradual erosion. High pressure discharges have therefore to be modified in order to obtain continuous generation of the excited species. These two major problems associated with conventional arc discharges of self-sustaining and electrode eroding tend to limit large scale applications of this mode of photon generation.

1.2- The silent discharge or dielectric barrier discharge

1.2.1- The electrode problem

To prevent the etching of the electrodes during discharge, it is essential to limit the amount of charge and energy that can be fed into the arc. One simple way is to cover the electrodes with a dielectric material (Fig 2.2).

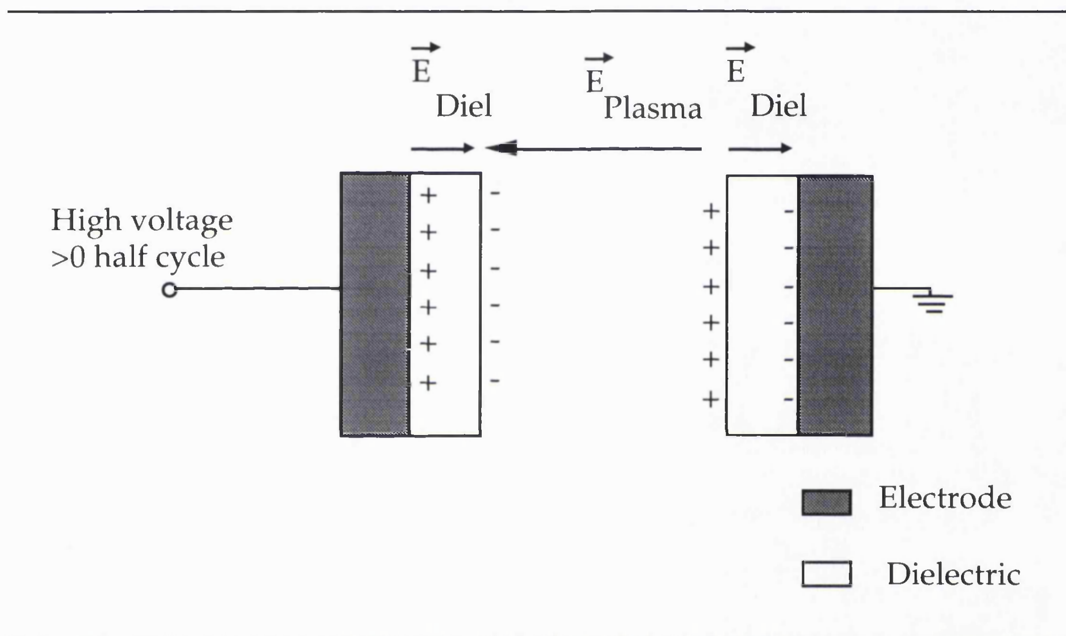

Figure 2.2 : Dielectric barrier discharge structure

Increasing the voltage on one electrode results in an increase in the charge build up on the inner surfaces of the dielectric and hence a rise in both E_{diel} values. When the breakdown voltage in the gap between the electrodes is reached by E_{plasma}, the arc appears causing the dielectric surfaces to discharge. Thus both E_{diel} and E_{plasma} values drop, thereby extinguishing the arc. In high pressure plasmas, covering the electrodes with a dielectric material solves both problems of electrode etching and self sustaining of the arc. When alternate voltages are used, such phenomena occur on each half cycle, resulting in a larger number of arcs per second and hence a higher optical efficiency. Consequently, very high frequency input signals (typically a few

hundreds of kHz) result in high efficiencies. Also, because of the partition of the charge on the total surface of the dielectric during the fast voltage rise, there is no possible equilibrium of the charge over the dielectric surface, hence many breakdown voltages can be reached simultaneously on various randomly distributed points, resulting in numerous microdischarges appearing on the same high frequency alternance (cf figure 2.3). Due to the fast rising voltages involved, long time delays are observed before breakdown, thus corresponding to an effective voltage higher ($\approx$ 50%) than the actual Paschen field for stationary breakdown [Kogelschatz-1990]. These modifications allow much greater UV power to be generated than is obtained from a high pressure arc discharge and therefore explain the higher efficiency of the dielectric barrier discharge.

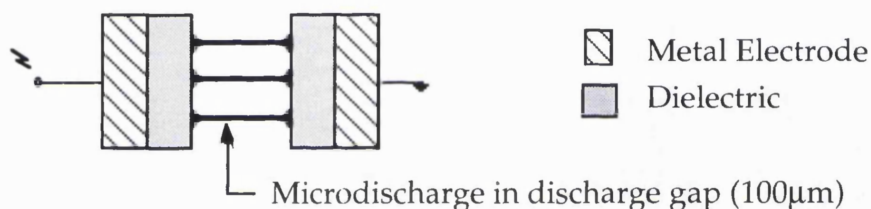

Figure 2.3 : Surface repartition of the dielectric barrier discharge at high frequency

Figure 2.4 shows the oscillogram of the electrical signal generated by a high frequency photodiode when exposed to the UV radiation. The top signal is the input high voltage fed to the lamp (x500 probe), oscillating at 300kHz. It appears that the frequency of the photodiode output is twice as high as that of the input signal, since the lamp discharges occur on each monoalternance of the AC voltage. The diode output signal is recorded as its summation over 40 scans, coadded and smoothed, and thus has excellent uniformity. Its dissymmetry is caused by the geometrical dissymmetry of both the lamp and the sensor, as the light is observed through one cylindrical electrode.

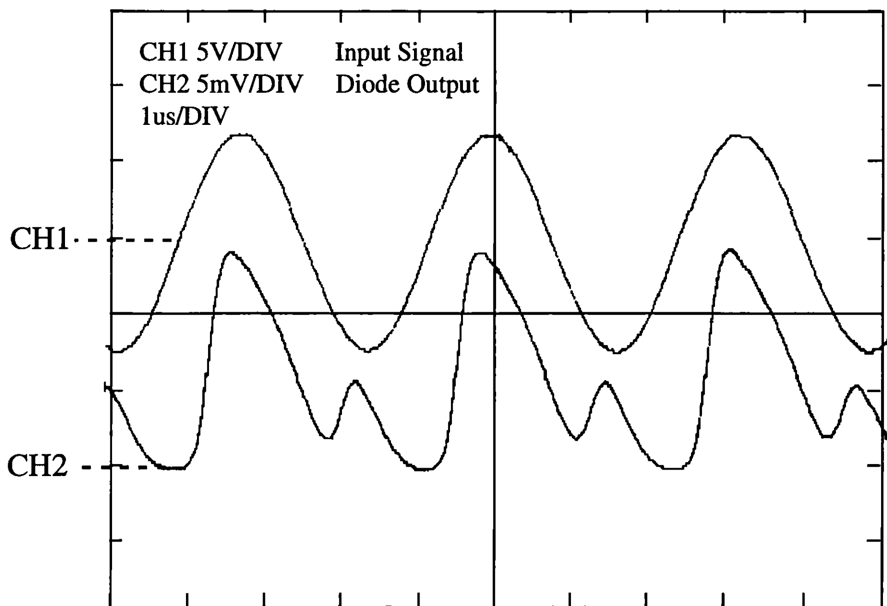

Figure 2.4 : Oscillogram of feeding voltage (upper trace), and photodiode output (λ=172nm).

1.2.2- The pressure effect

It has previously been mentioned that arc discharges, in contrast to glow discharges, are obtained in a high pressure plasma. In fact, glow discharges occur in a few torr and arc discharges above 50 to 100 torr. By increasing the pressure (and obviously the number of species) we can therefore modify the nature of the discharge. This increase of pressure changes the wavelength generated from resonance lines to higher continua. In the cases of pure or pure mixtures of gases, we can clearly observe this modification of the spectrum. This effect is illustrated in figure 2.5 for the case of xenon. This is due to the fact that at higher pressures, the probability of having direct recombination of an ionised molecule can be lower for certain gases than the competing reaction with the ground state. This is the case when excimer formation occurs, as will be explained in the next section.

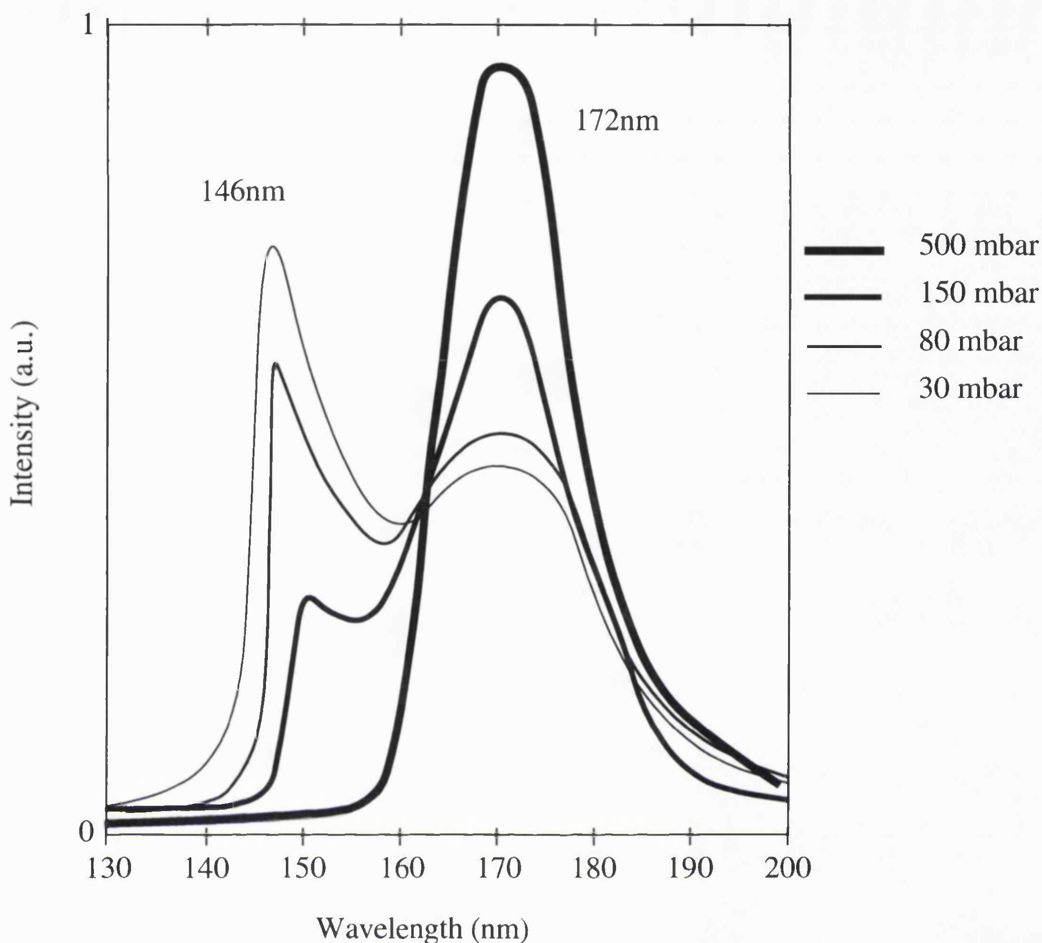

Figure 2.5: Pressure dependance in a xenon dielectric barrier discharge (the spectra have been re-drawn from scanned records). (Spectra obtained with the light source presented in § 3.3.1, figure 2.20).

1.2.3- The excimer formation

This phenomenon was first explained by Förster and Kasper in terms of the formation of a complex containing two pyrene molecules [Förster]. The complex has been given the name "excimer" since it is a d*imer*, which is stable in an electronically *exc*ited state [Gilbert]. The existence of excimer generation stands in the absence of an electronically stable ground state.

Excimer formation can be represented by

$$M^*+M \longrightarrow MM^* \qquad (2.1)$$

where M is a ground state, M^* an excited state, and MM^* the corresponding dimer.

To explain this process, reference is made to the following simplified energy diagram (figure 2.6).

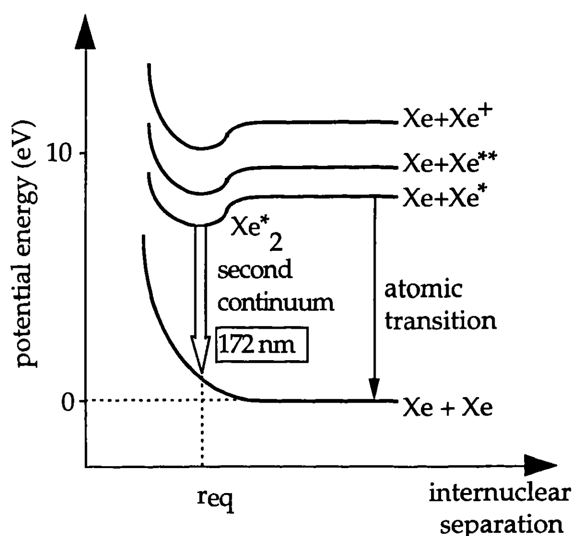

Figure 2.6 : Simplified band diagram for excimer generation

At low pressure, and hence at high intermolecular separation, if an M state is excited to an M^* level, this state can generate light by radiative recombination. Due to the flat shape of the bands, all photons emitted have the same energy, thus the corresponding emission spectrum is narrow (line). Also, the light generated can easily excite another M ground state to an M^* level, hence there will be self absorption of the emitted radiation. This contributes to limit the efficiency of low pressure discharges.

Another scenario that can be examined by reference to figure 2.6 is the case when two ground state molecules (level M) are brought closer together. These molecules feel no mutual attraction. In fact, at higher pressures (i.e., for small intermolecular separation), a mutual repulsion is experienced by these ground states. In contrast, if one of the M-states is provided with electronic excitation, the upper curve displays considerable attraction as the M and M* species are brought together. The result is the formation of a bound complex MM*. The binding energy of a typical excimer is substantially less than that of a typical diatomic molecule. Also, the absence of a bound ground state means that dissociation of the complex may lead to light emission.

$$(MM^*) \longrightarrow M + M + h\nu \qquad (2.2)$$

The vibrationless level of the bound excimer has an energy substantially below that of the separated components M*+M (the difference is the binding energy). Thus, emission of light from MM* involves a transition of a lower repulsive potential energy surface, with a smaller energy difference compared to that for emission from the M* monomer. Therefore, the emission will always involve the release of a photon of lower frequency (higher wavelength) compared to the monomer emission, thus explaining the shifted emission of xenon observed in figure 2.5. Also, the emitted radiation shows a substantial range of energies, explaining the broad continuum observed.

When further excitation is provided to the ground state monomer, the excited state is able to return to the ground state through numerous steps including monomer and dimer levels as detailed in figure 2.7. Such a form of molecular band structure characterises the existence of an excimer.

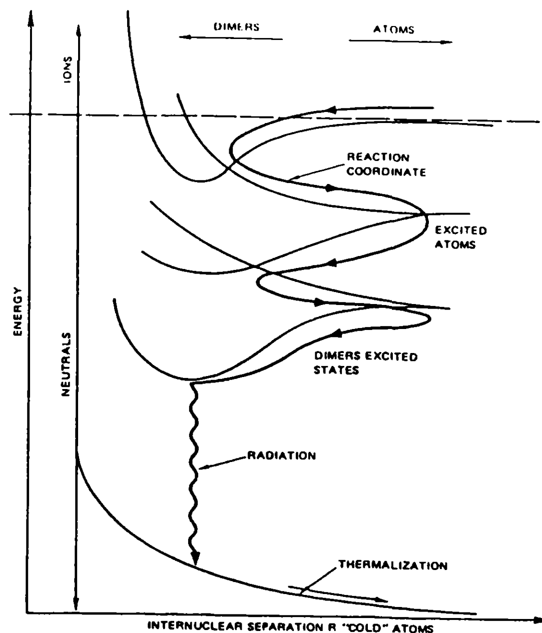

Figure 2.7: Dimer chemical pathway [Rhodes]

1.2.4- Excimer formation in dielectric barrier discharges

The principle of excimer lamp operation relies on the radiative dissociation of excimer states created by a dielectric barrier discharge. Therefore, if we build a device enabling excited state creation in high pressure plasma, the transition of charges between the two dielectric covered electrodes results in a number of randomly distributed filaments of excimer states. Each channel corresponds to a single transit, or streamer, breakdown. The microdischarge filaments are of submicrosecond duration and submillimeter radial extension [Eliason-1987]. We can discern three separate steps during the life cycle of such a filament: (*i*) the formation of the discharge from the electrical breakdown (within nanoseconds), (*ii*) the ensuing current pulse or transport of charges across the gap (1-100ns) and (*iii*) simultaneously the excitation of the atoms and molecules present and thus initiation of the reaction kinetics (from nanoseconds to seconds). Properties of a typical microdischarge are outlined in table 2.1.

Total Charge	10^{-10} A s
Current density	10^{3} A cm^{-2}
Electron density	10^{14} cm^{-3}
Electron energy	> 5 eV

Table 2.1 : Properties of the microdischarge

B. Eliasson and U. Kogelschatz have developed a theoretical model presenting the discharge physics and the plasma chemistry involved with time, input voltages, and gap spacing for various gases [Eliason-1991]. The overall theoretical efficiency of dielectric barrier discharge lamps can reach 40%. Experimental values of 10% have been obtained, losses are generally caused by the absorption from the window material, by geometrical losses, and by temperature increase. In fact, the high current density, passing through the gas when the discharge occurs, has a detrimental effect of heating the plasma. This increase of temperature reduces the amount of energy that electrons can provide to excite the ground state molecules and therefore results in a loss of efficiency. When high powers are required, it is essential to cool the lamp devices, generally by flowing water through the electrodes.

1.3- Application to rare gas molecules

1.3.1- Pure rare gas excimers

In 1955, Tanaka intensively studied the continuous emission spectra of rare gases [Tanaka]. In figure 2.8 is presented the inter-molecular energy curves for Xenon [Haaks]. We can observe the potential wells for the first and the second continua. The intense second continuum corresponds to a transition from the lowest vibrational level of the two lowest lying bound electronic excimer levels to the repulsive ground state.

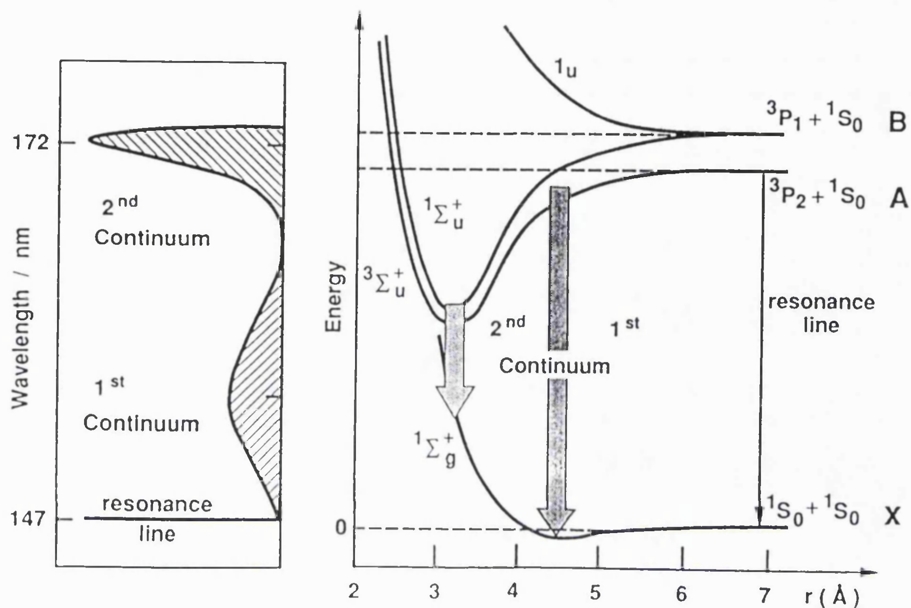

Figure 2.8 : Potential energy diagram of xenon and corresponding emission [Gellert]

Because of the experimental difficulties in measuring spectra below 120nm and the necessity for high pressure discharges to use transparent window materials, the emissions below 120nm will not be investigated in this thesis, and in particular the cases of helium and neon excimer radiations. The case of xenon is described, although a similar mechanism applies to the other rare gases. Kinetic models for rare gases pumping mechanisms have been presented by D.J. Eckstrom *et al.* [Eckstrom]. Figure 2.9 shows such simplified mechanism for xenon. Although we do not wish to discuss it in details within the framework of this thesis, a similar treatment has been proposed by Bergonzo *et al.* for the case of argon. The resulting publication can be found submitted in Appendix 5 [Bergonzo].

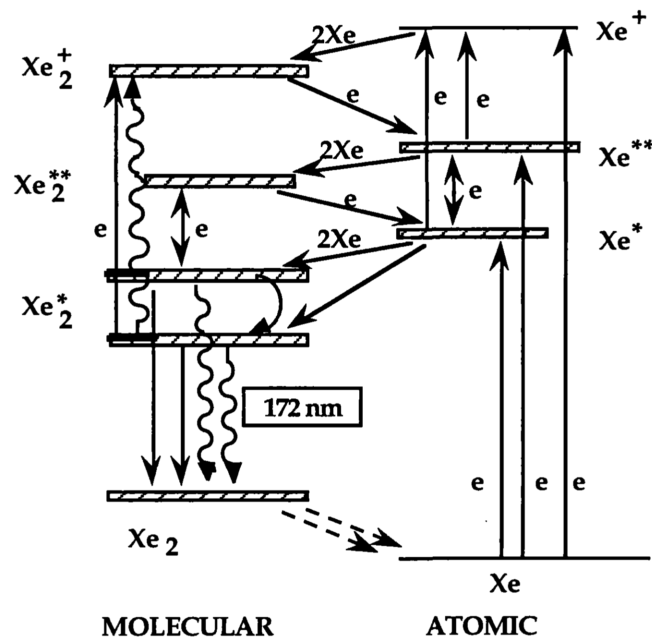

Figure 2.9 : Pumping mechanism in xenon (adapted from Rhodes)

Energetic electrons present in microdischarges excite and ionise the Xenon

$$e^- + Xe \rightarrow Xe^+ + 2e^- \qquad (2.3)$$

$$e^- + Xe \rightarrow Xe^* + e^- \qquad (2.4)$$

At high pressures (>50mbar), the formation of molecular ions becomes very efficient. This then leads to the formation of excited neutrals:

$$Xe^+ + 2Xe \rightarrow Xe_2^+ + Xe \qquad (2.5)$$

$$Xe_2^+ + e^- \rightarrow Xe + Xe \qquad (2.6)$$

Three body reactions can then lead to the formation of bound molecular levels:

$$Xe^{**} + 2Xe \rightarrow Xe_2^* + Xe \qquad (2.7)$$

When the Xe_2^{**} dissociates into 2 Xe atoms, it radiates a photon at 172nm

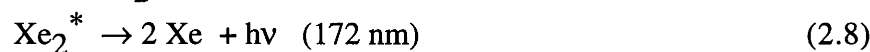

$$Xe_2^* \rightarrow 2\,Xe + h\nu \quad (172\ \text{nm}) \qquad (2.8)$$

Rare gas excimer continua radiate at 126nm, 146nm and 172nm for argon, krypton and xenon respectively (Fig. 2.10).

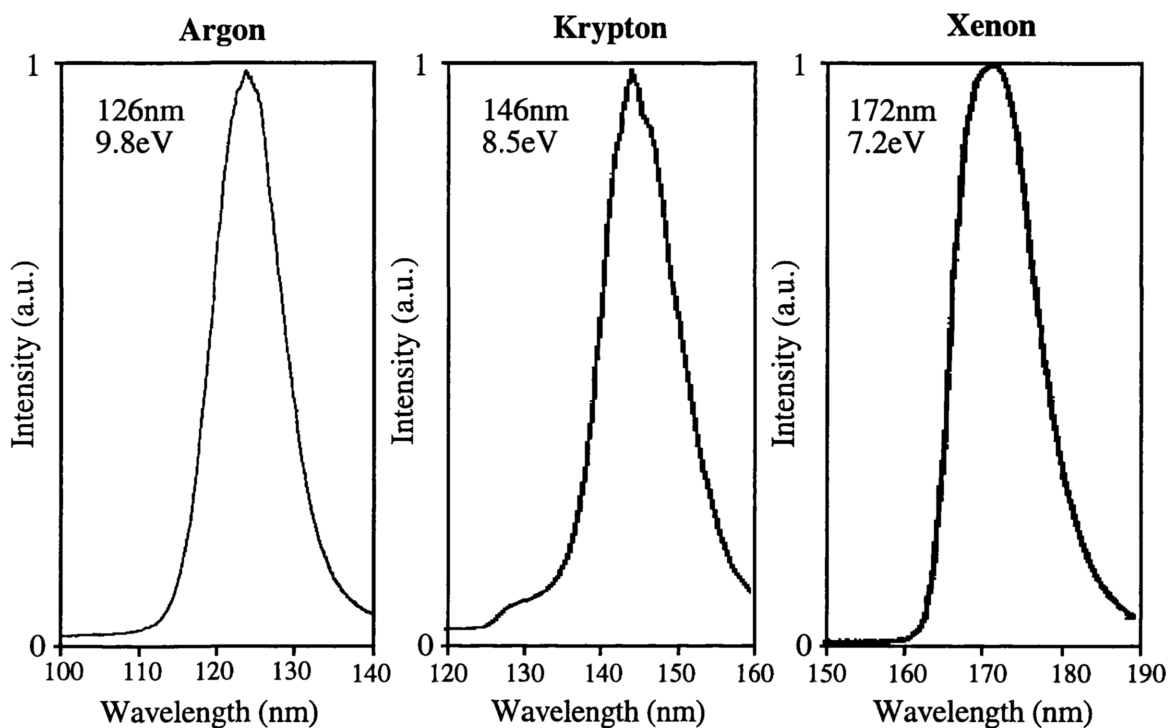

Figure 2.10 : Spectra measurements for Ar, Kr and Xe gases

1.3.2- Halogen dimers and rare gases/halogen exciplexes

Numerous excimers can be generated from dielectric barrier discharges. Halogen and rare gas mixture excimers are commonly used in excimer lasers, and these require less pumping energy than pure rare gases. However, as they emit in lower energy ranges, they are less of interest for direct photo-CVD. The principle of rare gas-halogen excimers is similar to that of the rare gases presented before. It involves the creation of $(RgH)^*$ states, which generate light by radiative dissociation. As such, the large number of excimers which can be generated in dielectric barrier discharges extends their emission bands from the VUV to the visible part of the spectrum (fig. 2.11).

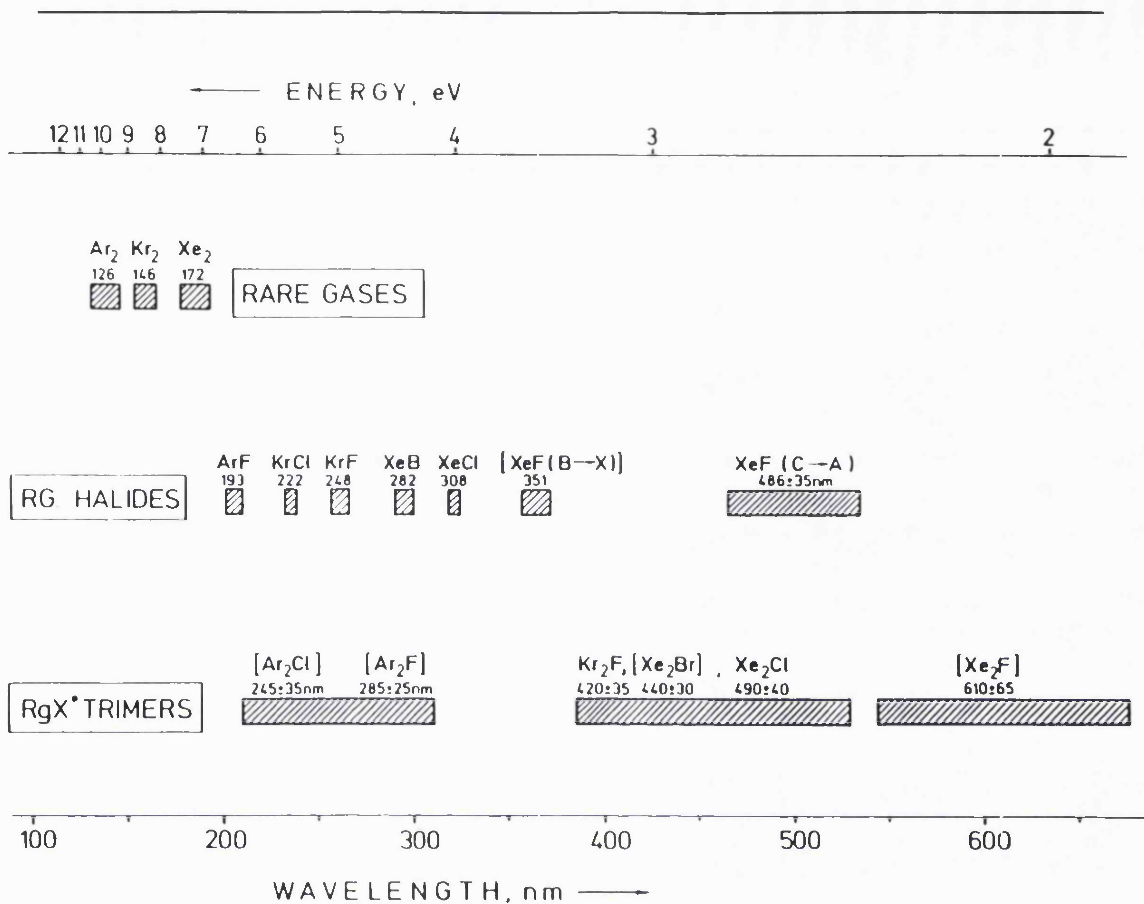

Figure 2.11 : Excimer emission bands [Rhodes]

2.- Excimer lamps ($\lambda \geq 160nm$)

2.1- Construction of excimer lamps

The kinetics of dielectric barrier discharges have been presented. To construct a device for UV light generation based on this principle, one requires two electrodes covered with a dielectric and a gas cell at a pressure of a few hundred torr. The purity of the gas is the most important parameter in order to avoid the generation of lower energy radiation from contaminants. Therefore, the gas has to be enclosed in a very clean chamber made of material which does not degas even when heated up to high temperatures. In this respect, quartz or similar compounds are ideal. An added advantage is that various shapes can be developed using these materials. Figure 2.12 presents 2 possible geometries: cylindrical and planar.

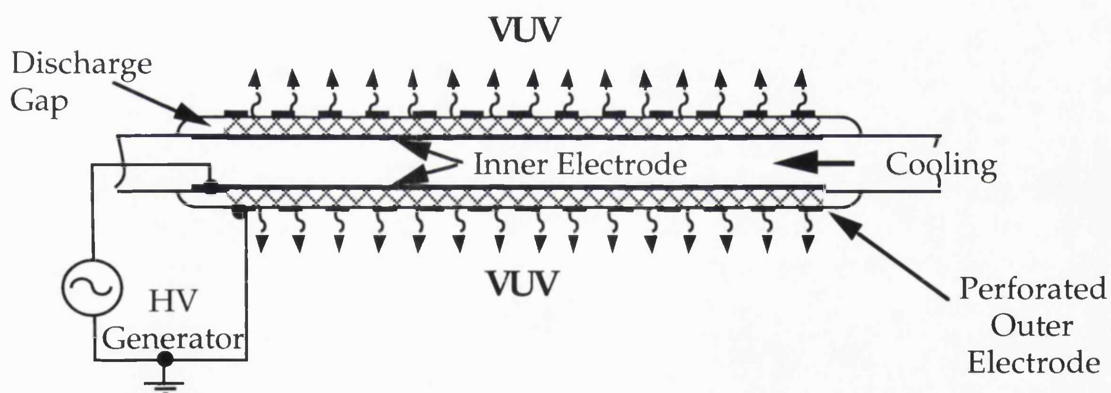

Figure 2.12 : (a) an example of cylindrical gas cell for excimer lamp

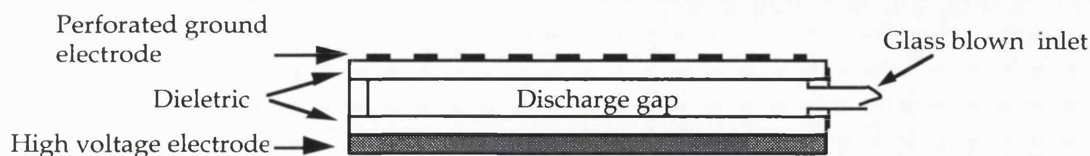

Figure 2.12 : (b) An example of planar gas cell for excimer lamps

The glass cells are pumped down to 10^{-6} torr, filled with the required gas or gas mixture, and then sealed. This technique eliminates concern about long term gas purity over long periods of use (over 500 hours for pure rare gases). With these devices, the radiation is generated inside the discharge volume and is transmitted through one of the dielectric material also acting as a window. The wavelengths produced are therefore limited by the cut-off frequency of the dielectric material. Also glass working requirements implying the use of non crystalline materials, this arrangement cannot be used for wavelengths shorter than 160nm, the transmission cut-off of the Suprasil fused quartz (table 1.3).

Various lamp prototypes using the cylindrical set-up presented in figure 2.12 (a) have been developed during this project. This configuration was in fact the most convenient for us and especially for our glass blowing workshop. The dimensions are 30cm in length, 30mm in outer diameter for the outer tube, and 16 to 20 mm diameter for the inner tube. Some of the results presented in chapter 3, section 2, regarding MOD experiments, are obtained from such a cylindrical krypton chloride (222nm) lamp used to irradiate various organometallic coatings. Two xenon chloride (308nm) lamps were also developed during this project for a parallel project interested in the direct photodissociation of fluorine which shows a strong absorption cross section around 300nm. However, most of these rare gas/halogen devices were developed in order to obtain a database on these systems, since our knowledge in the optimised ratios and pressures is currently limited. Also, it has been suggested that the halogen element used as the excimer precursor may progressively react with the outer tube material, ensuring the formation of opaque to the radiation crystal defects,

and therefore strongly limiting the life time of those devices. A few pictures of such a XeCl lamp are shown on figure 2.13 as well as the related spectrum.

For semiconducting or dielectric material deposition from direct photo-CVD, wavelengths below 200nm are required (§1.3.2). One can then use a cylindrical lamp set-up to generate 172nm photons from dielectric barrier discharges in xenon with a cell made of Suprasil. Films of silicon dielectric materials have been deposited during this project with such a device. Results are presented in chapter 4 and 5. These results are the first application of these lamps to dielectric material processing. Good quality films were obtained, such a photo-enhanced process can then compete with similar processes using the low pressure mercury lamp [Petitjean].

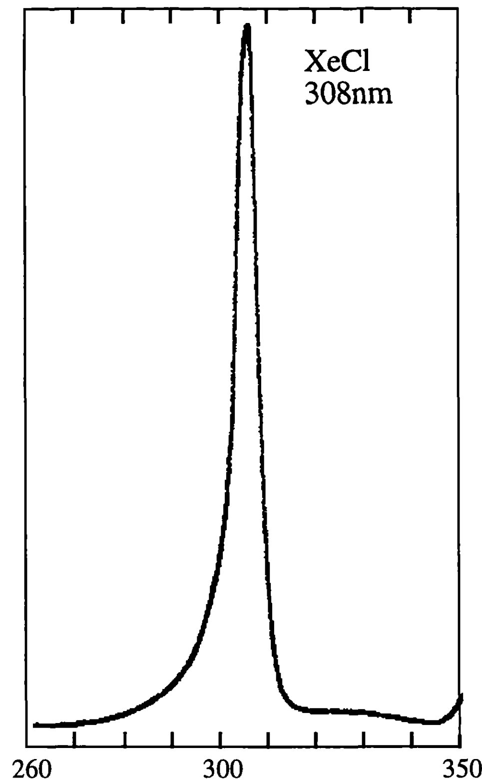

Figure 2.13 : Excimer continuum of a xenon chloride mixture

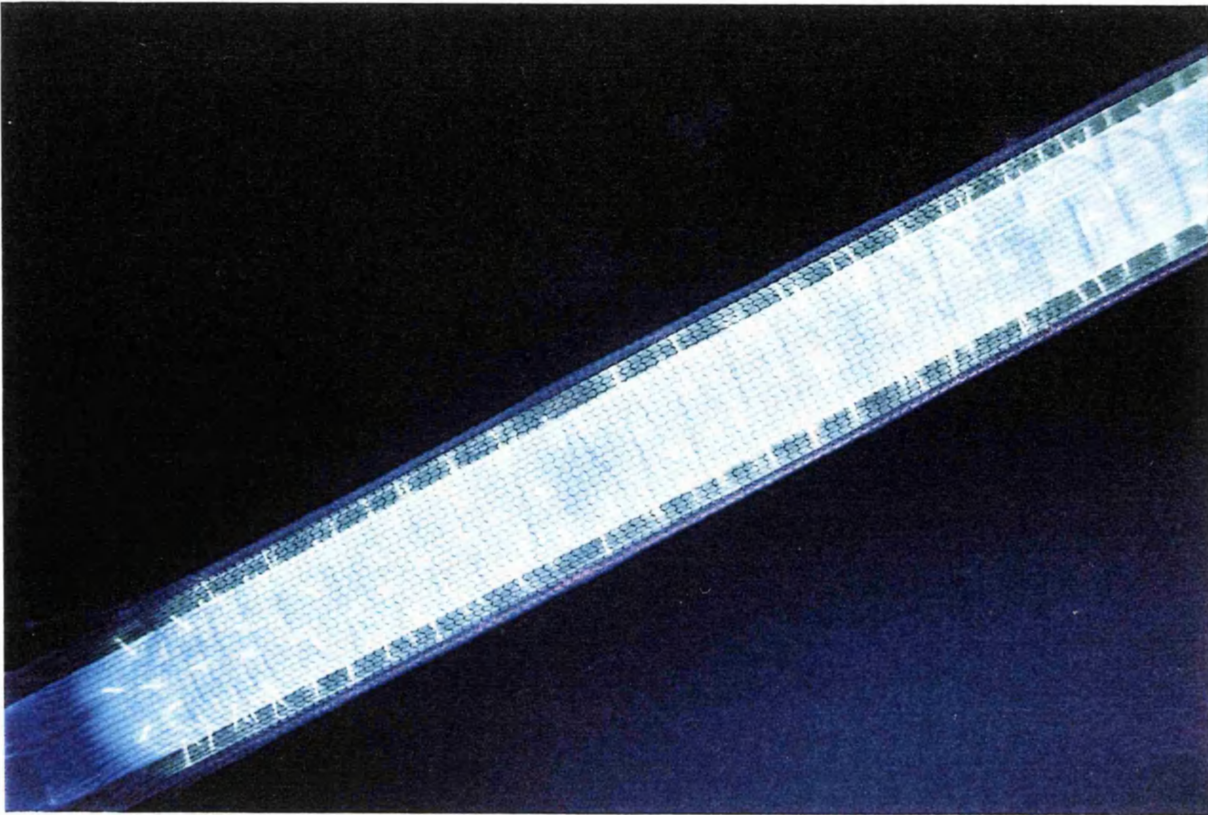

Picture of a ø30mm-30cm Xe excimer lamp

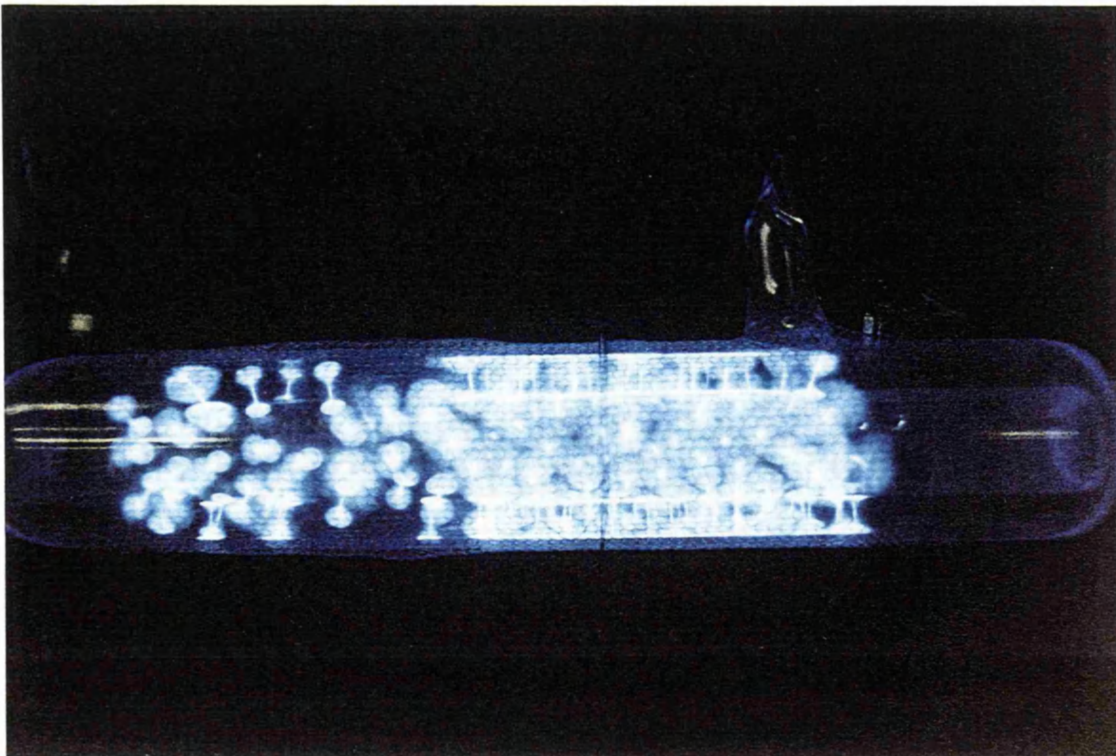

Pictures of a ø30mm-15cm XeCl excimer lamp

2.2- Power measurements

2.2.1- Electrical methods

The difficulties in handling very short wavelengths make the use of commercially available detectors very difficult. It is so far either impossible or extremely expensive to buy calibrated devices capable of measuring the VUV radiation. Common detectors as UV diodes or photo-multipliers will not respond to the emitted radiation without special expensive attentions for the window material used and the coupling of the sensor to the light source (under vacuum). One easier way is to use the fluorescent properties of some materials to *convert* the VUV energy to higher ranges of the spectrum where measurements can be performed with common light detectors.

The use of sodium salicylate is well documented for VUV measurements [Déjardin]. The relative quantum efficiency is showed to be constant from 100nm to 330nm [Watanabe]. The fluorescence occurs around 430nm, which allows the use of common photodiodes (fig. 2.14).

Following a design a presented by Robertson, such a VUV sensor based on the fluorescence properties of sodium salicylate has been developed [Robertson]. Sodium salicylate is readily soluble in methanol, and may then be sprayed or spin coated on any 430nm transparent material (or even on the detector surface). The solution may conveniently be sprayed with a scent atomiser directly towards the surface maintained at a temperature around 80°C on a hot plate. The ultra-violet to visible light conversion efficiency of the phosphor layer is close to unity for a Film of 2 to 4 mg/cm^2 [Allison][Samson]; which may be produced by multilayer applications until the surface has the appearance of quality white paper. Using an optical band pass filter centred around 430nm, it is possible to eliminate the influence of stray light. Figure 2.15 shows a schematic of the device. This set-up can be calibrated either using any other calibrated light source (e.g., a low pressure Hg lamp), or by considering the absolute conversion efficiency of the fluorescent film.

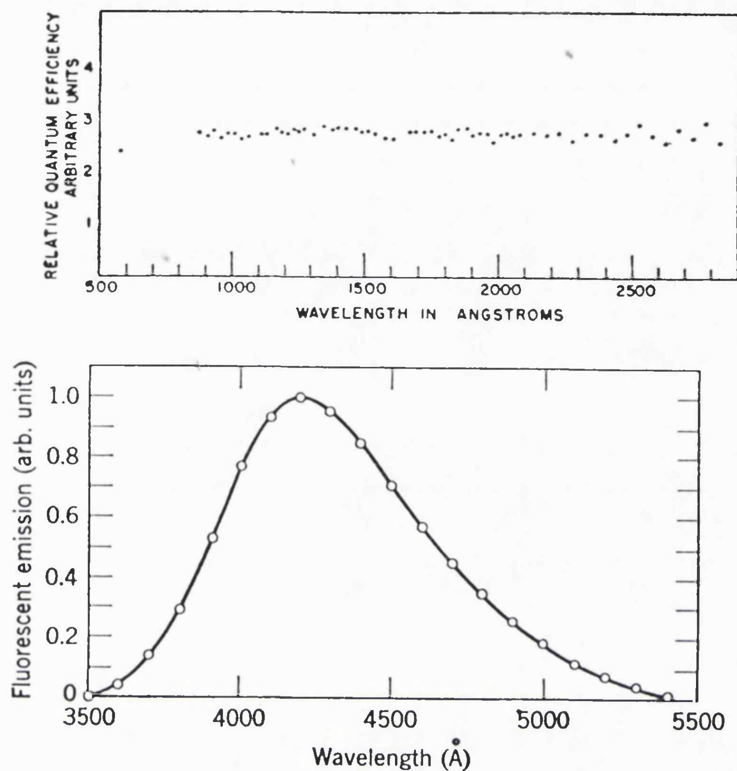

Figure 2.14 : Spectral response (top) [Watanabe] and fluorescence (bottom) [Thurnau] of sodium salicylate

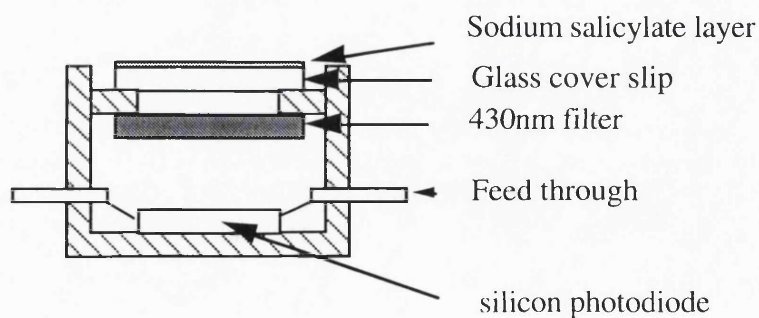

Figure 2.15: Relative emission intensity sensor

Such a sensor has been developed at UCL, but problems associated with its calibration limited its use to relative measurements. One of the problems is that the sodium salicylate film conversion efficiency decays with time, from around 1 to 0.65 within a few days. Films should therefore be renewed and re-calibrated for each set of measurement. This sensor was only used to obtain rough ideas of the light energies generated.

2.2.2- Chemical actinometric measurements

When a gas is irradiated by high energy photons, it may react leading to the formation of other products for which the analysis is simple and precise. Several systems have been studied and literature data provides accurate quantum yields over wide ranges of wavelengths of the absorbed light (e.g., [Calvert]). Such a method utilising oxygen has been used. When oxygen is submitted to UV radiation (λ<240nm), ozone (O_3) is formed. From the amount of ozone generated, the efficiency of the source can be estimated. This system was used to calculate the overall efficiency and power output of a 172nm xenon lamp as shown in figure 2.12(a).

2.2.2.1- Ozone generation

Ozone is essentially a colourless gas with a characteristic pungent odour. It is one of the strongest oxidants available. It has a particularly strong smell detectable at about 0.1ppm in air, and is toxic at concentrations above 1ppm. In fact, historically, the first use for the dielectric barrier discharge generation was for the direct excitation of oxygen molecules in the microdischarge leading to the formation of ozone [Kogelschatz-1988]. Today, many water purification plants in the world use such a technique. The ozone is bubbled through water for purification (removal of taste, colour, odour, decomplexing organically bound heavy metals such as manganese, iron and destruction of inorganic substances). With a short lifetime in air, ozone shows better environmental qualities than other oxidants where transport, storage, and decay products are concerned. The section 1 in chapter 3 will present experiments on the generation of ozone in a mechanism based on its photo-generation, using a similar principle to the one described for the present experiments.

2.2.2.2- Theory of VUV enhanced generation of ozone

Under the influence of photons, oxygen is dissociated via the reaction (2.9) [Baulch] (fig. 2.16):

$$O_2 + h\nu \rightarrow O + O \qquad (2.9)$$

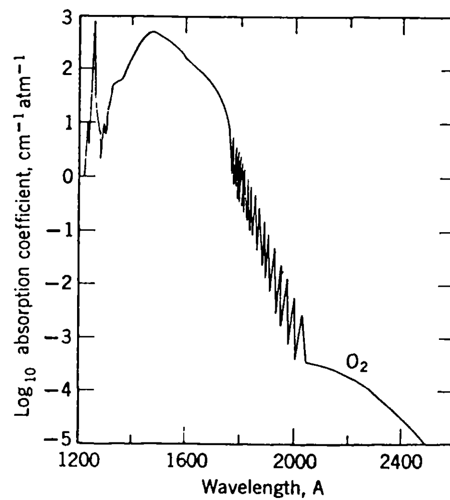

Figure 2.16 : oxygen absorption cross section

The ozone molecule is formed by the three body reaction of oxygen atoms with O_2, through an initially excited O_3^* state [Eliason-1989]

$$O + O_2 + O_2 \rightarrow O_3^* + O_2 \qquad (3.2)$$

Being exposed to the UV radiation, the ozone molecule will also be dissociated:

$$O_3 + h\nu \rightarrow O + O_2 \qquad (3.3)$$

Eliasson *et al.* developed a model of ozone generation under VUV irradiation, based on the assumption that the particle species are distributed homogeneously with the volume of the reaction chamber [Eliason-1990]. They concluded that the resulting concentration corresponds exactly to the formation of two O_3 molecules per incident VUV photon. The suggested quantum yield in this model is therefore equal to 2.

A quantitative method has been used to characterise the amount of ozone generated. The ozone gas is bubbled through a potassium iodide buffered solution (pH=7) (Figure 2.17) [Maier] :

$$O_3 + 2KI + H_2O \rightarrow I_2 + O_2 + 2KOH \qquad (3.4)$$

The released iodine is titrated with sodium thiosulfate after acidifying with diluted sulfuric acid, resulting in the disappearance of the colour of the solution:

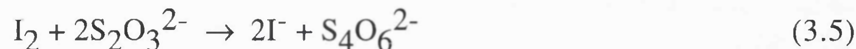

$$I_2 + 2S_2O_3^{2-} \rightarrow 2I^- + S_4O_6^{2-} \qquad (3.5)$$

From the amount of sodium thiosulfate used, calculations lead to the amount of ozone produced, from which efficiencies in term of photons and input power are deduced.

2.2.2.3- Experimental setup

The oxygen-ozone mixture generated is bubbled through a series of three different condensers. The first is empty, to avoid any possible suction of the KI solution back into the system. The second and third bubblers contain the KI solution. The third one allows constant check-up that the solution in the second bubbler is not saturated.

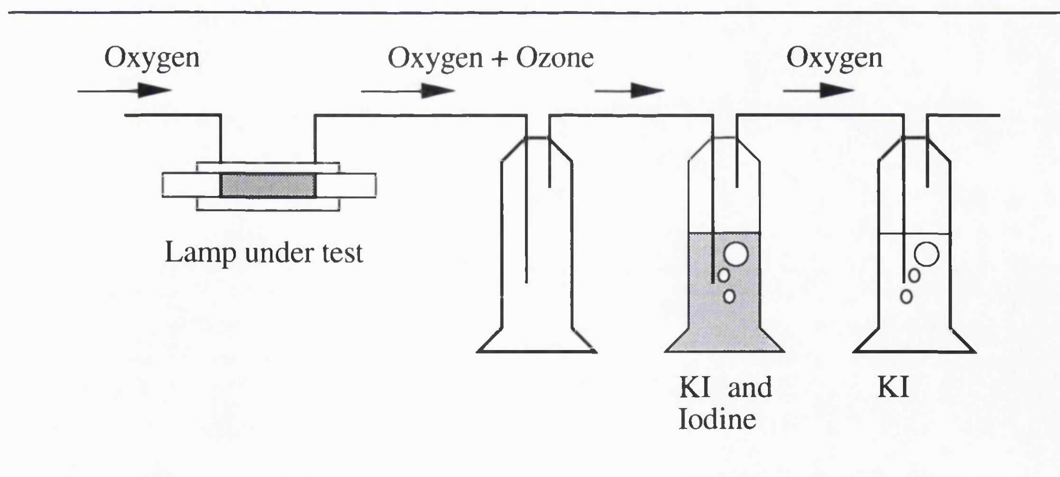

Figure 2.17 : Experimental set-up for ozone detection

The molecular absorption of oxygen at 172nm is about 10 $cm^{-1}atm^{-1}$ (fig. 2.16). Therefore, at 760torr of oxygen pressure, the absorption length of the emitted radiation is about only 1mm. A xenon excimer lamp is used, with 30mm external diameter, surrounded by a metal tube of 50mm inner diameter and a length of 16cm, allowing a radial depth of 10mm, which guarantees complete absorption of the 172nm radiation (Figure 3.5). The solution used was a potassium iodide (2%) with a N/10 sodium thiosulphate starch solution.

2.2.2.4- Results

From the titre obtained, the amount of ozone which has been bubbled through the solution can be calculated. After 4 minute experiments, the measurements gave values ranging around 65mg of ozone generated. The quantum yield of generation of ozone at 172nm being equal to 2, the mass of ozone obtained corresponds to 4.2 10^{20} quanta used in the reaction.

Also, assuming each photon emitted to be at the centred wavelength of 172nm (i.e., 7.22eV, or 1.16 10^{-18}J), it gives a total radiated energy from the lamp of 485 Joules, thus a power of 2W, or about 40mW/cm^2. This power was obtained with an input power of 50W, corresponding to an overall conversion efficiency of 4%. Since the measurement was made using an unoptimised ozone generator, it is assumed that some of the ozone generated molecules have been dissociated before being counted. The power obtained can therefore be considered as a lower limit, these measurements are then very promising; such a power of 40mW/cm^2 at 172nm being already comparable with those of powerful low pressure mercury lamps. Generally, the lamp input power hardly exceeded 30W (corresponding to 20mW output power) for deposition experiments.

3.- VUV excimer lamps

3.1- Introduction

For shorter wavelength generation, the cell has to be constructed from crystalline materials as detailed in §1.2.5. Due to the expensive nature of these materials and the difficulties involved with crystalline material glass work, one cheap and convenient solution is to use UHV chambers with crystalline view ports made of LiF or MgF_2. The light generated inside the cell volume is emitted through the view port to any attached deposition chamber. A few groups have also preferred this configuration for wavelengths above the cut-off of suprasil quartz and in particular for the xenon continuum generation (172nm) [Kessler][Manfredotti].

3.2- Initial VUV excimer lamp design

The key requirement for such a system is to allow radiations down to the argon continuum (126nm). Initial designs therefore comprised a light source inside a vacuum chamber from which the light was emitted through a crystalline viewport. The lamp possessed an interlocking cylindrical multi-electrode geometry (figure 2.18) [Patel-1991]. This planar light source allowed VUV generation in a multiple discharge gap. The chamber configuration is presented in figure 2.19.

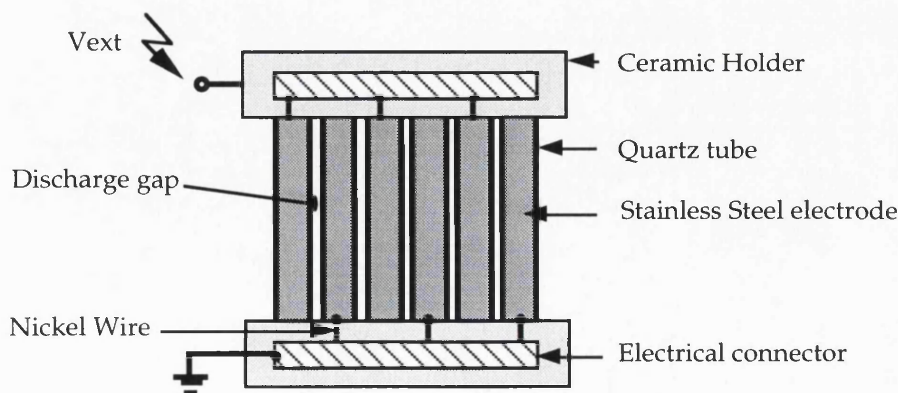

Figure 2.18 : Interlocking cylindrical multi-electrode geometry set-up

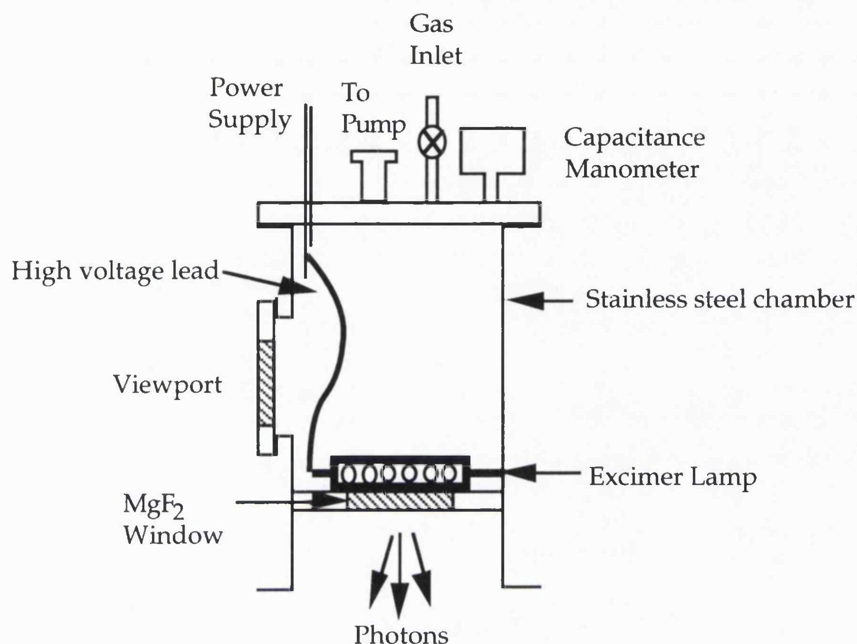

Figure 2.19 : Lamp house for the first prototype of excimer lamp at UCL

Radiation as energetic as 126nm (9.8eV) was able to be generated using the Argon excimer continuum with this lamp. However, the available intensity was limited: the power to be supplied (under several kV) had to be brought into the chamber via insulating feedthroughs. High voltages had then to be brought inside the volume containing the discharge. At high power, it is obviously difficult to avoid arc discharges between the high voltage feedthrough lead and any grounded part. This is caused by the fact that dielectric strengths of rare gases (around 10kV/cm [Meek]) are much lower than that of quartz (about 200kV/cm [CRC Handbook]). Even if generating the desired wavelength, these arcs were self-sustained and resulted in the etching of the feedthrough electrodes. Most deposition attempts with this lamp were in vain because of the power limitation. This set-up had to be modified to external energy feeding.

3.3- Improvements

3.3.1- Lamp configuration

To avoid the problem connected with energy feeding from the gas volume, the high voltage is introduced through an atmospheric pressure column feedthrough to the lamp. The lamp is also designed with a multi-cylindrical electrode geometry, and consists of half sealed quartz tubes containing a ground conductive material (iron filings) (figure 2.20). Each tube being assembled through a flange of the lamp chamber, a high voltage lead can be connected from the outside of the gas volume. See also pictures on the next page.

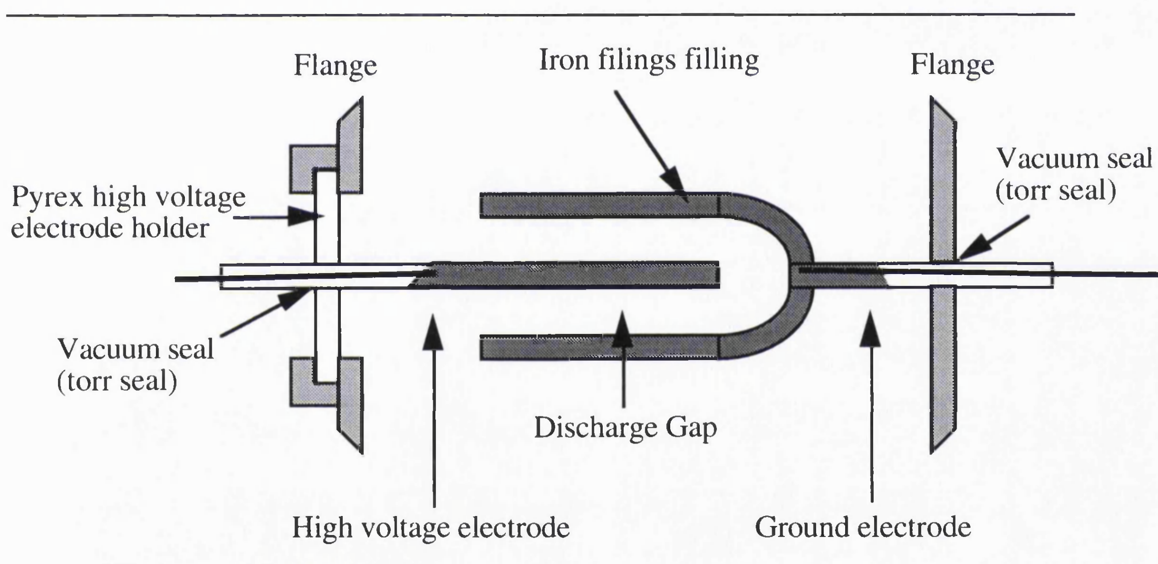

Figure 2.20 : Lamp set-up enabling the generation of radiations of wavelengths shorter below the suprasil wavelength cut-off (160nm)

Spectra of the rare gas continua were obtained for the cases of argon, krypton and xenon (figure 2.10). High pressure second continua of neon (86nm) and helium (73nm) could also be obtained with this lamp, but this implies the absence of a window between lamp and reaction chambers, hence it limits their use to high pressure reactions. The need for high purity of the excimer gas also implies the absence of any other gas plasma. Such a light source can therefore be used for curing or etching, patterning and surface reactions, but are incompatible with photolytic enhancement of gas phase reactions.

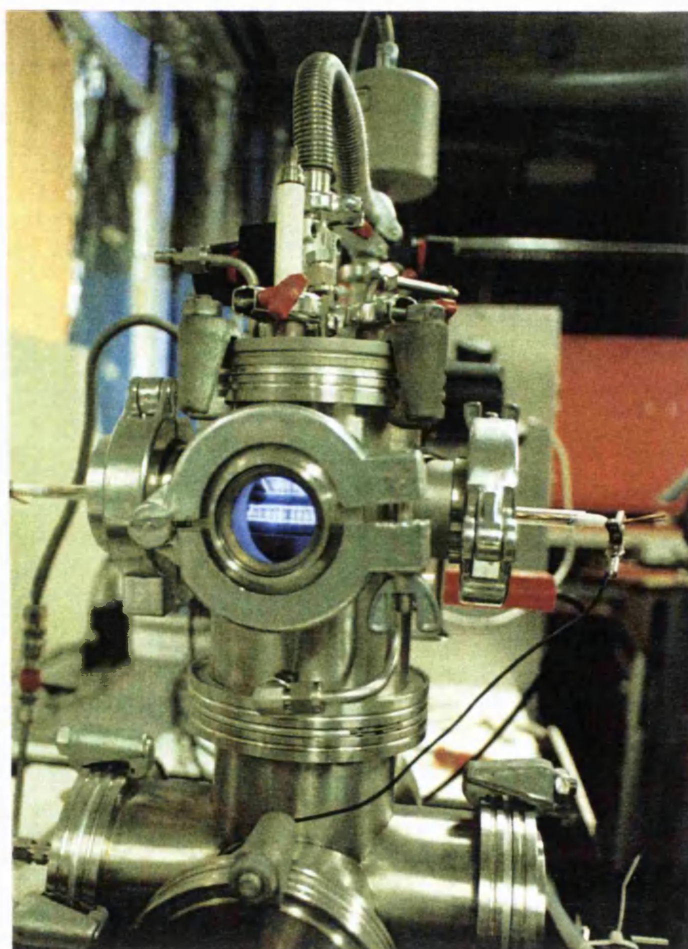

VUV Excimer lamp (top) and system (bottom).
This system allows radiations down to 126nm to be directed to a deposition chamber.

3.3.2- Optimisation for Ar_2^* continuum generation (126nm)

The device presented in figure 2.20 is mounted in a chamber where is introduced argon. The electrical microdischarges generated in the gap separating the three annular electrodes create Ar_2^* excimer species, and their radiative dissociation emits 126nm photons. This radiation correspond to a 9.8eV energy transition between the $^3\Sigma$ and $^1\Sigma$ states of the excimers to their stable ground states. It is clear that the higher the transition, the more it is likely that some impurities present energy levels located between the transient states. As such, the excimer generation of 126nm from a discharge in argon is a lot more exposed to purity problems than that of lower transition excimers (e.g., xenon at 7.2eV). Also, it has been shown that in the case of xenon most of the purity problems could be overcome by completely sealing the discharge gas in a quartz tube. Here, since the gas is directly in contact with the chamber volume, impurities trapped on the walls of the chamber may be released and alter severely the intensity of the spectrum. For instance, at the early stages of the development of this lamp, an unexplained peak at 300-305nm was measured in the spectrum of the lamp output. This peak was persistent with respect to lower background pressures, as well as higher cylinder purity. Eventually, it occurred that it was caused by the presence of a few tens of centimetres of PTFE piping in the argon feeding line, i.e. between the cylinder and the lamp chamber. As argon is know to be extremely non reactive at room temperature, and also since no degasing of the piping materials is likely to happen at high pressures (few atm), this shows well how dramatically an ultra low concentration of impurities can alter the spectrum output of such lamps. Also, unlike for the xenon cylindrical lamp, the development of this device did not consider the possible implementation of water cooling facilities. As a result, not only the photo-emission decreases due to the temperature increase (phonon losses), but also the heat generated by the lamp promotes impurities to degas from the chamber walls and to affect the spectrum output.

To overcome those purity problems, one empirical solution is to allow a permanent flow of the discharge gas to be flown through the discharge volume. With the use of an optimised 1.5l/min flow of argon, no such decrease of the output emission is observed It is to be noted that this flow is relatively high, and therefore the cost of

the gas has to be taken into consideration when further development is to be made. For instance, according to the excessive prices of xenon and krypton, it may be more appropriate to consider the use of a UHV bakeable chamber thus enabling higher gas purity and preventing the need for a flow.

3.3.3- Output power

Although the use of actinometry techniques was preferred for the measure of the xenon lamp intensities, less convenience is offered in the case of argon excimer emissions. In fact, a look at the absorption cross section data for oxygen shows that σ varies from 0.3 to 1000 and down to 1.6 $atm^{-1}cm^{-1}$ at 121, 125, and 127nm respectively [Calvert][Inn][Marr] (as known, oxygen shows very little absorption in the region of the spectrum close to the Lyman line (121.6 nm)). These huge dispersions on σ render quantum efficiency calculations almost impossible for the case of ozone formation. As a result, the present intensity measurements were limited to spectra and photo-detector evaluation, with reference to calibrations obtained with the xenon lamp devices. Using the device presented in § 2.2.1, *in-vacuo*, it comes that the lamp can emit intensities of 30 mW/cm^2 at a narrow range of wavelengths centred around 126nm.

3.4- Incorporation to a CVD reactor

The argon excimer lamp can be assembled to a deposition system as shown on figure 2.21. The radiation is directly generated inside the chamber volume, and emitted in all directions and particularly through the magnesium fluoride window towards the deposition reactor. Preliminary work, which concentrated on the photo-enhanced deposition of hydrogenated amorphous silicon using this system was investigated, and the results are given in appendix 1.

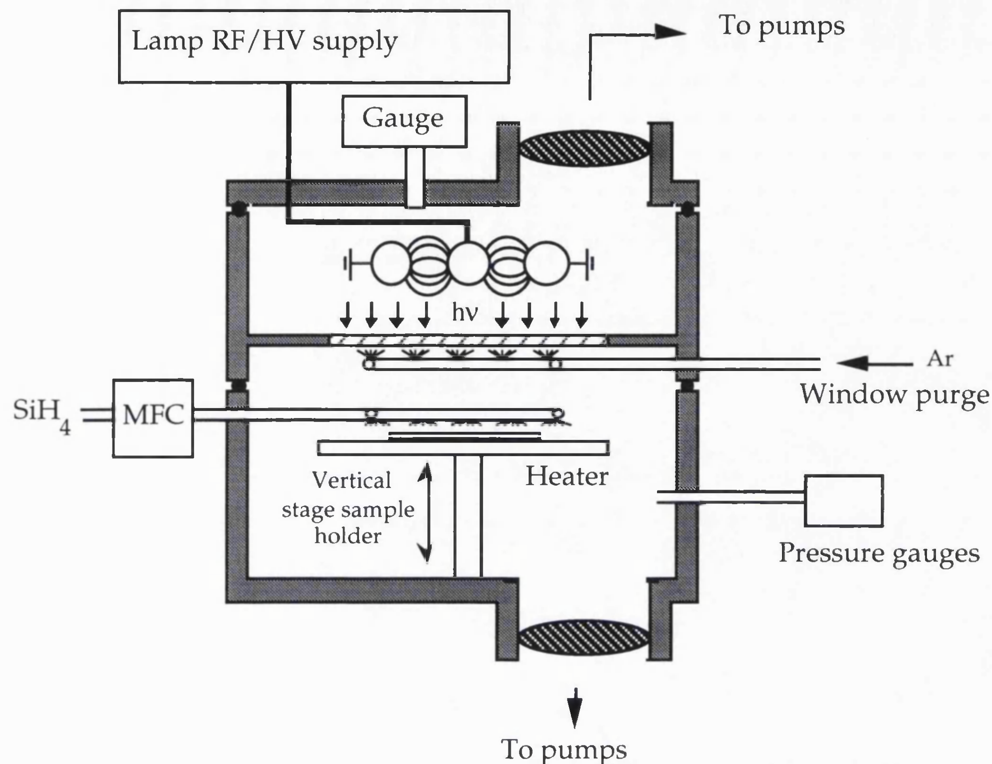

Figure 2.21 : Experimental setup of the argon lamp photo-CVD system

4.- Conclusion

In this chapter, the technologies involved with the fabrication and the use of excimer lamps have been presented. The initial steps of the *exc*ited di*mer* generation theory have been reviewed, together with a few essential VUV characterisation techniques. Using this type of light source, almost all domains of the ultraviolet range can be covered by selecting the appropriate gas mixture. The continua generated in the UV-A, B, and C ranges have already been used for various industrial applications, such as in UV curing (polymerisation) of special paints, varnishes and adhesives, with applications on wood, metal, paper, plastic parts, foils, compact disks, and glass fibers [ABB]. In the case of photo-CVD, the use of shorter wavelengths is necessary in order to cope with the absorption cross sections of the precursor gases. Consequently, mainly the radiations emitted from lamp devices using pure rare gases are of interest, and in particular the 172nm continuum of pure xenon excimer species.

References to chapter 2

[Allison] R. Allison, J. Burns, A.J. Tuzzolino,
J. Opt. Soc. Am., **54** (1964) 747

[ABB] U. Kogelschatz, B. Eliasson,and H. Esrom
in ABB Infocom, *New excimer UV sources for industrial applications*, (Internal Asea Brown Bovery Publication),
CH-E 3.30833.0 E , ABB Review (3/1991)

[Baulch] D.L. Baulch, R.A. Cox, P.J. Crutzen, R.F. Hampson, J.A. Kerr, J. Troe, R.T. Watson,
J. Phys. Chem. Ref. Data, **11** (1982) 359

[Bergonzo] P.Bergonzo, P. Patel, I.W. Boyd and U. Kogelschatz
Appl. Surf. Sci., **54** (1992) 424

[Calvert] J.G. Calvert & J.N. Pitts, *Photochemistry*,
J. Wiley & Sons, New york (1966)

[CRC Handbook] Handbook of Chemistry and Physics
(Chemical Rubber, Cleveland, OH) 1st stud. ed. (1988)

[Déjardin] G. Déjardin and R. Schwégler,
Revue d'Optique, **13** (1934) 313

[Eckstrom] D.J. Eckstrom, H.H. Nakano, D.C. Lorents, T. Rothem, J.A. Betts, M.E. Lainhart, D.A. Dakin, and J.E. Maenchen
J. Appl. Phys., **64** (1988) 1679
and
D.J. Eckstrom, H.H. Nakano, D.C. Lorents, T. Rothem, J.A. Betts, M.E. Lainhart, K.J. Triebes, D.A. Dakin,
J. Appl. Phys., **64** (1988) 1691

[Eliason-1987] B. Eliasson and U. Kogelschatz
J. Phys. D, Appl. Phys., **20** (1987) 1421

[Eliason-1989] B. Eliasson and U. Kogelschatz
2nd Int. Conf. on UV + Ozone in the treatment of water and other liquids (Vasser Berlin '89), Berlin, April 1989, pIV-6-1

[Eliason-1990] B. Eliasson and U. Kogelschatz
J. of the Int. Ozone Association ("Ozone"), **13** (1991) 365

[Eliason-1991] B. Eliasson, IEEE Transaction on plasma science **19** (april 1991) 309

[Förster] Th. Förster and K.Kasper, Z. Phys. Chem. NF, **1** (1954) 275 and Z. Electrochem., **59** (1955) 976

[Gellert] B. Gellert, U. Kogelschatz, Appl. Phys. B, **52** (1991) 14

[Gilbert] A.Gilbert & J. Baggot, in *Essential of Molecular Photochemistry*, Blackwell Scientific Pub., Oxford (1991)

[Haaks] D.Haaks, *Kinetic der Xe_2* excimere*, habilitationschrift, University of Wuppertal (1980)

[Hirsh] M.N. Hirsh, H.J. Oskam, *Electrical Discharges*, Vol.1 of *Gaseous Electronics*, Academic Press, New York, (1978)

[Inn] E.C.Y.Inn, Spectrochim. Acta, **7** (1955) 65

[Kessler] F. Kessler, H.D. Mohring, G.H. Bauer, Proc. of the 9th Int. Conf. on Plasma Chem., Vol. 3, (1989) 1383

[Kogelschatz-1988] U. Kogelschatz, *Advanced Ozone Generation*, in *Process Technologies for Water treatment*, edited by S. Stucki, Plenum Publishing Corporation, (1988) 87

[Kogelschatz-1990] U. Kogelschatz, Pure & Appl. Chem., **62** (1990) 1667

[Maier] D. Maier and G.E. Kurzmann in "Analytical Aspects of Ozone Treatment of Water and Wastewater", ed. by R.G. Rice, L.J. Bollyky, W.J. Lacy, Lewis Publishers, Chelsea, MI (1986) 271

[Manfredotti] C. Manfredotti, F. Fizotti, M. Boero, G. Piatti, Appl. Surf. Sci., **69** (1993) 127

[Marr] G.V. Marr, in *Photoionisation processes in gases*, (1967) 236

[Meek] J.M. Meek & J.D. Craggs, *Electrical Breakdown of gases* John Willey and Sons, New York (1978)

[Patel-1990] P. Patel and I.W. Boyd, Appl. Surf. Sci., **46** (1990) 352

[Patel-1991] P. Patel, P.Bergonzo, U. Kogelschatz and I.W. Boyd Proc. of the MRS 1991 Spring meeting, MRS Proc. Vol. 224, Los Angeles (1991)

[Petitjean, 1991] M. Petitjean, *Optimisation de structures MIS sur InP* rapport de thèse, Université Paris 6 (1991)

[Rhodes] Ch.K. Rhodes, Excimer Lasers, Vol. 30 of Topics of Applied Physics , Springer, Berlin (1984)

[Samson] J.A.R. Samson in *Techniques of Vacuum Ultraviolet spectroscopy*,. John Wiley & Sons, New York (1967)

[Tanaka] Y. Tanaka, J. Opt. Soc. of America, **45** (1955) 710
and
Y. Tanaka, A.S. Jursa, F.T. Leblanc,
J. Opt. Soc. of America, **48** (1958) 304

[Thurnau] D.H. Thurnau
J. Opt. Soc. of Am., **46** (1956) 346

[Watanabe] K. Watanabe, E.C.Y. Inn
J. Opt. Soc. of Am., **43** (1953) 32

Chapter 3

Initial Applications of Excimer Lamps

Since a new type of powerful vacuum ultraviolet source became available in this project, and further to the photo-CVD experiments, various new areas of applications have been investigated. Two new features are presented in this chapter, consisting of the development of an ozone generator using the 172nm radiation of a xenon excimer lamp, and in various applications of the ultraviolet enhanced organometallic deposition technique (MOD) of a few materials.

1.- Photochemical generation of ozone with vacuum ultraviolet radiation (VUV)

1.1- Fundamentals of ozone generation

1.1.1.- Introduction

A brief introduction to the various properties of ozone has been given in the previous chapter (§ 2.2.2). Mainly, ozone (O_3) is a commonly used gas with various applications in treating drinking water and industrial waste-waters. It is one of the strongest oxidants available. It has a characteristic pungent odour, which is not offensive [Rice]. In the earth stratosphere, ozone is formed photochemically under the effect of the sun VUV irradiation, but it also occurs at ground level in low concentrations due to photochemical decomposition of certain transient air pollutants. Under the conditions at which ozone is usually generated, concentrations above 9 to 10% cannot be obtained conveniently. At ambient temperatures, pure ozone is a blue coloured gas, although the colour is generally not noticeable at the concentrations at which it is generated. Ozone decays in air, with a half life of about 10 hours in the atmosphere at ambient temperature. Small increases in temperature reduce considerably the life time, down to about 2 seconds at 200°C [Masschelein]. In water, the half-life of ozone stands between 10 to 30 minutes.

Ozone mainly finds its applications as a cleaning reagent, since it is intensively used in the world on water and wastewater cleaning plants [Rice] [Kogelschatz]. However, ozone is also used for various electronic applications and material fabrication technologies, e.g., in superconductor MBE techniques [Siegrist], as well as for ultrathin gate oxide fabrications [Kazor], and elaborate wafer cleaning and oxide removal [Suemitsu] [Pidduck].

Because of the inherent instability of ozone, it cannot be purchased and stored until ready for use as can other oxidants/disinfectants currently employed. Instead, it is generated on-site, near its point of use, as it is required. This tends to motivate actual research on the development of new techniques for the generation of ozone, an environmentally clean disinfectant.

1.1.2- Toxicity of ozone to humans

The major concern for exposure to ozone is breathing it when ozone has leaked accidentally into the workplace atmosphere. This may happen when total destruction or evacuation of the ozone is not achieved on the site of an ozone generation experiment, or also when vacuum ultraviolet light leaks from a lamp system and causes photochemically enhanced generation of ozone in the laboratory. If ozone is detected in the laboratory atmosphere, the appropriate response procedure is to shut off the electrical power which then ceases its generation. Normally, human olfactory capabilities can detect ozone in the ambient air at levels around 0.1ppm. Exposure to atmospheric ozone levels below 1ppm for as long as 5 minutes is non-symptomatic [Langerwerf] [Bollyky]. For higher concentrations, figure 3.1 gives the relationships between exposure and human response.

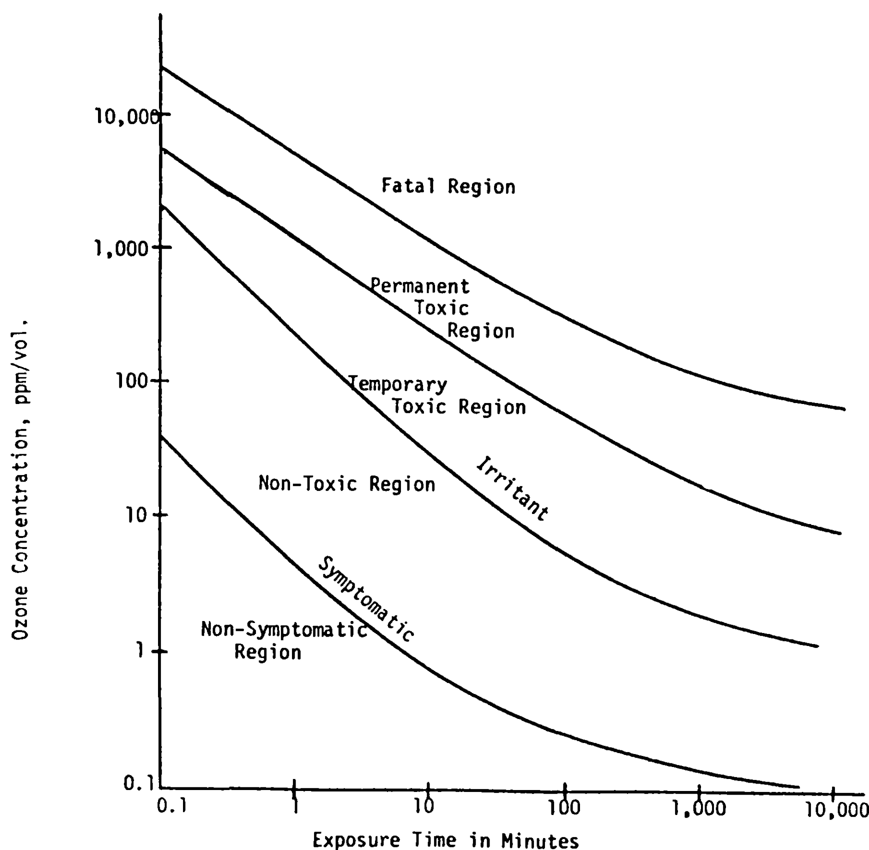

Figure 3.1 : Concentration vs time relationships between exposure to ozone and human response [Langerwerf]

1.1.3- Conventional generation of ozone

Among the methods by which ozone is generated, the corona discharge, or silent discharge, is the most widely used procedure. The main feature of this electrical discharge technique is the presence of a dielectric layer between the discharge gap and at least one of the electrodes (figure 3.2).

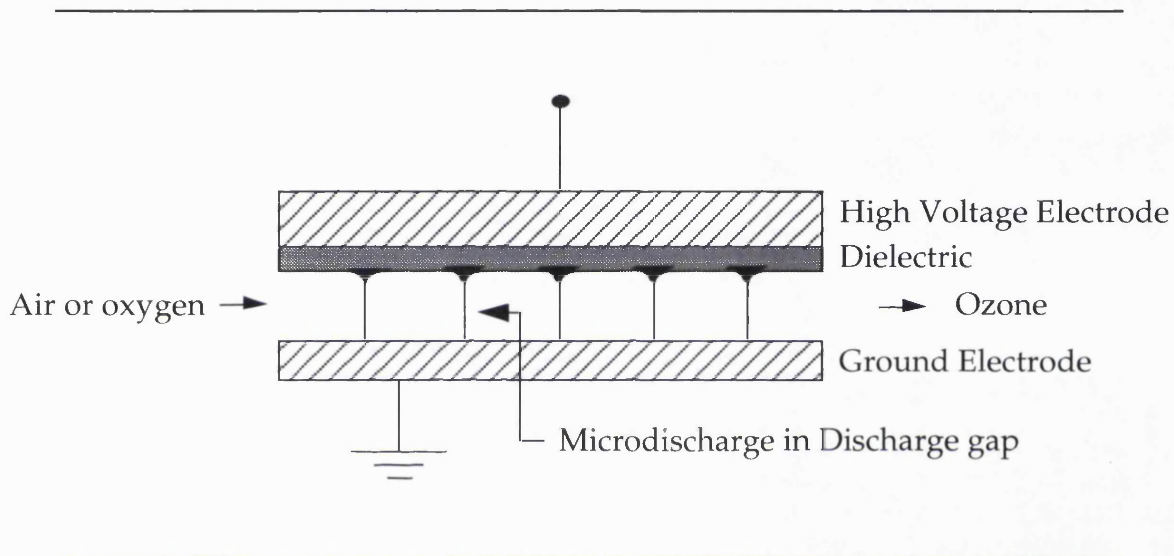

Figure 3.2 : Ozone generation in a corona discharge

The presence of the dielectric leads to the formation of a large number of micro-discharges of nanosecond duration. These micro-discharges are uniformly distributed with respect to space and time. The existence of the microdischarge is conditioned by the electrical breakdown in the gap. Figure 3.3 shows the breakdown voltages (Paschen curves) in air.

In oxygen, the main reactions are:

$$e + O_2 \rightarrow e + O + O \qquad (3.1)$$

$$O + O_2 + M \rightarrow O_3 + M \qquad (3.2)$$

in which M is a third collision partner, namely O_2, O_3 or N_2 in air.

The maximum efficiency of ozone generation would be obtained if every O atom reacted according to reaction (3.2) to form an ozone molecule. In practice, additional chemical side reactions can occur:

$$O + O + M \rightarrow O_2 + M \quad (3.3)$$

$$O + O_3 \rightarrow 2\,O_2 \quad (3.4)$$

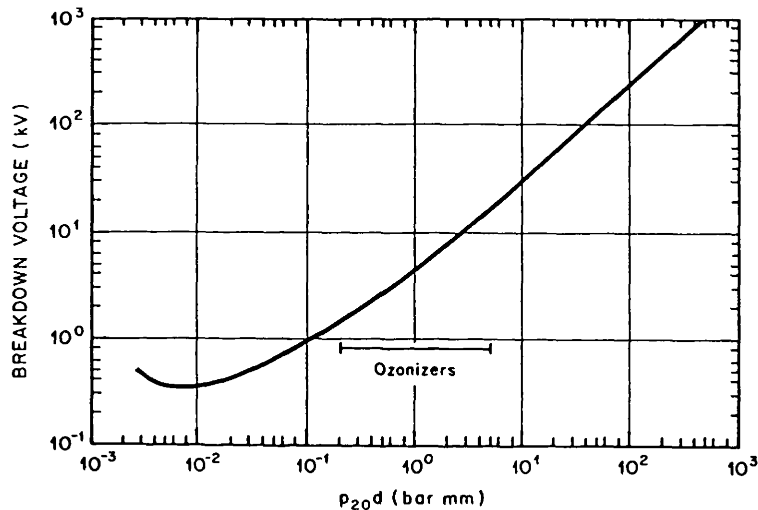

Figure 3.3 : Paschen curve for air

For oxygen discharge, calculations have proved that, at best, about one third of the discharge energy is channelled into ozone formation. The major part of the dissipated electrical energy is converted into heat and will have to be removed by a cooling circuit. In air, other reactions involving nitrogen atoms or excited nitrogen molecules may lead to the formation of oxygen atoms that eventually react to form ozone. Therefore, the generating efficiency can be higher (by a factor of 2) as one could expect from the oxygen content of air. Optimised values for ozone generators are in the range 2-3% for air-fed ozonisers to 7% for oxygen-fed.

1.2- Ozone generation with UV radiation

1.2.1- Oxygen photodissociation

The absorption spectrum of oxygen in the various regions of the UV spectrum was given in figure 2.16. In order not to create charged particles, the energetic requirements for the UV radiation used for the photo-dissociation of O_2 molecules are that the radiation must be energetic enough to dissociate O_2 (λ<242nm) but not energetic enough to produce ionization (λ>103nm). Practical considerations, such as the necessity to absorb the UV radiation in a laboratory experiment over a path length of a few centimetres lowers the upper wavelength limit below 190nm. In principle, the 185nm radiation of the low pressure mercury lamp can be used for the generation of ozone; but the low efficiency of these lamps at 185 nm and the intense 254nm line, which destroys the ozone, limit such applications.

1.2.2- Use of the xenon excimer source

Under the influence of the 172nm photons, oxygen undergoes dissociation, and the § 2.2.2 of chapter 2 gave details on the photochemistry. At an atmospheric pressure of pure oxygen, the absorption length of the radiation is about 1mm. The suggested quantum yield of such a generation of ozone is equal to 2, thus resulting in the formation of two ozone molecules per incident UV photon.

1.2.2.1- Measurements and efficiency

The methodology used was discussed in § 2.2.2 of chapter 2 on actinometric measurements. From the amount of ozone generated, efficiencies in terms of input gas flow and electrical power are deduced. The latter is the most significant efficiency in terms of process efficiency, the former being more strongly correlated with the reactor configuration. The electrical efficiency is generally expressed in terms of Wh/g or J/g necessary for the production of ozone. Expressions in g/kWh may also be used, since they are more convenient for a direct estimation from the amount of ozone generated.

1.2.2.2.- First prototype- Proof of principle

The molecular absorption of oxygen at this wavelength is about 10 $cm^{-1}atm^{-1}$. This means that in an atmospheric pressure of oxygen, the absorption length is about only 1mm. For the first experiment, a stainless steel chamber was used, containing the lamp element, through which was passed pure oxygen. The actual volume of the chamber was about of 1.5 litre, and the distance lamp-walls was close to 5 cm (figure 3.4). Also, according to the previous estimations of the *active* volume, this ozone generator is far from being optimised.

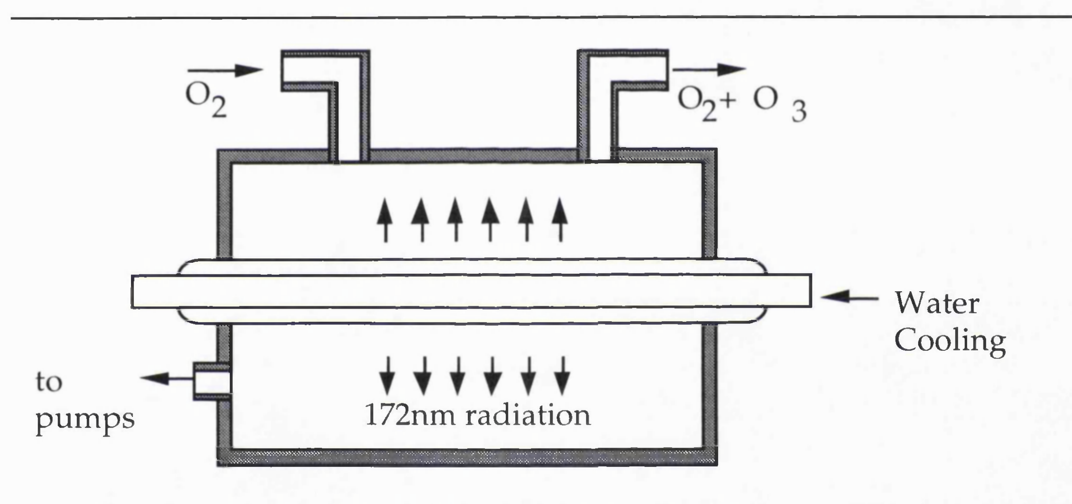

Figure 3.4 : First prototype.

A KI solution of 2% was used to titrate a N/10 sodium thiosulphate starch solution. From the titre is calculated the amount of ozone generated. For experiments lasting a few minutes, with 500 sccm O_2 flow, and at lamp input power ranging around 50W, titration measurements led to ozone generated yields around 400 mg/hour. From this value, VUV power generated is 1W, giving a lamp efficiency of 2%. In terms of ozone/oxygen efficiency, values are reaching 0.7%, leading to a process efficiency around 9 g/kWh.

1.2.3.- Improvements

The analysis of the further experiments performed with this prototype VUV ozoniser pointed out that the low efficiencies obtained were mainly caused by geometrical problems. In fact, by using smaller flows of oxygen, a much lower lamp efficiency was obtained, and with higher flows a higher calculated lamp efficiency (which so far is a constant value). Such a result leads to the conclusion that when low flows of gases are used, the ozone generated is not flushed out of the ozoniser and the input oxygen can leave the chamber without reacting. To limit this problem, one solution is to increase the flow, but of course this leads to lower efficiencies in terms of ozone/oxygen generation yield. It can therefore be estimated that the O_3/O_2 efficiency varies on an inverted parabolic basis with the gas flow in this ozoniser. The maximum efficiency being reached when a laminar flow of oxygen passes all along the tube before being flushed out.

From that point it is assumed that the efficiency of the device is directly linked with the flow around the lamp cell. The volume into which the oxygen is flushed has to be reduced so that the generated ozone can be automatically removed by the incoming oxygen, even at low flows. This requires a smaller volume between the lamp cell and the chamber walls. On the other hand, the total length of the oxygen path along the tube can be extended as much as the device enables it, so that the input oxygen flow can be increased to high values without limiting the maximum conversion efficiency.

1.3- The VUV enhanced ozone reactor

1.3.1- Description

The design is based on the use of a cylindrical shaped ozoniser, in which the radial diameter has to allow a laminar oxygen flow into the device. For such, an active radial depth of 10 mm is proposed (only 10^{-7} % of the incoming radiation is not absorbed). The actual lamp source has an external diameter of 30mm, and the device consists of a metal tube of 50mm inner diameter and a length of 16cm, which guarantees complete absorption of the 172nm radiation (Fig. 3.5).

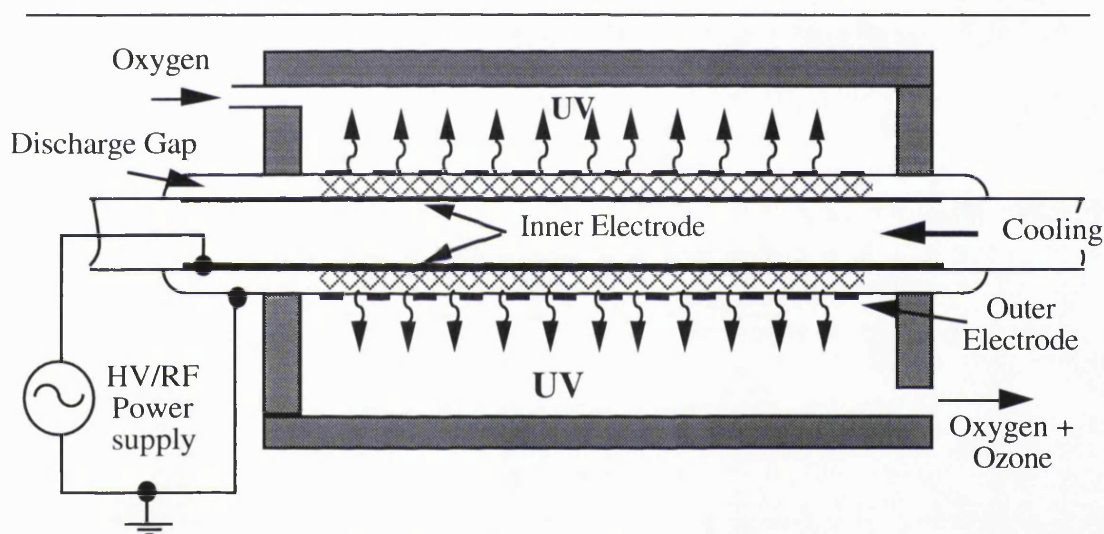

Figure 3.5 : VUV enhanced ozone reactor

1.3.2- Results

The first experiments concentrated on the influence of the lamp power and of the gas flow on the different efficiency coefficients. Figure 3.6 shows the evolution of the ozone generated at a constant input power of 50 Watts for low flows of oxygen (less than one litre/min). Values of 1g of ozone generated per hour can easily be obtained, but at very low corresponding electrical efficiencies (which are in this case proportional to the amount of ozone generated because of the fixed input power).

A low electrical efficiency can be expected, since in this case, in comparison with corona discharge ozonisers, the electrical power has firstly to be converted into light (and excimer lamp efficiencies generally range around 5 to 6%), and secondly into photochemical reactions. Nevertheless, figure 3.6 shows a strong increase of the overall efficiency with the flow, showing it to be critical for this reactor. This flow dependance will be discussed in the next section.

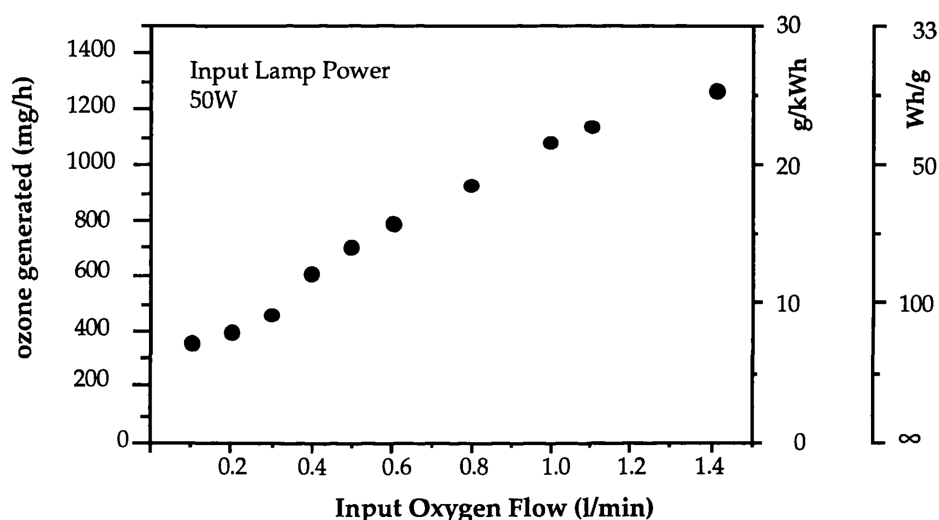

Figure 3.6 : Ozone generation as a function of oxygen flow at a constant light input power

In figure 3.7 is presented the ratio of ozone generated to the oxygen flow fed through the system. The highest efficiencies are obtained at the lowest flow rates. These high efficiencies, however, are not particularly beneficial in this configuration because of the very low absolute levels of ozone obtained. The curve shows a generally decreasing efficiency with increased flow rates, eventually levelling off at around 1%. The decrease in efficiency is in fact compensated by the increase of the absolute amount of ozone generated (cf. fig. 3.6). This motivates further investigations towards high flows of oxygen.

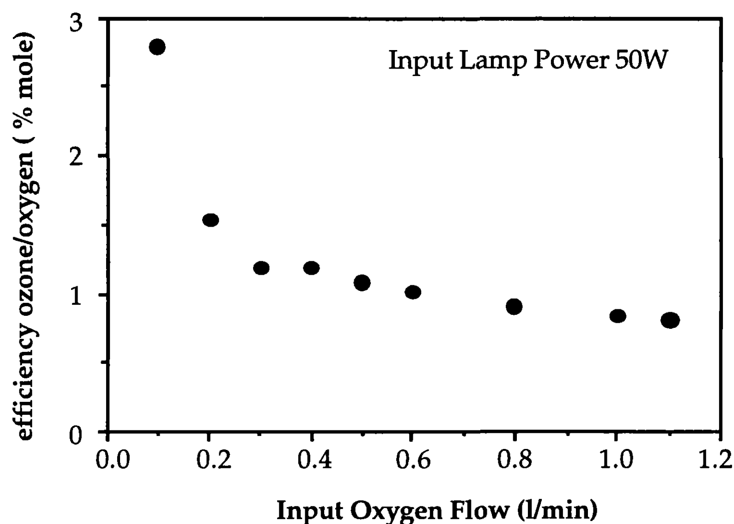

Figure 3.7 : Relationship of the Ozone/Oxygen ratio to oxygen flow for a constant input lamp power

The average input power levels of the light used were around a few 10s of Watts. The effect of the light input power on a constant oxygen flow of 1 litre/min is shown in figure 3.8 (a). The amount of ozone generated is clearly directly correlated with the UV power used. Figure 3.8 (b) shows the electrical efficiency in terms of the quantity of ozone generated for values of input lamp power around 20 to 30W. It comes that a higher ozone production may be obtained with an increased VUV power, but at a lower efficiency.

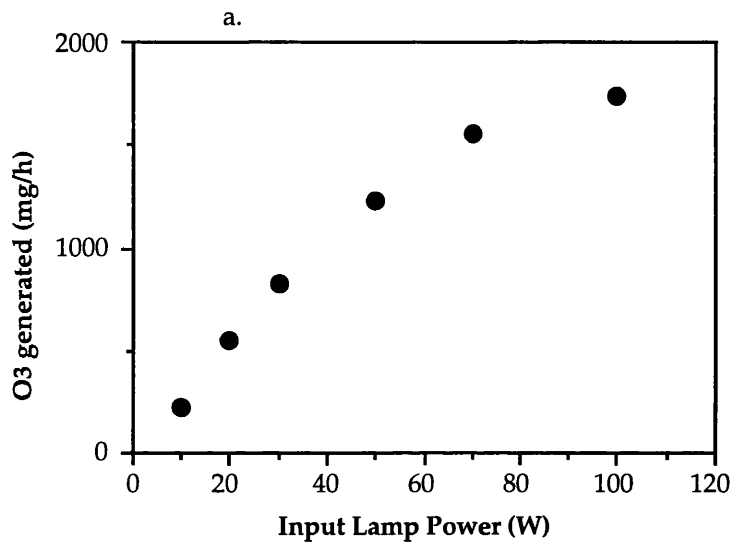

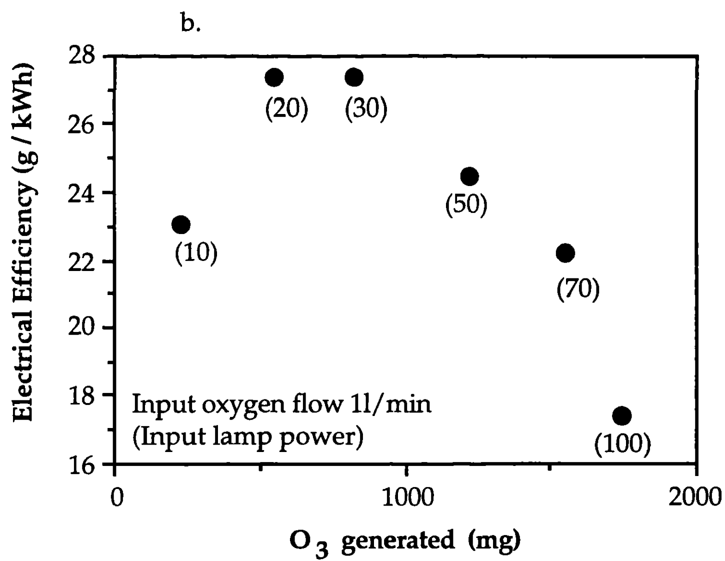

Figure 3.8(a) (top) and 3.8(b) (below) : Effect of the light input power on the ozone generated (constant flow 1l/min oxygen)

1.3.3- Discussion of the effect of the flow on the ozoniser efficiency

As seen in figure 3.6, the production of ozone increases with the gas flow, although as Figure 3.7 shows, the overall efficiency decreases. These low ozone/oxygen efficiencies at low flows cannot be caused by a reactant gas limitation. Thus, the ozone generated may decay or dissociate along the reactor. In fact, it is well known that the ozone may be dissociated at high temperatures, and also under the 172 nm radiation. The literature shows that a fixed volume of ozone decays by about 95% within about 2 seconds when heated up to 200°C [Coste]. Since only the inner electrode is cooled, the outer electrode of the lamp may reach high temperatures. Thus some of the ozone may be thermally dissociated before leaving the reactor. Similarly, ozone absorbing the 172nm radiation emitted from the lamp may also be photo-dissociated under the effect of the photons.

The importance of such phenomena was checked by varying the length of the reactor. Figure 3.9 shows the amount of ozone produced and the corresponding electrical efficiency when the length of the reactor varies from 4 to 12cm. This curve does not show any obvious reduction of the efficiency when the ozoniser length is extended, but a small *plateau* appears above 90mm. This therefore shows that a scaled up version of this prototype may be obtained more appropriately by adding a number of short ozonisers in parallel, rather than increasing the length of one reactor.

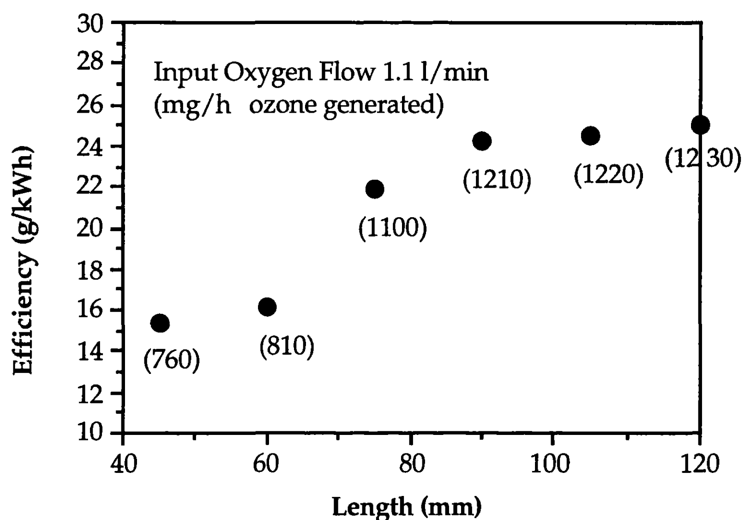

Figure 3.9 : Effect of the length of the reactor (Constant Flow)

The graph shown in figure 3.9 was obtained at a fixed constant flow and input power. These settings, however, may not be optimum for each of the different lengths investigated. Figure 3.8(a) showed that the ozone generation varied linearly with the input power. On the other hand, the effect of the flow is more critical, as can be seen in figure 3.10. Here, the different lengths of lamp show a different efficiency-flow relationship. This may be due to the fact that if some of the ozone is thermally destroyed, variations in the flow may change the cooling of the outer electrode hence the temperature induced decay of the ozone. In other words, the *plateau* which appeared at around 90 mm for a flow of 1l/min will be different for different flow rates. When such an ozoniser is to be developed to produce a certain amount of ozone, the cost of oxygen against the optimised flow must be considered, after which the length must be optimised to avoid ozone destruction along the reactor.

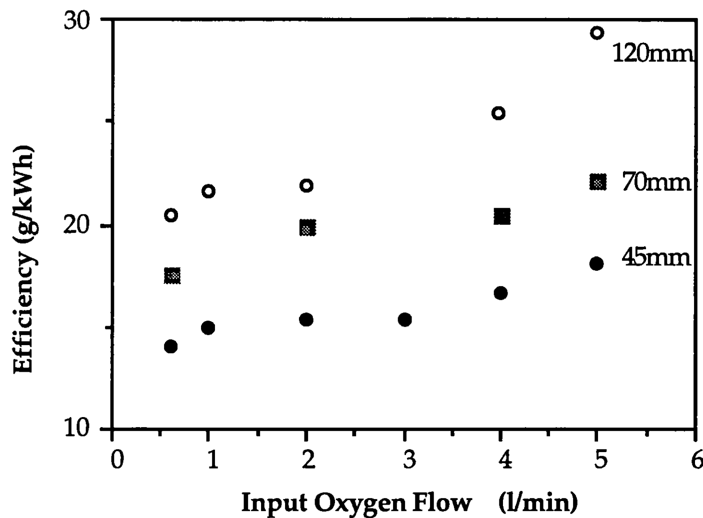

Figure 3.10 : Influence of the flow on the efficiency for different reactor lengths

1.3.4- Air fed VUV enhanced ozoniser

Since the highest efficiencies are obtained with large (and costly) oxygen flow rates, it is pertinent to consider air-feeding of such reactors. This approach does not necessitate to preliminary dry the air, an expensive constraint with corona discharge ozonisers.

Figure 3.11 compares the efficiencies of the oxygen and air fed ultraviolet enhanced ozonisers. It shows, in particular, that values obtained with 5l/min of air easily reach those obtained with 1l/min oxygen. This 5 to 1 ratio may correspond to the normal oxygen content in air (20%), although secondary photolytic reactions may also occur to lower the decay of ozone in the reactor. Further studies involving air should carefully check if other products such as nitrogen oxygenated compounds are generated in proportions which can be dangerous to nearby animal-life. Figure 3.12 inter-relates the efficiencies achievable for various amounts of ozone generated (by different input powers at a constant flow rate), using air or oxygen.

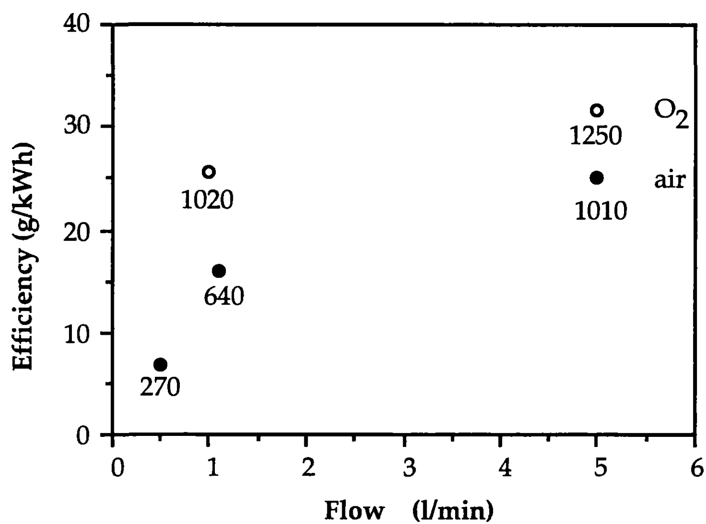

Figure 3.11 : Comparison between air and oxygen efficiencies. Values indicate the mass of ozone generated per hour (mg/h)

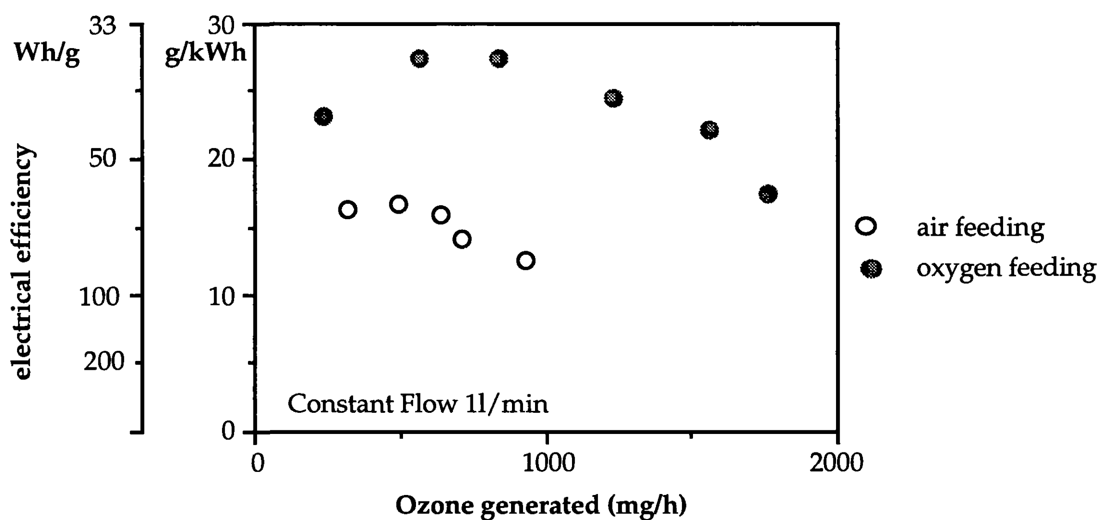

Figure 3.12 : Variation of the efficiency for various input power for air and oxygen at a constant flow rate of 1 litre/minute

1.4- Conclusion

The primary target for this work was to reach ozone production values higher than 1g/hour, which has been achieved. However, the measured electrical efficiencies remain lower than those of corona discharge ozonisers. This is due to the fact that the electrical energy supplied has first to be converted into light, and therefore the process is limited by the efficiency of the VUV lamp. Efficiencies of a comparable order could only have been achieved in this process if the lamp efficiencies had reached 14%. In theory, excimer discharge efficiencies could reach 40%. However, experimental values have so far never exceeded 10%, even though these are very high values for such short wavelength light sources.

Nevertheless, this work showed that many other possibilities are offered with this type of reactor. In particular, the generation of ozone from air, without treatment, gives promising results which may interest industrial applications. Also, the absence of any particular requirement on the kind of gas to be processed in this reactor, opens new applications towards direct treatment of various products under short wavelength ultraviolet illumination. Such lamps can be used for direct photo-oxidation in aqueous solutions, as water can be dissociated by such radiation. New applications can therefore be studied as a continuation of this work towards the UV disinfection and destruction of pollutants in the liquid phase, thus opening new applications from biology to environmental cleaning: it has been reported that similar laser photo-dynamic therapies are already studied in the US for blood treatment and virus disinfection (such as HIV), as well as for CHCs destruction [Klein]. The study of the effect of UV photons (e.g., aging) on new compounds and the life time of very stable pollutants can also be explored.

2.- Applications of excimer lamps to organometallic depositions (MOD)

As powerful producers of selective radiation at specific wavelengths, the excimer lamps contrast with the other commonly used UV lamps, such as xenon or mercury lamps, which often produce unwanted radiations. Under the UV radiation, molecular bonds can be broken selectively by photo dissociation or photolysis. In chapter 1, a discussion on photo-CVD has been presented, and it implies the existence of dissociative reactions in a gas phase. Similarly, here is proposed the study of the enhancement of this type of reactions, but in thin solid films. In fact, the decomposition of the spin-on organometallic films can be performed in air or inert gases, with no need for specialised reactors and gas transport or distribution systems. The literature gives various examples of the pyrolytic decomposition of spin-on films in furnaces [Schroeder], or under the effect of powerful lasers [Ehrlich] [Preuss] [Boyd]. However, the application of those deposition methods to thermally fragile substrates implies the development of low temperature processing, e.g., the photolytic activation.

2.1- Experimental set-up

Most of the thin solid film expositions were performed on spin-on coated samples in a very basic lamp chamber. Figure 3.13 shows the experimental arrangement used to hold the lamp and to provide a primary vacuum to the process. There was no heating element to hold the substrate, since all depositions were performed at room temperature. The lamp was cooled with a cooling circuitry unit flowing deionised water through the inner high voltage electrode. For experiments performed in vacuo, no significant heating was measured on the sample, although small temperature increases (60 to 70°C) due to the proximity of the outer electrode of the lamp were measured on certain samples processed for long runs at atmospheric pressures.

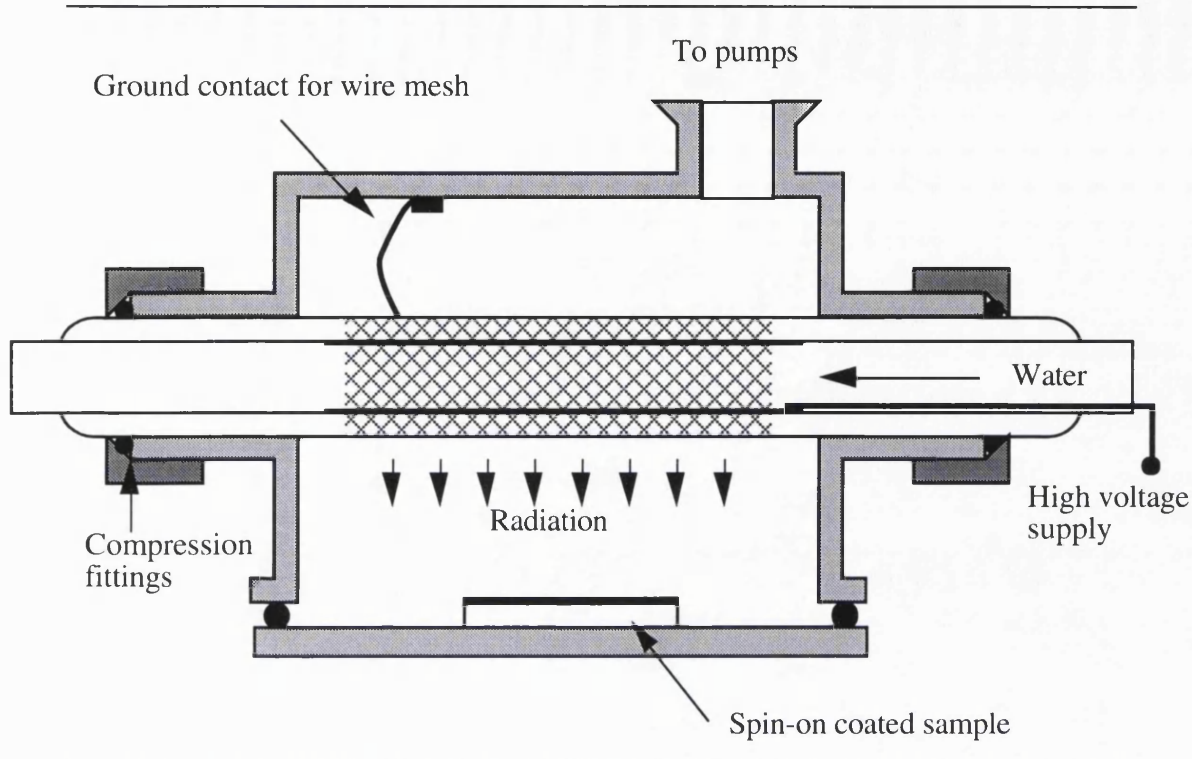

Figure 3.13 : Experimental apparatus used for spin-on coated organometallic thin solid film processing

The sample characterisation was performed using a Shimadzu UV-160A, UV-visible transmission spectrometer working in the range 200-800 nm, combined with simple four probes electrical measurements. The thicknesses were monitored using an alpha-step, performed on edges obtained with the use of a masking tape. The processed samples were spun on crystalline quartz substrates with sizes up to one inch in diameter. Although the study of the photochemistry may have been very fruitful, the interest here is to investigate the potential applications of the UV radiations available, and therefore no volumetric nor mass analysis was performed on those samples. Also, this presentation concentrates on a wide range of materials to be deposited, without extending thoroughly on the UV enhanced chemical reactions occurring on the sample surface.

2.2- UV induced metal depositions

2.2.1- Palladium

In this process, vacuum UV radiation from a xenon excimer source was used to initiate palladium nucleation by selective photodissociation of palladium acetate [Esrom-1989, -1990]. The palladium acetate film was obtained by dissolving palladium acetate in chloroform, then by coating the substrate (e.g., quartz) using spin-coating or dip-coating methods, from which the solvent evaporates. By varying the dissolution ratio or the speed used for spinning, various uniform thicknesses were obtained. A typical ratio is of 1g of Pd(2)-acetate in 30ml of chloroform, spin on coated at 2000 rot/min. Figure 3.14 shows the UV transmission spectrum evolution vs exposure time under 50W of input power. At t=0, the spectrum shows strong absorption in the wavelength range around 200nm. Using a xenon lamp emitting at 172nm to irradiate the sample, the light is absorbed, leading to photo induced chemical modification of the dry palladium acetate film. Strong modifications of the UV transmission spectrum were observed, leading after exposure to a flat spectrum characteristic of a metallic film. The coatings show very good uniformity and smoothness.

Palladium film thicknesses from a few nanometers to a few tens of nanometers can be easily obtainable by this process. These layers can be used as initiators for thicker metal coating: the palladium acts as an activator for subsequent chemical metal-deposition baths in which the micrometer-thick copper, nickel or gold layer can be grown on top of the palladium. Such coating thicknesses provide a level of electrical conductivity which is sufficient for applications such as the production of printed circuits or for shielding electromagnetic fields. With this method, only a few simple and economical process stages are needed to obtain a metal pattern on any required substrate.

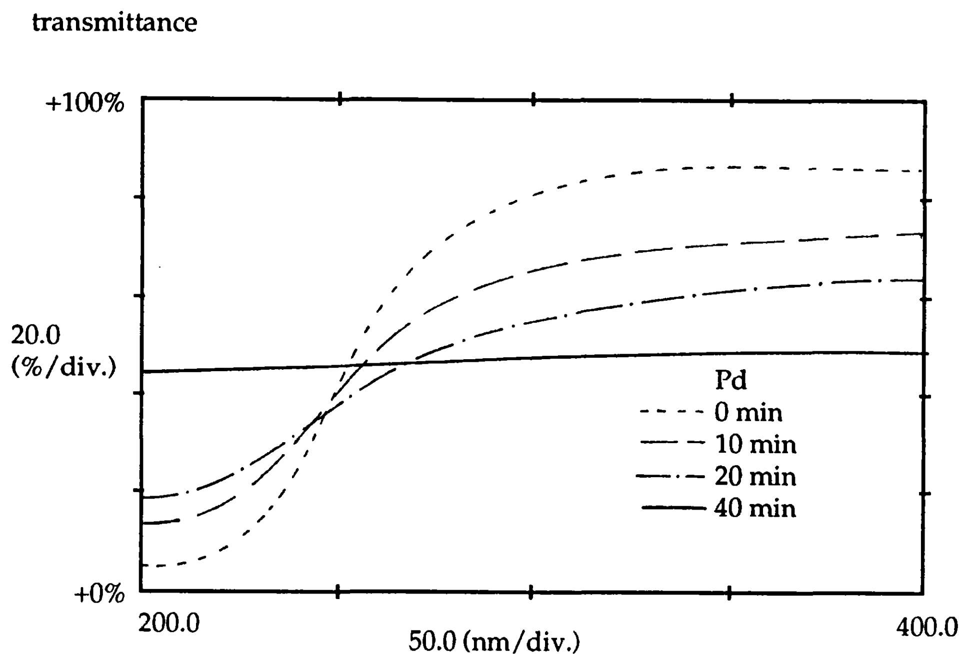

Figure 3.14: UV transmission spectrum evolution of Pd-acetate coating under Xe_2^* radiation

The palladium film can also be used by itself as a thin metallic layer, such a thinness offering for example a high UV transmission property. Figure 3.15 presents the UV absorption spectrum of a very thin palladium film. The dilution in that case is that of 1g Pd(2)-acetate in 150ml of chloroform, and a rotating speed of 2000 rot/min. As can be seen, the optical transmission reaches 80% from 400nm down to 200nm. The estimated thickness (or thinness !) of such a sample is a few Ångströms. Four probes resistivity measurements were performed using silver-paint contacts. The square resistivity of this film, was 600 Ω_{square}. One interesting application of such a film is to use it instead of the perforated external electrode of excimer lamps. The total voltage drop over a length of 10 cm for the currents used barely reaches values of a few volts, which are negligible when compared with the few kilovolts which are fed into the lamps. However, these film were scratch sensitive and therefore required passivation from dielectric materials with similar optical characteristics.

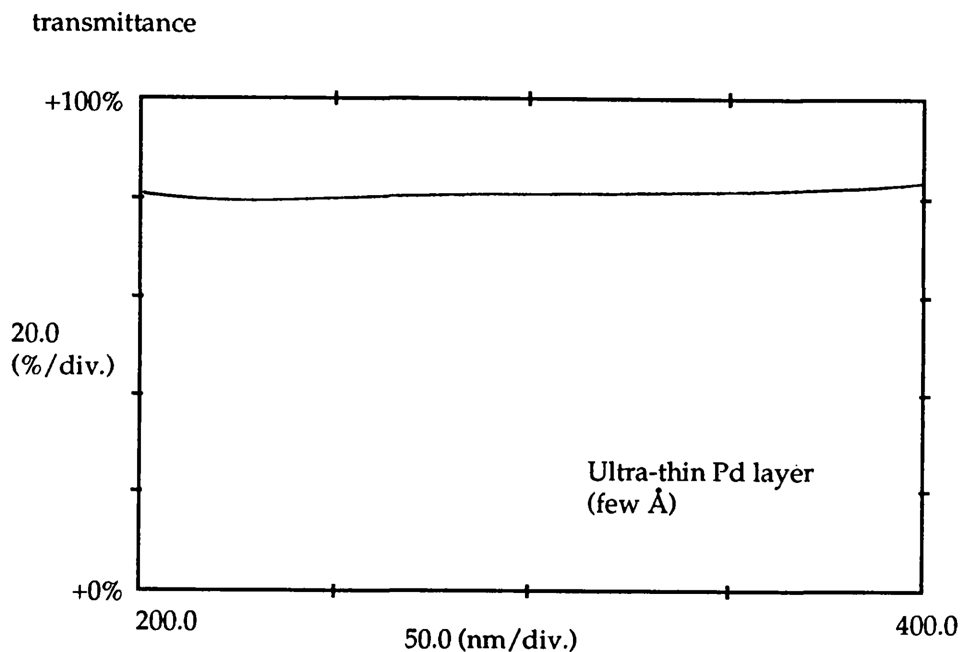

Figure 3.15 : UV transmission spectrum of a very thin film of Palladium

2.2.2- Copper

The copper deposition attempts used cupric acetylacetonate ($C_{10}H_{14}CuO_4$) as the precursor, dissolved in chloroform at various ratios (typical: 1g/20ml). Irradiations were attempted under the xenon lamp at various powers for times up to 2 hours. No significant modification of the spectrum, as well as no electrical conductivity of the sample was observed. The 172nm assisted processing of spin-on cupric acetylacetonate for the deposition of copper was abandoned.

2.3.- UV induced dielectric material depositions

Organometallic deposition techniques have already enabled various dielectric material depositions from pyrolytic processes [Schroeder] [Gobrecht]. This UV assisted process is very similar to that of palladium MOD. However, for oxide materials, the oxygen from the atmosphere is incorporated, hence vacuum conditions are not required. This implies the use of longer radiations than 200nm, and thus a xenon chloride excimer lamp (222nm) was used.

2.3.1- Aluminium oxide (Al_2O_3)

Films of aluminium oxide were deposited at room temperature, using the irradiation of a KrCl excimer lamp on a solution prepared from:

- 10% Aluminium di(i-propoxide) acetoacetic ester chelate $Al(OC_3H_7)_2(C_6H_9O_3)$
- 90% Hexane (Aq)
- spin-on coated at 1000 rot/min.

Figure 3.16 shows the evolution of the UV spectrum of this compound during irradiation as a function of time. The curves tend to a flat band and show a small loss in transmission towards very low wavelengths (theoretical cut-off: 250nm for Al_2O_3). The films were insulating layers, with resistivities higher than 10MV/cm. The films obtained were scratch resistant (Mose Hardness higher than 5.5: Stainless steel) and adherent, with thicknesses of a few 100s of nanometers obtained per process. This explains the low absorption measured at 200nm. The films were amorphous and are not expected to be perfectly stoichiometric. Their properties are of interest as protecting or insulating layers for various uses, especially when high temperature processing is impossible. The growth of these aluminium oxide films over the very thin palladium films grown in § 2.2.1 was achieved. Optical and electrical properties were not modified greatly, so that it was possible to get scratch resistant and adherent electrically conducting ($R_{square}=600\Omega_{square}$), far UV low absorption films (over 70 % transmittance at 200nm).

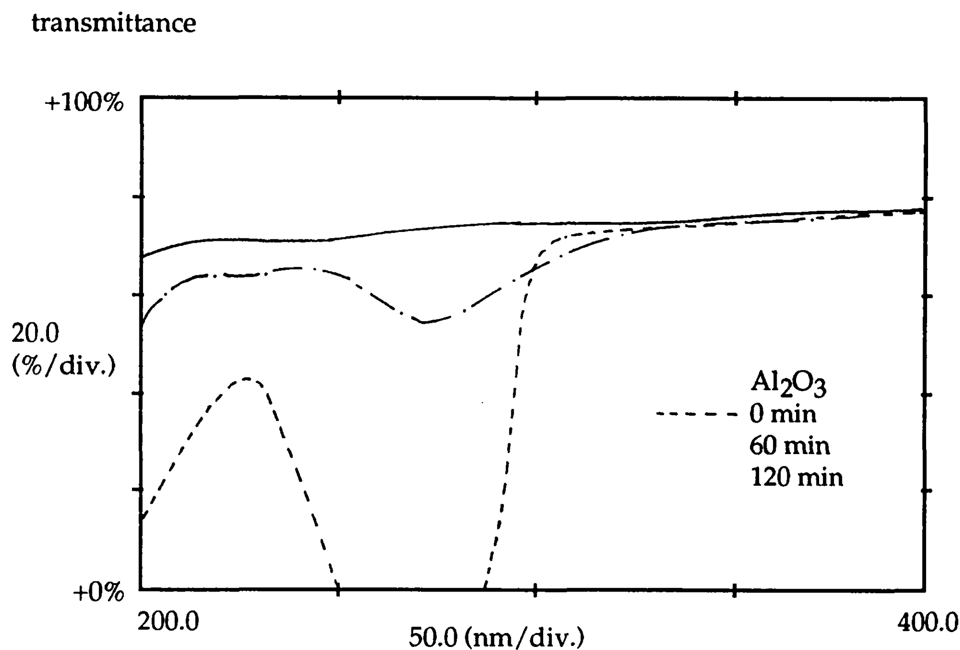

Figure 3.16: UV transmission spectrum evolution of dielectric coating of Al_2O_3

2.3.2- Lanthanum oxide (La_2O_3)

Films of lanthanum oxide were deposited at room temperature, using the irradiation of a KrCl excimer lamp on a solution prepared from:

- 0.1mg Lanthanum 2,4-pentanedionate (crystalline at room temperature) $La(C_5H_7O_2)_3$
- 20 ml ethanol
- spin-on coated at 1000 rot/min.

Since saturation is reached at very low concentrations, a high dissolution is used. Figure 3.17 shows the evolution of the UV transmission spectrum of this compound during exposition as a function of time. The curves tend to a flat band and shows a small loss in transmission towards very low wavelengths (theoretical cut-off: 220nm for La_2O_3). The electrical properties were those of a dielectric (square resistance ≥10MV/cm). Due to the high dissolution, only very thin layers per spin-on can be obtained (≈500Å), but the process can be repeated in order to increase thickness.

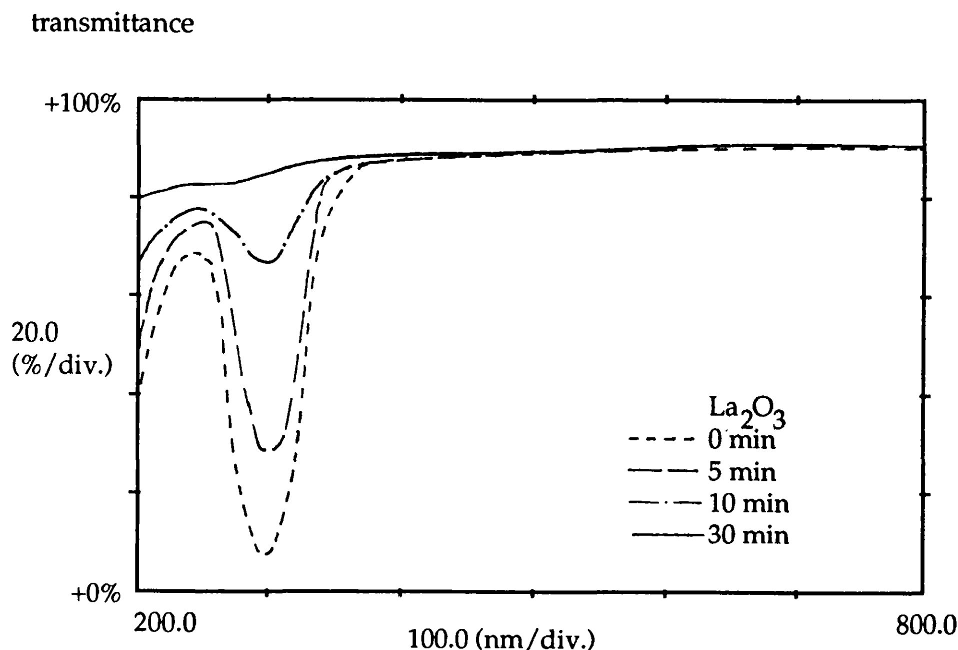

Figure 3.17: UV transmission spectrum evolution of dielectric coating of La_2O_3

2.3.3- Titanium nitride (TiN)

The excellent high temperature stability, hardness, corrosion resistance, and electrical properties provide TiN with many applications from cutting tools and anaesthetic coatings to VLSI microelectronics [Wittmer]. TiN films can be obtained by a large number of different techniques such as physical vapour deposition [Sundgren], ion implantation [Armogliato], CVD [Takahashi], or laser assisted techniques [Craciun] [Elders]. The difficulty for depositing titanium at low temperature from spin-on coatings stands in the very high oxidising capability of Titanium.

The first attempt consisted of the irradiation of films spin coated from

- titanium (disopropoxide)bis (2,4-pentanedionate),

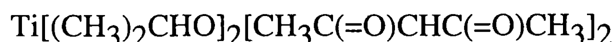

$$Ti[(CH_3)_2CHO]_2[CH_3C(=O)CHC(=O)CH_3]_2$$

- dissolved in hexane,

These were then exposed to the radiation in vacuo.

No evidence of deposition was observed, and the aspect of the films was closer to that of titanium oxide or dioxide than to TiN. Other experiments with the same organometallic precursor used gaseous nitrogen pressures of a few tens of mbar, as well as gaseous ammonia pressures of a few mbars. No difference was observed, and titanium oxides obtained.

Other titanium precursors were studied, such as

- titanocene dichloride : $(C_5H_5)_2TiCl_2$,
  also called bis (cyclopentadienyl) titanium dichloride
- dissolved in toluene $(C_6H_5CH_3)$
- exposed to the 172nm radiation from a xenon excimer lamp.

The results were no more encouraging than in the previous set of experiments, whatever the nitrogen or ammonia gas phase compositions or pressures used.

Finally, attempts to deposit TiN from the photo-enhanced gas phase reaction between titanium tetrachloride $TiCl_4$ and ammonia were performed. Titanium tetrachloride has been used successfully in laser assisted techniques to deposit titanium and titanium silicide compounds [Kubát] [Tsao] [Gupta].

However, $TiCl_4$ reacting very strongly with air to form HCl, thus spin-on coating is impossible. The risks associated with the use of these chemicals, as well as the contamination of the deposition chamber which would have occurred ended our involvement in this system. However, we note with interest that the gas phase of titanium tetrachloride can be obtained in low pressures by heating up the liquid precursor (53mbar at 50°C) [CRC Handbook], and ammonia radicals such as NH and NH_2 can be obtained by irradiating NH_3 to the 172nm from a xenon excimer lamp. This approach may be a fruitful route to eventual film growth and certainly deserves investigation.

2.4.- Conclusion

A new area of application of excimer lamps is the low temperature thin film growth from spin-on coatings of organometallic compounds. The room temperature growth of palladium, aluminium oxide and lanthanum oxide were successfully performed. These materials can readily be deposited on any type of substrates, and particularly on heat sensitive materials, such as wood, plastics, paper, cardboard, synthetic fibre, etc [ABB]. Although the characterisation methods used did not give detailed information on the stoichiometry of the films obtained, the film characteristics were in agreement with literature data, and we can consider these MOD experiments successful. In fact, at the time of writing this thesis, a new project is about to begin at UCL to further extend those MOD experiments.

References to chapter 3

[ABB] U. Kogelschatz, B. Eliasson,and H. Esrom in ABB Infocom, *New excimer UV sources for industrial applications*, (Internal Asea Brown Bovery Publication), CH-E 3.30833.0 E , ABB Review (3/1991)

[Armogliato] A. Armogliato, G. Celotti, A. Garulli, S. Guerri, R. Lotti, P. Ostoja, Appl. Phys. Lett., **41** (1982) 446

[Bollyky] L.J. Bollyky, *Ozone safety and health considerations*, in Proc. of the seminar on the "design and operation of drinking water facilities using ozone or chlorine dioxide", ed. by R.G. Rice (1979) 281

[Boyd] I.W. Boyd, *Laser Processing of Thin Films and Microstructures*, Springer, New York (1987)

[Coste] C. Coste, in *Ozonization Manual for Water and Wastewater Treatment*, ed. by W.J. Masschelein, J. Wiley & Sons, Chichester (1982)

[Craciun] V. Craciun, I.N. Mihailescu, I. Ursu, F. Craciunoiu, A. Corici, G. Leggieri, A. Luches, V. Nassisi, M. Martino, Appl. Phys. Lett., **53** (1988) 1225

[CRC Handbook] Handbook of Chemistry and Physics (Chemical Rubber, Cleveland, OH) 1st stud. ed., 1988.

[Elders] J. Elders, *Laser induced chemical vapor deposition of titanium diboride*, PhD Thesis, University of Amsterdam, (1992)

[Ehrlich] D.J. Ehrlich, J.Y. Tsao, J. Vac. Sci. Technol., **B14** (1983) 969

[Esrom-1989] H. Esrom, J. Demmy, U. Kogelschatz Chemtronics, **4** (1989) 202

[Esrom-1989] H. Esrom, U. Kogelschatz Appl. Surf. Sci., **46** (1990) 158

[Gobrecht] J. Gobrecht & M. Rossinelli J. Electrochem. Soc., **131(8)** (1984)

[Gupta] A. Gupta, G.A. West, K.W. Beeson, J. Appl. Phys., **58** (1985) 3573

[Kazor] A. Kazor, I.W. Boyd, Appl. Phys. Lett., **63** (1993) 2517,
and also
Elect. Lett., **29** (1993) 115

[Klein] A. Klein, Photonics spectra, (august 1992) 70 and 90

[Kogelschatz] U. Kogelschatz in *Process Technologies for water treatment*, ed. by S. Stucki, Plenum Publishing Corp., (1988) 87

[Kubát] P. Kubát, P. Engst, Appl. Surf. Sci, **64** (1993) 97

[Langerwerf] J.M. Langerwerf, Aerospace Medicine, **36** (June 1963)

[Masschelein] W.J. Masschelein, in *Ozonization Manual for Water and Wastewater Treatment*, J. Wiley and Sons, Chichester, (1982)

[Pidduck] A.J. Pidduck, D.J. Robbins, J.L. Glasper, I.M. Young, Conf. Publication, University College Swansea, (Jul. 1988) 410

[Preuss] S. Preuss, M. Stuke, Appl. Surf. Sci., **54** (1992) 308

[Rice] R.G. Rice, L.J. Bollyky, W.J. Lacy, in *Analytical Aspects of Ozone Treatment of Water and Wastewater*, Lewis Publishers, Chelsea, MI, (1986)

[Schroeder] H. Schroeder, Phys. of Thin Films, **5** (1969) 87

[Siegrist] T. Siegrist, D.A. Mixon, E. Coleman, T.H. Tiefel, Appl. Phys. Lett., **60** (1992) 20

[Suemitsu] M. Suemitsu, T. Kaneko, M. Miyamoto, Jpn. J. Appl. Phys., **28** (1989) 2421

[Sundgren] J.E. Sundgren, B.O. Johansson, S.E. Karlsson, Thin Sol. Films, **105** (1983) 353

[Takahashi] T. Takahashi, H. Itoh, J. Electrochem. Soc., **124** (1977) 797

[Tsao] J.Y. Tsao, R.A. Becker, D.J. Ehrlich, F.J. Leonberger, Appl. Phys. Lett., **42** (1983) 559
and J. Y. Tsao, D.J. Ehrlich, J. Chem. Phys., **81** (1984) 4620

[Wittmer] M. Wittmer, J. Vac. Sci. Technol., **A3** (1985) 1797

Chapter 4

The Photochemical Deposition and Characterisation of Silicon Dioxide Layers

The deposition of silicon dioxide SiO_2 layers from the photo-CVD technique using a xenon excimer lamp radiating at 172nm is investigated. This work was the first published application of excimer lamps to the photo-enhanced deposition of such dielectric thin films. Recently, similar subsequent publications have given evidence of the general interest this work initiated [González] [Manfredotti].

After giving details on the apparatus and the experimental arrangements, two different approaches are reported, whether the gaseous mixture uses nitrous oxide (N_2O) or oxygen (O_2) as the oxidant gas in combination with silane (SiH_4).

1.- The photo-CVD of silicon dioxide from silane and nitrous oxide gas mixtures

1.1- Experimental Conditions

1.1.1- Experimental set-up

The reactor used in these investigations has been previously presented in detail in chapter 1. Briefly, it comprises a vertical stage holder above which are fed the precursor gases. The flows are controlled by a set of mass flow controllers. The substrate may be heated up to 500°C, and its temperature is monitored via a k-type thermocouple probe. A high vacuum environment (10^{-6} mbar) is provided by a turbomolecular pump, with a subsidiary high volume rotary pump in parallel to evacuate the residual gases during experiments.

The main precursor of the photo-enhanced reaction, the Xe_2^* excimer lamp has a cylindrical shape geometry identical to the one presented in figure 2.12 (a). It comprises an annular arrangement of two concentric quartz tubes, of 20 and 30mm in diameter respectively. This leaves an annular gap of 4mm where microdischarges may occur uniformly. The total length of the lamp is of 260 mm, although only an active region of 50mm in length is used for the generation of the light. The tube is attached to the lamp chamber using vacuum tight compression flanges, similar to the fittings used on the device presented on figure 3.13. The outer ground electrode is fabricated from a metallic wire netting, grounded via the host chamber. The radiating section of the lamp is facing the magnesium fluoride MgF_2 window separating the lamp chamber from the reactor. Since the lamp emission is omnidirectional, an important quantity of photons (≈70%) is lost in the chamber, and does not intervene in the reaction. Nevertheless, since high photons intensities are accessible, the implementation of VUV reflector was not considered necessary.

An independent deionised (DI) water cooling circuitry enabling water to be passed through the lamp, and allowing the cooling of even high voltage devices in a safe

environment, was included in the system design. A quantity of about 15 litres of DI water is permanently kept in a container located below the system, from which it is raised to the lamp with a 12V DC pump. The connections between the water pipes and the lamp are of a Schott compression type, ensuring water-tight quick-release connections. There is no need for a water chiller, since it was observed that for experiments as long as two hours, the temperature of the DI water in the container increased only to 40°C. To prime the water pump, aspiration is performed on the circuit. The level of ionisation (≈10MV/cm) of the water in the tank is also regularly checked, since low levels of isolation would induce power losses in the lamp device. In practical terms, the water needs to be changed every few months, corresponding to an average of 50 hours of use. The feeding voltage of the lamp is supplied using a metallic coil passing trough the inner quartz tube, and the cooling water acts as the inner electrode due to capacitance coupling effects. Voltages between 5 to 7kV are fed to the inner electrode from an ENI® RF (100-300kHz, 150W) power supply.

Prior to each experiment, the lamp chamber is evacuated to 10^{-3}mbar, since the generated radiations would be absorbed in oxygen. By probing the radiation output, it was observed, however, that it is preferable to keep the lamp in a few hundred mbars (typically 400mbar) of nitrogen during prolonged experiments. This buffer gas is expected to act in two manners:

- to help thermal exchanges between the chamber walls and the outer electrode, and consequently to reduce over-heating,
- to increase the dielectric strength in the lamp chamber volume, and particularly in the lamp neighbourhood, between the outer quartz tube and the metallic wire mesh used as a ground electrode. In fact, the mechanical tensions of the wire mesh prevent from the existence of a uniform contact between the metal and the quartz. When the pressure is low (≤1mbar), small arcs may appear between the tube and the mesh, resulting in the progressive corrosion of the wire netting. The presence of a buffer gas in the chamber volume suppresses this problem.

Figure 4.1 shows the final experimental set-up used for silicon dioxide photo-CVD. The typical lamp powers used for prolonged experiments were ranging around 10 to 20mW/cm^2, which corresponds to 20 to 40 W input power.

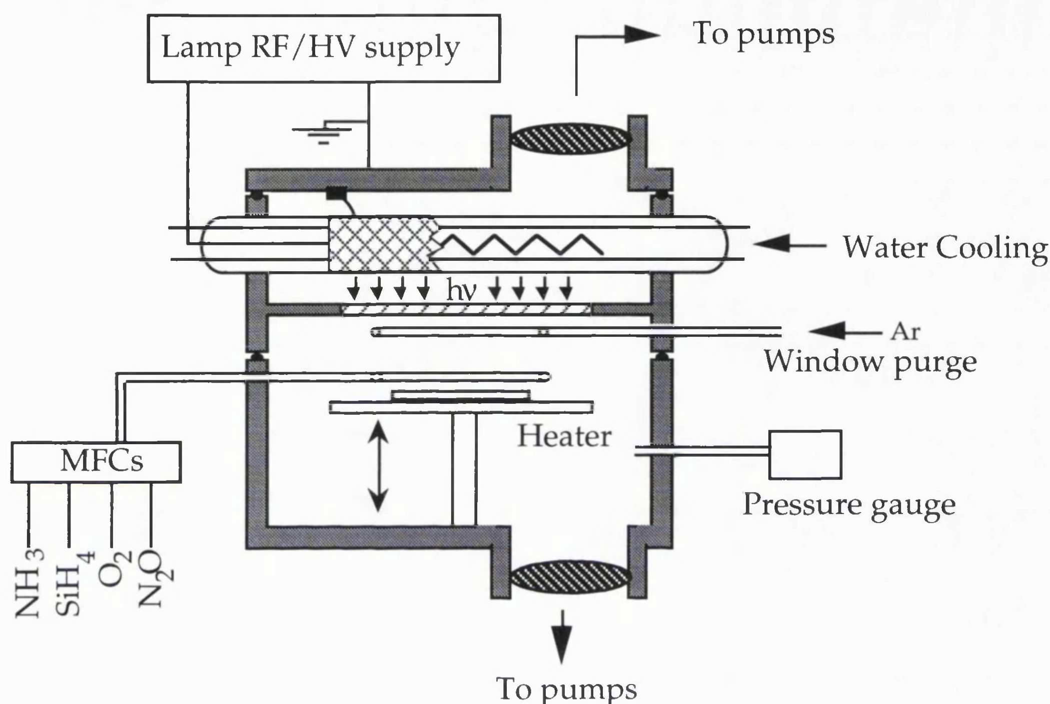

Figure 4.1: Experimental set-up for xenon excimer lamp enhanced photo-CVD experiments (only half of the wire mesh is shown).

1.1.2- Photochemistry

The VUV induced reaction scheme between SiH_4 and N_2O has previously been studied, using a low pressure mercury lamp [Petitjean-1991], or an internal nitrogen lamp [Baker]. In our case, the silane is known not to be dissociated at the wavelengths and intensities used [Itoh]. The photochemical dissociation of nitrous oxide is written as:

$$N_2O + h\nu \rightarrow N_2 + O \qquad (4.1)$$

The reactive oxygen radicals produced here will react in the gas phase with silane species, leading to SiO_2 deposition. The absorption coefficient σ of N_2O at 172nm is typically of $3 atm^{-1} cm^{-1}$ (figure 4.2) [Calvert] [Baulch] [Okabe]. This value of σ appears to be very low since only 0.3% of the incoming radiation would be absorbed by 1 cm of N_2O gas phase, when kept at a pressure of 1mbar. Figure 4.3 gives an

abacus for the determination of the cross sectional absorption for various deposition pressures and window substrate distances. To appreciate cross-sectional absorption ranging around half of the incoming radiation, the pressure and window to substrate distance d_{WS} are increased to 50mbar and 5cm respectively. Petitjean *et al.*, who studied the SiO_2 deposition from the same gas phase photolysis (SiH_4/N_2O) under the 185nm line emitted from a low pressure mercury lamp, reported the use of window to substrate distances of 12mm, at maximum deposition pressures of 12mbar. Although σ_{N_2O} shows slightly greater cross sectional values at 185nm ($4atm^{-1}cm^{-1}$), such values of the deposition parameters would surprisingly lead to very little cross sectional absorption [Petitjean-1992].

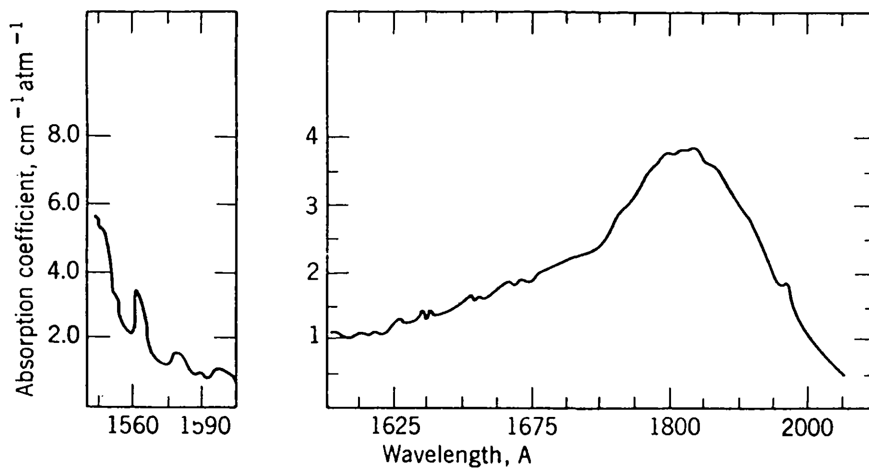

Figure 4.2 : Absorption cross section of nitrous oxide [Calvert]

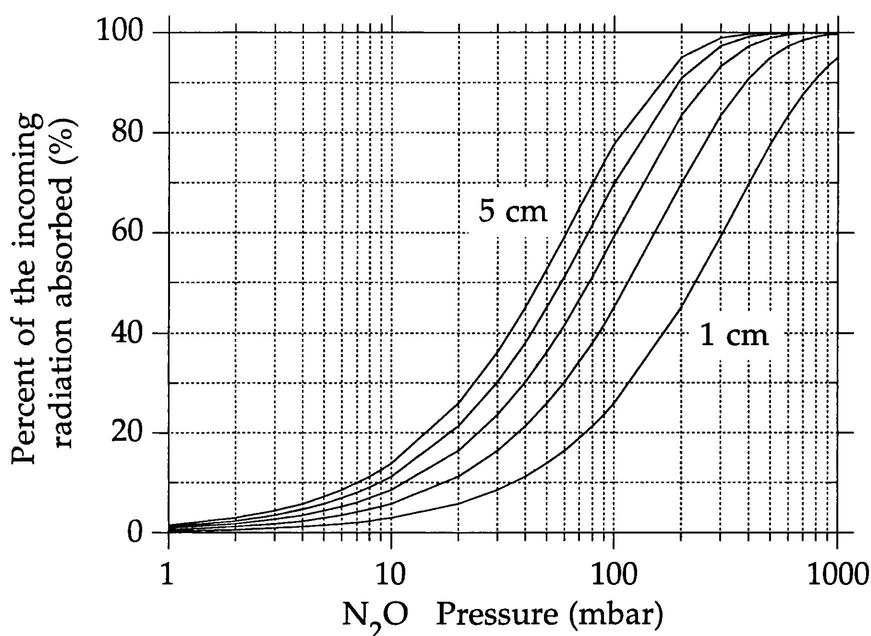

Figure 4.3 : Abacus for 172nm photons absorption in pure N_2O.
Various window-substrate distances are considered, from 1 to 5 centimetres.

To study the photochemistry induced in the reactor, here is proposed a simple growth mechanism based on that proposed by Robertson [Robertson], involving the photochemistry, the branching reactions in the gas phase, and the dissociation of products on the sample surface. Under 7.2eV irradiation, the silane is transparent, and only the nitrous oxide species undergo dissociation:

$$N_2O + h\nu \rightarrow N_2 + O \qquad (4.1)$$

Oxygen radicals react with the silane:

$$O + SiH_4 \rightarrow SiH_3 + OH \qquad (4.2)$$

$$O + SiH_4 \rightarrow SiH_2 + H_2O \qquad (4.3)$$

Although (4.2) is predominant when low pressures are used, (4.3) becomes significant above 100mbar [Petitjean-1991].

Branching reactions occur between the reactive species:

$$SiH_4 + OH \rightarrow SiH_3 + H_2O \qquad (4.4)$$

$$SiH_2 + O \rightarrow SiH_2O \qquad (4.5)$$

$$SiH_3 + O \rightarrow SiH_2O + H \qquad (4.6)$$

$$SiH_2O + O_2 \rightarrow SiH_2O_2 + O \qquad (4.7)$$

$$SiH_2O_2 + O_2 \rightarrow SiO_2 + H_2O + O \qquad (4.8)$$

SiH_2O known as silanone, is very likely to undergo rapid secondary reactions on the substrate surface [Kudo]. If a SiH_xO_y radical is absorbed onto the growing film surface, hydrogen may be incorporated into the film or may combine with oxygen and be driven off as water at high deposition temperatures. Deposited SiO_2 films, therefore, usually contain several atomic percent of H (up to 10% [Adams-1979][Hess]).

Petitjean has computed equations (4.1) to (4.8) and concluded that OH and SiH_3 are the major species which contribute to SiO_2 deposition. However, the oxygen radicals formed under (4.2) and (4.3) can also react with N_2O to form O_2 (redissociated), N_2 (non-reactive) and finally 2NO, especially at high pressures. It is acknowledged that powder formation occurs as a result of the reaction of NO radicals on SiH_3, thus promoting nuclei formation at high pressures.

1.1.3- Preliminary experiments

Deposition experiments were performed on p-type silicon samples, (100) oriented, preliminary cleaned in a propanol solution in ultrasonic bath. The processing chamber was evacuated to 10^{-6} mbar prior to deposition. Mixtures of 0.5 to 10% SiH_4 in N_2O were introduced into the chamber at a constant total flow of 40sccm. The samples were characterised using FTIR spectroscopy, while thickness measurements were carried out using a Rudolf AutoEl ellipsometer at 632.8nm. Exposure times from 10 minutes to a maximum of 30 minutes were investigated. The films obtained were scratch resistant and adherent (Moh's hardness between 6 and 7).

The first experiment was carried out to control the absence of pyrolytic growth. Setting the substrate temperature at values up to 400°C, it was found that no measurable layer could be detected. The pyrolytic dissociation of the precursors does not occur at those temperatures.

The second experiment consisted of the study at constant parameters of the evolution of the thickness of the grown layer with the duration of the experiment. No decrease of the growth rate with time was observed for times up to 2 hours (≈0.1μm deposited thickness). This attests the absence of any significant absorption by the products deposited on the magnesium fluoride window. A similar observation has been reported by Petitjean, depositing SiO_2 from the same precursors using 185nm photons [Petitjean-1991]. This dispenses with the use of an elaborate window purging set-up. It is a great technological advantage, since the window fogging problem has often been reported as the ultimate restriction to the popular acceptance of photo-CVD.

1.2- Results and discussion

1.2.1- Optimisation of the deposition parameters

• Window-substrate distance and total pressure

Since very little absorption is observed in the gas phase, there is a need to increase the window substrate distance to a high value, typically 5cm. In that case, and with pressures ranging around 50mbar, the absorption by N_2O of the incident radiation is about 50% (figure 4.3).

The deposition rates are extremely low for pressures below 100mbar. In contrast, at pressures exceeding 150 mbar, powders were formed as a consequence of secondary gas phase reactions being stimulated, leading to radical recombination and polysiloxane formation [Kamaratos]. Those films were opalescent and very scratch sensitive. Since this is detrimental to the film quality, intermediate pressures are chosen, typically from 100 to 130mbar.

• Light intensity

Figure 4.4 shows the variation of the deposition rate at 300°C with input light power (40W input power corresponds to ≈ 20mW/cm^2). It clearly shows that thermal deposition of SiO_2 is insignificant within the operating conditions. Since a constant precursor flow is used in this experiment, an attenuation of the growth rate increase is observed while increasing the lamp power, consequence of the limitation of the diffusion of photoproducts and reactants to the substrate surface.

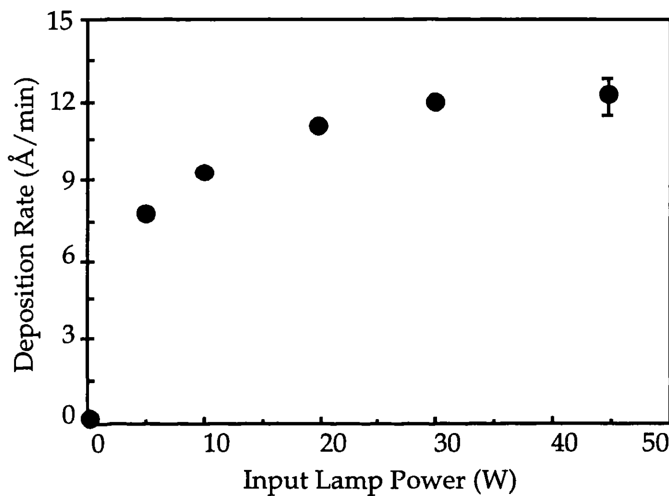

Figure 4.4 : Evolution of the deposition rate for silicon dioxide samples with light exposure (Substrate temperature is 300°C)

• SiH_4/N_2O precursor ratio R

Figure 4.5 shows the variation of the deposition rate with R, the SiH_4/N_2O ratio. For R<1%, the growth rate is limited by the silane concentration. For R>2% nucleation reactions are promoted in the gas phase, limiting film deposition. The decrease of the growth rate can mainly be attributed to a decrease in the SiH_3 species concentration which are able to react with O species, since some are reacting with NO species. High values of R may lead to the deposition on the window of materials which have higher absorption to the incoming radiation (e.g., SiO_xN_y or SiO_xH_y), thus further reducing the growth rate. Figure 4.6 shows the refractive index (n)

evolution as a function of R. Optimised values of 1-2% for R lead to films presenting the 1.462 theoretical value for n in SiO_2. For higher R values, higher values of n are observed, reflecting an increase in either H or N incorporation.

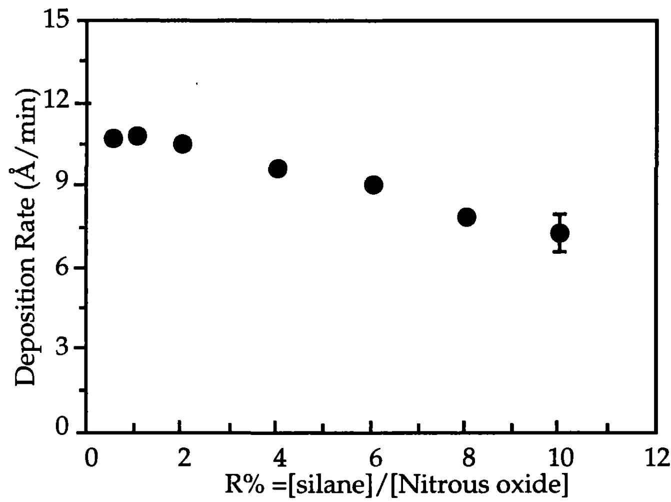

Figure 4.5 : Evolution of the deposition rate vs. precursor mixture ratio (P= 100mbar, T=300°C)

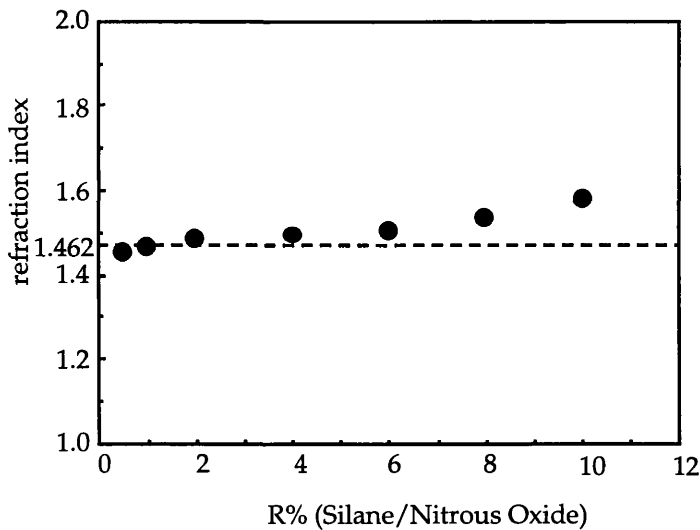

Figure 4.6 : Evolution of the refractive index with the precursor mixture ratio (P=100mbar, T=300°C)

• Substrate temperature

Figure 4.7 shows an Arrhenius plot of the growth rate. An activation energy of 0.25eV is extrapolated from those data. Purely pyrolytic reactions give activation energies in the range 0.42eV to 0.95eV [Cobianu] [Vasilyeva] [Taft]. The very low value obtained gives evidence of the reduced importance of the substrate temperature and therefore of a less dominant role of thermally induced surface reactions. The modified chemical pathways induced by the photons clearly enable lower substrate temperatures to be used. No significant variation of the refractive index was observed for temperatures varying from 200 to 400°C.

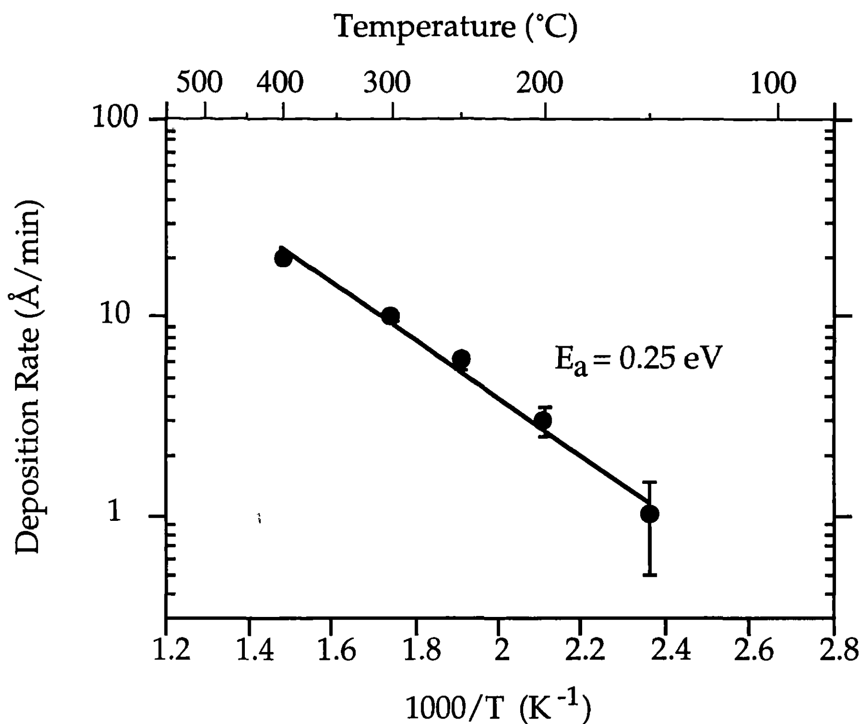

Figure 4.7 : Arrhenius plot for the growth of SiO_2 from SiH_4 and N_2O mixtures.

1.2.1- FTIR spectroscopy

The structural properties of the films were characterised by their vibrational spectra using FTIR spectrometry. Figure 4.8 shows a FTIR spectrum of an oxide film photo-deposited at a substrate temperature of 300°C. The spectrum consists of three characteristic peaks at $1065cm^{-1}$ (Si-O-Si stretching), $800cm^{-1}$ (O-Si-O bending), and $480cm^{-1}$ (Si-O-Si rocking) [Boyd-1982] [Lucovsky]. The full width half maximum (FWHM) for the dominant IR mode around $1065cm^{-1}$ has a value of $70cm^{-1}$, characteristic of a stoichiometric SiO_2, and remains essentially the same for all the oxides studied. The small peak centred around $885cm^{-1}$ can be attributed either to Si-H, Si-OH, Si_2O_3 or to non bridging oxygen [Boyd, 1982-b]. It is most likely the reflection of a few percent of hydrogen in the film, due to the incomplete desorption of H species at low temperatures. However, the presence of Si-H and Si-OH bonds in concentrations higher than 5% would have led to the presence of other peaks centred around $2270cm^{-1}$ and $3620cm^{-1}$, which were not observed.

The absorption spectra of figures 4.9-a and 4.9-b show that the quality of the film is not significantly affected by either lamp power or precursor mixture ratio used. These parameter however affect the deposition rate more appreciably (e.g., 6Å/min for R=10%).

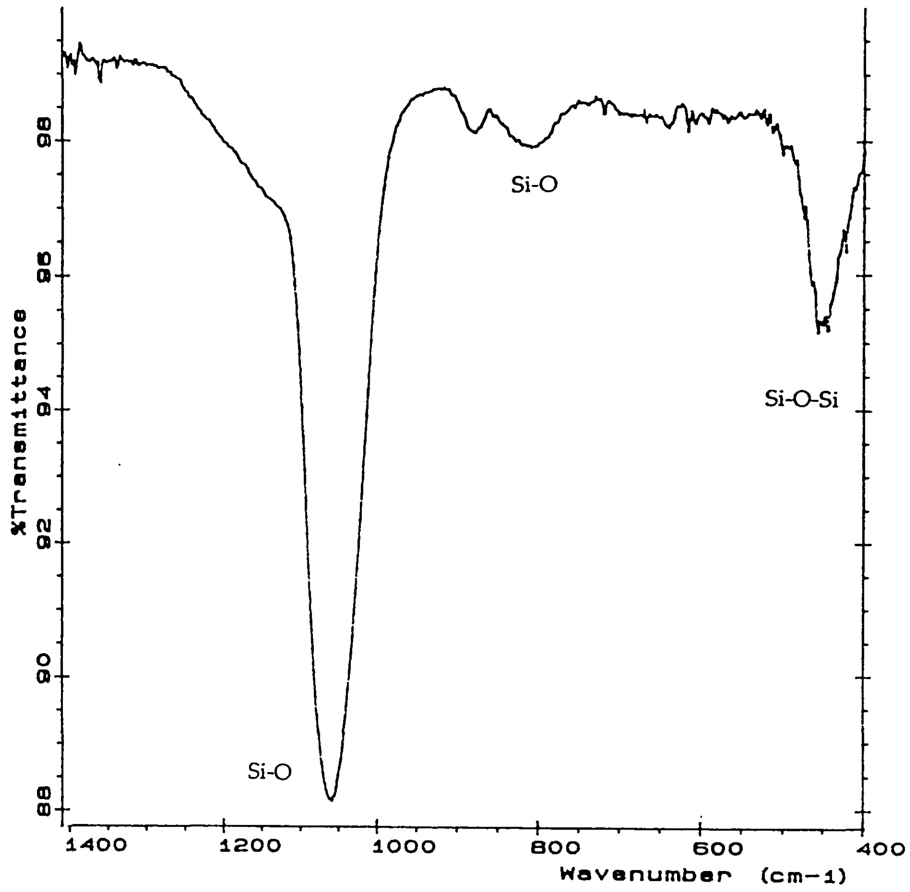

Figure 4.8 : FTIR spectrum of a 400Å SiO_2 film deposited at 300°C

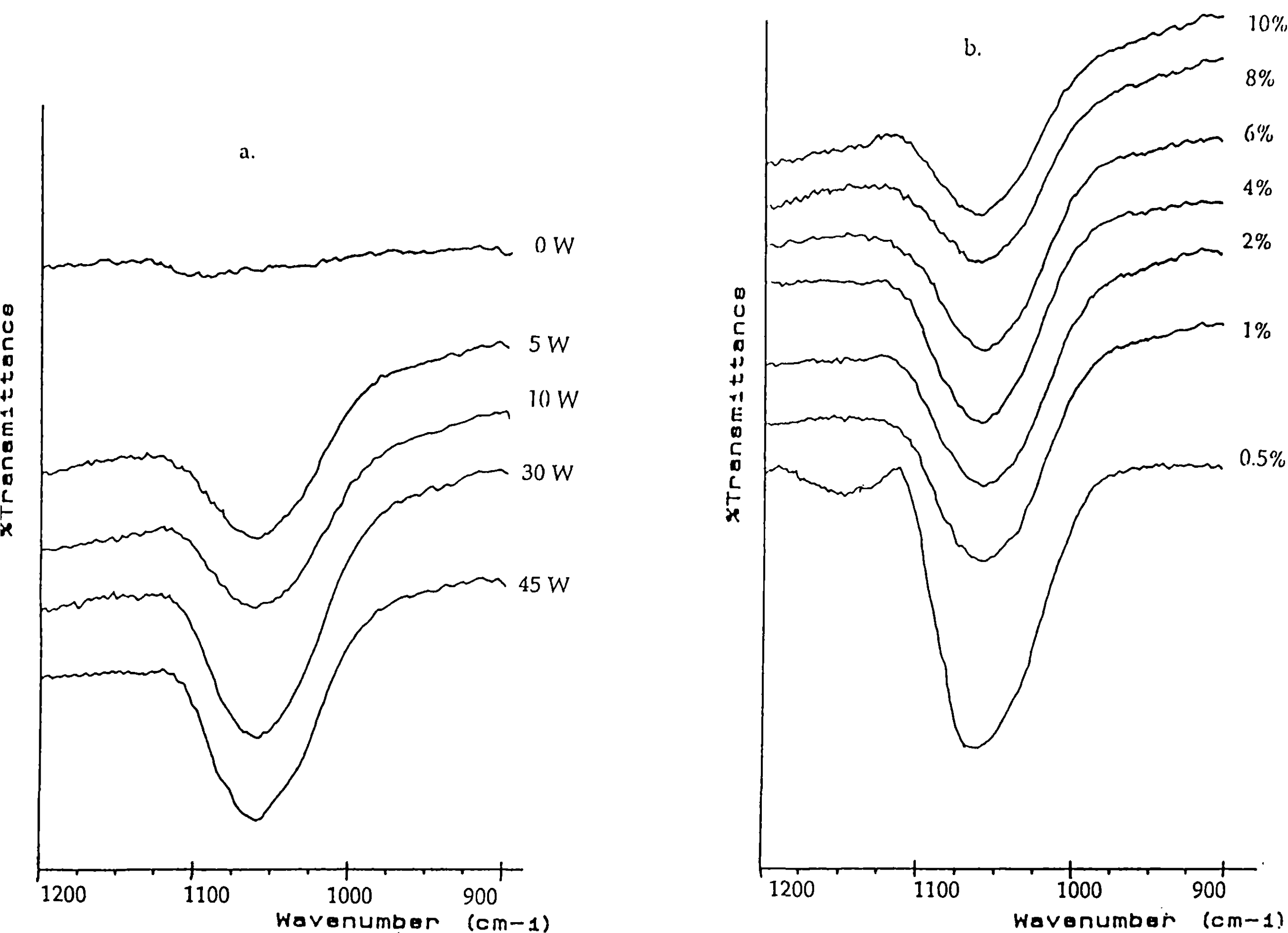

Figure 4.9: Sets of FTIR spectra of the 1065cm^{-1} peak for various a-lamp power input, b-precursor mixture ratio R.

1.2.3- Film properties

Film properties were investigated on p-type silicon samples, exhibiting a resistivity ρ ≈10 Ω.cm. For each sample, the value E_b of the electrical breakdown field was estimated as an average of the measured values on N devices (N≥10). Typical E_b values were measured around 5 MV/cm, although lower values have been obtained for samples deposited at elevated pressures, or at temperatures below 200°C. Values as high as 8 MV/cm were obtained on some devices, although several dots exhibited a

very low E_b value, consequently strongly reducing the averaged values. This was assumed to be due to particle contamination of the substrates in the laboratory, which is not a clean room facility. This contamination is further affecting the measurements on the very thin films studied. Figure 4.10 gives the evolution of the breakdown field when the precursor mixture ratio R is increased from 1 to 10%.

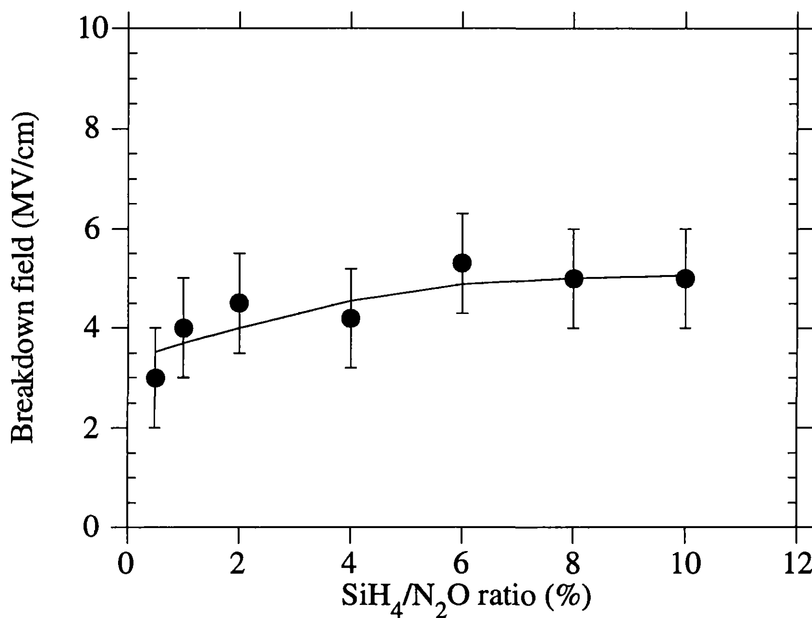

Figure 4.10 : Evolution of E_b with precursor ratio R

As can be seen, although high R ratios were the cause of high N incorporation, which was reflected by high refractive indices, the breakdown field does not appear to be altered, since no particular decrease of the electrical properties would be expected from SiO_xN_y layers (y « x).

Capacitance-Voltage (CV) measurements also revealed that the typical surface state charges were ranging around 10^{11}-10^{12} cm^{-2}, value which appears to be high comparatively with other conventionally deposited SiO_2 films ($10^{10}cm^{-2}$). This may

be caused by the absence of native oxide cleaning prior to deposition, thus resulting in a high number of interface traps between the silicon substrate and the native oxide, as well as between the native oxide and the deposited layer.

Etch rates measurements were finally performed on the silicon dioxide layers, using a buffered hydrofluoric acid solution, diluted in water at a concentration of $1 mol.l^{-1}$. Typical values of 25Å/s were obtained, to be compared with 16Å/s, characteristic etch rate for thermally grown silicon dioxide [Sze]. This is a much lower value than typically reported for CVD grown oxides (e.g., 50Å/s in HF, $0.25 mol.l^{-1}$ by Adams *et al.* using PECVD [Adams-1983], and ≈80Å/s in HF, $3 mol.l^{-1}$ for films deposited at 300°C by Boyer *et al.* with laser CVD [Boyer]).

1.3- Conclusion

The low etch rates of the films reveal that they can be used *as grown* as thin films for barrier layers, and to protect and passivate any type of surface. Further sample cleaning prior to deposition, using chemical or in-situ etching, would also benefit towards applications as gate oxides. The method has successfully been extended to other substrate materials such as quartz and gallium arsenide.

Table 4.1 summarises the growth parameters and properties for the SiO_2 films obtained in this 172nm photo-CVD process. This work consisted the first use of an excimer lamp to the direct photo-deposition of silicon dioxide from silane and nitrous oxide mixtures. The deposition rates achieved on this unoptimised system are comparable with those obtained with low pressure mercury lamps. The thicknesses of the layers deposited were constant within a few percent over the 4 cm^2 surfaces studied. This technique of depositing SiO_2 film, in a xenon excimer assisted process, can then compete with the other existing techniques of the day. The results indicate promising further applications of such lamps towards semiconductor and optoelectronic material processing. As mentioned in the introduction to this chapter, other groups have now concentrated on a similar technique based on a xenon excimer lamp to deposit thin SiO_2 films [González] [Manfredotti]. To date, however, only Gonzáles *et al.* seem to have been successful, although they reported films exhibiting lower growth rates (8Å/min), as well as higher FWHM (76-82cm^{-1}).

SiO_2 from SiH_4/N_2O	
Initiated photo-dissociation at 172 nm	$N_2O + h\nu \rightarrow NO + O$ $\sigma = 2\ atm^{-1}cm^{-1}$
Deposition Conditions	100 mbar < P < 130 mbar 200°C < T <300°C 1% < R= SiH_4/N_2O < 2% F_{tot}= 40 sccm Window-Subst. Dist.= 50 mm
Deposition Properties	12-15 Å/min n = 1.46
FTIR	Si-O stretch at 1065 cm^{-1} FWHM = 70 cm^{-1}
Electrical Properties	E_b= 5 MV/cm Q_{ss}= $10^{11}$to $10^{12}cm^{-2}$

Table 4.1 : Summary of SiO_2 deposition conditions and essential properties obtained from the photo-CVD of SiH_4/N_2O mixtures

2.- The photo-CVD of silicon dioxide from silane and oxygen gas mixtures

2.1- Introduction

In the previous section have been reported the use of novel excimer lamps that provide a new route to growing SiO_2 layers using mixtures of silane and nitrous oxide. Several groups have previously reported the use of ultraviolet lasers [Boyer] [Szörényi] and lamps [Petitjean-1991] [Patel] to induce the required photo-CVD heterogeneous reactions that encourage thin film growth. However, the layers grown with an acceptable quality at low temperatures have been obtained using SiH_4 and N_2O precursor mixtures, from processes which exhibit generally slow growth rates (20Å/min) [Petitjean-1990] [Bergonzo]. So far, using such a gas mixture, growth rates reaching 100Å/min have only been reported from techniques based on windowless lamps [Marks] [Baker] [Robertson]. Despite these excellent results, internal lamp technologies seem not to have been extensively developed, probably since a potential disadvantage of this approach is that the plasma generating the VUV radiation is not insulated from the thin film precursors.

Here is extended the xenon excimer lamp deposition technique to different gas mixtures, namely silane and molecular oxygen, to produce growth rates of high quality silicon dioxide, which are some 40 times faster than previously achieved using N_2O, and also some 200% faster than using either low temperature CVD or traditional optical sources [Bennett] [Inoue] [Okuyama]. When gas mixtures of silane and oxygen are used, the high reactivity between those precursors allows far higher growth rates (up to 100s of Å/min), but the film quality is generally affected at low temperatures, resulting in poor film properties. The deposition of silica films by low pressure pyrolysis of silane in oxygen is a routine process in the semiconductor technology. Layers of this type are commonly used as interconnect insulators and for device passivation in MOS circuit fabrication, as well as for packaging of completed microcircuits to provide mechanical and chemical protection. However, purely pyrolytic films generally show very poor properties when deposited at temperatures below 500°C. High etch rates in buffered hydrofluoric acid (e.g., 50Å/s at

0.25mol.l^{-1}) and low electrical breakdown field characteristics (e.g., 5 MV/cm) are often found, as well as a high hydrogen content (typically up to 10%) [Adams-1983] [Weber] [Liehr] [Kawahara]. Here is showed that the use of 172nm photons in the deposition reaction allows improved film properties to be obtained at temperatures as low as 200°C, rendering this technique highly compatible with the low thermal budget material processing philosophy.

2.2- Experimental details and sample preparation

2.2.1- Safety

The highly explosive nature of silane and oxygen mixtures has been recognised since the pioneering work of Freidel and Ladenburg in 1867 [Friedel]. Emeléus and Stewart also reported in 1936 that the ignition of such a mixture could be enhanced by ultraviolet light. However, it is almost impossible to find coherent and complete literature data from those days. It is only recently that Hartman et al. reported precisely the aspects of SiH_4-O_2 explosions in terms of gas mixture ratios and pressures [Hartman]. In summary, SiH_4/O_2 mixtures are pyrophoric in the range 30/70% to 95/5%. For the present experiments, only mixtures containing a few percent of silane in oxygen are considered, thus far below the 30/70% range. Furthermore, the minimum pressures required to ignite this 30/70% mixture is reported above 250mbar, far above the range of interest. Pure silane with diluted oxygen in argon (15%) is used, with ratios of silane in oxygen ranging from 1 to 10%, and pressures kept below 12mbar. Stoichiometric explosive mixtures in this range are therefore definitely precluded.

2.2.2- Photochemistry

Under the 7.2eV photon irradiation, the silane is transparent to the radiation and therefore not photo-dissociated. O_2, however, undergoes dissociation into oxygen radicals, with an absorption cross section σ of 20atm^{-1}cm^{-1} (assuming that the emitted continuum centred at 172nm is restricted to this wavelength) [Calvert].

$$O_2 + h\nu \rightarrow O + O \qquad (4.9)$$

In addition to an increased reactivity of oxygen species towards the reaction with silane, the high absorption cross section σ of oxygen allows far lower pressures to be used than for the case of nitrous oxide. Figure 4.11 shows an abacus where the percentage of the incoming 172nm radiation traversing oxygen is plotted as a function of the pressure.

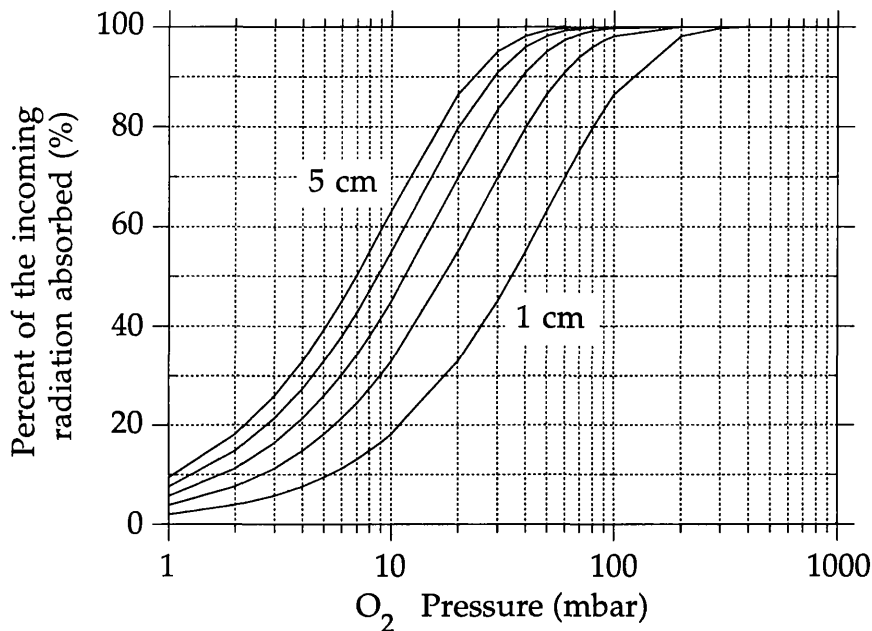

Figure 4.11 : Abacus for 172nm photon absorption in pure oxygen. Various window substrates distances are considered, from 1 to 5 cm.

The reaction of oxygen radicals with molecular oxygen also produces ozone (O_3) which has a longer life time than the atomic radical (≈4.10^{-2}s for O_3, compare with 7.10^{-8}s for $O(^1D)$ in N_2O at 10 mbar and 25°C [Baulch]).

$$O + O_2 + M \rightarrow O_3 + M \qquad (4.10) \text{ or } (3.2)$$

$$O_3 \rightarrow O + O_2 \qquad (4.11)$$

$$O_3 + O_2 \rightarrow O + 2\,O_2 \qquad (4.12)$$

Ozone thermally dissociates at temperatures higher than 50°C via (4.11) [Coste] [Wen], and with molecular oxygen (4.12) [Aiken], and therefore in this scheme acts as a long term source of oxygen radicals [Kazor]. Because of the elevated temperature of the substrate, ozone will be dissociated in its close neighbourhood, thus releasing oxygen radicals on the sample surface. This feature is limited when a similar photochemistry is initiated by a low pressure mercury lamp, since the ozone is also strongly dissociated in the gas phase by the 254 nm radiation.

The active oxygen radicals formed strongly react with silane causing its dissociation through a series of reactions, leading to the formation of SiO_xH_y nuclei [Robertson] [Petitjean-1991]:

$$SiH_4 + O \rightarrow SiH_3 + OH \qquad (4.13)$$

$$SiH_4 + OH \rightarrow SiH_3 + H_2O \qquad (4.14)$$

$$SiH_3 + O \rightarrow SiH_2 + OH \qquad (4.15)$$

$$SiH_3 + OH \rightarrow SiH_2 + H_2O \qquad (4.16)$$

$$SiH_3 + SiH_3 \rightarrow \text{products} \qquad (4.17)$$

$$SiH_2 + O \rightarrow SiHOH \qquad (4.18)$$

$$SiH_2O + O_2 \rightarrow SiH_2O_2 + O \qquad (4.19)$$

$$SiH_2O_2 + O \rightarrow SiO_2 + H_2O \qquad (4.20)$$

Of the products formed in (4.17) through (4.12) to (4.19), SiHOH (silanone) is known to undergo rapid secondary reactions on the substrate [Kudo] [Giunta].

2.2.3- Experimental apparatus

The system used is as described in § 1.1.1 of this chapter for SiH_4/N_2O experiments (figure 4.1). The window to substrate distance, however, is reduced as discussed in the next section. The samples used were 1" diameter, crystalline p-type silicon (100), and irradiated typically for up to 5 minutes. The dilution ratios and the total pressure inside the reactor are optimised for rapid deposition of SiO_2 films, with values of refractive index close to those expected for typical thermal oxide layers (n=1.46).

2.2.4- Sample preparation and preliminary experiments

Prior to deposition, the samples were cleaned in a propanol solution in an ultrasonic bath. The processing chamber was evacuated to 10^{-6} mbar prior to deposition. As a first experiment, and to confirm the hypothesis submitted in § 1.1.3, which asserted that the absorption of the photons by the layer deposited on the window is insignificant at this wavelength, the evolution of the deposited thickness with time was studied. In fact, as the growth rates achieved with the present precursor mixture give values around 40 times higher than in the N_2O experiments, such thicknesses would more severely affect the window fogging. For deposition times as long as 15 minutes, corresponding to thicknesses around 0.5μm, the evolution of the growth rate was still not showing any attenuation with time. There is no absorption of the 172nm photons by the films deposited on the window, and still no need for elaborate window cleaning procedures.

The window to substrate distance was varied from 20mm down to 12mm, the minimum distance allowed by the system configuration. No significant difference in the film thicknesses was observed for those values. However, since the gas phase reactions are here supposed to be very reactive, there is an interest in reducing the window to substrate distance to a minimum, in order to keep the heated substrate as close as possible to the newly generated species. A distance of 12mm is adopted.

One resulting experimental artefact from the use of a short window to substrate distance is the heavy photon bombardment on the substrate surface (≈70% of the incoming radiation at 10mbar, figure 4.11). The effect of the substrate surface irradiation on the growth characteristics was therefore investigated. In separate experiments, a portion of the substrate was masked from direct UV exposure (care was taken not to modify the gas flows with the mask). No significant difference was observed between the shadowed and irradiated surfaces, in terms of growth rates, refractive indices, or FTIR characteristics.

2.3- Results and discussion

2.3.1-Activation energy

Prior to illumination, pyrolytic depositions were performed at various temperatures. As can be seen in figure 4.12, a very strong decrease in the growth rate is observed as the substrate temperature is reduced below 400°C. An activation energy of 0.6eV was extrapolated from these data, which agrees well with other reported pyrolytic work in cold wall reactors (0.42eV- 0.95eV) [Cobianu] [Vasilyeva] [Taft]. The average temperature increase of the gas phase species due to the proximity of the hot substrate was measured to be around 100°C for the highest pressures used (10mbar). This temperature is known to be too low to induce any significant thermal dissociation in the gas phase, indicating that the growth mechanism is entirely promoted by surface reactions [Bennett].

Under otherwise identical conditions, but with illumination at an intensity of 20mW/cm^2 with 7.2eV radiation, the new deposition rate of the films deposited was measured as a function of the substrate temperature. The data, also plotted in figure 4.12, clearly reveals a modified activation energy of 0.13eV. This is much lower than the 0.6eV value obtained for the purely pyrolytic reaction, providing evidence for the reduced importance of substrate temperature under these conditions and therefore a less dominant role of thermally induced surface reactions. The modified chemical pathways induced by the photons clearly enable lower substrate temperatures to be used.

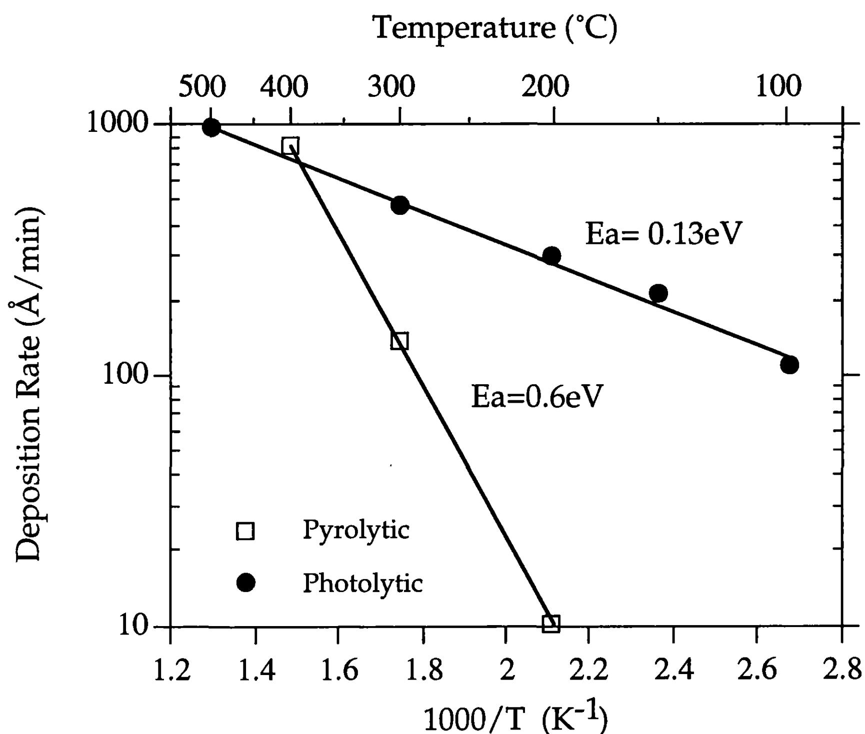

Figure 4.12: Arrhenius plot of the growth rate of pyrolytically and photolytically enhanced deposition of SiO_2 ($SiH_4 : O_2 : Ar = 1 : 10 : 55$, P= 10 mbar).

2.3.2- FTIR Spectroscopy

Fourier Transform Infrared (FTIR) spectroscopy measurements were carried out on the UV-deposited films using a Perkin Elmer 2000 spectrometer. A spectrum of a typical 200nm layer deposited in 5 minutes is shown in figure 4.13. The small absorption peak visible around 880cm^{-1} reveals the presence of a few percent of hydrogen impurities bonded as Si-H within the deposited film [Taft]. No additional absorption peaks were observed in the higher wavenumber ranges, particularly between 2000cm^{-1} and 2300cm^{-1}, the region which is reportedly associated with the presence of a high percentage (i.e., $\geq 5\%$) of Si-H [Tsu]. The characteristic Si-O-Si stretching, bending and rocking vibration modes, representative of stoichiometric SiO_2, are visible at 1065, 810 and 460cm^{-1} respectively [Boyd-1982]. The stretching vibration mode has a full width half maximum (FWHM) value in this case

of 75cm^{-1}, which agrees well with published data for thermally grown SiO_2 (70cm^{-1}) [Boyd-1987] and is lower than that for thermally deposited SiO_2 (85 cm^{-1}) from the same gas mixtures [Kawahara]. As will be discussed later, the hydrogen incorporation can be significantly minimised by fine adjustment of the deposition conditions.

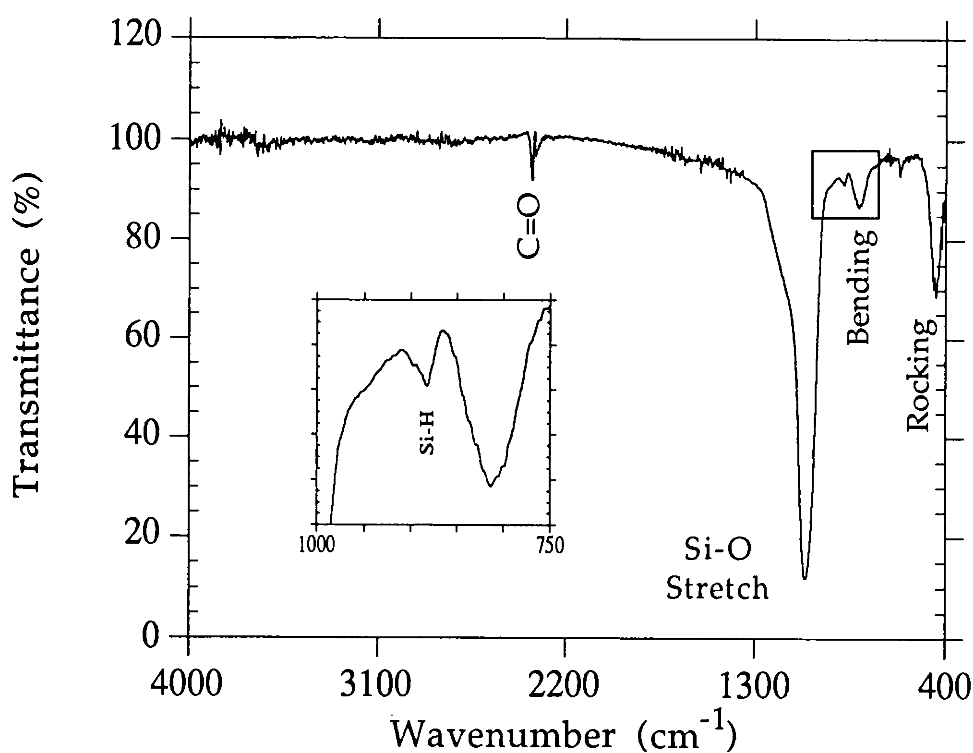

Figure 4.13 : FTIR Spectrum of a 200nm SiO_2 layer deposited in 5min at 300°C at a total pressure of 10mbar and flows of $SiH_4/O_2/Ar$ at 0.7/10/55 sccm respectively.

2.3.3- Optimisation of the deposition parameters

• SiH_4/O_2 precursor ratio R

Figure 4.14 shows the influence of the silane to oxygen precursor mixture ratio (R), on the deposition rate and refractive index of the deposited films. Very small differences in the silane to oxygen concentration are seen to strongly affect the deposition rate. Changes in the film properties are observed for high values of the precursor mixture R, as is reflected by a significant increase in both the refractive index and the amount of hydrogen incorporated (figure 4.15).

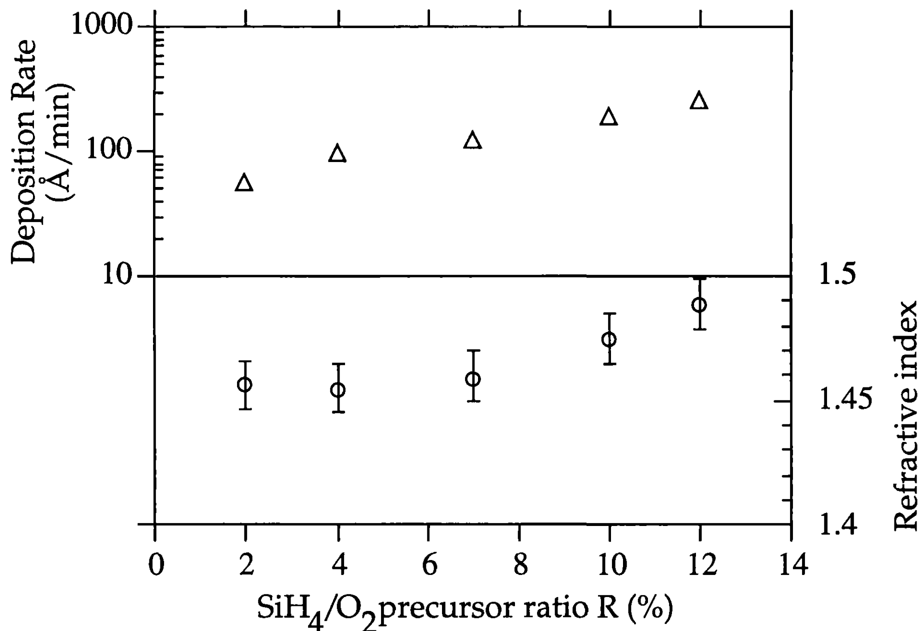

Figure 4.14 : Deposition rate and refractive index of layers deposited for various precursor ratios R (P= 7mbar, T= 200°C).

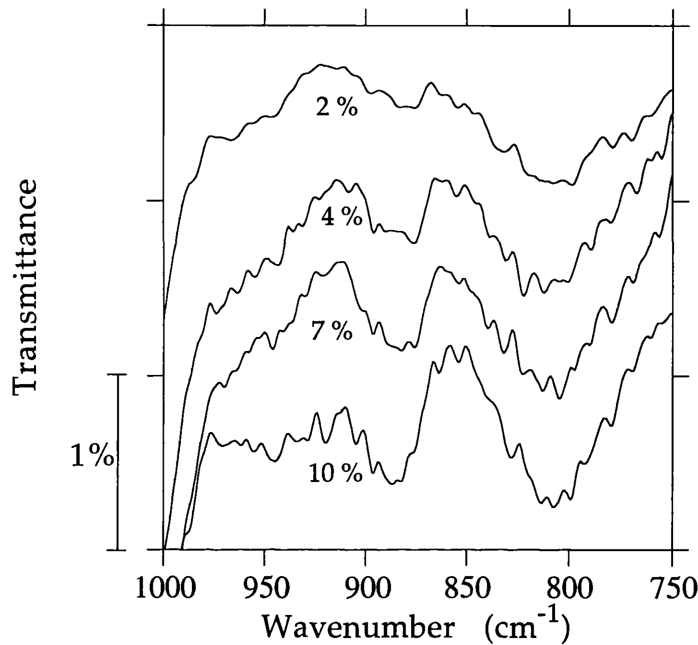

Figure 4.15 : Detail of the 880cm^{-1} vibrational absorption for several ratios of SiH_4/O_2.

• Total pressure

The effect of the total deposition pressure on the film deposition was studied for a constant total gas flow (60sccm). Figure 4.16, for example, shows that growth rates of 400Å/min can be achieved at 10mbar at only 200°C. Films up to 2000Å may be grown in only 5 minutes under these conditions. However, the figure also reveals that these layers exhibit low refractive index values, indicating high film porosity. This was confirmed by the measurement of high etch rates in buffered hydrofluoric acid (up to 60Å/s in buffered HF, 1mol.l^{-1}), and larger FWHM values (110cm^{-1}) at 1065cm^{-1}.

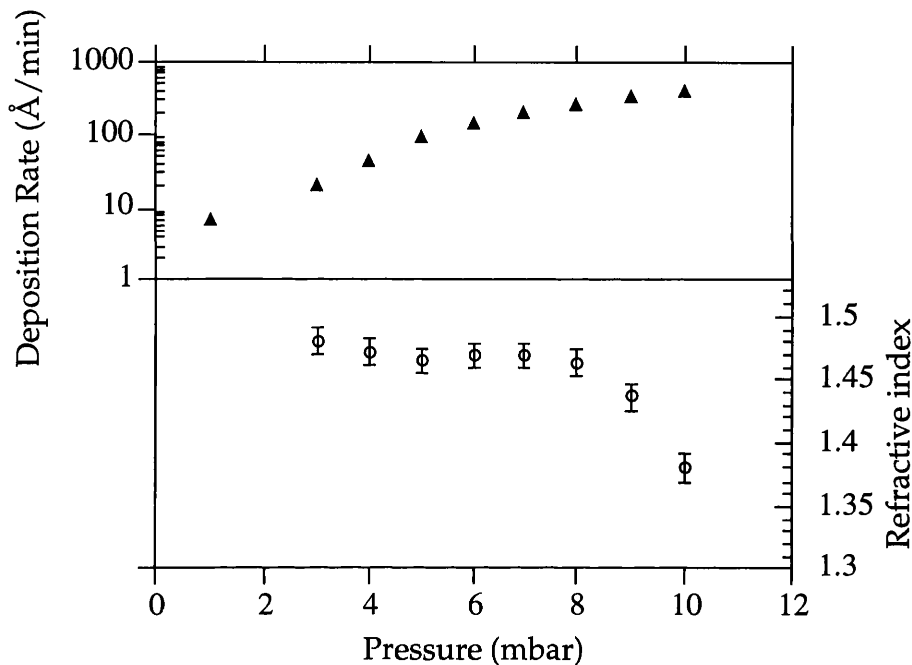

Figure 4.16 : Effect of pressure on the deposition rate and refractive index. (R=10%, T= 200°C).

Figure 4.17 shows the evolution of the normalised Si-H vibration mode at 880cm^{-1} as a function of pressure. The presence of the broad peak at the higher pressures confirms the existence of a significant amount of bonded hydrogen (≈ 10% at 10mbar) within the layers grown. This feature is strongly diminished when the processing pressure is reduced. Higher pressures generally lead to an increased rate of gas phase collisions. Thus more efficient gas phase nucleation will occur, which in turn will lead to larger-sized products reaching the substrate. These nuclei, however, will not be fully dissociated on the sample surface, since the growth temperatures used are not high enough to provide sufficient energy for the process to occur efficiently. This effect highlights the very high importance of gas phase processes in the deposition mechanism. Also, when the working pressure is increased from 5 to 10mbar, the photon flux reaching the substrate drops from 90% to 80% of the 20mW/cm^2 radiation. However, since in earlier experiments the

insignificant effect of UV irradiation on the substrate was investigated, this indirect effect of increased pressures should not be taken as a cause of the modification of the properties observed. It can then be concluded that the final step of the silanone dissociation may only significantly be influenced by the surface temperature of the substrate.

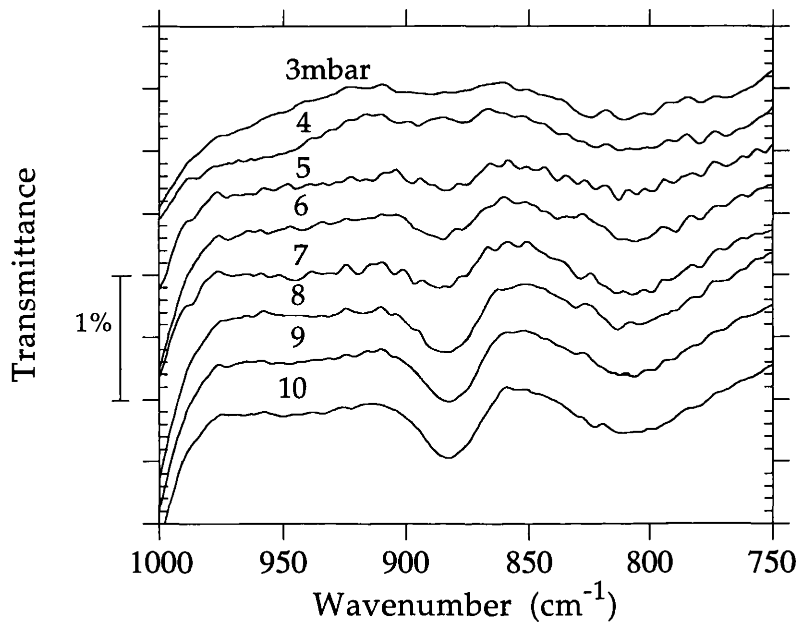

Figure 4.17 : Detail of the 880cm^{-1} vibrational absorption of films grown at different pressures with T= 200°C.

• Substrate temperature

The influence of the substrate temperature on the characteristics of the films grown was also studied and figure 4.18 shows its effect on the deposition rate and refractive index of layers deposited at pressures of 5 and 10mbar. For both pressures, as the temperature is increased, higher deposition rates are obtained, and refractive indices approach those for stoichiometric SiO_2 values. At 10mbar, generally lower refractive

index values and hence more porous films are obtained. Following the preceding hypothesis attesting that a higher pressure promotes gas phase nucleation, it is observed that an increased temperature is needed to dissociate the nuclei formed. Therefore, high quality films can also be produced at very low temperatures by using low processing pressures. One must balance this attractive proposition against a much decreased growth rate.

Figure 4.19 shows the effect of the substrate temperature on the normalised 880cm^{-1} Si-H vibration mode for layers deposited at 10mbar. Very low substrate temperatures clearly lead to high H incorporation due to the limitation of the nuclei dissociation kinetics on the sample surface and confirms the importance of the temperature in promoting the necessary surface reactions.

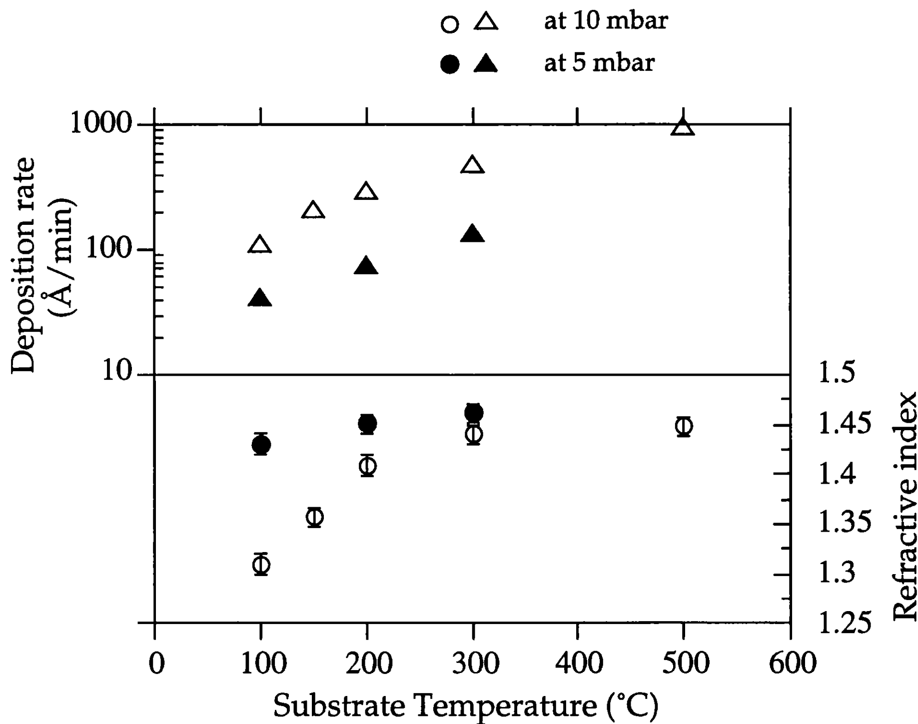

Figure 4.18 : Deposition rate and refractive index of films grown at different substrate temperatures at 10 mbar (open) and 5mbar (closed) for R=7%.

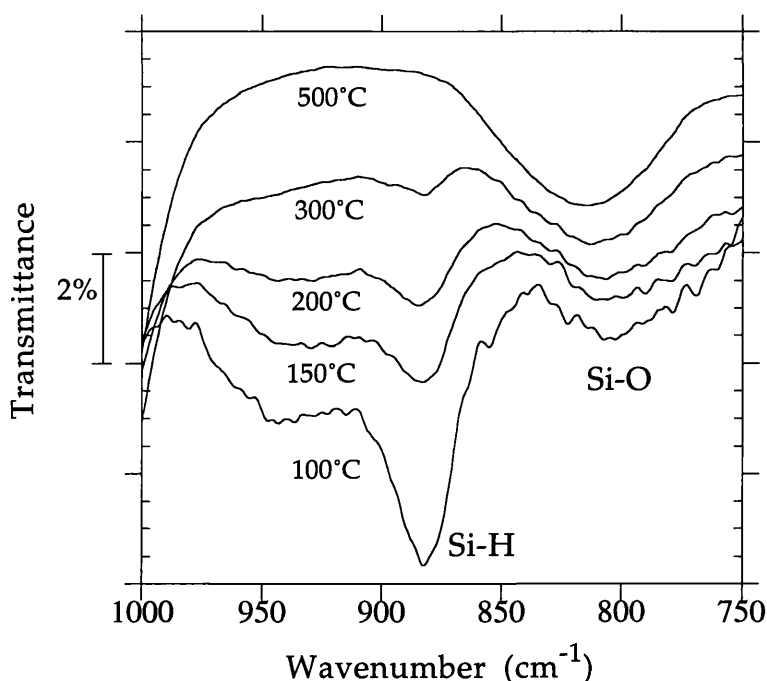

Figure 4.19: Comparison of the 880cm^{-1} vibrational peaks for films grown between 100°C and 500°C at a pressure of 10mbar.

2.3.4- Annealings

To study the form of the incorporated hydrogen, films grown at 200°C were annealed in wet N_2 at temperatures of 300°C for a period of three hours. Figure 4.20 shows that there is very little change in the overall FTIR spectra with respect to the contributions of the Si-O bonding. However, a particularly dramatic reduction of the Si-H peak located at 880cm^{-1} is apparent. A resulting small decrease in the film thickness (≈5%) and an increase of the refractive index (1.40 to 1.45) are also observed. This is explained by an onset of densification of the annealed film, and the release of weakly bonded H from within the oxide [Eagle] [Lan], although Lucovsky *et al.* have suggested that similar modifications of the Si-H vibration mode could also be the result of silica network modifications [Lucovsky].

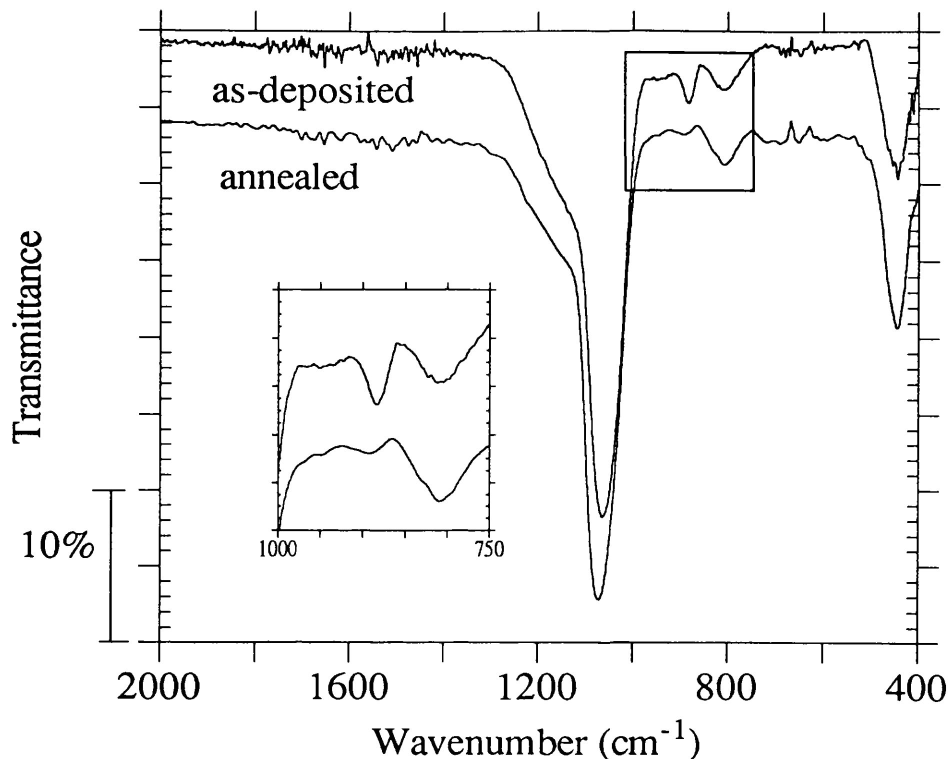

Figure 4.20: Effect of a 3 hour anneal at 300°C on a 200nm film grown at 10mbar.

2.3.5- Electrical characterisation

The SiO_2 layers were characterised electrically on MOS capacitors obtained by evaporating aluminium dots. The substrates used were p-type silicon ($\rho \approx 10\Omega$.cm). The breakdown voltages were measured by ramping a DC voltage applied on the device towards negative values. Since the sample thicknesses were relatively thick, (around 0.1μm), high bias voltages were used, up to the maximum value of 100V of the IV tester. Although most breakdowns were recorded around 60 to 80V (6-8MV/cm), some devices did not breakdown at 100V (>10MV/cm). The dielectric strength of those films seems therefore to be surprisingly very high, almost as high as thermally grown oxides. High frequency capacitance-voltage measurements were also performed, and revealed high Q_{ss} values (10^{12}cm^{-2}), probably due to particle contamination, since the substrates were not etched prior to deposition.

2.4- Conclusion

The possibility of depositing at high deposition rates has been demonstrated, and at very low temperatures silicon dioxide films using a novel photo-CVD technique based on the photochemistry of silane and oxygen. Table 4.2 summarizes the deposition conditions and the film properties obtained. Optimised deposition conditions produced, at 200°C, films exhibiting refractive index values of 1.46, etch rates of 20Å/s in buffered HF (1mol/l) and electrical breakdown voltages of 6 to 10MV/cm, all values representative of good quality CVD grown silicon dioxide obtained at high temperatures [Ortiz] [Chau]. The advantage of this method is the good control of the gas phase photochemistry and therefore of the final stoichiometry obtained, and it has been showed that the nuclei dissociation reactions on the substrate are strongly enhanced by the substrate temperature and limited by the total pressure.

This entire photo-CVD process is compatible with many industrial requirements for electronic manufacturing as well as for optical coatings. The low operating temperature also makes it compatible with III-V semiconducting materials, glass, and many heat sensitive compounds.

SiO_2 from SiH_4/O_2:Ar (15:100)	
Initiated photo-dissociation at 172 nm	$O_2 + h\nu \rightarrow O + O$ σ= 20 atm^{-1}cm^{-1}
Deposition Conditions	5 mbar < P < 7 mbar 200°C < T <300°C 2% < R= SiH_4/N_2O < 6% $F_{tot} \approx$ 60 sccm Window-Subst. Dist.= 12 mm
Deposition Properties	100-250 Å/min n = 1.46
FTIR	Si-O stretch at 1065 cm^{-1} FWHM = 75 cm^{-1}
Electrical Properties	E_b= 6-8 MV/cm Q_{ss}= 10^{12} cm^{-2}

Table 4.2 : Summary of SiO_2 deposition conditions and essential properties obtained from the photo-CVD of SiH_4/O_2 mixtures

References to chapter 4

[Adams-1983] A.C. Adams, Sol. State Technol., **26** (1983) 135

[Adams-1979] A.C. Adams, C.D. Capio, S.E. Haszko, G.I. Parisi, E.I. Pouilonis, McD. Robinson, J. Electrochem. Soc., **126** (1979) 313

[Aiken] R.C. Aiken, L. Lapidus, AIChE J., **20** (1974) 368

[Baker] S.D. Baker, W.I. Milne, P.A. Robertson, Appl. Phys., **A 46** (1988) 243

[Baulch] L. Baulch, R.A. Cox, R.F. Hampson Jr., J.A. Kerr, J. Troe, R.T. Watson, J. Phys. Chem. Ref. Data, **13** (1984) 1259 and also D.L. Baulch, R.A. Cox, P.J. Crutzen, R.F. Hampson, J.A.Kerr, J. Troe, R.T. Watson, J. Phys. Chem. Ref. Data, **11** (1982) 359

[Bennett] B.R. Bennett, J.P. Lorenzo, K. Vaccaro, United States Patent N°4,900,591 (13 Feb 1990)

[Bergonzo] P.Bergonzo, U. Kogelschatz, I.W. Boyd, Appl. Surf. Sci., **69** (1993) 393

[Boyd-1982] I.W. Boyd, J.I.B. Wilson, J. Appl. Phys., 53 (1982) 4166

[Boyd-1982-b] I.W. Boyd, *Laser processing of Si and the growth and structure of Si oxides*, PhD Thesis, Herriot Watt University (1982)

[Boyd-1987] I.W. Boyd, J.I.B. Wilson, Appl. Phys. Lett., **50** (1987) 320

[Boyer] P.K. Boyer, G.A. Roche, W.H. Ritchie, G.J. Collins, Appl. Phys. Lett., **40** (1982) 716

[Calvert] J.G. Calvert, J.N. Pitts, in *Photochemistry*, J. Wiley & Sons New York (1966)

[Chau] T.T. Chau, S. R. Meija, K.C. Kao, J. Electrochem. Soc., **138** (1991) 325

[Cobianu] C. Cobianu, C. Pavalescu, J. Electrochem. Soc., Sol. State Sci. and Technol., **130** (1983) 1888

[Coste]	C. Coste, in *Ozonation Manual for Water Treatment*, Ed. by W.J. Masschelein, John Wiley & Sons, Chichester, (1982) 204
[Eagle]	D.J. Eagle, W.I. Milne, Semicond. Sci. Technol., **2** (1987) 56
[Friedel]	C. Friedel and A. Ladenburg, Annal. Chem. Pharm. **CXLIII**, (1867) 118-128
[Giunta]	C.J. Giunta, J.D. Chapple-Sokol, R.G. Gordon, J. Electrochem. Soc., **137** (1990) 3237
[González]	P. González, E. Garcia, J. Pou, D. Fernández, J. Serra, B. Léon, M. Perez-Amor, presented at the 1993 E-MRS Spring Meeting, Strasbourg, to be published in Thin Solid Films
[Hartman]	J.R. Hartman, J. Famil-Ghiriha, M.A. Ring, H.E. O'Neal, Combustion and Flame, **68** (1987) 43
[Inoue]	K. Inoue, Y. Nakatani, M. Okuyama, Y. Hamakawa, J. Appl. Phys., **64** (1988) 6496
[Itoh]	U. Itoh, Y. Toyoshima, H. Onuki, N. Washida, T. Ibuki, J. Chem. Phys., **85** (1986) 4867
[Kamaratos]	E. Kamaratos, F.W. Lampe, J. Chem. Phys., **74** (1970) 2267
[Kawahara]	T. Kawahara, A. Yuuki, Y. Matsui, Jpn. J. Appl. Phys., **30** (1991) 431
[Kazor]	A. Kazor, I.W. Boyd, Appl. Phys. Lett., **63** (1993) 2517, and also Elect. Lett., **29** (1993) 115
[Kudo]	T. Kudo, S. Nagase, J. Phys. Chem., **88** (1984) 2833
[Hess]	D.Hess, J. Vac. Sci. Technol., A2 (1984) 244
[Lan]	W.H. Lan, S.L. Tu, S.J. Yang, K.F. Huang, Jpn. J. Appl. Phys., **29** (1990) 997
[Liehr]	M. Liehr, S.A. Cohen, Appl. Phys. Lett., **60** (1992) 198
[Lucovsky]	G. Lucovsky, Solid State Commun., **29** (1979) 571
[Manfredotti]	C. Manfredotti, F. Fizotti, M. Boero, G. Piatti, Appl. Surf. Sci., **69** (1993) 127
[Marks]	J. Marks, R.E. Robertson, Appl. Phys. Lett., **52** (1988) 810
[Nissim]	Y. I. Nissim, J.M. Moisson, F. Houzay, F. Leblanc, C. Licoppe and M. Bensoussan, Appl. Surf. Sci., **46** (1990) 175

[Okabe] H. Okabe, in *Photochemistry of small molecules* J. Wiley and Sons, New York (1978)

[Okuyama] M. Okuyama, Y. Toyoda, Y. Hamakawa, Jpn. J. Appl. Phys., **23** (1984) L9713

[Ortiz] A. Ortiz, S. Lopez, C. Falcony, M. Marias, L. Cota-Araiza, G. Soto, J. Elec. Mat., **19** (1990) 1411

[Patel] P. Patel and I.W. Boyd, Appl. Surf. Sci., **46** (1990) 352

[Petitjean-1990] M. Petitjean, N. Proust, J.F. Chapeaublanc, Appl. Surf. Sci., **46** (1990) 189

[Petitjean-1991] M. Petitjean, *Optimisation de structures MIS sur InP*, rapport de thèse, Université Paris 6 (1991)

[Petitjean-1992] M. Petitjean, N. Proust, J.F. Chapeaublanc, J. Perrin, Appl. Surf. Sci., **54** (1992) 453

[Robertson] P.A. Robertson, *The photo-enhanced deposition of amorphous Silicon and Silicon oxide thin films*, PhD Thesis, University of Cambridge (1987)

[Sze] S.M. Sze, *Semiconductor Devices, Physics and Technology,* J. Wiley & Sons, New York (1985)

[Szörényi] T. Szörényi, P. González, D. Fernández, J. Pou, B. León, M. Pérez-Amor, Appl. Surf. Sci, **46** (1990) 206

[Taft] E.A. Taft, J. Electrochem. Soc., Sol. State Sci. and Technol., **126** (1979) 1728

[Tsu] D.V. Tsu, G. Lucovsky, B.N. Davidson, Phys. Rev. B, **40** (1989) 1794

[Vasilyeva] L.L.Vasilyeva, V.N. Drozdov, S.M. Repinsky, K.K. Svitashev, Thin Solid Films, **55** (1978) 221

[Weber] R. Weber, G. Wahl, R. Huber, Journal de Physique, Colloque C5, Suppl. 5, Tome **50**, (1989), C5-411

[Wen] J. Wen, M.H. Thiemens, Chem. Phys. Lett., **172** (1990) 416

The Photochemical Deposition and Characterisation of Silicon Nitride and Oxynitride Layers

The ability to deposit high quality silicon nitride (Si_3N_4) at low temperatures makes this material an important candidate for large area microelectronic applications. Here is presented the deposition of this material from a technique based on the photo-CVD of silane and ammonia mixtures, under the VUV irradiation emitted from a xenon excimer lamp radiating at 172nm.

By combining this novel technique with that of the deposition of silicon dioxide films presented in the earlier section, this work is extended to the photo-CVD of oxide-nitride-oxide stacked layers and of silicon oxynitrides SiO_xN_y.

1.- The photo-CVD of silicon nitride from silane and ammonia gaseous mixtures

1.1- Introduction

1.1.1- Interest in silicon nitride

Amorphous silicon nitride is a dielectric which is widely used, most often as a layer to mask the oxidation of the underlying silicon layers. Those films have superior dielectric properties to silicon dioxide, especially in the very thin film regime. They have the potential for extensive application in passive and active elements in electronic Metal Insulator Semiconductor (MIS) devices [Paloura]. They are also a very good barrier to water, which may cause devices to corrode. In silicon nitride, the mobility of sodium or alkali metal ions, typical sources of interface charge defects in devices, is known to be significantly slower than in silicon dioxide. As a result, amorphous silicon nitride is commonly used as a barrier layer, between a silicon dioxide gate oxide and the Si/SiO_2 interface, as a way to inhibit the drift of ions towards the interface, thus reducing charge defects by protecting the device from contamination [Navon] [Lee-1990]. Furthermore, silicon nitride MIS transistors benefit from the high ε value exhibited by silicon nitride, i.e., 7.5 c.f. silicon dioxide (3.9), hence lowering the threshold voltages.

1.1.2- Brief review on silicon nitride deposition techniques

Pyrolytic CVD, which yields silicon nitride films with high stoichiometry, requires high deposition temperatures (in the range of 800°C). In order to decrease the overall thermal budget, plasma techniques have been utilised [Rand], and remain today the conventional method [Gupta]. However, silicon nitride films grown using this technique may suffer from plasma damage [Smith], and often contain a large amount of hydrogen, typically up to 20 to 35 at.% [Claassen] [Seager] [Lustig], and are often substoichiometric in nitrogen [Jauberteau]. Various other novel techniques have been developed with varying degrees of success. As such, a very promising technique based on the remote pyrolytic dissociation of a silane (SiH_4) and hydrazine (N_2H_4)

mixture has been developed in Japan by Matsumara, allowing growth rates as high as 1000 Å/min at 300°C, and for films very close to the Si_3N_4 stoichiometry [Matsumura].

Photolytic nitridation of the silicon surfaces has also been intensively studied, using either UV lasers [Sugii] or lamps [Ishikawa]. Similarly, the CVD of silicon nitride thin films has also been achieved using lasers [Eisele] or lamps. Silicon nitride deposition techniques using lamps have essentially consisted of mercury (Hg) sensitisation techniques, since the work of Collet in 1969 [Collet] [Brekel] [Nikolic] [Lemiti] [Berti]. The contamination and hazards associated with the use of mercury tended to motivate research towards techniques using direct photo-enhanced CVD, i.e., when the available energy provided by the photons is transferred photolytically to the reactive species such as disilane and ammonia mixtures [Inushima], or silane and ammonia mixtures [Numasawa-1983] [Guizot] [Petitjean]. However, the general low levels of vacuum ultraviolet radiation associated with the low pressures Hg lamps have limited the deposition rates and thus further expansion of these techniques.

Here is proposed to study a novel way to deposit silicon nitride films, involving the use of a xenon excimer lamp emitting in the VUV domain in a continuum centred at 172nm.

1.2- Experimental details

1.2.1- Photochemistry of SiH_4 and NH_3 mixtures under 172nm photons

Whilst silane is transparent to the UV radiation, the ammonia molecules are excited by the photons and undergo dissociation:

$$NH_3 + h\nu \rightarrow NH_2 + H \qquad (5.1)$$

$$NH_3 + h\nu \rightarrow NH + 2\,H \qquad (5.2)$$

$$NH_3 + h\nu \rightarrow NH + H_2 \qquad (5.3)$$

Mainly reaction (5.1) occurs around 172nm (≥ 96%). The absorption cross section, σ, of NH_3 species varies from 20 to 100 $atm^{-1}cm^{-1}$ in the 165-180 nm range with sharp peaks at 176 and 179nm, exhibiting values of 200 and 260 $atm^{-1}cm^{-1}$, respectively [Tannenbaum]. The quantum yield of NH_3 dissociation at 185nm may approach unity at low pressure [Calvert]. Figure 5.1 gives an abacus of the corresponding absorptions for various ammonia pressures (at room temperature and assuming σ=50$atm^{-1}cm^{-1}$), and for photon pathways varied from 1 to 5 cm. It shows that 172nm absorption cross sections of 40 % are obtained through 1cm of ammonia at 10mbar.

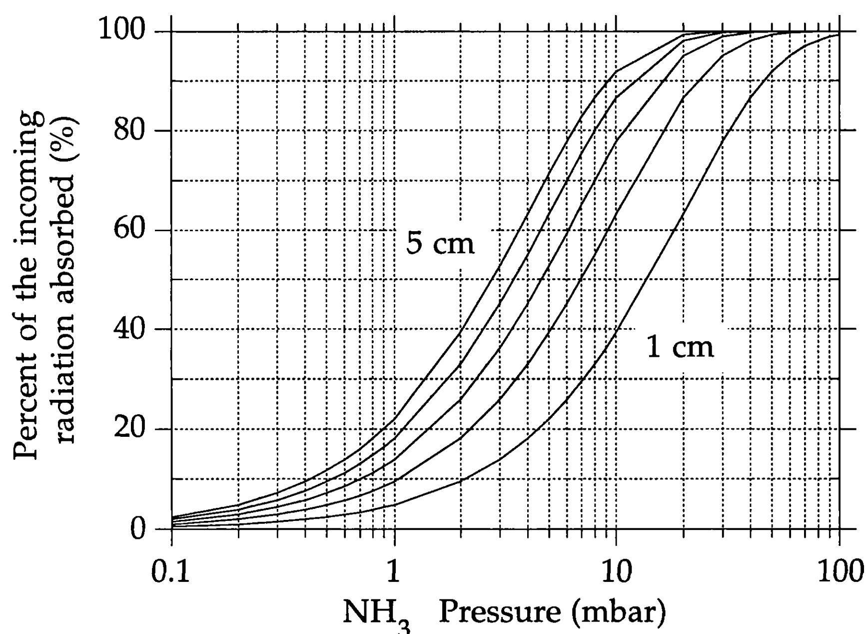

Figure 5.1: Abacus for 172nm photon absorption in pure ammonia, various window to substrate distances are considered, from 1 to 5cm, (assuming σ = 50 $atm^{-1}cm^{-1}$).

The NH_2 radicals then react with silane molecules, under

$$NH_2 + SiH_4 \rightarrow NH_3 + SiH_3 \quad (5.4)$$

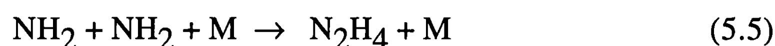

$$NH_2 + NH_2 + M \rightarrow N_2H_4 + M \quad (5.5)$$

where M is a third body, and N_2H_4 is hydrazine which also undergoes photodissociation under

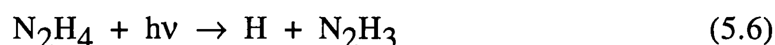

$$N_2H_4 + h\nu \rightarrow H + N_2H_3 \quad (5.6)$$

$$N_2H_4 + h\nu \rightarrow NH_2 + NH_2 \quad (5.7)$$

Secondary reactions occur:

$$H + SiH_4 \rightarrow H_2 + SiH_3 \quad (5.8)$$

$$H + SiH_3 \rightarrow SiH_2 + H_2 \quad (5.9)$$

$$N_2H_3 + H \rightarrow N_2 + 2H_2 \quad (5.10)$$

$$SiH_3 + NH_2 \rightarrow SiH_3NH_2 \quad (5.11)$$

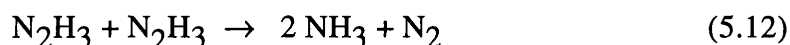

$$N_2H_3 + N_2H_3 \rightarrow 2\,NH_3 + N_2 \quad (5.12)$$

The primary reaction products, such as H and NH_2 radicals, can undergo rapid secondary reactions such as (5.8) to (5.11) in the gas phase. Further reactions of other minority and short lived species such as NH and SiH_2, produced by secondary reactions, are here neglected. SiH_3NH_2 is silylamine, which actively contributes, with NH_2 and SiH_3 to surface reactions [Guizot].

1.2.2- Precursor gas purity

At the early stages of this study, experiments indicated that the process requires the use of ultrahigh purity gases. In fact, impurities of only a few hundred ppm (part per million) (especially O_2, H_2O and CO_2 for ammonia), were sufficient to drastically pollute the deposited film with oxygen, leading to film stoichiometries more closely resembling SiO_2 rather than Si_3N_4. This was due to a higher degree of reactivity exhibited by these impurities than by the ammonia, towards the reaction with silane, therefore rendering them predominant in the deposition photochemistry. Accordingly, the precursor gas purities used were grade 5.0 (i.e., 99.999%) for the silane and 5.5 (99.9995%) for the ammonia.

1.2.3- Sample preparation and preliminary experiments

The experimental set up has been presented in details in chapter 1, and with the study of silicon dioxide depositions in figure 4.1. Portions of p-type silicon wafers, (100) oriented, are used as substrates. Prior to deposition, the samples are cleaned in a propanol solution in ultrasonic bath and the chamber is evacuated to 10^{-6} mbar.

A first experiment was carried out to measure the extent of pyrolytic growth. Setting the substrate temperature at values up to 400°C, resulted in no measurable layer being detectable. The pyrolytic dissociation of the precursors does not occur at those temperatures.

The next experiment studied the evolution of the thickness of the deposited layer as a function of the duration of the experiment. Samples prepared using identical deposition parameters were processed for various times, and their thicknesses, as measured with ellipsometry, were plotted. For example, figure 5.2 shows the evolution of the thickness with process time up to 30 minutes, for films deposited at 10mbar, 300°C, and using a 10% silane in ammonia mixture. The thickness evolution for two window-substrate distances of 12 and 40mm, and for various total precursor flows are plotted.

The instantaneous growth rate is obtained from the slope of the curves. A significant decrease is observed with time, and can be attributed to the attenuation of the incident photon flux, caused by the absorption of the film deposited onto the magnesium fluoride window. This problem is well known to photo-CVD experimenters and is commonly referred as the window fogging problem.

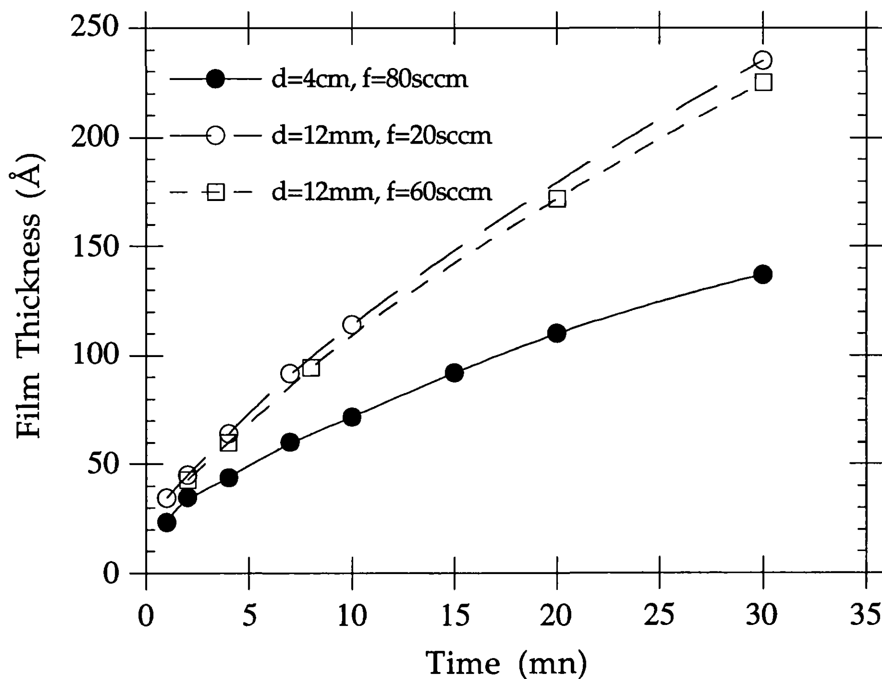

Figure 5.2 : Evolution of the deposited layer thickness with the duration of the experiment, at various window to substrate distances (d) and total gas flows (f).

1.3- The window fogging problem

1.3.1- Outline of the problem

As mentioned in chapter 1, § 2.2.1, a practical limitation of most photo-CVD processes stands in the attenuation of the ultraviolet light due to film deposition on the window. In the case of the 172nm photons, absorption is exhibited by the SiN products condensing on the window separating the lamp and deposition chambers, and this results in the decrease of the deposition rate during the experiment. In the particular case of hydrogenated amorphous silicon (a-Si:H), this problem is a further limitation, since the deposited products show very high absorption cross sections in the UV domain. A number of solutions, used with varying degrees of success, includes a directed etching XeF_2 jet at the window [Langford], a thin layer of low vapour pressure oil (Fomblin) on the window [Inoue], the previous solution

combined with a wiper blade system [Bhatnagar] or a flexible transparent film held against the window [Peters] [Rocheleau]. However, contaminations resulting from the use of oil or fluorinated compounds may result in the deposited layers.

Other groups have preferred the use of a purging gas in the vicinity of the window, to prevent the condensation of deposition products [Tanimoto]. This type of gas purge is often used with laser assisted techniques [Tsuji] [Nishino] [Shirafuji]. In fact, as the laser light is highly collimated, the window through which the beam enters may be located relatively far from the region where the reactions occur, and as such the purge may not interfere with the reactive species. However, in the case of lamp assisted techniques, this solution is more difficult to implement, since the added purging gas often results in local turbulences close to the substrate region. Numasawa *et al.* reported the use of an optically transparent "separator plate", perforated about 1200 times with ø0.6mm holes, and located between the window and the reactor, to prevent the precursor gases reaching the window, as well as to limit the flow turbulences to a minimum [Numasawa-1986]. This ingenious method seems so far to have offered the best answer to the window fogging problem, although it requires expensive and technologically difficult preparation of the perforated "separator plate".

1.3.2- Gas purge configuration

The gas purge configuration utilised in these experiments exploits the use of a secondary flow of argon. As was previously mentioned, a very fine tuning of both the precursor gas flows and the purging gas geometries is required since the purging gas flow may create undesirable local turbulences in the neighbourhood of the substrate. Furthermore, to be efficient, this approach implies the use of pressures for which the mean free path of the species is shorter than the chamber dimensions (viscous mode). Consequently, this type of window purge gives constraints on the pressures to be used in the reactor. Also, although the configuration would greatly benefit from the implementation of a "separator plate", it is technologically too demanding for this study.

Figure 5.3 gives a schematic diagram of the configuration used between window and substrate, and shows typical gas flow characteristics for this geometry. The "shower" used to feed the purging gas is made from a ø2mm stainless-steel straw, onto which have been perforated about ten ø0.4mm holes at regular intervals.

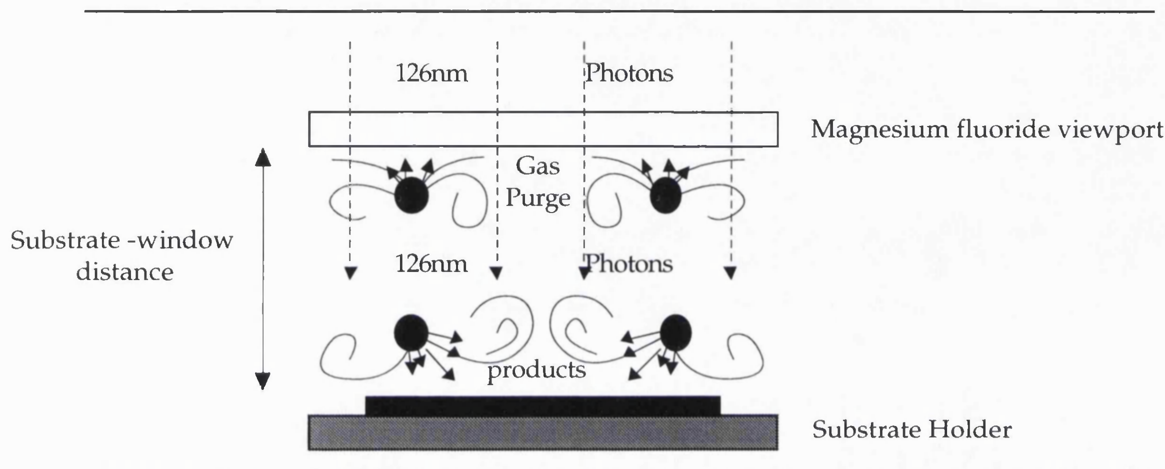

Figure 5.3 : Schematic diagram of the effect of the window purge

1.3.3- Lateral approach

• Introduction

In the previous configuration, it appears that the effects of the window purge may be strongly influenced by many of the deposition parameters, such as the window-to-substrate distance, the total deposition pressure, the precursor and purge gas flows, the shower-to-substrate and purge-to-window distances, and the surrounding chamber geometry. Similarly, the optimisation of the deposition conditions would also strongly be influenced by the window purge itself. It is therefore not advisable to try to optimise both the deposition conditions and the window purge at the same time, and consequently an experimental artifice is adopted. From the behaviour of the curves presented in figure 5.2, the consequence of material absorption on the window can be expressed mathematically. From this point, it would become possible to draw a model on the growth kinetics, and then to calculate for each experiment the relative growth rate which would have been obtained without any window absorption. This

will enable us to optimise fully the deposition conditions before optimising the window purge.

• Mathematical expression

Considering x(t) as the expression of the thickness of the deposited layer on the sample surface, and v(t) as the corresponding deposition rate, i.e., its derivative. Assuming that the time dependant deposition rate is proportional to the decreasing 172nm radiation, the expression of the Beer-Lambert law on the intensity, I, of the light traversing the window can be written as:

$$v(t) = K I = K I_0 \exp(-\sigma\, x_{window}(t)) \qquad (5.13)$$

where I_0 is the light entering the reactor, $\sigma(t)$ the absorption coefficient of the film deposited on the window, and $x_{window}(t)$ the thickness of the deposited coating on the window.

To a first approximation, the gas phase chemistry, and hence the deposition products, do not depend upon the radiation intensity, therefore σ is not time dependant and can be written as $\sigma(t) = \sigma$. Furthermore, assuming that $x_{window}(t)$ is proportional to x(t), at a ξ coefficient ($\xi \geq 1$) :

$$x_{window}(t) = \xi\, x(t) \qquad (5.14)$$

Therefore:

$$v(t) = K I = K I_0 \exp(-\sigma\, \xi\, x(t)) \qquad (5.15)$$

$$= v_0 \exp(-\sigma\, \xi\, x(t)) \qquad \text{since } v(t)_{t=0} = K I_0 = v_0 \qquad (5.16)$$

By derivating (5.16) in respect to t, it comes:

$$dv(t) / dt = -v_0\, \sigma\, \xi\, [dx(t)/dt]\, \exp(-\sigma\, \xi\, x(t)) \qquad (5.17)$$

$$= -v_0\, \sigma\, \xi\, v(t)\, \exp(-\sigma\, \xi\, x(t)) \qquad (5.18)$$

$$= -\sigma\, \xi\, v^2(t) \qquad (5.19)$$

And therefore,

$$dv(t) / v^2(t) = -\sigma\, \xi\, dt \qquad (5.20)$$

The solution of equation (5.20) is :

$$1/v(t) = \sigma\,\xi\,t + cte = \sigma\,\xi\,t + 1/v_0 \quad \text{(since } v(t) = v_0 \text{ at } t=0) \qquad (5.21)$$

Thus,

$$v(t) = v_0 / (1 + \sigma\,\xi\,v_0\,t) \qquad (5.22)$$

Therefore, x(t) obtained by integrating (5.22) becomes:

$$\boxed{x(t) = \frac{1}{\sigma\xi} \ln(1+\sigma\xi\,v_0\,t) + x_0} \qquad (5.23)$$

taking $x(t) = x_0$ at t=0 (native oxide).

Equation (5.23) is the expression of the deposited thickness evolution with the duration of the experiment.

• Curve fitting

From the evolution of the thickness as measured in figure 5.2, a computed algorithm [Press] is used to calculate a curve fit in the form of equation (5.23), to obtain the corresponding experimental values for σ and ξ. Experimental values for the product $\sigma\xi$ of 3.8 $10^5 cm^{-1}$ and 8.8 $10^5 cm^{-1}$ were obtained, at window to substrate distances, d_{ws}, of 12 and 40mm respectively. The absorption cross section σ of silicon nitride at 172nm has been reported as 3 $10^5 cm^{-1}$ [Borghesi]. The corresponding values for the coefficient ξ are of 1.2 and 2.9, at 12 and 40mm, respectively. As expected, the efficiency of the deposition on the substrate is greater at small distances d_{ws}.

The ratio ξ, representative of the deposition thickness on the substrate compared to that on the window, is calculated to be strongly dependant on d_{ws}. The influences of the total precursor and of the deposition pressure were measured, and they did not percepti bly affect the values of σ and ξ. From that point, it can be assumed that only d_{ws} influences ξ, and the value ξ=1.2 (d_{ws}=12mm) is kept constant for the remainder of the discussion.

From equation (5.23), an estimation of the initial growth rate v_0, which is independent of the window fogging effects, can be given:

$$v_0 = \frac{\exp((x - x_0)\sigma\xi) - 1}{\sigma\xi \quad \Delta t} \qquad (5.24)$$

where x is the measured thickness of the sample,
x_0 is the native oxide thickness,
Δt is the duration of the experiment.

Only the values of v_0 are considered in the forthcoming discussion of the kinetics of the deposition. Numerically, have been used:

$x_0 = 20Å$,
$\sigma\xi = 0.0038\ Å^{-1} = 3.8\ 10^5\ cm^{-1}$, deduced from analytical fittings, at d=12mm.

• Precision and accuracy

For each experiment, the value of v_0 is calculated from equation (5.24). Uncertainties on the values of x_0 and $\xi\sigma$ result in an error on v_0. Here is proposed to numerically estimate that error. Firstly, the error on x_0 is ranging around 10 to 20% (native oxide thicknesses varying from 15 to 25Å). The repercussion of that error on v_0 is very small, and tends towards zero for increasing values of the thickness (≥100Å). Similarly, the relative error on the product $\sigma\xi$, fitted at 0.0038Å, may reach 10%. By calculating the partial derivative of v_0 with respect to the product $\sigma\xi$, it can be shown that an expression of the following form is obtained:

$$\frac{\Delta v_0}{v_0} = f^n(\sigma\xi, x) \cdot \frac{\Delta(\sigma\xi)}{(\sigma\xi)} \qquad (5.25)$$

Where $f^n(\sigma\xi, x)$ is a function that essentially remains between 0.1 and 1 in the 20Å to 400Å range (appendix 4), therefore indicating that a 10% relative error on $(\sigma\xi)$ would be compensated and maintained to a few percent error on v_0. As a result, the resulting total influences of the small errors on the values of x_0, σ and ξ are not strongly counteracting on the calculated values of v_0.

1.3.4- Optimisation of the gas purge

The optimisation of the purge concentrated on the size of the areas on the window from which product deposition has been prevented. Figure 5.4 shows the differences in behaviour observed on the window after deposition experiments for two different pressures and for exposition times up to 30 minutes.

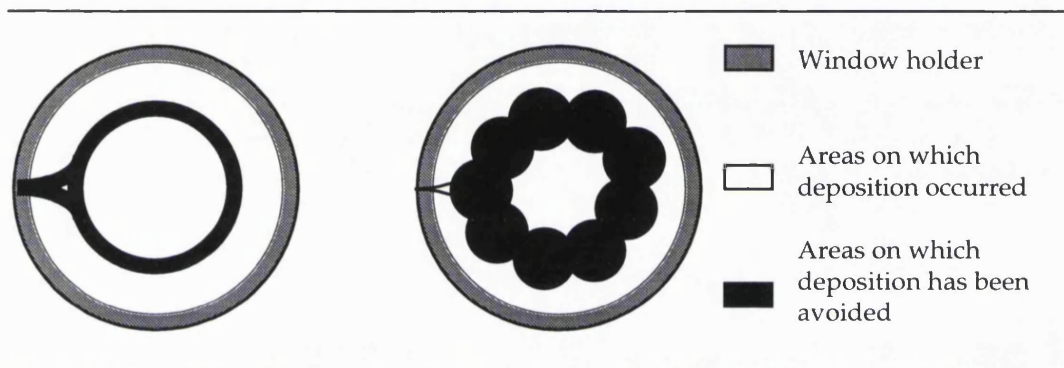

Figure 5.4 : Schematic of the aspect of the window after deposition, when observed in white light. Total pressure is 1mbar (Left) and 5mbar (right) (see text).

The drawing on the left represents the shadow of the purging shower on the window when a total pressure of 1mbar is used. At this pressure, silane and reactive molecules have not been affected by the purging flow and condensed on the window. When the total pressure in the chamber is increased, the probability for a reactive species to reach the magnesium fluoride window is reduced due to a high collision rate with argon species sprayed in the neighbourhood of the window, and so a darker area with hardly any coating appears. As a preliminary experiment, the width of the "clean" area on the window versus the total chamber pressure (figure 5.5) is probed. As expected, the pressure increase motivates strongly the effect of the window purge, which becomes less efficient below 5 mbar.

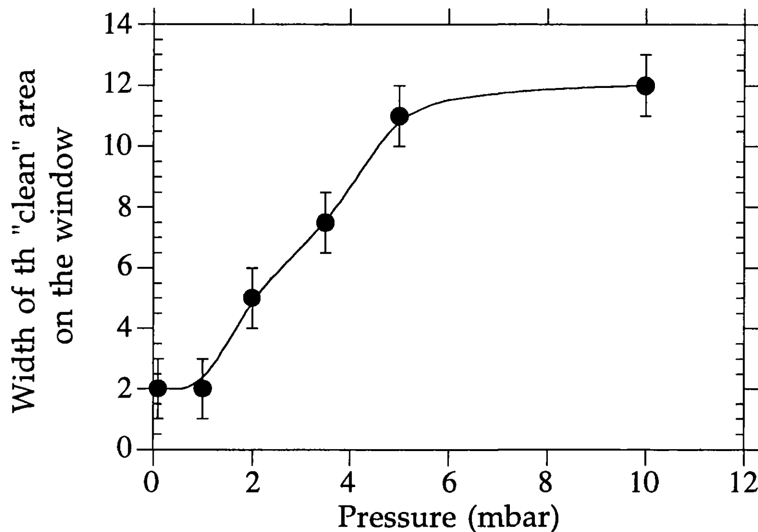

Figure 5.5 : effect of the total chamber pressure on the purge (argon: 200sccm, precursors: 50sccm, SiH_4/NH_3 = 10%).

1.3.5- Conclusion

The absorption of the 172nm incoming radiation by the deposition products condensing on the window, namely the window fogging problem, contributes to attenuate the incident photon flux, and as such is very depreciative when silicon nitride photo-CVD is attempted. From the numerous techniques which can be used, it would be preferable to use a gas stream across the window, in combination with a "separator plate" in order to avoid experimental constraints created by the use of a gas purge. Due to experimental limitations, a simpler device is to be used during this project, and its optimisation has been presented. Furthermore, with the use of a simple mathematical model, it has been showed how the growth kinetics could be optimised without concerning the window fogging problem, since the deposited products do not absorb strongly the incoming radiation. In the next paragraph, a study of the growth kinetics and silicon nitride film properties is presented, with no further consideration of this problem. By ensuring that the total deposition pressure exceeds 5mbar, this is a valid assertion.

1.4- Growth Kinetics

Silicon substrates prepared as described in §1.2.3 are studied. The temperature is kept in the 200-300°C range, with a typical lamp input power up to 40W, which corresponds to 20mW/cm^2. The experiments were carried out for 10 to 20 minutes, and the initial growth rates v_0 were extrapolated from equation (5.24).

1.4.1- Effect of the total precursor flow

The influence of the total precursor flow on the growth rate was studied from 5 to 140sccm, at 10mbar, using a lamp input power of 40W, and a precursor mixture of 5% silane in ammonia (figure 5.6). For flows below 10sccm, the deposition is limited by the gas phase diffusion of precursors, whether for values higher to 50sccm, the growth is limited by the photon intensity (lower rates are achieved at 20 and 30W input power). Also, a higher non-uniformity of the deposited layer could be observed above 120sccm. In the intermediate range, i.e., between 10 and 30sccm, the growth rates exhibit slightly higher values, as a result of the laminar condition of the flow in this region. The use of a total precursor flow of 20sccm is therefore advisable. At this flow and a d_{ws} of 12mm, very good thickness uniformity on the 20x20mm samples is obtained (non-uniformity ≤5%).

1.4.2- Effect of the total pressure

The effect of the total pressure was studied and figure 5.7 shows its influence on the deposition rate, at a temperature of 300°C and using a 5% precursor mixture of silane in ammonia. In order to study the effect of the window to substrate distance d_{ws}, characteristics obtained at d_{ws}=4cm are also shown.

The initial deposition rate v_0 exhibits a linear evolution with the pressure in the low range, up to a critical value at which v_0 saturates. Similar behaviour was also observed by Guizot using a low pressure mercury lamp [Guizot]. At low pressures, the process is limited by the diffusion of the precursors. At higher pressures, other mechanisms occur, with secondary and recombination reactions becoming important in the gas phase. This leads to a reduction in the film growth efficiency.

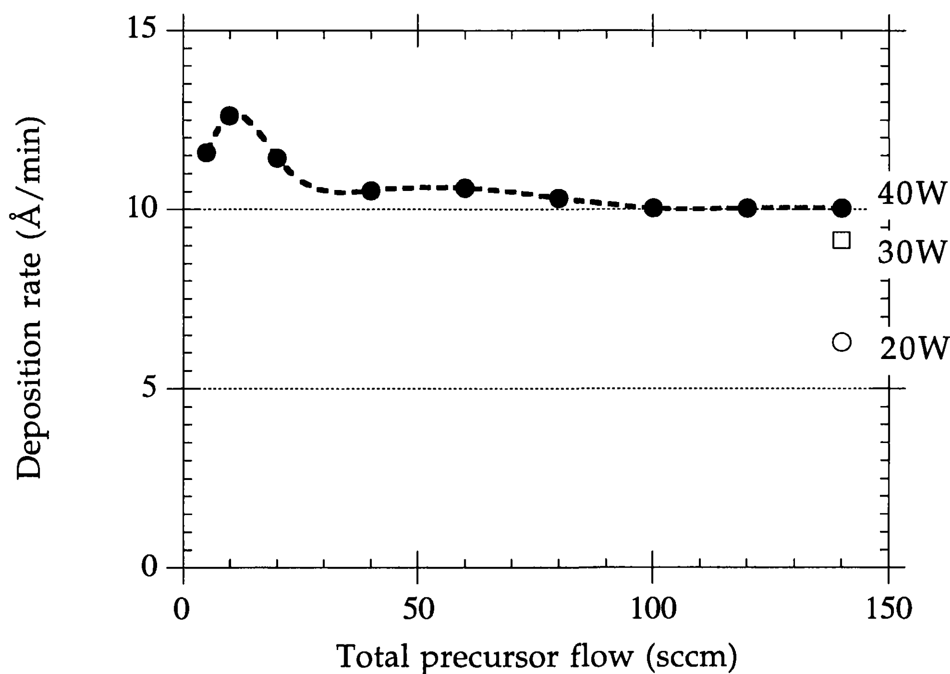

Figure 5.6 : Evolution of the growth rate vs. the total precursor flow
(Open : at 140sccm only for input power comparisons)

At a d_{WS} of 12mm, the maximum value for v_0 is obtained at 11mbar, whereas at 40mm, this occurs at 6mbar. In fact, by using data in figure 5.2, it appears that at 6mbar and 40mm, roughly 70% of the incoming radiation is absorbed, and this is a close value to that obtained at 11mbar and 12mm. The limitation of v_0 is therefore related to the number of photons reaching the substrate. Since these photons are likely to limit the recombination reactions, this reinforces the suggestion proposing that the limitation is caused by gas phase recombination reactions.

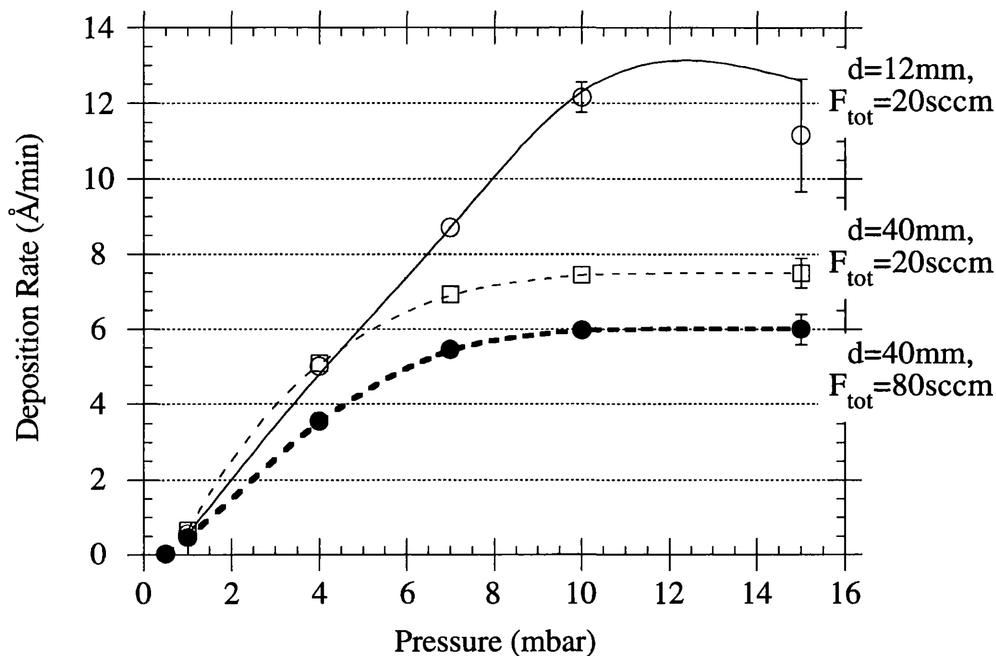

Figure 5.7 : Evolution of the growth rate with the chamber pressure (5% silane in ammonia, at 300°C)

At a d_{WS} value of 12mm, a slight decrease of v_0 at 15mbar is observed. In fact, the appearance of this film was almost opalescent, giving evidence of powder formation in the gas phase. This causes inaccuracy in the film thickness, measured using ellipsometry, and a greater error should be considered on the point. This did not happen at 40mm, probably since the powder formation reactions only occur in the vicinity of the window, and hence the products are more likely to be pumped away than to deposit on the sample.

Comparison of the two behaviours observed at d=40mm, using precursor gas flows of 20 and 80sccm, reveals that greater values of v_0 are obtained at low flows. This suggests that the secondary reactions, which limit the deposition mechanism, are also promoted by the gas turbulences.

1.4.3- Effect of the precursor mixture ratio R of silane in ammonia

Figure 5.8 presents the growth rate and refractive indices obtained for various precursor mixtures. These growth rates were obtained at a temperature of 300°C, an NH_3 flow of 20sccm, a d_{ws} of 12mm, a total pressure of 10mbar, and a lamp intensity of 10 to 15mW/cm^2. Growth rates higher than the 10Å/min rate obtained here should be readily achievable due to the much higher fluxes of photons that can be generated with the lamp. The value of the refractive index is clearly very strongly dependant on the silane concentration within the ammonia. Values as high as 1.85 were obtained for low SiH_4/NH_3 ratios. Direct photo-CVD rarely leads to values higher than this due to the difficulties of routinely achieving completely oxygen free processing conditions, and with the very high reactivity of those oxygen based impurities. There is evidence of such an unequal reactivity of active oxygen species compare with that of NH or NH_2 radicals. For example, Watanabe and Hanabusa reported the deposition of $SiO_{1.9}N_{0.03}$ oxynitride layers with a deuterium lamp, and using a precursor mixture of $SiH_4/NH_3/NO_2$ of 13/130/0.5 sccm, respectively [Watanabe-1989]. In the present case, the O_2 source is mainly due to the precursor purity and to the background pressure, and therefore could be reduced with more elaborate gas handling.

Petitjean *et al.*, as well as Guizot *et al.*, who in similar processes used low pressure mercury lamps, reported a different behaviour for the refractive index evolution with the precursor mixture [Petitjean] [Guizot]. In fact, in their case, the highest values were obtained at precursor mixtures of 10 to 12%, and stoichiometries close to Si_3N_4 were obtained at ratios below 1%, but exhibiting lower refractive index values of 1.75. In fact, they reported, at high R, film compositions closer to SiN_xH_y, which exhibit higher refractive index values. This will be further discussed when considerations on the composition of the films are made.

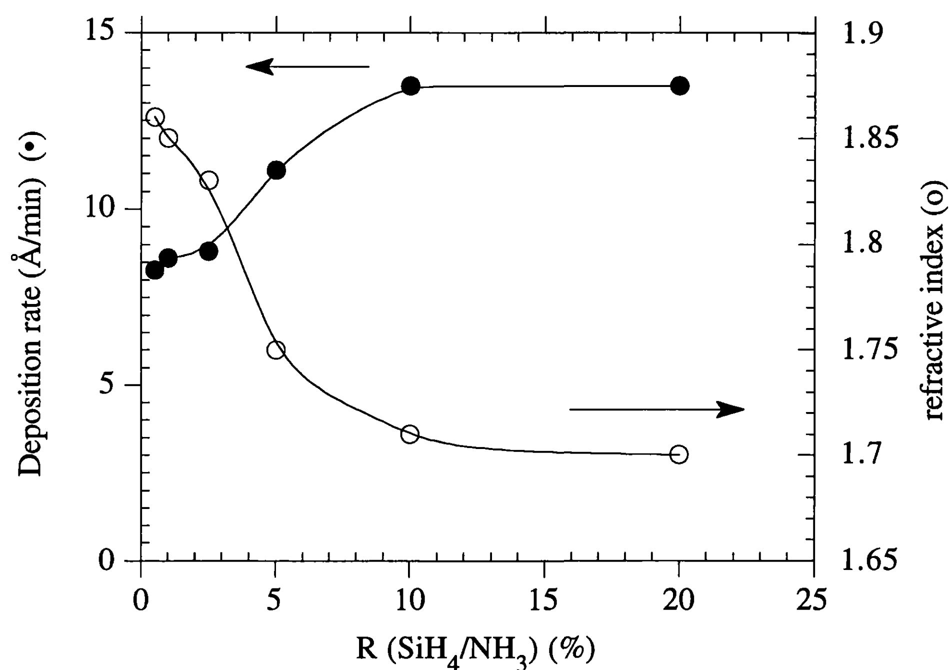

Figure 5.8 : Deposition rate and refractive index vs SiH_4/NH_3 ratios

1.5- Thin film characterisation

1.5.1- Fourier transform Infra-Red spectrometry

FTIR spectrometry was carried out on the UV deposited films. The spectrum of a silicon nitride layer obtained at 300°C, 10mbar and a mixture of .5% of silane in ammonia is shown in figure 5.9. It essentially consists of the characteristic absorption peak observed for the infra-red stretching vibration mode of Si-N centred at 840cm^{-1} [Berti] [Parsons].

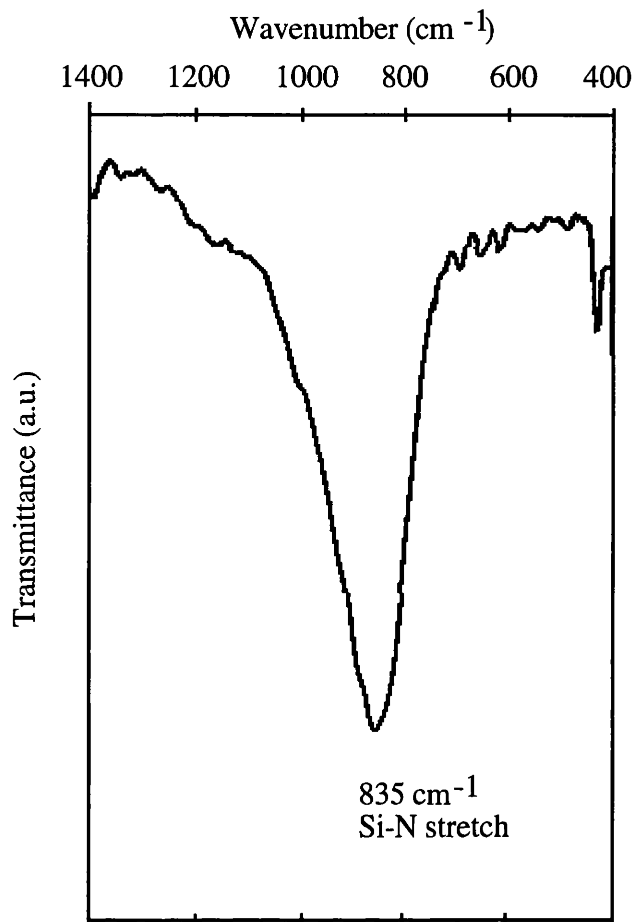

Figure 5.9 : FTIR characteristic absorption spectra of silicon nitride

FTIR spectrometry was also used to identify the effect of the gas mixture on the stoichiometric content of the films. No dominant peak was observed in the region where the Si-H vibrational modes are located (around 2175 cm^{-1}) [Berti]. This gives an upper limit to the content of bonded hydrogen in the films of a few percent, thus indicating a much lower concentration to that typically found in plasma enhanced CVD nitride films, where it can vary up to 35% [Chou]. In figure 5.10, the relationship between the Si-N stretching vibration mode and the SiH_4/NH_3 ratio R is shown. These measurements were obtained for 300Å thick silicon nitride films deposited at 300°C at a constant ammonia flow.

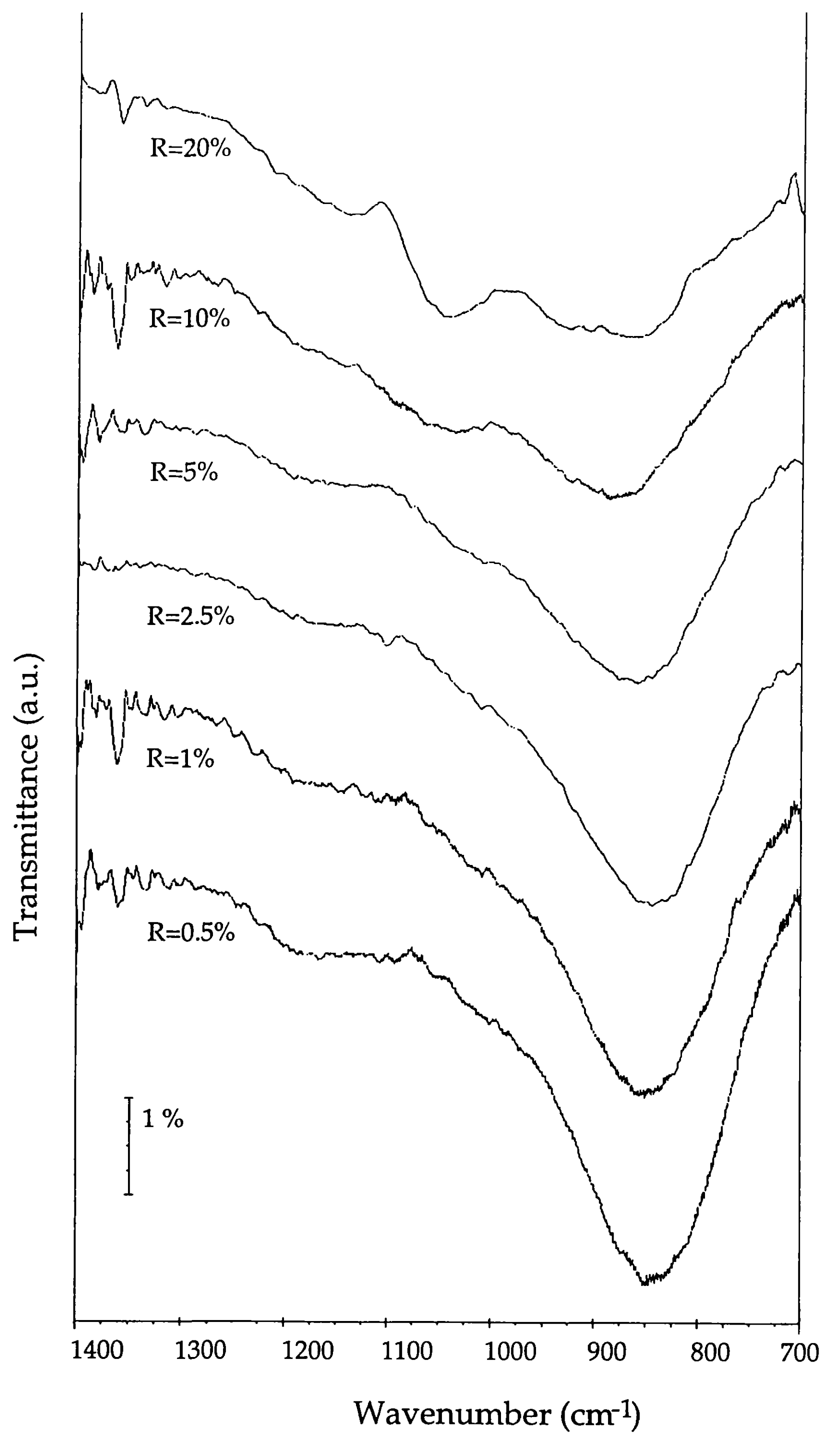

Figure 5.10 : Evolution of the Si-N vibrational mode with precursor mixture ratio R

As can be seen in figure 5.10, the characteristic broad peak centred around $840cm^{-1}$ observed for low R ratios is strongly diminished at higher silane concentrations. Therefore, the refractive index reduction observed for high silane concentrations corresponds to a decrease in the concentration of Si-N bonds in the films. This is explained by the fact that when R is increased at a constant NH_3 total flow, the ratio of dissociated active NH and NH_2 species to the number of silane molecules decreases, rendering the complete dissociation of the silane to be less probable, leading to a poorer Si-N bond concentration in the film. Further, at very high ratios (20%), the Si-N bond concentration is so low that the relative increase in the concentration of Si-O impurities bonds become visible by the associated increase in the absorption near $1060cm^{-1}$ due to the presence of Si-O units in the film. These observations confirm that it is possible to accurately control the stoichiometry of the deposited films by altering the precursor mixture. This selective precursor excitation feature is an added advantage of this technique over other deposition processes, since mutual excitation of the gas phase often leads to SiN_xH_y (e.g., plasma CVD and Hg sensitised photo-CVD).

1.5.2- Secondary Ion Mass Spectroscopy (SIMS)

SIMS analysis performed on the samples showed that the hydrogen and oxygen contents were very low and that the stoichiometry of the film was constant in depth. Figure 5.11 shows such a profile for a 600Å silicon nitride film deposited on silicon. This film, exhibiting a refractive index of 1.83, was obtained using a precursor mixture of 2.5% silane in ammonia. The tail on the N profile visible after the interface is due to recoil mixing commonly found in SIMS measurements.

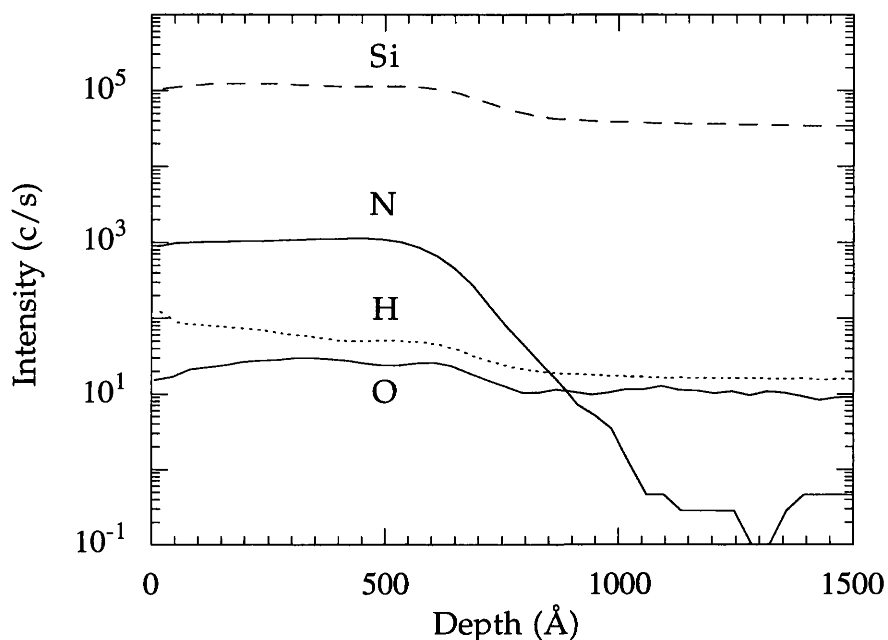

Figure 5.11 : SIMS profile of a 600Å silicon nitride film deposited on silicon

1.5.3- X-ray Photoelectron Spectroscopy (XPS)

XPS is a characterisation technique that enables the chemical analysis of a surface layer with thickness around or below 100Å. This technique enables the detection of any element, except hydrogen, incorporated in the films. The principle relies on the detection of electrons emitted from the surface, when exposed to a X-ray beam. The electron kinetic energy is equal to the difference between the incident X-ray photon energy, and the energy necessary to extract one electron from the lower atomic level of an atom. It is as such a signature of the atom from where the electron has been emitted, but also of the electronic boundaries of that atom (chemical bindings with neighbour atoms). The composition of a silicon nitride layer deposited on silicon has been studied, using a precursor ratio of 0.5% silane in ammonia, at 300°C and a total pressure of 10mbar (same sample as the one studied using FTIR spectroscopy in figure 5.9). Typical portions of the XPS spectrum corresponding to the regions O 1*s*, N 1*s*, and Si 2*p*, are shown on figure 5.12(a)-5.12(c) respectively.

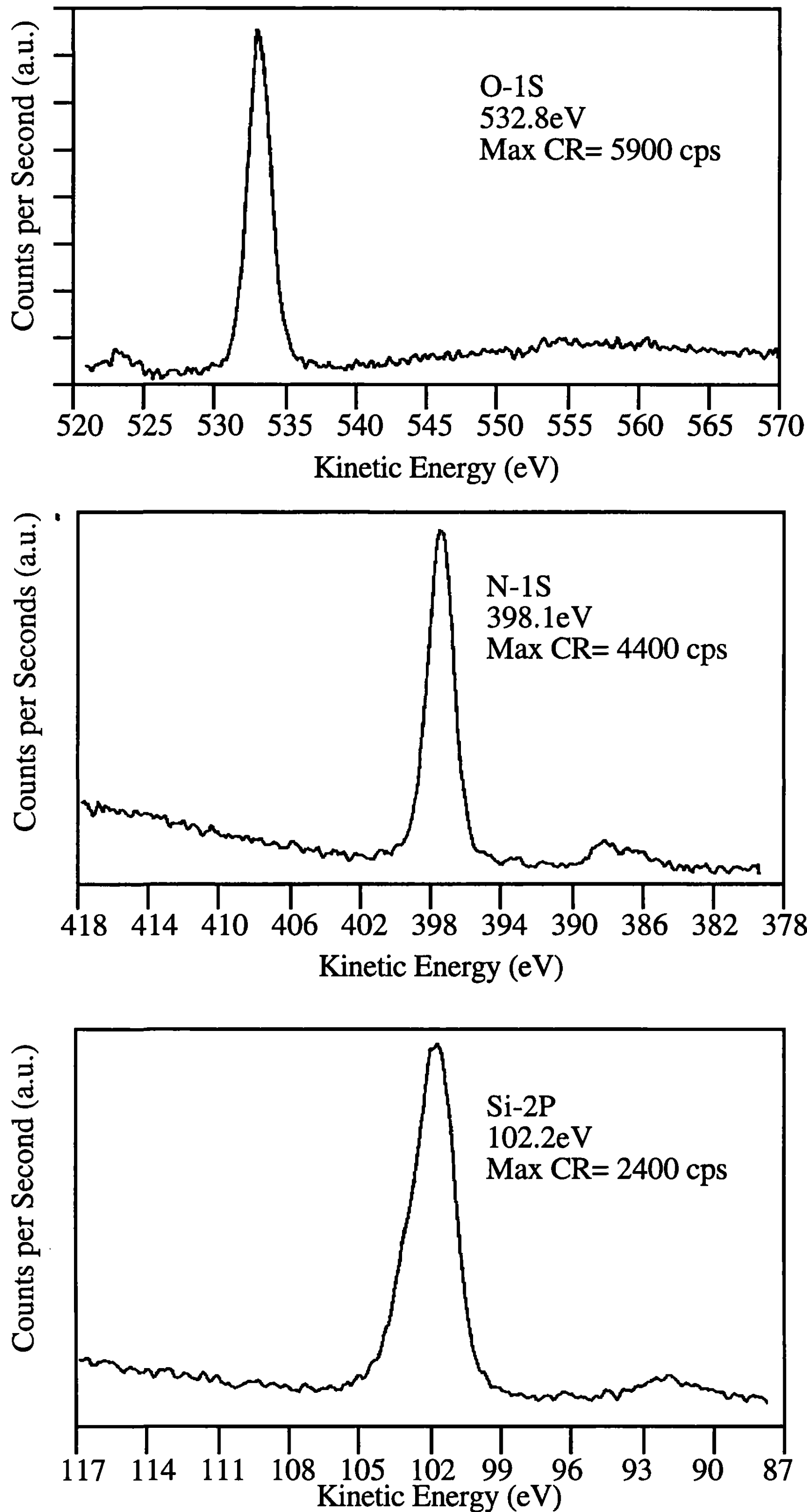

Figure 5.12 : XPS spectrum of a photo-deposited silicon nitride film, 3 regions corresponding to (a) the O 1s, (b) the N 1s, (c) the Si 2p peaks are presented.

The O 1*s* peak reveals the presence of several percent of oxygen in the area of the XPS analysis, its position at 532.8eV being in good agreement with data in the literature [Jo]. However, the absolute intensity of the peak is measured at one order of magnitude below that observed for thermally grown SiO_2 films on the same apparatus; also, since oxygen was not detected at the time of the FTIR measurement, this peak may be caused by a surface contamination of the film after its long exposition to air before the XPS measurements (≈2 months). This is in fact commonly observed on silicon nitride layers [Padmanabhan]. Within the N 1*s* zone, a maximum at 398.1eV is observed in accordance with N bound to Si in Si_3N_4 [Jo] [Sobalewski]. The small peak located around 388eV may be caused by the N (KLL) Auger emission [Kyuragi]. The position of the Si 2*p* peak at 102.2eV finally corresponds to Si bound to N, as reported by Aritome *et al.* [Aritome]. The presence of oxygen in the film would have led to a shift in this peak towards higher values of 103.8eV, value obtained on the same machine for a silicon dioxide layer. Since a much lower value of 102.2eV is observed, this confirms that the presence of oxygen is limited to a few percent, and that the O 1*s* peak was indeed due to surface contamination.

1.5.4- Physico-chemical properties

Simple hardness measurements were performed on the films, using a scratch test with various stones of known Moh's hardness. It showed that silicon nitride was not scratched by feldspar (H=6), although it was by quartz (H=7). This estimation of the hardness agrees with the values expected.

Etch rates measurements were performed on the silicon nitride deposited layers, using a buffered hydro-fluoric acid (HF) solution, diluted in water at a concentration of $1mol.l^{-1}$. Sze reported a quasi insolubility of silicon nitride in HF ($\approx 13mol.l^{-1}$), with a value of 5-10Å/min [Sze]. However, due to the unavoidable content of H or O impurities in the film, some weaker bonds can be broken, and etch rates as high as 2000Å/min have been reported [Hess]. Claassen *et al.* also reported a relationship between etch rates, the Si/N atomic concentration, and the film density [Claassen]. This is the cause for great differences in the reported values found in the literature.

Generally, the films deposited using a plasma enhanced technique, show very high etch rates, particularly since they always present a very high hydrogen content. Values vary from 200Å/min in 3mol.l^{-1} solutions [Sinha], down to 30-70Å/min in 2.5mol.l^{-1} reported in more recent work [Parsons]. Photo-CVD nitride etch rates of 100Å/min in HF, 3mol.l^{-1} have been reported, using the mercury sensitised technique [Berti]. In the case of the present experiments, a buffered HF solution with concentration of 1mol.l^{-1} was used. Etch rates of 30Å/min were obtained, for films deposited at 300°C and with a precursor mixture ratio of 0.5% silane in ammonia. Higher values of 100Å/min were also obtained at precursor ratios of 5%.

1.5.5- Electrical characterisation

The film properties were probed electrically using I(V) measurements. MOS capacitors were prepared by evaporating aluminium dots (0.001cm^2) on the silicon nitride layers deposited on p-type silicon substrates ($\rho \approx 10\Omega$.cm). In order to measure the I(V) characteristics of those devices, the gate was biased, and the ramp rate was 1V/s. Figure 5.13 shows the distribution of breakdown values obtained on one sample deposited using the optimised conditions (R=0.5%). As can be seen, a very high deviation from the mean of the measurements is obtained, probably due to particle contamination of the substrates in the laboratory, which is not a clean room facility. Dielectric breakdown values of 6 to 8MV/cm are readily achievable, although greater mean values of 8MV/cm may be obtained with improved sample handling.

Capacitance voltage measurements were also performed on optimised samples, and figure 5.14 shows a typical characteristic. A significant increase of the value of the capacitance during inversion is observed. This effect was present in most of the thin films, and it was supposedly caused by charges trapped at the interface between the deposited layer and the native oxide. High Surface state charge values were also obtained (around 10^{12}/cm^2), such high values probably caused by the absence of *in-situ* cleaning prior to deposition, and therefore to a high number of states trapped in the native oxide and at its interface with the nitride layer. These defects are not related to the deposited layer properties, but to its interface with the substrate. In fact, when the *deposition* of thin films is achieved, the interface between the substrate and

the deposited coating remains at the same position during all the process, and therefore pollutant particles which were present on the surface of the sample remain sandwiched exactly at the position of the electrical interface of the junction, together with the native oxide. This is an ideal location for impurities and surface states, and therefore it limits the application of deposited thin films towards gate dielectrics, unless *in-situ* cleaning of the interface is made available. This problem could however be overcome, for industrial applications, with the implementation of substrate cleaning techniques.

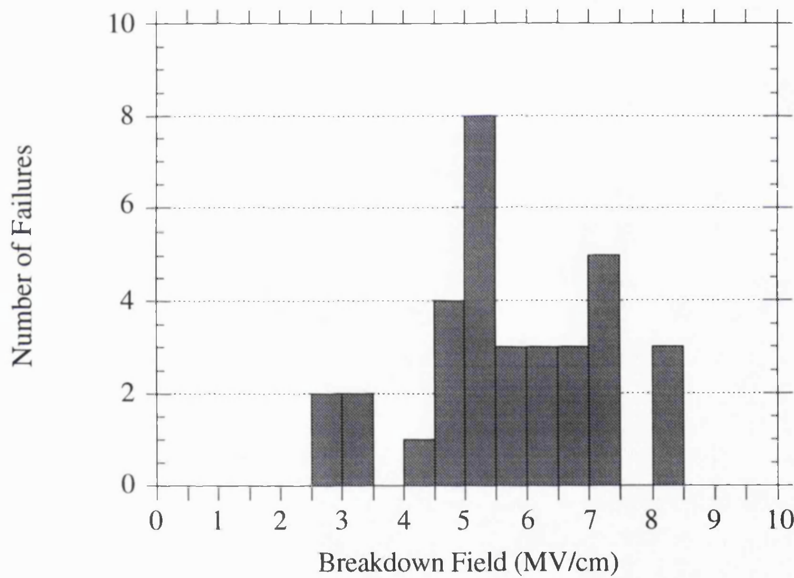

Figure 5.13 : Breakdown fields measured on a 300Å silicon nitride sample obtained at 300°C.

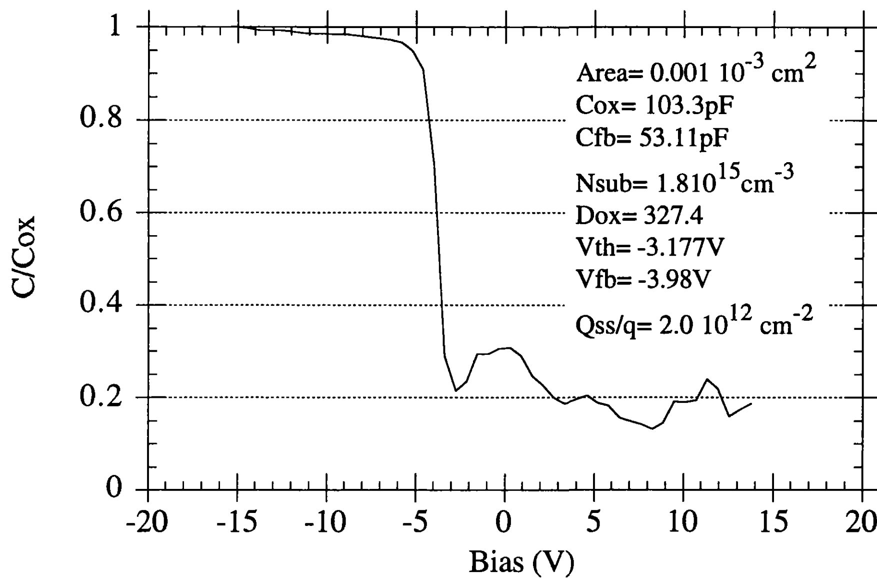

Figure 5.14 : Capacitance-Voltage measurement

1.6- Conclusion

The possibility to deposit, at low temperatures, good quality silicon nitride films has been demonstrated, using a photochemical process based on the 172nm continuum of xenon in a dielectric barrier discharge lamp. In table 5.1 are summarised the optimised deposition conditions as well as the essential film properties obtained. Such a deposition process has now been described for both SiO_2 and Si_3N_4 layers. It has been demonstrated that deposition rates comparable to those obtained with mercury lamps can be obtained, with generally higher refractive indexes and better control of the stoichiometry. These observations open a potentially new area for the application of excimer lamps, since the deposition of dielectric films for industrial applications at even higher rates and larger areas may be achieved by scaling up the geometry of the apparatus used.

Si_3N_4 from SiH_4/NH_3	
Initiated photo-dissociation at 172 nm	$NH_3 + h\nu \rightarrow NH_2 + H$ $\sigma = 50\ atm^{-1}cm^{-1}$
Deposition Conditions	P = 10 mbar 200°C < T <300°C 0.5% < R= SiH_4/NH_3 < 1% F_{tot}= 20 sccm Window-Subst. Dist.= 12 mm
Deposition Properties	15 Å/min n = 1.85
FTIR	Si-N stretch at 845 cm^{-1} FWHM = 150 cm^{-1}
Electrical Properties	E_b= 6-8 MV/cm $Q_{ss} = 10^{12}cm^{-2}$

Table 5.1 : Summary of Silicon nitride deposition and essential properties obtained from the photo-CVD of SiH_4/NH_3 mixtures.

2.- The *in-situ* photo-CVD of silicon Oxide-Nitride-Oxide multilayers

The main purpose of this short section is to give a proof of principle of the possibility to deposit *in-situ* oxide-nitride-oxide multilayers of silicon using the photo-CVD technique enhanced by 172nm photons emitted from a xenon excimer lamp.

2.1- Interests

Thin Oxide-Nitride-Oxide (ONO) stacked films are of considerable interest as dielectric layers for dynamic random access memories [Watanabe-1984] [Suzuki], and low voltage electronically erasable and programmable read-only memories [Chan]. They combine the high interfacial integrity of SiO_2 with the good diffusion barrier property, the low leakage current, and the higher dielectric constant of Si_3N_4 [Ting] [Lee1988], as well as the high yield of the stacked film, and the possibility to be processed at relatively low temperatures [Manzini] [Banerjee].

2.2- Experimental conditions

The deposition conditions are the same as those presented in earlier sections for the deposition of silicon dioxide and nitride layers. The light source is a xenon excimer lamp, capable of generating at 172nm up to $20mW/cm^2$ fluxes of photons. The silicon dioxide layers were deposited using a silane and nitrous oxide gaseous mixture, and the optimised conditions presented in table 4.1. The silicon nitride layer was obtained using a silane and ammonia mixture, with the optimised parameters presented in table 5.1. Between the multiple depositions, the sample was kept under heat at 300°C, and the chamber was evacuated to 10^{-5}mbar.

2.3- SIMS analysis

Three layers with thicknesses around 100Å have been deposited, and the film was characterised using SIMS analysis. On figure 5.15 is shown the depth profile of an

oxide-nitride-oxide silicon multilayered structure on silicon. Four distinct zones are found, and the ONO layers are well recognisable. From the bulk of the silicon substrate (right), a first silicon oxide layer which thickness is about 150Å is visible. The nitrogen tail under the N profile may be caused by recoil mixing probably due to a too high erosion rate during the measurement. The nitrogen rich layer, of 100Å in thickness, is visible in the middle of the ONO structure. The O profile seems also to be high under this layer, still probably because of recoil mixing. Finally, the surface silicon oxide layer is seen on the left of the depth profile. In that case, the relatively high N content cannot be caused by recoil mixing, and therefore gives evidence of a small interdiffusion between the layers. This may be enhanced by the small thicknesses considered. The surface layer seems also to be slightly thinner, although deposited in the same conditions, than the buried oxide layer, probably due to a small window fogging absorption caused by the deposition of the N rich layer. This could however have been compensated by increasing the lamp power during the deposition of the surface oxide.

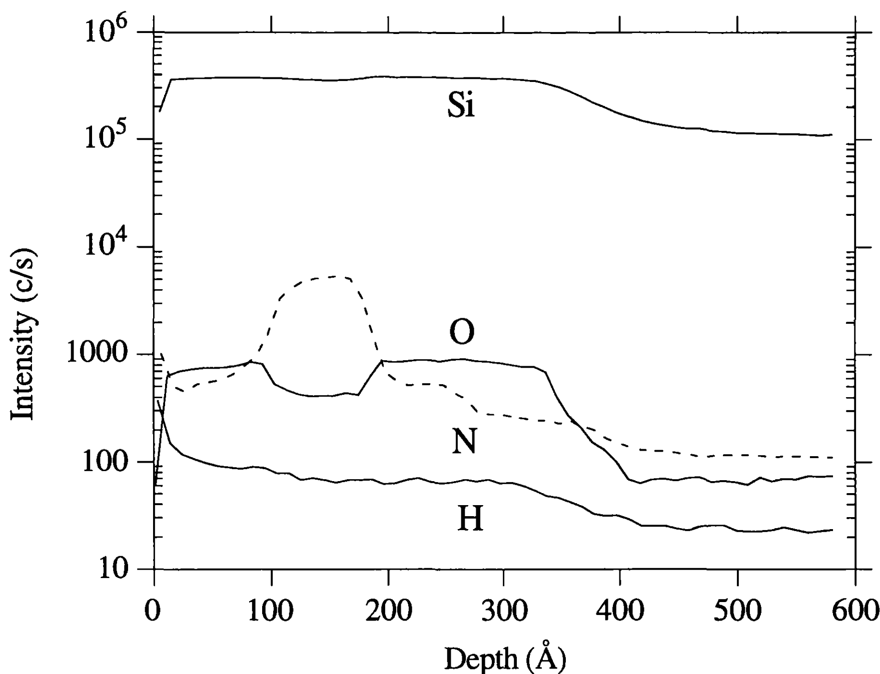

Figure 5.15 : SIMS profile of an oxide-nitride-oxide multilayered structure on silicon

3.- The photo-CVD of silicon oxynitride SiO_xN_y

In the previous sections have been reported the use of a 172nm radiation to deposit pure discrete layers of silicon dioxide and silicon nitride. Here, by directly combining the two processes, is achieved the photo-enhanced CVD of SiO_xN_y layers.

3.1- Interests in silicon oxynitride

Silicon oxynitride thin films present several advantages as layers for the fabrication of integrated-optical circuits. They can be deposited as a transparent amorphous film whose refractive index can be varied from 1.46 (SiO_2) to 2.0 (Si_3N_4), therefore permitting a controlled matching of waveguide structures. Further, for passive optical components applications, doping of a silicon oxynitride waveguide can be achieved by using nitrogen, whose use obviates the handling hazards and safety problems introduced by other dopants such as boron and phosphorous [Bruno]. Finally, Silicon nitride films are also fully compatible with microelectronics, and offer other advantageous properties over SiO_2 and Si_3N_4, e.g., lower mechanical stress [Watanabe-1989], and tunable density and stoichiometry. SiO_xN_y films are usually obtained in a two step process: silicon dioxide deposition and nitridation in a NH_3 flow at high temperature (≈ 800°C) [Hori]. As a result, the possibility to deposit *directly* the SiO_xN_y layers reduces the manufacturing overall thermal budget.

3.2- Thin SiO_xN_y film deposition

3.2.1- Experimental conditions

The photo-CVD reactor used is the same as previously described for the depositions of silicon dioxide and silicon nitride. P-type silicon wafers were used as substrates. The window to substrate distance was kept at 12mm, in order to keep the optimised geometry conditions obtained with the deposition of silicon nitrides. No particular window purge was used for those experiments. Various mixtures of silane, ammonia and nitrous oxide were used, and the sample properties were probed using ellipsometry and FTIR spectrometry.

Figure 5.16 shows the growth rate and refractive index of the films grown using different N_2O/NH_3 ratios at a constant pressure of 10mbar, and a substrate temperature of 300°C. The flow of silane is maintained at a constant value of 0.5 sccm, whether the sum of the ammonia and nitrous oxide flows is maintained constant at 50sccm. The smooth and continuous evolution of the refractive index with the variation of the N_2O/NH_3 mixture indicates a progressive evolution from nitride rich films towards stoichiometric oxides.

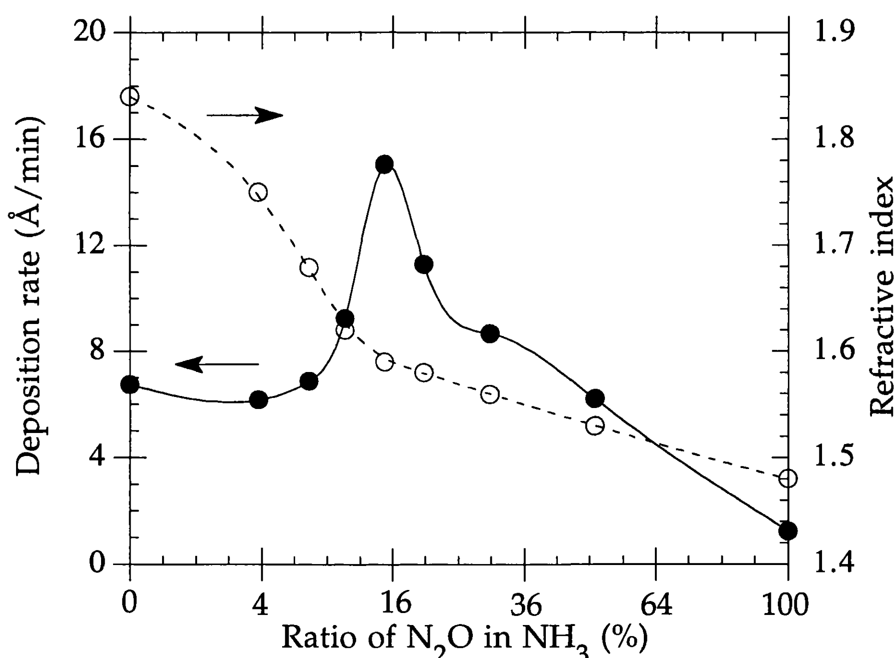

Figure 5.16: Relationship of the growth rate (•) and the refractive index (o) with the N_2O/NH_3 precursor mixture ratio (square root scale).

When only NH_3 is used, the nitride-rich films (n=1.83) grow around 5 times faster than the oxide-rich layers (n=1.48) produced in pure N_2O, reflecting the stronger absorption cross-section of the ammonia at this wavelength. As more NH_3 replaces the N_2O mixtures used, the deposition rate increases and the higher refractive index values of the films grown indicate a steadily increasing N content. Once the gas

values of the films grown indicate a steadily increasing N content. Once the gas mixture is dominated by NH_3 species (i.e., the N_2O/NH_3 ratio < 50%) the deposition rate exceeds that achieved for pure NH_3 alone, and reaches a maximum value at a ratio of N_2O/NH_3 of 16%. The films grown with this gas mixture, however, are still predominantly oxide-based, the refractive index being 1.58. This indicates that while the ammonia strongly absorbs the radiation, it is the oxide species that are being efficiently incorporated into the films. This effect is most likely controlled by an energy transfer (photo-sensitisation) process between the NH_3 and the N_2O species. At lower N_2O levels (N_2O/NH_3 ratios between 10 and 16%), the collisional transfer mechanism occurs less frequently and the film growth rate decreases abruptly whilst the layers formed become significantly more nitride-based. For N_2O/NH_3 ratios less than 10%, the N_2O content ceases to affect the growth rate, but nevertheless plays a continuing role in determining the refractive index of the films.

To further evaluate the structure of the deposited films, Fourier Transform Infra-Red spectrometry (FTIR) measurements were carried out. Figure 5.17 shows the FTIR spectra obtained from films whose refractive indices varied from 1.48 to 1.85. A clear transition from a Si-N predominant vibration mode to a Si-O is strongly visible in the spectra, and this corresponds directly to the change in refractive index. This evolution of the main stretching vibration mode is well in agreement with other published PECVD grown SiO_xN_y studies [Hirao] [Cros] [Tsu] [Denisse]. Table 5.2 summarises the properties of these films by showing the relationship between the refractive index and the position of the peak, resulting from the convolution of the main Si-O and Si-N stretching vibration modes located at 1065 and $835 cm^{-1}$, respectively [Boyd] [Berti]. Since the relationship between the refractive index and the SiO_xN_y stoichiometry has been reported as being quasi-linear [Knolle] [Xiong], the evolution of the stoichiometry with the precursor mixture ratio is in the present case very different, giving evidence (further to figure 5.16) of selective excitation of the gas phase precursors, due to the combination of the higher cross section exhibited by ammonia species, and the high degree of reactivity of O species. This ability to selectively predetermine the reactive precursor composition that will ultimately react with the silane gives this photo-CVD process an added advantage over conventional plasma deposition processes for optical coatings and optical fibre material manufacturing.

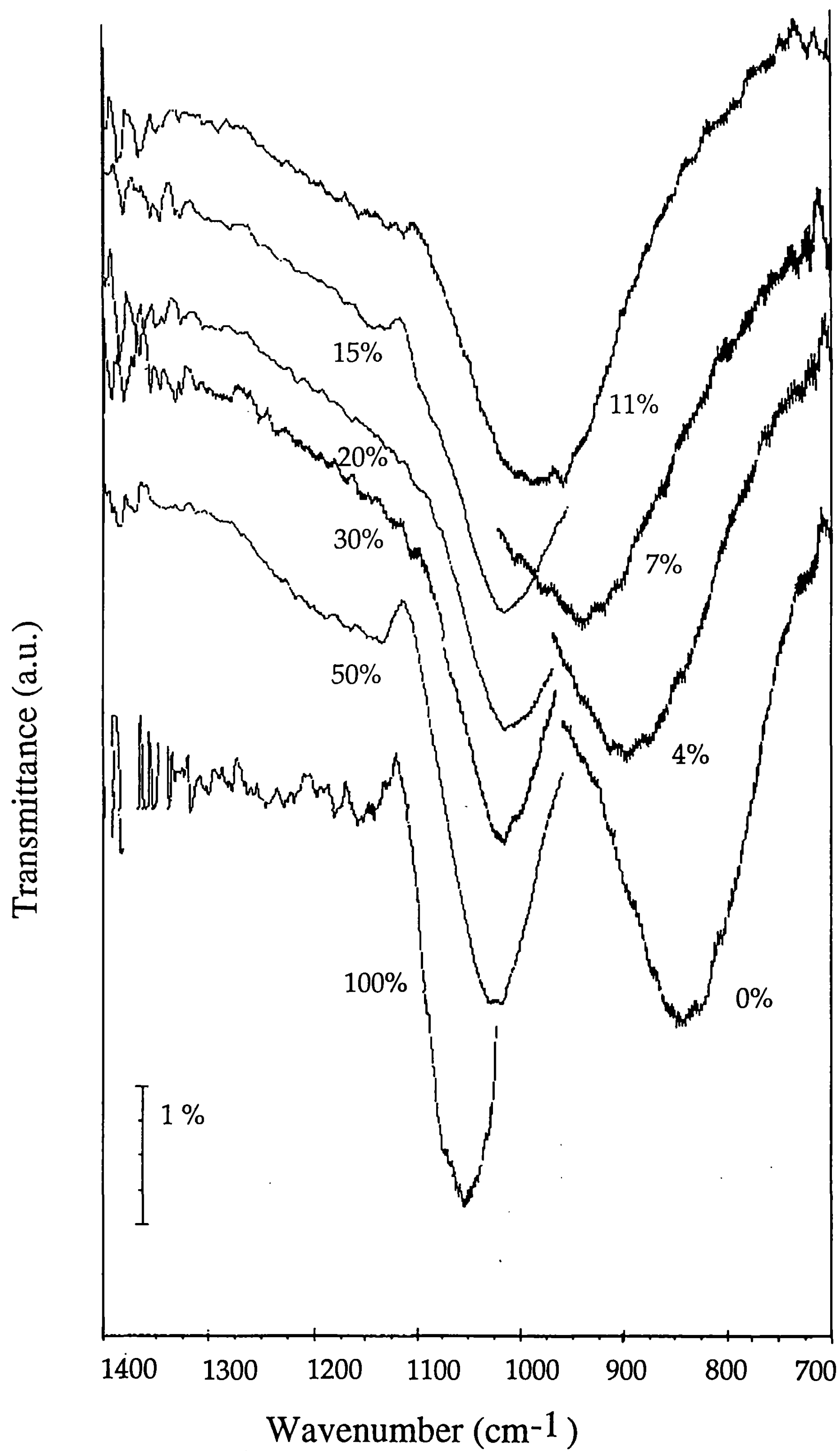

Figure 5.17: Evolution of the FTIR main stretching vibration peak with the N_2O/NH_3 precursor mixture ratio.

$SiH_4:NH_3:N_2O$	N_2O/NH_3 (%)	n	growth rate (Å/min)	Main Stretching Vibrational Mode (cm^{-1})	FWHM (cm^{-1})
0.5 : 50 : 0	0	1.84	6.74	$845 \pm 2\ cm^{-1}$	$125 \pm 5\ cm^{-1}$
0.5 : 50 : 2	3.8	1.75	6.16	$910 \pm 2\ cm^{-1}$	$175 \pm 5\ cm^{-1}$
0.5 : 50 : 4	7.4	1.68	6.88	$940 \pm 2\ cm^{-1}$	$175 \pm 5\ cm^{-1}$
0.5 : 50 : 6	10.7	1.62	9.25	$975 \pm 3\ cm^{-1}$	$150 \pm 5\ cm^{-1}$
0.5 : 42.5 : 7.5	15	1.59	15.03	$1000 \pm 2\ cm^{-1}$	$125 \pm 5\ cm^{-1}$
0.5 : 40 : 10	20	1.58	11.31	$1001 \pm 2\ cm^{-1}$	$125 \pm 5\ cm^{-1}$
0.5 : 35 : 15	30	1.56	8.68	$1015 \pm 2\ cm^{-1}$	$110 \pm 5\ cm^{-1}$
0.5 : 25 : 25	50	1.53	6.22	$1025 \pm 2\ cm^{-1}$	$100 \pm 5\ cm^{-1}$
0.5 : 0 : 50	100	1.47	1.25	$1050 \pm 1\ cm^{-1}$	$65 \pm 3\ cm^{-1}$

Table 5.2: FTIR results for oxynitride thin films

3.3- Conclusion

The possibility to deposit a variety of high quality SiO_xN_y dielectric films using a photochemical technique based on an excimer lamp has been demonstrated. This process is based on the 172nm wavelength from the excimer continuum of xenon in a dielectric barrier discharge lamp. The process has been shown to produce any predetermined SiO_xN_y mixture. The excellent control of the stoichiometry offered by this method potentially opens up new areas for the application of such lamps, especially since deposition at even higher rates and much larger areas can readily be achieved by scaling up the geometry of the apparatus used.

References to chapter 5

[Aritome] S.Aritome, M. Morita, T. Tanaka, M. Hiroshe, Appl. Phys. Lett., **51** (1987) 918

[Banerjee] I. Banerjee, D. Kuzminov, Appl. Phys. Lett., **62** (1993) 1541

[Berti] M. Berti, M. Meliga, G. Rovai, S. Stano, S. Tamagno, Thin Solid Films, **165** (1988) 279

[Bhatnagar] Y.K. Bhatnagar, in *Photo-CVD of hydrogenated amorphous silicon and silicon dioxide using an external deuterium lamp*, PhD thesis, University of Cambridge (1989)

[Borghesi] A. Borghesi, E. Bellandi, G. Guizetti, A. Sassella, S. Rojas, L. Zanotti, Appl. Phys., **A 56** (1993) 147

[Boyd] I.W. Boyd, J.I.B. Wilson, J. Appl. Phys., **53** (1982) 4166

[Brekel] C.H.J.v.d. Brekel, P.J. Severin, J. Electrochem. Soc., Sol. State Sci. and Technol., **119** (1972) 372

[Bruno] F. Bruno, M. del Guidice, R. Recca, F. Testa, Appl. Optics, **30** (1991) 4560

[Calvert] J.G. Calvert, J.N. Pitts, “Photochemistry”, John Wiley and Sons, New York (1966)

[Chan] T.Y. Chan, K.K. Young, C. Hu, IEEE Electron. Dev. Lett., **8** (1987) 93

[Chou] R. Chou, W.A. Lanford, W. Ke-Ming, R.S. Rosler, J. Appl. Phys., **53** (1982) 5630

[Claassen] W.A.P. Claassen, W.G.J.N. Valkenburg, F.H.P.M. Habraken, Y. Tamminga, J. Electrochem. Soc., Solid State Sci. and Technol., **130** (1983) 2419

[Collet] M.G. Collet, J. Electrochem. Soc.: Solid State Science, **116** (1969) 110

[Cros] Y. Cros, N. Jaffrezic-Renault, J.M. Chovelon, J.J. Fombon, J. Electrochem. Soc., **139** (1992) 507

[Denisse] C.M.M. Denisse, K.Z. Troost, J.B. Oude, F.H.P.M. Habraken, W.F. van der Weg, J. Appl. Phys., **60** (1986) 2536

[Eisele] K.M. Eisele, W. Rothemund, B. Dischler,
Vacuum, **41** (1990) 108

[Guizot] J.L. Guizot, P. Alnot, F. Wyczisk, J. Perrin, B. Allain,
Semicon. Sci. Technol., **6** (1991) 582

[Gupta] M. Gupta, V.K. Rathi, R. Thangaraj, O.P. Agnihotri,
Thin Solid Films, **204** (1991) 77

[Hess] D.W. Hess, J. Vac. Sci. Technol., **A2** (1984) 244

[Hirao] T. Hirao, K. Setsune, M. Kitagawa, T. Kamada, T. Ohmura,
K. Wasa, T. Izumi, Jpn. J. Appl. Phys., **27** (1988) L21

[Hori] T. Hori, H. Iwasaki, H. Esaki,
IEEE Transactions on Electron. Dev., **ED-34** (1987) 2238

[Inoue] T. Inoue, M. Konagai, K. Takahashi,
Jpn. J. Appl. Phys., **24** (1985) 678

[Inushima] T. Inushima, N. Hirose, K. Urata, K. Ito, S. Yamazaki,
Appl. Phys., **A 47** (1988) 229

[Ishikawa] Y. Ishikawa, I. Kobayashi, I. Nakamichi,
Jpn. J. Appl. Phys., **31** (1992) L443

[Jauberteau] J.L. Jauberteau, D. Conte, M.I. Baraton, P. Quintard,
J. Aubreton, A.. Catherinot, Thin Sol. Films, **189** (1990) 111

[Jo] Y.-S. Jo, J.A. Schultz, S. Tache, S. Constanini, J.W. Rablais,
J. Appl. Phys. 60 (1986) 2564

[Knolle] W.R. Knolle, J.W. Osenbach, A. Elia,
J. Electrochem. Soc., **139** (1992) 3310

[Kyuragi] H. Kyuragi, T. Urisu, J. Electrochem. Soc., **138** (1991) 3412

[Langford] A.A. Langford, J. Bender, M.L. Fleet, B.L. Stafford,
J. Vac. Sci. Technol., **B7** (1989) 437

[Lee-1990] H.H. Lee, *Fundamentals of microelectronics processing*,
McGraw-Hill Publishing Company, New York, (1990)

[Lee-1988] S.K. Lee, J.H. Chen, Y.H. Yu, D.L. Kwong, B.Y. Nguyen,
K.W. Teng, Solid-State Electronics, **31** (1988) 1501

[Lemiti] M. Lemiti, S. Audisio, J.C. Dupuy, B. Balland,
J. non-Crystalline Sol., **144** (1992) 261

[Lustig] N. Lustig, J. Kanicki, J. Appl. Phys., **65** (1989) 3951

[Matsumura] H. Matsumura, Jpn. J. Appl. Phys., **28** (1989) 2157

[Manzini] S.Manzini, G. Queirolo, Sol. State. Electronics, **30** (1987) 587

[Navon] D.H. Navon in *Semiconductor microdevices and materials*, CBS Publishing Japan Ltd, Tokyo, (1986)

[Nikolic] G.M. Nikolic, Vacuum, **40** (1990) 143

[Nishino] S. Nishino, H. Honda, H. Matsunami, Jpn. J. Appl. Phys., **25** (1986) L87

[Numasawa-1983] Y. Numasawa, K. Yamazaki, K. Hamano, Jpn. J. Appl. Phys., **22** (1983) L792

[Numasawa-1986] Y. Numasawa, K. Yamazaki, K. Hamano, J. Elect. Mat., **15** (1986) 27

[Padmanabhan] R. Padmanabhan, N.C. Saka, J. Vac. Sci. Technol., **A6** (1988) 2226

[Paloura] E.C. Paloura, S. Logothetidis, S. Boultadakis, S. Ves, Appl. Phys. Lett., **59** (1991) 280

[Parsons] G.N. Parsons, J.H. Souk, J. Batey, J. Appl. Phys., **70** (1991) 1553

[Peters] J.W. Peters, F.L. Gebhart, U.S. Patent No. 4265 932

[Petitjean] M Petitjean, N. Proust, J.F. Chapeaublanc, J. Perrin, Appl. Phys., **A 54** (1992) 95

[Press] W.H. Press, B.P. Flannery, S.A. Teukolsky, W.T. Vetterling, *Numerical Recipes in C*, Cambridge University Press (1986)

[Rand] M.J. Rand, D.R. Wonsidler, J. Electrochem. Soc., Solid State Sci. and Technol., **125** (1978) 99

[Rocheleau] R.E. Rocheleau, S.S. Hegedus, W.A. Buchanan, S.C. Jackson, Appl. Phys. Lett., **51** (1987) 133

[Seager] C.H. Seager, J. Kanicki, MRS. Symp. Proceedings,Vol. **284** (1993) 89

[Shirafuji] J. Shirafuji, S. Miyoshi, H. Aoki, Thin Sol. Films., **157** (1987) 105

[Sinha] A.K. Sinha, H.J. Levinstein, T.E. Smith, G. Quintana, S.E. Hasko, J. Electrochem. Soc., Solid State Sci. and Technology, **125** (1978) 601

[Smith] D.L. Smith, A.S. Alimonda, C-C. Chen, H.C. Tuan, J. Elect. Mat., **19** (1990) 19

[Sobalewski] M.A. Sobalewski, C.R. Helms,
J.Vac. Sci. Technol., **A6** (1988) 1358

[Sugii] T. Sugii, T. Ito, H. Ishikawa,
Jpn. J. Appl. Phys., **45** (1984) 966

[Suzuki] E. Suzuki, H. Hiraishi, K. Ishii, Y. Hayashi,
IEEE Trans. Electron. Dev., **ED-30** (1983) 122

[Sze] S.M. Sze, *Semiconductor Devices, Physics and Technology,*
J. Wiley & Sons, New York (1985)

[Tanimoto] S. Tanimoto, M. Matsui, K. Kamisako, K. Kuroiwa, Y.
Tarui, J. Electrochem. Soc., **139** (1992) 320

[Tannenbaum] E. Tannenbaum, E.M. Coffin, A.J. Harrison,
J. Chem. Phys., **21** (1953) 311

[Ting] W. Ting, S.N. Lin, D.L. Kwong,
Appl. Phys. Lett., **55** (1989) 2313

[Tsu] D.V. Tsu, G. Lucovsky, M.J. Mantini, S.S. Chao,
J. Vac. Sci. Technol., **A5** (1987) 1998

[Tsuji] M.Tsuji, N. Itoh, Y. Nishimura,
Jpn. J. Appl. Phys., 30 (1991) 2868

[Watanabe-1984] T. Watanabe, A. Menjoh, M. Ishikawa, J. Kumagai,
IEEE IEDM Techn. Dig., **173** (1984)

[Watanabe-1989] J. Watanabe, M. Hanabusa, J. Mat. Res., **4** (1989) 882

[Xiong] Y-M. Xiong, P.G. Snyder, J.A. Woollam, G.A. Al-Jumaily,
F.J. Gagliardi, L.J. Mizerka,
Surface and Interface analysis, **18** (1992) 124

Conclusions

In this work, new deposition methods have been devised, that involve some of the first applications of recently developed excimer lamps. The development of these excimer lamps is potentially a major breakthrough since they now make available a much extended range of wavelengths in the VUV, UV and visible range at higher power densities than currently available, and low cost. The deposition procedures followed utilised the photochemical initiation of gas phase reactions at low temperatures (below 300°C). Specifically, this project focused on the growth of silicon dioxide and nitride thin films, as well as of silicon oxide-nitride-oxide stacked multilayers, and silicon oxynitrides. These results indicate a new method of thin film fabrication for electronic and optical applications.

Chapter 1 describes the development of the prototype reactor used, highlighting design requirements, which include geometry, cost, control apparatus, and safety considerations. In chapter 2, the theory of light generation from excimer states is presented, together with the description of a few devices which radiate a few watts in the UV and VUV parts of the spectrum. The excimer-photo-CVD system developed offered excellent reliability, and a high degree of flexibility which enabled a diverse set of applications to be studied.

Chapter 3 describes a series of additional experiments that were devised during this project which take advantage of the high fluxes of UV radiation now available. These include the generation of ozone, an environmentally clean oxidant with numerous applications from water treating to elaborate wafer cleaning, which is achieved in a similar manner to that occurring in the upper atmosphere. A brief study of the use of

UV radiation to stimulate chemical changes in several organometallic spin-on coatings is also reported. Such processes have potential uses for room temperature thin film fabrication.

In chapter 4, the radiation emitted from a xenon excimer lamp, centred at 172nm, is used to initiate low temperature photo-deposition of silicon dioxide films from the gas phase. By studying the effect of pressure, temperature, precursor gas flows and mixtures, the film growth has been optimised. Film quality was assessed in terms of optical and physical properties, and layers with refractive index values of 1.46, and high SiO_2 stoichiometry were produced at 300°C. Two different gaseous mixtures were studied. While silane was common to both, the oxygen was supplied either as molecular N_2O or as O_2. In the first case, low growth rates of about 10Å/min at 300°C were only achieved, but this enabled excellent thickness control for thin layer growth. When O_2 and silane are used, much faster deposition rates (≈100-250Å/min) were obtained, even at temperatures as low as 200°C. Although window fogging (i.e., deposition of material on the inside of the cell window through which the radiation is transmitted) has often been reported as a possible limitation to photo-CVD, this work has found that the effect of the product deposition on the window was insignificant, opening up applications towards the deposition of passivating layers, diffusion barriers, as well as optical coatings used in many technological applications.

Photo-CVD of silicon nitride thin films from various silane/ammonia mixtures using a radiation centred at 172nm is presented in chapter 5. The physico-chemical properties of the films obtained at 300°C were in very good agreement with literature data reported from processes using much higher substrate temperatures. The deposition of films with refractive indices of 1.85 is reported, a high value for photo-CVD nitrides, especially since the films did not exhibit a high hydrogen content. By combining the deposition of silicon nitride layers with that of silicon dioxide, the direct *in-situ* photo-stimulated deposition of ONO stacked layers is presented, together with that of SiO_xN_y mixed coatings. The process demonstrated the possibility of depositing any predetermined SiO_xN_y mixture, with refractive index tuning from 1.48 to 1.85. The excellent control of the stoichiometry offered by the method potentially opens up new areas of applications of the xenon excimer lamp

techniques towards optical waveguide or low mechanical stress coating depositions. Preferential photo-excitation pathways in the photochemistry have been demonstrated, and evidence was given that this selective excitation feature enables a better control of the SiO_xN_y composition. Compatibility of the deposition processes was demonstrated on gallium arsenide and quartz substrates. The technique can be extended to other III-V semiconducting materials, glass, and several heat sensitive compounds.

The ability to modify the wavelength of the generated radiation in excimer lamps by simply refilling the lamp discharge volume also opens up new applications for this technique, essentially since other photochemistries could be enhanced selectively using other wavelength continua. In particular, with a lamp device radiating $30mW/cm^2$ at 126nm, the direct photo-dissociation of silane was attempted, in order to deposit hydrogenated amorphous silicon. Promising aspects were exhibited by those experiments, as presented in appendix 1. The latter work, however, gave evidence of inherent limitations in our photo-CVD reactor, since major modifications should be implemented in order to reduce the window fogging absorption. Nevertheless, this work has potentially opened up other areas of investigations for excimer lamp users.

The Photochemical Deposition of Hydrogenated Amorphous Silicon using an Argon Excimer Lamp

In chapter 2, the possibility of generating wavelengths shorter than the xenon continuum centred at 172nm has been demonstrated, and particularly that of the 126nm continuum of argon. Here, it is proposed to use this radiation to enhance the photo-chemical deposition of hydrogenated amorphous silicon (a-Si:H). The reactor used for those experiments is the same as previously described for silicon dielectric depositions, and very few modifications have been made. The aim of this appendix is to give a proof a feasibility of this technique.

1.- Hydrogenated amorphous silicon (a-Si:H)

1.1- Introduction

Over the last decade, amorphous silicon has emerged as an economically viable semiconducting material for various electronic applications. In the particular case of solar cell applications, it gives promising alternatives to the use of crystalline (c-Si) silicon, by offering reduced manufacturing cost per watt generated (table 6.1). Solar energy, which is clean and practically unlimited, is expected to be a desirable alternative energy source to conventional power supplies, and demand for the photovoltaic system has increased throughout the world, especially in Europe and the United States. Photovoltaic cells are probably the most effective method for capturing solar energy, since they are easy to use and are the most effective means of directly generating electricity. However, the present high levels of manufacturing costs have limited their applications to remote areas where electricity is given a high value, or where a clean, quiet and reliable generator is needed. The promising improvements in manufacturing costs offered by hydrogenated amorphous silicon towards crystalline silicon have motivated industrial interests. To date, however, the light to electrical conversion efficiency of solar cells using a-Si:H is far lower than that of those using c-Si (table 6.1), thus motivating intense research throughout the world.

Technique	Cost (US$)	Typical module efficiency
Typical electricity plant	$0.25 to $1	
photovoltaic material in solar cells:		
c-Si	$8-$12	16-18%
poly-Si	$2-$5	10-12%
a-Si-H	$0.5-$1	5-7%

Table A1.1: Electricity generation costs per watt and corresponding module efficiencies for typical solar cells (adapted from [Takashi] and [Hamakawa])

The wide variety of R&D efforts aimed at high efficiency and low cost have been in progress on each part of the photovoltaic cell and module processing. Among these, remarkable advances have been seen in new technologies (e.g., heterojunctions, graded band profiling, doping, superlattices and stacked junctions), resulting in a steadily improving amorphous silicon solar cell efficiency. As such, one can quote the promising recent efficiency of 21% reported by Ma *et al.* from Osaka University on a laboratory solar cell based on a-Si:H. [Ma]

1.2- Interests

Amorphous silicon is an interesting material since it does not have a long range regularity, so there is a slight variation in the Si-Si bond length. The result is that the forbidden band gap is slightly different, depending on location. Consequently, the state density, as a function of energy, does not present the sharp feature found in crystalline silicon, and tails off at its edges. There is a continuous distribution of states throughout the energy range between the conduction and valence band regions (figure 6.1). The levels present in the forbidden band are called "localised states". Their high concentration is due to the large density of "dangling bonds" inside the material. In pure amorphous silicon, the state density presents a decrease in the middle of the resulting "band gap", but the defect level being very high, it is difficult to determine the structure of the energy bands. In fact, considering a typical 1% of dangling bonds in amorphous silicon, the resulting state density concentration around the Fermi level is only of two orders of magnitude lower than in the conduction and valence bands, a far too small value for a band gap behaviour to be observed. This material presents very little interest as a semiconducting material as changes cannot be produced by doping impurities, since the defect levels already present are more numerous.

However, it has been found that when a small concentration of hydrogen is added to the a-Si structure, the state density sharply decreases by several orders of magnitude around the Fermi level, thus rendering p-n control possible, making a-Si:H an interesting semiconducting and photovoltaic material [Carlson] [Pankove]. It is generally assessed that an optimum hydrogen incorporation stands between 12 and

15% of the silicon. The hydrogen atoms do not serve only to fill the localised states (1%), but also to relax local strain and preserve short-range order. Further, when hydrogen is added to Si, since the Si-H bond energy (3.4eV) is greater than the Si-Si bond energy (2.2eV), the forbidden bandgap increases with added hydrogen concentration (figure A1.1). The optical band gap obtained from the measurement of the absorption coefficient (see § 3.3.1) is often employed to describe the resulting forbidden band gap. Typical values for a-Si:H are in the range of 1.6 to 1.8eV. Also, in contrast to c-Si, an indirect gap semiconductor, a-Si:H exhibits a sharp "non direct" optical absorption edge, that gives rise to a large optical absorption coefficient and facilitates the development of thin film photoreceptor [Kruzelecky].

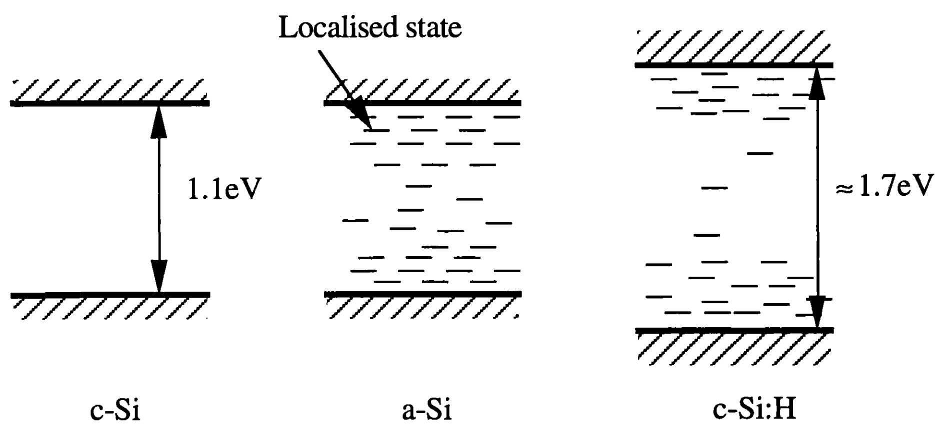

Figure A1.1: Schematic of band structure for crystalline Si, amorphous Si, and amorphous Si:H.

1.3- Usual deposition techniques of a-Si:H

In using a-Si:H for device applications, there is a particular difficulty in growing this material using the usual c-Si processing techniques. For instance, the hydrogen evolves from the material at temperatures above 350°C [Shanks] (see § 3.4.1), and since the importance of the hydrogen concentration in the optical band gap energy has been mentioned, higher processing temperatures imply difficult stoichiometry control, which mostly results in poor electronic properties. This is the main reason to search for ways to develop low temperature processes which do not involve heating the material beyond this threshold.

Initially, the known conventional methods for depositing amorphous silicon were by evaporation, sputtering, and chemical vapour deposition. The hydrogen concentration was adjusted using an additional implantation step. At present, the glow discharge method, or PECVD method, is the best for solar cell manufacturing [Gallagher] [Hamakawa]. The film is grown by dissociating silane (SiH_4) in a plasma, with or without the use of a diluting gas, and with substrate temperatures in the 200-300°C range. The dissociation of silane leads to the formation of SiH, SiH_2, and H radicals, which diffuse to the substrate surface and react for film growth. So far, the glow discharge technique appears in the literature as being the more widely used since it offers the best properties and growth characteristics. However, as ion bombardment is present during growth, the resulting damage may limit the fields of applications to solar cells applications, and new techniques have to be investigated for other microelectronic applications of a-Si:H such as for thin film transistors (TFT).

To overcome this problem, recent techniques using photo-CVD have been developed for the deposition of a-Si:H. Similarly to the cases of silicon dioxide and other dielectrics studied in this thesis, the principle relies on the dissociation of the precursors using high energy photons. However, silane photodissociation requires the use of photons below 150nm, much shorter wavelengths than those involved with the dielectric thin film deposition previously described. As a direct consequence, the problems of the unavailability of high intensity continuous sources radiating in this range, as well as that of the window fogging are more difficult to overcome. One alternative consists of using mercury sensitised photo-CVD (Ch.1, §1.3.1) [Tachibana], but hazards connected with the use of mercury motivated research for the development of other methods. Other groups have concentrated on the use of other silicon hydrides compounds such as Si_2H_6 or Si_3H_8, which require the use of lower energies for direct photo-dissociation [Fuyuki] [Yamada] [Zarnani]. Kessler *et al.* have also applied successfully the excimer lamp techniques to such depositions. Their method was based on the photodissociation of disilane Si_2H_6 by 172 nm photons generated in a xenon excimer lamp [Kessler]. The window fogging problem was overcome using a thin layer of Fomblin oil to prevent from the deposition of an absorbing thin film layer on the window. Other groups have also concentrated on the use of internal lamps [Yoshida]. In fact, suppressing the window

between the chamber and the lamp enables the use of much shorter wavelengths, as well as the complete absence of the troublesome window fogging problem. This technique was first developed by W.I. Milne *et al.*, to deposit good quality hydrogenated amorphous silicon [Robertson-1986] [Milne-1992]. However, it was reported that in the case of a-Si:H deposition using the 160 to 90nm continuum emission from a hydrogen discharge lamp, almost 30% of the hydrogen incorporated into the film results from energetic hydrogen radicals generated in the lamp discharge volume [Milne-1989]. As a result, and for the same reason as in plasma CVD, this may lead to detrimental bombardment of the film.

2.- Photo-CVD of a-Si:H

2.1- Photochemistry

Here is discussed the use of the 126nm argon continuum to enhance the deposition of amorphous silicon from the direct photo-dissociation of silane (SiH_4), which absorbs radiations of wavelengths below 150nm. Under the 126nm photons, silane shows an absorption cross section σ of 0.8 to 1 $10^{-16}cm^2$ [Kawai] [Harada] [Itoh], corresponding to 2100 to 2700 $atm^{-1}cm^{-1}$. As a comparison, pressures lower by one and a half order of magnitude than those used for the ammonia experiments would exhibit a similar light attenuation in the irradiated gas phase.

Under the argon excimer continuum radiations, the silane molecules are photo-dissociated

$$SiH_4 + h\nu \rightarrow SiH_2 + 2H \qquad (A1\text{-}1)$$

$$SiH_4 + h\nu \rightarrow SiH_3 + H \qquad (A1\text{-}2)$$

Secondary reactions will lead to the formation of other silicon hydrides to be dissociated.

$SiH_4 + H \rightarrow SiH_3 + H_2$ (A1-3)

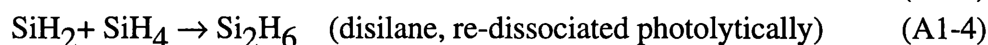

$SiH_2 + SiH_4 \rightarrow Si_2H_6$ (disilane, re-dissociated photolytically) (A1-4)

$SiH_2 + SiH_4 \rightarrow SiH_3SiH + H_2$ (A1.5)

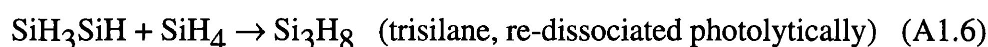

$SiH_3SiH + SiH_4 \rightarrow Si_3H_8$ (trisilane, re-dissociated photolytically) (A1.6)

The reactive radicals SiH_2 & SiH_3 formed in the gas phase lead to surface reactions and film deposition on the substrate surface.

2.2- Experimental set-up and apparatus

2.2.1- Introduction

The reactor configuration is shown on figure 2.21 (chapter 2). It consists of a light generation chamber, located above a reaction chamber. The 126nm radiation enters the reactor through a MgF_2 window ($\lambda \geq 120$nm), and irradiates a substrate above which is fed the silane gas. Due to absorption problems on the window (window fogging, see chapter 5, § 1.3), an argon gas purge is used to flush reactive precursors away from the window. Since the amorphous silicon products which condense on the window are opaque to the radiation, a very high purging flow has to be used, and experiments with duration longer than 10 minutes are ineffective.

2.2.2- Optimisation of the total pressure for fast deposition

Since in chapter 5, § 1.3.4 (figure 5.5), the effect of the total chamber pressure on the window purge was investigated, here is studied this effect on the growth rate (figure A1.2). The absorption on the window is reduced when the pressure is increased from 0.1 to 5mbar, and consequently a significant increase in the growth rate is observed. However, if the pressure is further increased, the exponential absorption of the radiation in the gas phase reduces strongly the deposition on the substrate. Optimum pressure conditions stand between 5 and 7 mbar.

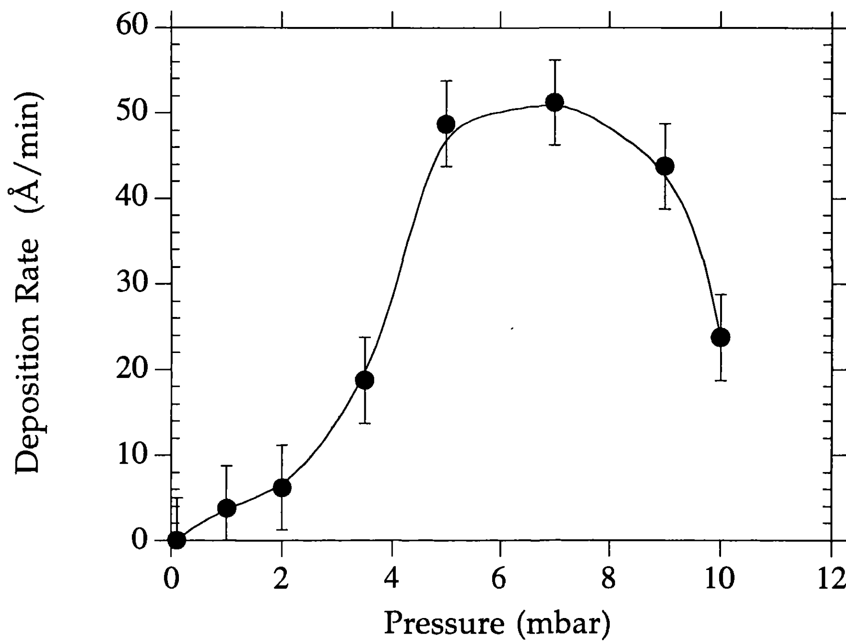

Figure A1.2 : Effect of the pressure on the deposition rate

2.2.3-Effect of the window to substrate distance

The flow perturbations caused by the window purging gas in the neighbourhood of the substrate can be reduced while increasing the window to substrate distance. However, when the distance is too high, a decrease of the deposition rate is observed since the absorption of the radiation in the gas phase occurs too far from the substrate. The distance used is of 12 millimetres.

2.2.4- Effect of the SiH_4/Ar ratio

A high flow of argon gas purge leads to turbulences in the neighbourhood of the substrate and therefore decreases the growth rate. However, the efficiency of the gas purge would benefit from an increase in the ratio of the two flows. A flow of 200sccm is chosen (maximum of the MFC). An increasing value in the silane flow induces a very high increase in the deposition rate. The highest flow available from

the attached silane MFC was of 12 sccm. Also, a local "over pressure" in the neighbourhood of the substrate was created by confining the precursor gases using a metal ring around the substrate holder (figure A1.3).

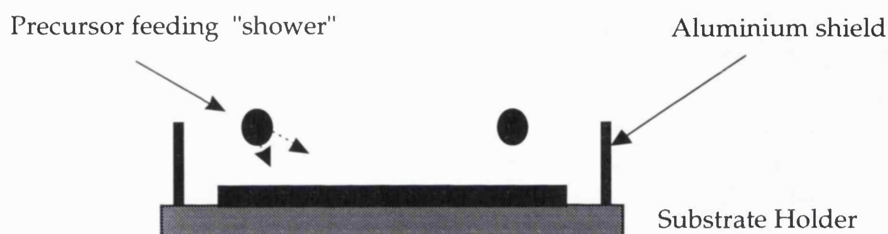

Figure A1.3 : Aluminium shield used to confine the precursor gases in the vicinity of the substrate.

2.2.5- Summary

The final configuration used for the deposition of amorphous silicon has been presented, and table A2.2 summarizes the optimised deposition parameters. As the aim of those experiments is to give a proof of principle of the photo-CVD of a-Si:H with the argon excimer lamp, most of the modifications added to the system are empirical and it is agreed that a further development should consider the complete redesign of the reactor, and in particular that of the widow purging configuration. With the actual design, thin films of a-Si:H with thicknesses up to 300Å can be grown, and the deposition of thicker films implies successive repetitions of the process. Also, since the system has been used for several months to deposit dielectric films, and particularly oxygenated layers, clearly a residual contamination may occur.

Parameter	Value
Total Pressure (mbar)	5
SiH_4/Ar flows (sccm)	12 / 200
Purge-shower/window distance Precursor-shower/substrate distance Window/Substrate distance	2 mm 3 mm 20 mm
Circular ring to confine precursor gases in the neighbourhood of the substrate	Yes

Table A2.2 : Optimised geometry condition for a-Si:H deposition

3.- Thin Film deposition

3.1- Sample preparation

In thin a-Si:H films, since surface effects may alter the electrical characteristics, it is generally agreed to grow films with thicknesses superior to 0.3 μm. Due to the limitations associated with the reactor and essentially window fogging problems, only a-Si:H layer of 300Å in thickness can be obtained. Therefore, higher thicknesses can only be achieved by repetitive deposition experiments with intermediate window cleaning operations. Table A1.3 summarizes the thicknesses and properties obtained for different samples prepared at various substrate temperatures.

Sample Name	Substrate Temperature (°C)	Number of successive experiments	Duration of one individual experiment (min)	Thickness (Å) (±15Å)	Refractive index at 632.8nm
L1	200	8	10	1240	3.9±0.2
L2	250	8	10	1340	4.1±0.2
L3	300	8	10	1460	4.2±0.2
L4	400	6	10	1580	3.7±0.2

Table A1.3 : a-Si:H sample preparation for various substrate temperatures.

Each sample processed consists of the combination of portions of fused quartz as well as intrinsic silicon crystalline substrates, (111) oriented. The thicknesses and refractive indices are measured using a Rudolph AutoEl ellipsometer. A relative high error on the measurements is considered since this equipment is calibrated for films exhibiting lower refractive indices (1.4-2.0).

3.2- Fourier Transformed Infrared Spectroscopy

The L1 to L4 silicon samples were measured using FTIR spectroscopy on a Perkin-Elmer 2000 unit. The spectrum of the bare Si wafer is subtracted numerically to the transmission signal obtained. Using this technique, it is difficult to analyse accurately the Si-Si bond concentration in the deposited layer, since the silicon substrate itself is responsible for such vibration modes. However, FTIR spectroscopy will enable us to study accurately the behaviour of the incorporated hydrogen atoms, from the study of Si-H vibration modes.

Two major domains of the infrared spectrum are of interest, located around 2000 to 2100 cm^{-1} and 600 to 900 cm^{-1}, respectively. The stretching vibration mode of Si-H is observed as a sharp peak at 2000 cm^{-1}. However, this peak may be shifted towards higher wavelengths due to the convolution with Si-H_2 stretching vibration mode located at 2070 cm^{-1} (Appendix 3). The inherent relatively high concentrations of hydrogen in amorphous silicon are often found as a combination of atomic and molecular hydrogen, and since only atomic H is desirable, the study of the exact position of this peak gives a good information on the quality of the film.

Figure A1.4 shows the detail of the 1800 to 2200 cm^{-1} range for samples L1 to L4. The substrate temperature increase causes a perceptive transition from a peak centred around 2100 cm^{-1} down to the Si-H stretching vibration of 2000 cm^{-1}. At 200°C, mostly H_2 species bonded with Si are present in the film, whether at 300°C atomic hydrogen becomes predominant in the binding concentration. When the temperature is further increased towards 400°C, the H concentration drops, resulting in a reduction of the 2000cm^{-1} vibration mode. The shift from 2070 to 2000cm^{-1} is thus related to a decrease in the molecular hydrogen concentration. In fact, while silicon

hydrides (SiH_x) products are formed in the gas phase, some molecular hydrogen may be trapped on the sample surface during growth. Increasing the substrate temperatures to values greater than 250°C helps H_2 dissociation during growth and hence reduces its incorporation.

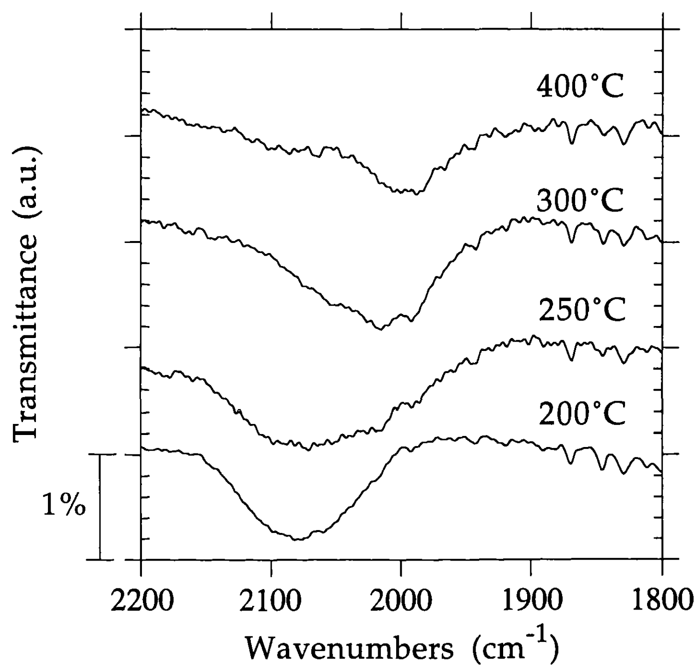

Figure A1.4 : 1800 to 2200 cm^{-1} detail of the FTIR spectrum

In the wavenumber range located between 600 and 900 cm^{-1}, a peak greater than the one located at 2000cm^{-1} is visible at 630cm^{-1}. It corresponds to the Si-H bond bending vibration mode, and it allows to calculate the percentage of atomic hydrogen incorporated in the film. Adams reported that the H concentration may be related to the number of bonds by the equation

$$N_H = K \int \alpha(\omega)\, d\omega \approx K \alpha H \qquad \text{(A1.7)}$$

Where α is the maximum value of the absorption coefficient, H the full bandwidth at half absorbance (FWHM), and K=2.5 10^{16} cm^{-1} [Brodsky] [Adams][John-1981-a]. Other vibration modes have been observed in this region, although not visible in the present case, and particularly at 845cm^{-1} ($(SiH_2)_n$ bending scissors) and at 880cm^{-1}(SiH bending mode), thus giving further information on the form (atomic or molecular) of hydrogen [Yamada]. Figure A1.5 shows the detail of this region of the spectrum for different deposition temperatures. Broad peaks are observed around 650 cm^{-1}, which decrease when higher deposition temperatures are used. A small absorption characteristic is also observed around 1010 cm^{-1}. This peak is caused by atomic oxygen appearing in the form of Si-O groups in the a-Si:H films [Tsu] [Ritter] [Sato]. This may be caused by oxygen contamination induced by the successive expositions of the sample to atmosphere between the deposition experiments (window cleaning procedures). Therefore, this problem would be overcome while implementing a more efficient window purge.

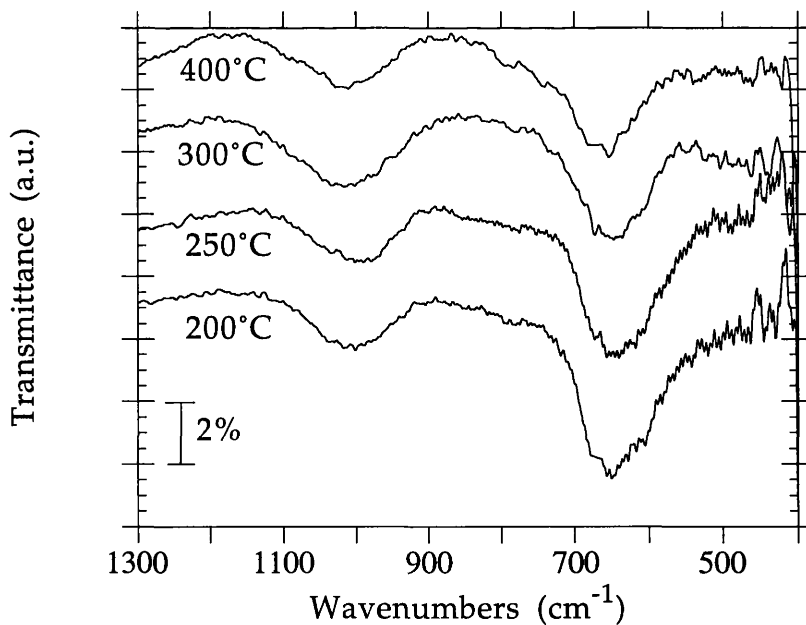

Figure A1.5 : Evolution of the FTIR spectrum located between 400 and 1300cm^{-1} with the deposition temperature.

The concentrations of atomic hydrogen were calculated from equation (A1.7), and from the Si-H bond bending vibration mode peaks, assuming a film density of 2.0g/cm^3 (Table A1.4) [Yamada].

Deposition Temperature (°C)	200	250	300	400
Absorption coefficient α at Si-H peak ($\approx$630cm^{-1}) (cm^{-1})	4270	3175	2260	1760
Full Width Half Maximum (cm^{-1})	104	109	97	85
n_H (at./cm^3)	$1.1\ 10^{22}$	$8.5\ 10^{21}$	$5.5\ 10^{21}$	$3.7\ 10^{21}$
H/Si Concentration (%) (ρ=2.0g/cm^3) ($\pm\approx$3%)	25.8	20.1	12.7	8.7

Table A1.4 : Evolution of the hydrogen incorporation with the temperature

3.3- Optical and electrical characterisation

3.3.1- Optical bandgap

The a-Si:H layers deposited on quartz samples were probed using a double beam Shimadzu UV-160A UV-visible spectrometer scanning in the 200-1000nm range. Optical absorption measurements in this region give important information about the thickness, the chemical composition [Maessen], and the optical bandgap of the deposited layers. Optical propagation of light through an absorptive medium can be described by:

$$I(h\nu) = I_0 \exp(-\alpha(h\nu)\ x) \qquad \text{(A1.8)}$$

where x is the sample thickness.

In amorphous semiconducting materials such as silicon, and assuming a parabolic density of extended states, Tauc *et al.* proposed an expression of the absorption coefficient α as:

$$\alpha(h\nu) = B\ (h\nu - E_{opt})^2 / h\nu \qquad \text{(A1.9)}$$

where B is a constant, and E_{opt} the resulting optical band gap [Tauc].

The plot of $(\alpha(h\nu))^{1/2}$ against $h\nu$ will therefore intercept the energy axis at E_{opt} (Tauc plot). From the measurement of the transmittance T, the absorbance A=log (100/T), and the absorption coefficient $\alpha = 2.303\ A/x$ are deduced. In Figure A1.6 is given the optical transmission spectra, and in figure A1.7 the corresponding Tauc plots for samples L1 to L4 deposited at 200 to 400°C respectively. Finally are plotted the E_{opt} values as a function of the deposition temperature in figure A1.8 (the plotted E_{opt} values were *calculated* using the best fit through the linear parts of the curves, and not using figure A1.7).

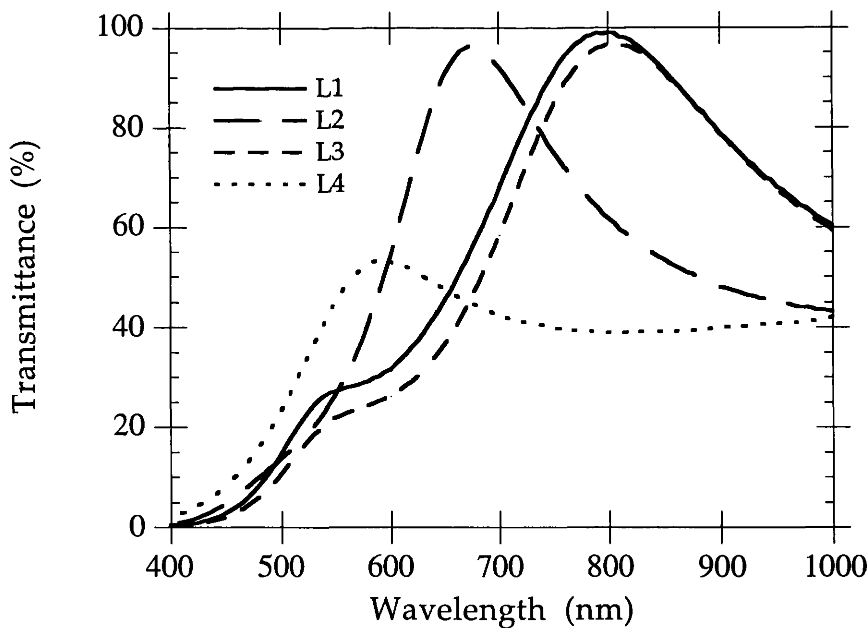

Figure A1.6 : Optical absorption spectra for samples L1 to L4

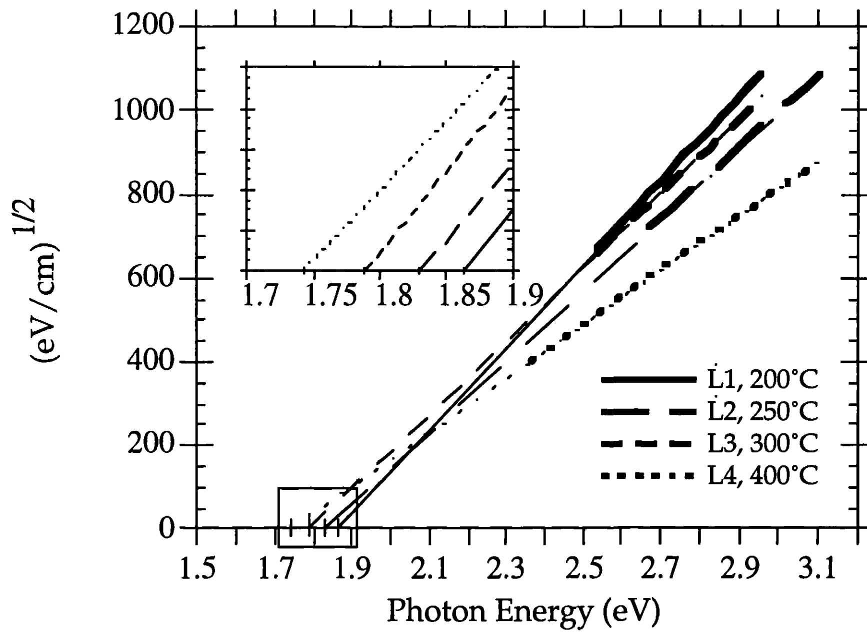

Figure A1.7 : Tauc plots of a-Si:H films for sample L1 to L4.

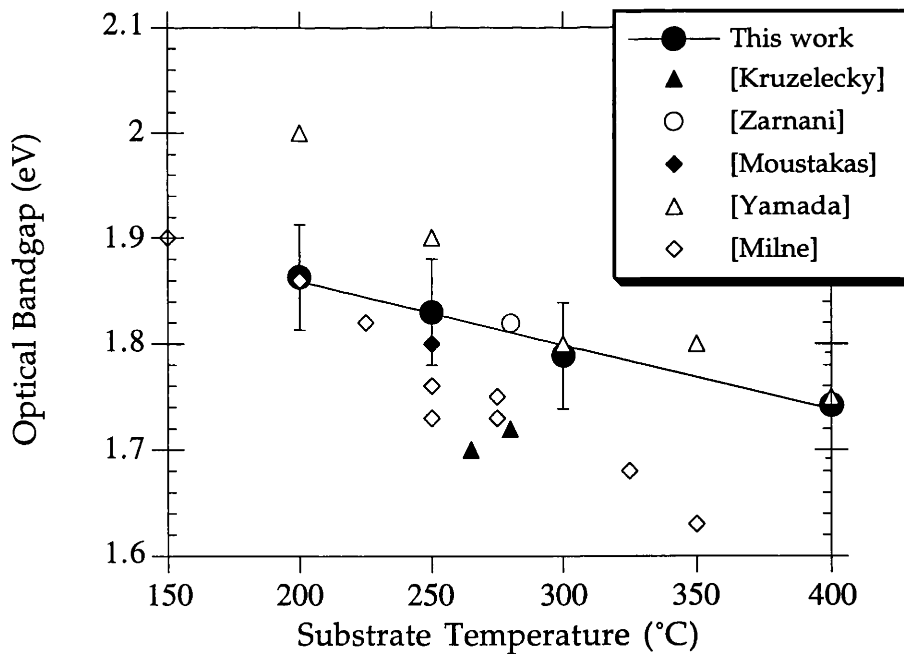

Figure A1.8 : Comparative evolution of the optical bandgap E_{opt} with substrate temperature (●). Other group data are also shown, using photo-CVD (open) or the glow discharge method (closed)

3.3.2- Conductivity measurements

The photo-conductivities of the material are measured in the dark (σ_d), and under illuminated conditions (σ_{ph}). The value of the ratio σ_{ph}/σ_d is a figure of merit for the quality of the material. A low dark conductivity is indicative of a low density of defect states in the bandgap, if it is accompanied by a high photoconductivity, corresponding to a high extended state density and mobility. Reported values in the ratio σ_{ph}/σ_d are in the range of 4 to 6 orders of magnitude, for films of 0.3 to 1µm in thickness [Yamada] [Milne-1989] [Fuyuki]. Generally speaking, AM1, $100mWcm^{-1}$, solar-simulator illumination (solar spectrum at ground level), is recognised as the agreed light source for σ_{ph} measurements. In the absence of such a calibrated apparatus, a Tungsten white light was used, which was empirically tuned in power to create the same bias on a large bandwidth photo-cell than that initiated by the sun itself (on a sunny september day in London).

The measurements were probed using a Hewlett-Packard picoameter on the samples L1 to L4 onto which contacts had been deposited. Values are reported on table A1.5. As can be noted, the ratios σ_{ph}/σ_d obtained hardly exceed 2 orders of magnitude. In fact, it is agreed that the conductivity values measured may be lower than they actually are if the layers are less than 0.3µm in thickness [Takahashi]. This is caused by the bending of the energy bands at the surfaces of the deposited layers which thicknesses hardly exceed 0.12µm. Also, as mentioned in § 3.2, a high H_2 concentration was trapped in the films deposited at 200 and 250°C, which strongly reduces the photo-conductivity. The sample L_4 exhibits a very small value, probably due to an error in the measurement.

Sample	σ_d (pA)	σ_{ph} (pA)	σ_{ph}/σ_d
L1	0.03	7	230
L2	0.1	80	800
L3	0.03	190	6000
L4	0.08	1.2	*15*

Table A1.5 : dark and photo-conductivities for photo-deposited a-Si:H layers

3.3.3- Activation energy

By measuring the evolution of the dark currents in the a-Si:H layers with increasing temperature, an activation energy is obtained, which corresponds to the position of the Fermi level in the material. Values around 0.54eV were obtained, thus exhibiting a strong N-type behaviour of our undoped layers (with $E_{opt} \approx 1.75eV$). In fact, this measurement would also be strongly affected in very thin layers, and those values subjected to high errors.

3.4- Further analysis of the physical properties

3.4.1- Annealings

In 1984, John et al. reported a new technique of optical storage based on surface non-uniformity of amorphous silicon layers [John-1984]. The process is based on the formation of surface irregularities by low temperature annealings of the layers. The technique is based on the fact that a-Si:H deshydrogenates at 350°C, leading to microbubbles and, ultimately, circular craters in the film [John-1981-b]. Using a furnace, 20 minutes annealings were performed at 350°C on the L1, L2 and L3 samples, and the films were probed under a SEM. As expected, circular craters were formed on the sample surfaces. Two behaviours are observed, whether a blister is formed, or a crater resulting of the burst of the blister. The size of the craters agrees with Shanks *et al.* report on the linear evolution of their diameter with the layer thickness (≈ ø70 µm for 0.15µm in thickness) [Shanks].

3.4.2- Study of VUV induced morphology modifications of a-Si:H layers

With the availability of a high intensity source of 9.8eV photons, far above the band gap of a-Si:H, it is interesting to verify that the structure of the films may not be altered after prolonged exposure to VUV light. Such experiments were performed on the previously prepared samples, for exposure times as long as 1 hour, and at various temperatures (up to 300°C). No particular modification of the morphology or of the crystallinity of the samples was observed.

4.- Conclusions and Improvements

A proof of principle of the possibility of depositing thin films of hydrogenated amorphous silicon has been given, using the direct photo-dissociation of silane under 126nm photons generated in an argon excimer lamp. Some of the film properties are in good agreement with those reported for films obtained using other techniques such as the glow discharge or the internal lamp photo-CVD. However, important modifications of the deposition reactor should be implemented, since here the thicknesses were essentially limited by window fogging problems. In fact, as the radiations were completely absorbed by the products deposited on the window, a purging gas was used to prevent product condensation on the window, but the mean of increasing the growth rate therefore implied the augmentation of the working pressure, which in turns led to poor film quality from high H_2 incorporation. Furthermore, it has been observed that the use of successive depositions is not viable, since atmospheric contamination occurs during processing and results in oxygen incorporation in the bulk of the material. Although the window purge approach is the most appropriate for the use of very short VUV radiations, it is essential to be able to limit the interaction of the window purging gas with the reaction precursors, since it causes turbulences, which are detrimental to the film growth process.

A geometry enabling the use of a perforated separator plate, acting as a *double* window, would be appropriate. Technologically, it implies to drill holes through a magnesium fluoride window, which is feasible, the size of the holes being calculated to offer a high conductance to a purging gas fed between the lamp cell and the separator plate. The purging flow could then be strongly reduced to minimum values and its interaction on the precursor flows hence minimised.

References to appendix 1

[Adams] A.C. Adams, Sol. State Technol., **26** (1983) 135

[Bhatnagar] Y.K. Bhatnagar, in *Photo-CVD of hydrogenated amorphous silicon and silicon dioxide using an external deuterium lamp*, PhD thesis, University of Cambridge (1989)

[Brodsky] M.H.Brodsky, M. Cardona, J.J. Cuomo, Phys. Rev. B, **16** (1977) 3556

[Calvert] J.G. Calvert & J.N. Pitts, "Photochemistry", Wiley & Sons, New york (1966)

[Carlson] D.E. Carlson, C.W. Magee, A.R. Triano, J. Electrochem. Soc., Sol.-St. Sci. and Technol., **126** (1979) 688

[Fuyuki] T. Fuyuki, KY. Du, S. Okamoto, S, Yasuda, T. Kimoto, M. Yoshimoto, H. Matsunami, J. Appl. Phys., 64 (1988) 2380

[Gallagher] A. Gallagher, MRS Proc. Vol. **70** (1986) 3

[Hamakawa] Y. Hamakawa, W. Ma, H. Okamoto, MRS Bulletin, Vol. **18** (1993) 38

[Harada] Y. Harada, J. Murrell, H. Sheena, Chem. Phys. Lett., **1** (1968) 595

[John-1981-a] P. John, I.M. Odeh, M.K.J. Thomas, M.J. Tricker, J.I.B. Wilson, J.B.A. England, D. Newton, J. Phys. C: Solid State Phys., **14** (1981) 309

[John-1981-b] P. John, I.M. Odeh, M.J.K. Thomas, M.J. Tricker, J.I.B. Wilson, R.S. Dhariwal, J. Mat. Sci., **16** (1981) 1305

[John-1984] P. John, B.L. Jones, Appl. Phys. Lett., **45** (1984) 39

[Kessler] F. Kessler, H.-D. Mohring, G.H. Bauer, Proc. of the 9th Int. Conf. on Plasma Chemie, Vol. **3** (1989) 1383

[Kruzeleki] R.V. Kruzeleki, S. Zukotynski, C.I. Ukah, F. Gaspari, J.M. Perz, J. Vac. Sci. Technol,. **A7** (1989) 2632

[Itoh] U. Itoh, Y. Toyoshima, H. Onuki, J. Chem. Phys., **85** (1986) 4867

[Kawai] E. Kawai, K. Kasatani, M. Kawasaki, H. Sato, K. Hirao,

Jpn. J. Appl. Phys., **28** (1989) 247

[Ma] W. Ma, Y. Hamakawa, in Proc. 23rd IEEE photovoltaics specialists conf., IEEE, New York, (1993) session 4A-5

[Maessen] K.M.H. Maessen, M.J.M. Pruppers, J. Bezemer, F.H.P.M. Habraken, W.F. Van der Weg, Proceedings of the MRS meeting, Vol. **95** (1987) 201

[Milne-1989] W.I. Milne, F.J. Clough, S.C. Deane, S.D. Baker, P.A. Robertson, Appl. Surf. Sci., **43** (1989) 277

[Milne-1992] W.I. Milne, P.A. Robertson, in *photochemical processing of electronic materials*, ed. by I.W. Boyd and R.B. Jackman, Academic Press Inc., San Diego (1992)

[Pankove] J.I. Pankove, D.E. Carlson Ann. Rev. Mater. Sci., **10** (1980) 43

[Ritter] E. Ritter, Opt. Acta, **9** (1962) 197

[Robertson-1986] P.A. Robertson and W.I. Milne, MRS Proc., Vol. **70** (1986) 31

[Robertson-1987] P.A. Robertson, *The photo-enhanced deposition of amorphous silicon and silicon oxide thin films*, PhD Thesis, University of Cambridge, (1987)

[Sato] K. Sato, J. Electrochem. Soc., Sol. St. Sci., **117** (1970) 1065

[Shanks] H.R. Shanks, L.Ley, J.Appl. Phys., **52** (1981) 811

[Tachibana] K. Tachibana, H. Harima, Y. Matsui, A. Yuki, N. Morita, Y. Urano, Appl. Phys., **B41** (1986) p103

[Takashi] K. Takashi, M. Konagai, in *Amorphous silicon solar cells*, North Oxford academic publishers Ltd, London (1986)

[Tauc] J. Tauc, R. Grigorovici, A. Vancu, Phys. Stat. Sol., **15** (1966) 627

[Tsu] D.V. Tsu, G. Lucovsky, B.N. Davidson, Phys. Rev. B, **40** (1989) 1795

[Yamada] A. Yamada, M. Konagai, K. Takahashi, Jpn. J. Appl. Phys., **24** (1985) 1586

[Yoshida] A. Yoshida, K. Inoue, H. Ohashi, Y. Saito, Appl. Phys. Lett., **57** (1990) 484

[Zarnani] H. Zarnani, H. Demiryont, G.J. Collins, J. Appl. Phys., **60** (1986) 2523

Colours presented by silicon dioxide films (in perpendicular white light)

Thickness (Å)	Colour
500	Beige -light brown
700	Brown
1000	Dark purple to violet
1200	Royal blue
1500	Light blue to metallic
1750	Metallic to light yellow-green
2000	Light gold - light metallic yellow
2200	Gold - orangey yellow
2500	yellowy orange
2700	Red-violet
3000	Blue to purple
3100	Blue
3200	Blue to green blue
3400	Light green
3500	Green to yellowy green
3600	Greeny yellow
3700	Yellowy green
3900	Yellow
4100	Light orange
4200	Buff
4400	Redy-violet
4600	Violet-tinged-red
4700	Violet
4800	Purple
4900	Blue
5000	Green-Blue
5200	Green
5400	Greeny-Yellow
5600	Yellowy-green
5700	Yellow to light mustard
5800	Yellowy orange to light salmon
6000	Buff
6300	Violet
6800	Violet-tinged-blue to green-blue
7200	Green-blue to green
7700	Light mustard
8000	Orange
8200	Salmon, orangey pink
8500	Strong and dark red-violet
8600	Violet
8700	Purple
8900	Blue
9200	Green-Blue
9500	Dark greeny-yellow
9700	Yellow, light mustard
9900	Orange
1.0 μm	Buff
1.02	Violet
1.05	Violet-tinged-red
1.06	Violet
1.07	Violet-blue
1.10	Green
1.11	Greeny-yellow
1.12	Green
1.18	Purple
1.19	Violet
1.21	Redy-violet
1.24	Pink to salmon
1.25	Orange
1.28	Light mustard
1.32	Sky blue to blue-tinged-green
1.40	Orange

Translated from French
Courtesy of the Université Scientifique et Médicale de Grenoble

Assignments of the principal infrared features for the study of silicon dielectric materials

Band Position (cm^{-1})	Structural Group	Reference
470 (sharp)	SiO_2	Taft et al., J. Electrochem. Soc., SST, 126 (1979) 1728
515	O in Si characteristic absorption	Boyd et al., J. Appl. Phys., 53 (1982) 4166
568	Si characteristic absorption	Boyd et al., J. Appl. Phys., 53 (1982) 4166
602	C in Si characteristic absorption	Boyd et al., J. Appl. Phys., 53 (1982) 4166
607	Si characteristic absorption	Boyd et al., J. Appl. Phys., 53 (1982) 4166
630	≈SiH Rocking	Boyd, PhD
630	$=SiH_2$ Rocking	Boyd, PhD
630	$-(SiH_2)n-$ Rocking	Boyd, PhD
630	$-SiH_3$ Rocking	Boyd, PhD
685	Si characteristic absorption	Boyd et al., J. Appl. Phys., 53 (1982) 4166
740	Si characteristic absorption	Boyd et al., J. Appl. Phys., 53 (1982) 4166
800 (sharp)	SiO_2	Taft et al., J. Electrochem. Soc., SST, 126 (1979) 1728
800	SiO	Mishima et al., J. Appl. Phys., 55 (1984) 1234
815	Si characteristic absorption	Boyd et al., J. Appl. Phys., 53 (1982) 4166
835	Si-N stretch	Berti et al., Thin Sol. Films., 165 (1988) 279
840	$=SiH_2$ wagging	Boyd, PhD
845	$-(SiH_2)n-$ Wagging	Boyd, PhD
845	$(SiH_2)n$	Yamada et al., Jap. J. Appl. Phys., 24 (1985) 1586
860	$-SiH_3$ Symmetric deformation	Boyd, PhD
880	$=SiH_2$ (Scissors) bending	Boyd, PhD
880	SiH_2 & SiH_3 bending	Kruzelecky et al., J. Vac.Sci. Technol., A7 (1989) 2632
880	SiH_2, scissors bending	Yamada et al., Jap. J. Appl. Phys., 24 (1985) 1586
880	SiH	Taft et al., J. Electrochem. Soc., SST, 126 (1979) 1728
880	Si_2O_3	Mishima et al., J. Appl. Phys., 55 (1984) 1234
880	Si_2O_3	Ritter et al., Opt. Acta, 9 (1962) 197
880	non bridging SiO interaction	Knolle et al., J. Appl. Phys. 51 (1980) 4385
890	$-(SiH_2)n-$ (Scissor bending)	Boyd, PhD
890	Si characteristic absorption	Boyd et al., J. Appl. Phys., 53 (1982) 4166
908	$-SiH_3$ degenerate formation	Boyd, PhD
930	SiOH deformation	Mishima et al., J. Appl. Phys., 55 (1984) 1234

964	Si characteristic absorption	Boyd et al., J. Appl. Phys., 53 (1982) 4166
1060	SiO	Mishima et al., J. Appl. Phys., 55 (1984) 1234
1090	(sharp) SiO_2	Taft et al., J. Electrochem. Soc., SST, 126 (1979) 1728
1095	$=SiH_2$ Sym & antisymm Stretch	Boyd, PhD
1107	Si characteristic absorption	Boyd et al., J. Appl. Phys., 53 (1982) 4166
1107	O in Si characteristic absorption	Boyd et al., J. Appl. Phys., 53 (1982) 4166
1302	Si characteristic absorption	Boyd et al., J. Appl. Phys., 53 (1982) 4166
2000	≈SiH stretch	Boyd, PhD
2000	(broad) Si-H stretching. Extends from 2000 to 2700	Kruzelecky et al., J. Vac.Sci. Technol., A7 (1989) 2632
2100	$-(SiH_2)n-$ Sym & antisymm Stretch	Boyd, PhD
2140	$-SiH_3$ Sym & antisymm Stretch	Boyd, PHD
2175	Si-H stretch	Berti et al., Thin Sol. Films., 165 (1988) 279
2240	SiH	Mishima et al., J. Appl. Phys., 55 (1984) 1234
2260	SiH	Taft et al., J. Electrochem. Soc., SST, 126 (1979) 1728
2349	(sharp) O=C=O in air due to beam path length inequalities	Lange 's Handbook of Chemistry
3350	N-H stretch	Berti et al., Thin Sol. Films., 165 (1988) 279
3400	(broad) SiO_2	Taft et al., J. Electrochem. Soc., SST, 126 (1979) 1728
3500	SiOH	Mishima et al., J. Appl. Phys., 55 (1984) 1234
3650	(broad) SiO_2	Taft et al., J. Electrochem. Soc., SST, 126 (1979) 1728

Estimation of the error on v_0 (chapter5, § 1.3.3)

The expression of v_0 was given as:

$$v_0 = \frac{\exp((x - x_0)\sigma\xi) - 1}{\sigma\xi \quad \Delta t} \qquad \text{(equation 5.24)}$$

Since the error on x_0 is agreed not to be significant, only the error on the predetermined product $\sigma\xi$ is to be considered (assuming no error on Δt). The error on v_0 can then be expressed as:

$$\frac{\Delta v_0}{v_0} = f^n(\sigma\xi, x) \cdot \frac{\Delta(\sigma\xi)}{(\sigma\xi)} \qquad \text{(equation 5.25)}$$

The expression of $f^n(\sigma\xi,x)$ is calculated:

$$\frac{\partial V_0}{\partial(\sigma\xi)} = \frac{\sigma\xi\,(x - x_0)\exp(\sigma\xi(x - x_0)) - \exp(\sigma\xi(x - x_0)) + 1}{(\sigma\xi)^2 \quad \Delta t}$$

which becomes:

$$\frac{\partial V_0}{V_0} = \frac{\sigma\xi \exp(\sigma\xi(x - x_0)) - \exp(\sigma\xi(x - x_0)) + 1}{\exp(\sigma\xi(x - x_0)) - 1} \; \frac{\partial(\sigma\xi)}{\sigma\xi}$$

or

$$\frac{\partial V_0}{V_0} = \left(\frac{\sigma\xi}{1 - \dfrac{1}{\exp(\sigma\xi(x - x_0))}} - 1\right) \frac{\partial(\sigma\xi)}{\sigma\xi}$$

The error $\partial V_0/V_0$ is plotted on figure A4.1 as a function of the sample thickness, for a value of the product $(\sigma\xi)$ of 0.0038Å^{-1} and a maximised relative error $\partial(\sigma\xi)/(\sigma\xi)$ of 10%. The curve shows that for a film of 400Å, a relative error on the product $(\sigma\xi)$ of 10% around 0.0038Å^{-1} would lead to less than a 10% relative error on v_0. In other words, as long as the sample thicknesses studied remain below this range, there is no risk to commit an important error on the calculated value of v_0.

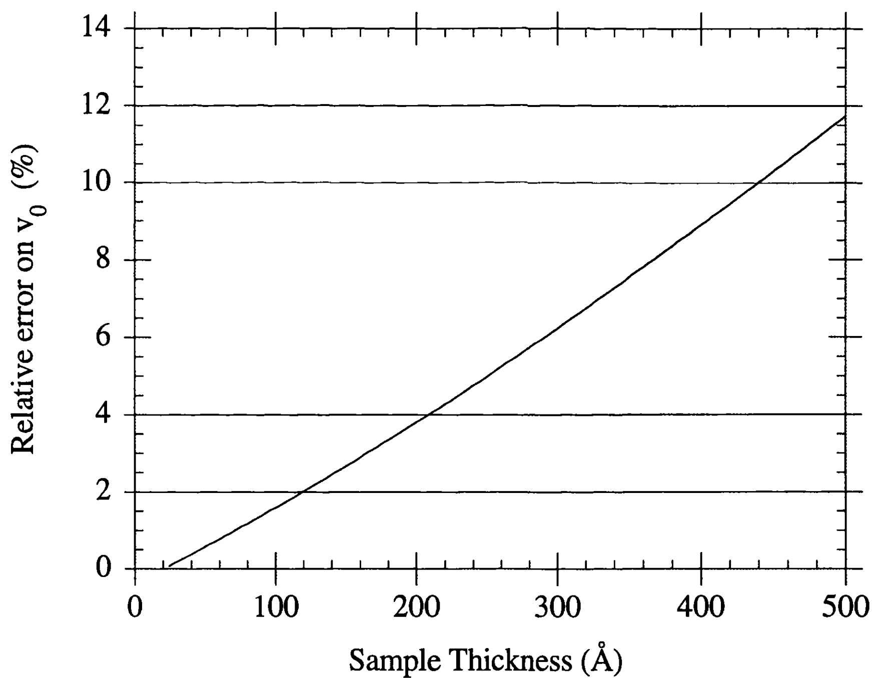

Figure A4.1 : Evolution of the relative error on v_0 with the sample thickness (Product $(\sigma\xi)$ at 0,0038Å^{-1}, relative error on $\sigma\xi$ is 10%).

List of publications based on this work

- P. Patel, P. Bergonzo, U. Kogelschatz et I.W. Boyd
  "Photo- induced deposition of thin silicon dioxide films using a novel large area excimer lamp", presented at the *Materials Research Society (MRS)* Spring meeting Anaheim, 1991, Symposium F.
  Published in the MRS proceedings, Volume. 224 (1992).

- P. Bergonzo, P. Patel, U. Kogelschatz et I. W. Boyd
  "Development of a novel large area excimer lamp for direct photo deposition of thin films", presented at the *European- Materials Research Society (E-MRS)* Spring meeting, Strasbourg, 1991.
  Published in Applied Surface Science, 54 (1992) 424-429

- P. Bergonzo, U. Kogelschatz, I.W. Boyd
  "Direct photo-deposition of silicon dioxide films using a xenon excimer lamp", presented at the *European- Materials Research Society (E-MRS)* Spring meeting, Strasbourg, 1992.
  Published in Applied Surface Science, 69 (1993) 393-397

- P. Bergonzo et I. W. Boyd
  "Photo-deposition of oxynitride and nitride films using excimer lamps", presented at the *European- Materials Research Society (E-MRS)* Spring meeting, Strasbourg, 1993.
  To be published in Microelectronics Engineering

- P. Bergonzo et I. W. Boyd
  "Photo-CVD of dielectric materials by pseudo-continuous excimer sources", presented at the Optics Québec '93 conference, organised by *The International Society of Optical Engineering (SPIE)* Québec, August 1993.
  To be published in the SPIE proceedings, Vol. 2045, "Thin Films and micro-structures", (1994) 174-183

- P. Bergonzo, I.W. Boyd,
  "Low pressure photo-deposition of silicon nitride films using a xenon excimer lamp"
  Published in Applied Physics Letters, 63 (1993) 1757-1759.

- P. Bergonzo and I.W. Boyd
  "Rapid Photo-Deposition of Silicon Dioxide Films using 172nm VUV light."
  To be published in Electronics Letters

- P. Bergonzo, I.W. Boyd,
  "Fast deposition of silicon dioxide films in a photo-chemical vapour deposition reactor using an excimer lamp"
  Sent for publication to the Journal of Applied Physics.

plied Surface Science 54 (1992) 424–429
rth-Holland

applied
surface science

evelopment of a novel large area excimer lamp for direct photo eposition of thin films

. Bergonzo, P. Patel, I.W. Boyd

partment of Electrical and Electronic Engineering, University College London, London, UK

nd

. Kogelschatz

ea Brown Boveri Corporate Research, CH-5405 Baden, Switzerland

eceived 27 May 1991; accepted for publication 4 July 1991

The desire for low-temperature processing in order to minimize undesirable effects has brought about an extensive use of otochemical vapour deposition (photo-CVD). Photo-enhanced processing is one of the techniques which has received consider- le interest. One of the major limitations of photo-processing is the lack of sufficiently intense ultra-violet (UV) sources.

In this paper we report the design of a new and intense large area UV lamp based on the dielectric barrier discharge. We shall so discuss the direct (i.e. without intermediate photo-sensitisation reactions) photo-induced deposition of thin silicon dioxide ms using SiH_4 and N_2O which are photo-dissociated by 126 nm photons generated by this variable wavelength excimer lamp.

. Introduction

As integrated circuits have become smaller nd more densely packed, and because of the nherent problems associated with high tempera- ure processing for thin film deposition (defect eneration in the underlying substrate, dopant edistribution, wafer warpage,...), low tempera- ure processing is extremely important for future eneration Si ultra large scale integration (ULSI). n addition, lower temperatures allow greater ex- loitation of new material opportunities which ave not been previously possible due to their igh temperature incompatibility. Several tech- iques which reduce the overall "thermal budget" ave emerged in recent years. Of these, photo-in- uced processing [1,2] has received considerable nterest because it does not produce the highly nergetic ionic species present in plasma-assisted rocessing [3,4], which can have sufficient energy o cause damage to the growing film.

As a matter of fact, UV wavelength photons can initiate or enhance a variety of chemical reactions for micro-electronics applications such as film deposition, etching, doping, cleaning or oxidation [5–8]. Also, deep UV sources can be used for several applications like sterilisation, dis- infection, water treatment [9], phototherapy, or industrial synthesis of organic products. But these processes suffer from the lack of availability of intense deep UV sources. Here, we will describe a new design of an intense deep UV source, and consider its application to the deposition of thin films for microelectronics.

Silicon dioxide films are widely used in semi- conductor manufacturing as passivation layers, diffusion barriers, and gate dielectrics for transis- tor structures. Silicon dioxide can be deposited from either silane SiH_4 or disilane Si_2H_6, with nitrous oxide N_2O, nitric oxide NO_2, or O_2 using pyrolysis or plasma deposition methods. Using these precursors, UV radiation can also produce

169-4332/92/$05.00 © 1992 – Elsevier Science Publishers B.V. All rights reserved

SiO_2 layers. For photo-deposition or growth of silicon dioxide layers, several techniques have been developed for the generation of UV radiation. One of the most commonly used UV sources is the low pressure mercury lamp [2,10]. However, in most of the cases using Hg lamps there is a need to photo-sensitise the reaction with mercury. This presents the drawback effects of health hazards and trace quantities of contamination in the deposited films [11].

Windowless discharge lamps have hence been developed in order to initiate direct, rather than sensitised photo-deposition processes [1], but quantities of ionic species used for the photon generation are often found in the film. Recent advances in excimer laser technology have encouraged the development of new techniques for film deposition [12]. Excimers laser, however, are extremely expensive, costly to operate, and only give limited area photo-coverage. In this paper, we will describe a novel large area variable wavelength excimer lamp design based on the dielectric barrier discharge.

2. Dielectric barrier discharge

When a current path is created through a gas separating two metallic electrodes, a conventional electric discharge occurs. As is shown schematically in fig. 1, dielectric barrier discharges are characterised by the presence of at least one dielectric layer in the current path in the discharge gap between the electrodes. The configuration with dielectric layers on both electrodes has the added advantage that there is no danger of electrode corrosion during the discharge process.

It is well known that if a slowly increasing voltage is applied across a pair of parallel electrodes separated by a distance, d, and immersed in gas of number density n, then an electrical breakdown of the gas occurs at some critical voltage (breakdown voltage, V_{bd}). The functional relationship bewteen V_{bd}, d, and n is referred to as Paschen's law, defined as:

$$V_{bd} = f(nd). \quad (1)$$

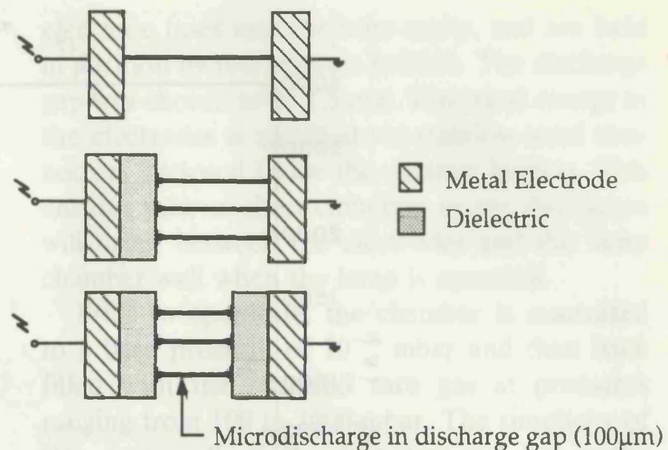

Fig. 1. Schematic of classical (top) and dielectric barrier discharges.

The breakdown condition is a unique curve for each gas (fig. 2) and depends on the gas pressure P, and the electrode separation [13]. Experimental work has shown that the same Paschen curves apply when one or both the electrodes are covered with a dielectric layer [14]. Microdischarges have been studied extensively [15] and their main properties are outlined in table 1.

The electron energies and electron densities found in such discharges are comparable to those found in modern excimer lasers. The added advantage of the dielectric barrier discharge is that the electron energy and density can be optimised for excimer formation by external parameters and geometry. It is of crucial importance to get maximum power into the microdischarge. Due to the capacitive nature of the barrier discharge this is most easily accomplished by using at least one of the following:
- a large dielectric area,
- a smaller dielectric thickness,
- a dielectric with a higher dielectric constant,
- higher frequencies.

Table 1
Typical properties of a dielectric microdischarge

Total charge	10^{-10} A s
Current density	10^{3} A cm^{-2}
Electron density	10^{14} cm^{-3}
Electron energy	> 5 eV

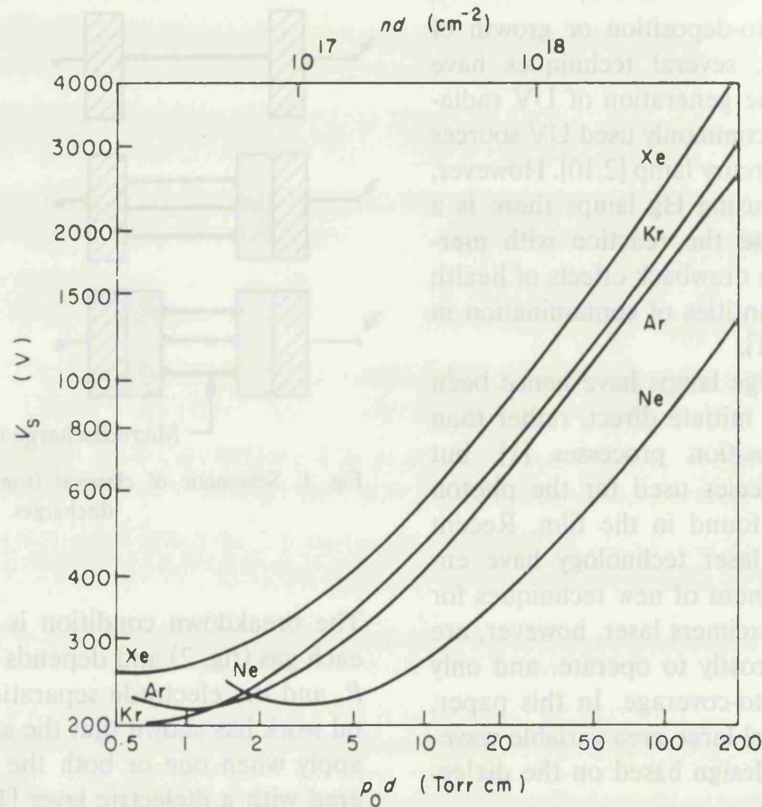

Fig. 2. Breakdown voltage in Ne, Ar, Kr and Xe with a copper cathode; $d = 10$ mm [13].

In our present work, we have concentrated on increasing the area of dielectric to increase the optical output.

3. Excimer formation in dielectric barrier discharges

The most investigated excimers are the rare-gas excimers (He_2^*, Ne_2^*, Ar_2^*, Kr_2^*, Xe_2^*) and the rare-gas-halide excimers (ArF^*, KrF^*, $XeCl^*$, XeF^*) which are commonly used in excimer lasers. The pumping mechanism involved in the formation of excimers is complex. Fig. 3, adapted from Rhodes [16], shows schematically an example of the interactions between atomic and molecular argon. Energetic electrons present in microdischarges excite and ionise the argon:

$$e^- + Ar \rightarrow Ar^+ + 2\,e^-, \qquad (2)$$

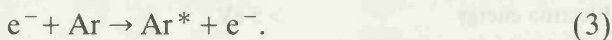

$$e^- + Ar \rightarrow Ar^* + e^-. \qquad (3)$$

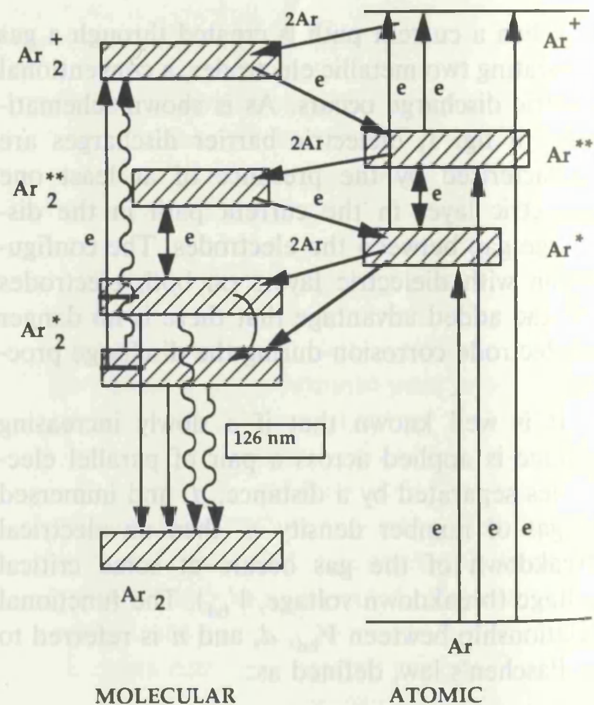

Fig. 3. Pumping mechanism for Ar.

At high pressures (> 50 mbar), relevant to the dielectric barrier discharge, the formation of molecular ions is rapid. This then leads to the formation of excited neutrals:

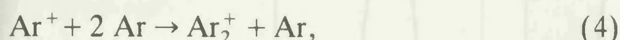

$$Ar^+ + 2\,Ar \rightarrow Ar_2^+ + Ar, \qquad (4)$$

$$Ar_2^+ + e^- \rightarrow Ar^{**} + Ar. \qquad (5)$$

Three-body association reactions then lead to the formation of bound molecular levels:

$$Ar^{**} + 2\,Ar \rightarrow Ar_2^* + Ar. \qquad (6)$$

When the Ar_2^* excimer falls back to the ground state it radiates a photon at 126 nm and disintegrates into two Ar atoms:

$$Ar_2^* \rightarrow 2\,Ar + h\nu(126\ \text{nm}). \qquad (7)$$

4. Design of a novel large area excimer lamp for deposition

So far, the excimer lamp has only been developed with one discharge gap. Here, we describe a new "interlocking electrode" geometry to generate excimer radiation over a large area. The lamp element consists of a series of quartz tubes. Every tube is connected to one pole of the power supply so that an alternating high voltage is applied between the adjacent tubes (fig. 4). The tubes are arbitrarily 70 mm long, each with a stainless steel electrode inset into the tube cavity, and are held in position by two ceramic holders. The discharge gap was chosen to be 1.5 mm. Electrical energy to the electrodes is supplied via stainless steel connectors enclosed inside the ceramic holders. This ensures that no short circuiting or arc discharges will occur between the electrodes and the lamp chamber wall when the lamp is operated.

Prior to operation, the chamber is evacuated to a base pressure of 10^{-3} mbar and then back filled with the required rare gas at pressures ranging from 100 to 1000 mbar. The simplicity of this design allows the rare gas, and hence the photon wavelength, to be easily changed. Equally importantly the lamp area, and hence the photon flux, can be increased by scaling up the size or number of the lamp elements.

The discharge was operated at a few kV at 250 kHz, and activity was confined between adjacent quartz tubes. Spectral measurements, using various gases, were performed using a vacuum monochromator [17]. Fig. 5 shows the spectra for the rare-gas excimers peaking at 126, 146 and 172 nm for Ar_2^*, Kr_2^*, and Xe_2^*. Using actinometric methods [18] efficiencies of 5%–10% (the optical output as a fraction of the electrical input energy) were obtained for xenon.

For thin film deposition, the lamp element is placed in a purpose-built chamber with a MgF_2 window separating it from a second chamber

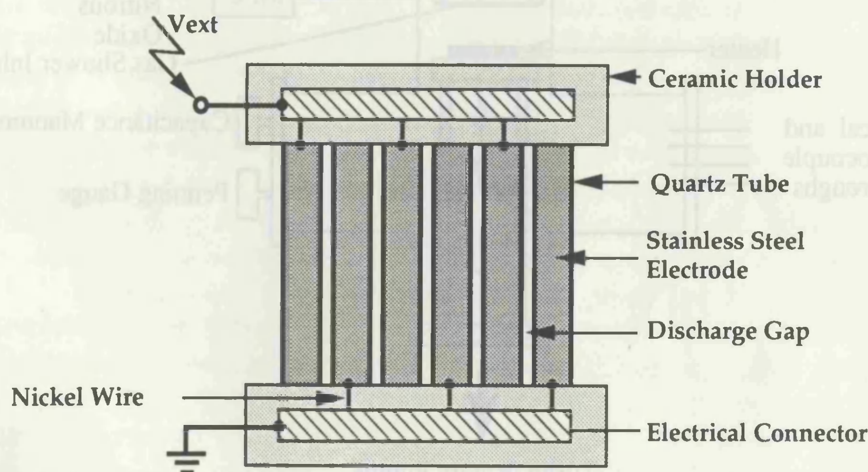

Fig. 4. Large area excimer lamp.

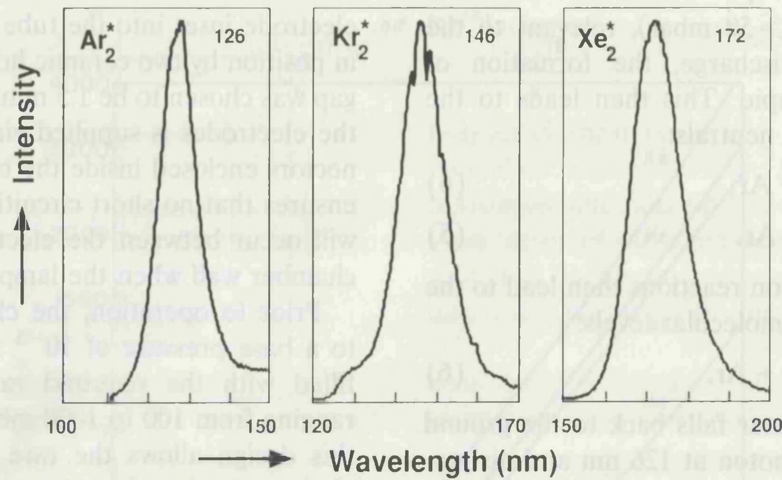

Fig. 5. Spectra measurements for Ar, Kr, and Xe gases.

specially designed for thin film growth (fig. 6). Initial experiments have shown that various powders may be readily formed by photo-dissociation of SiH_4 and N_2O mixtures followed by gas-phase nucleation. This nucleation indicates the extremely high efficiency of the UV photon initiated mechanisms. The controlling parameters of the gas mixture pressure, flow-rate and substrate

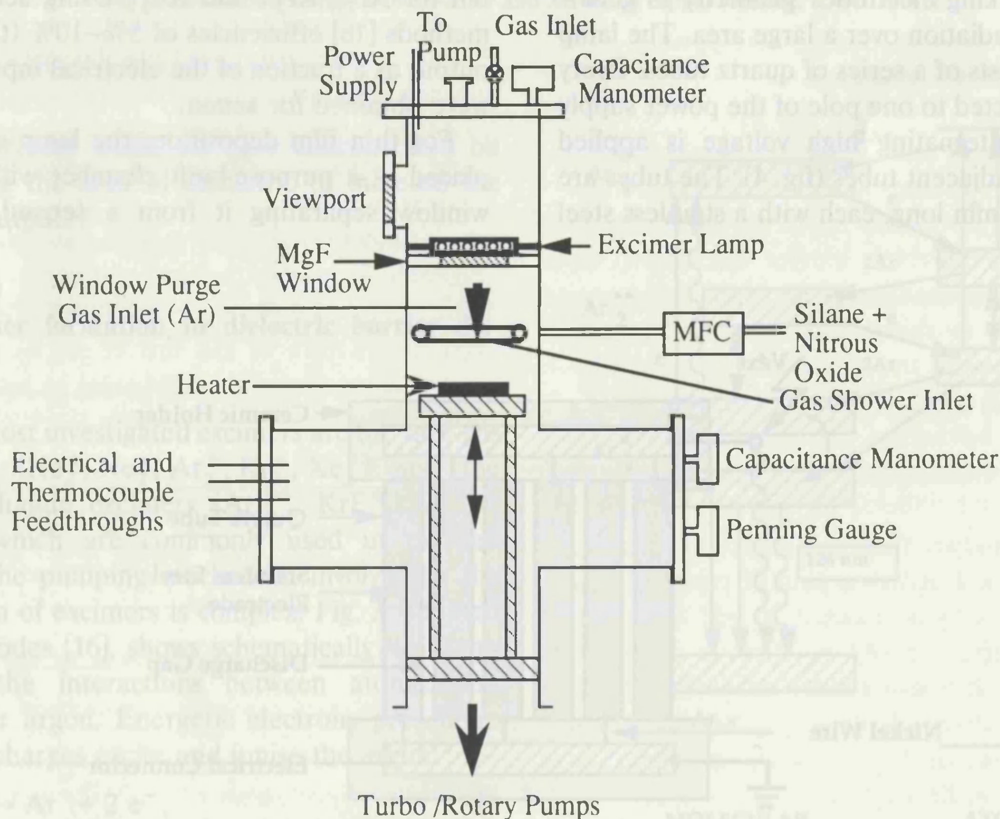

Fig. 6. Excimer lamp system used for direct photo-deposition.

temperature are currently being optimised to produce uniform thin film growth on a range of substrates.

5. Conclusion

Using a very simple geometry based on the dielectric barrier discharge, we have developed a large area excimer lamp. The flexibility of the design enables excimer radiation from the near-visible to deep-VUV to be easily generated. This has the added advantage that it allows sequential deposition of various thin films using different precursors without exposing the films to the atmosphere.

Additionally, this ability to fine-tune the photon energy, which will enable maximum energy to be coupled into the reaction, and the high efficiency of the lamp will allow high deposition rates to be achieved and therefore promise to make photo-enhanced processing a reality for the semiconductor and related industries in the foreseeable future.

Acknowledgements

This work was partially funded by SERC (contract No. GR/F 02229), ABB Corporate Research, and the EEC/SCIENCE programme.

References

[1] P. Patel and I.W. Boyd, Appl. Surf. Sci. 46 (1990) 352.

[2] V. Nayar, P. Patel and I.W. Boyd, Electron. Lett. 26 (1990) 205.

[3] C. Vinckier and S. De Jaegere, J. Electrochem. Soc. 137 (1990) 628.

[4] D.A. Buchanan, Appl. Phys. Lett. 56 (1990) 1037.

[5] M. Suemitsu, T. Kaneko and N. Miymoto, Jpn. J. Appl. Phys. 28 (1989) 2421.

[6] J. Marks and R.E. Robertson, Appl. Phys. Lett. 52 (1988) 810.

[7] B.S. Krusor, D.K. Biegelsen, R.D. Yingling and J.R. Abelson, J. Vac. Sci. Technol. B 7 (1989) 129.

[8] I.W. Boyd, Laser Processing of Thin Films and Microstructures (Springer, New York, 1987).

[9] U. Kogelschatz, in: Process Technologies for Water Treatment, Ed. S. Stucki (Plenum, New York, 1988).

[10] R. Padmanabham and B.J. Miller, J. Vac. Sci. Technol. A 4 (1986) 363.

[11] K. Usami, Y. Mochizuki, T. Minagawa, A. Iida and Y. Gohshi, Jpn. J. Appl. Phys. 25 (1986) 1449.

[12] P.K. Boyer, G.A. Roche, W. Ritchie and G. Collins, Appl. Phys. Lett. 40 (1982) 716.

[13] J.M. Meek and J.D. Craggs, Electrical Breakdown of Gases (Wiley–Interscience, New York, 1978).

[14] B. Eliasson, U. Kogelschatz and H.J. Stein, EPA NewsLett. 32 (1988) 29.

[15] B. Eliasson and U. Kogelschatz, J. Phys. D (Appl. Phys.) 20 (1987) 1421.

[16] Ch.K. Rhodes, Excimer Lasers, Vol. 30 of Topics in Applied Physics (Springer, Berlin, 1984).

[17] B. Gellert and U. Kogelschatz, Appl. Phys. B 52 (1991) 14.

[18] B. Eliasson and U. Kogelschatz, Appl. Phys. B 46 (1988) 299.

Applied Surface Science 69 (1993) 393–397
North-Holland

applied
surface science

Direct photo-deposition of silicon dioxide films using a xenon excimer lamp

P. Bergonzo [a], U. Kogelschatz [b] and I.W. Boyd [a]
[a] *Electronic and Electrical Engineering, University College London, Torrington Place, London WC1E 7JE, UK*
[b] *Asea Brown Boveri, Corporate Research, CH-5405 Baden, Switzerland*

Received 2 June 1992; accepted for publication 30 October 1992

Recently excimer lamps have opened up the field of intense vacuum ultra-violet (VUV) light generation. With theoretical efficiencies reaching 40%, the power available from such lamps based on dielectric barrier discharge generation can be superior to those of typical low pressure mercury lamps with shorter UV wavelengths generated. Here we present, for the first time, the use of these lamps for the direct photo-deposition of silicon dioxide from silane and nitrous oxide mixtures. Deposition rates achieved on our unoptimised system are comparable with those obtained with low pressure mercury lamps. The results indicate promising further applications of such lamps towards semiconductor and optoelectronic materials processing.

1. Introduction

Over the last decade, a general requirement for low temperature processing in the semiconductor industry has become apparent. This is due, in part, to the continued reduction in device geometries and, amongst other reasons, the emergence of temperature sensitive materials such as amorphous silicon, gallium arsenide and indium phosphide (a-Si:H, GaAs, InP) [1]. Of the low temperature processing techniques now being investigated, photo-enhanced processing of materials is very promising since the processed surfaces and growing films are not subjected to damaging ionic bombardment such as can be present in plasma-assisted processing systems [2,3].

The recent development of novel excimer lamps [4] has opened up the field for relatively inexpensive, large area, direct photo-CVD to wafer scale technologies. As new powerful sources of low wavelength photons, these lamps have received considerable attention during the past few years [5,10], producing wavelengths extending to the vacuum ultra-violet domain (VUV) at higher intensities than can otherwise be currently routinely achieved. In fact, such lamps have already been used successfully to enhance various photochemical reactions such as ozone generation and metallorganic processing [7–9].

The principle of the excimer lamp relies on the radiative decomposition of excimer states created by a dielectric barrier discharge in a rare gas such as Xe, Kr, or Ar [25]. Such a principle has of course already been used in excimer lasers with rare gas halogen mixtures [11], but simplicity and reliability as well as scalability give these lamps a definite advantage over lasers when large scale industrial processes are envisaged. In photo-CVD there is no need for purely monochromatic coherent light, since the UV absorption mechanisms associated with the gas phase exhibit extended band-like properties rather than discrete transitions. Furthermore, the intense excitation levels required in such laser cavities limit their emission to a pulsed mode, hence requiring long exposure times for most reactions. Another advantage of lamps is that the excitation densities required are

0169-4332/93/$06.00 © 1993 – Elsevier Science Publishers B.V. All rights reserved

much lower than for lasers and, therefore, pure rare gas excitation can be successfully obtained, enabling shorter wavelengths to be produced.

At present, intensities of 100 mW/cm^2 are achievable at the excimer lamp surface at reasonable cost, compared with excimer lasers [4], and this bodes for photo-CVD applications. Till now, no such source has been used for direct deposition of dielectric films relevant to VLSI devices, such as silicon dioxide, oxynitride, or nitride. Direct photo deposition has previously been obtained with the 185 nm radiation of the low pressure mercury lamps [12,13] and with various discharge lamps (nitrogen, argon, krypton, xenon). However, the very low efficiencies involved with these systems have somewhat limited the deposition rate of the films [14,15].

Silicon dioxide has been extensively used and studied in semiconductor manufacturing applications. Highly compatible with silicon-based technologies because of its highly desirable chemical, electrical, and mechanical properties, it is used for gate and field oxides, and masks and passivating layers, as well as for tunnel oxide applications. For such a material, conventional pyrolytic deposition occurs above 600°C [24] while traditional oxidation occurs at temperatures around and above 900°C. The aim of this paper is to demonstrate the possibility and inherent advantages of depositing silicon dioxide at low temperatures with excimer lamps. With this "proof of principle" shown, the case for other VLSI materials to be deposited with deeper wavelengths with these lamps can readily be made.

2. Experimental

Excimer lamps, particularly those using the Xe_2^* generated radiation and the reaction kinetics of excimer formation, have been extensively described elsewhere [6,10,16]. The second continuum of xenon emitting at 172 nm, when excited by non-equilibrium high pressure discharges, enables high UV power levels to be generated. In this study we have used 172 nm power densities around 10 mW/cm^2. The lamp system used comprised two sections. In the first, a cell containing the pure gas in a suprasil envelope generated the radiation which was directed through a MgF_2 window. The transmitted light entered a second chamber, a reaction cell. Here, gas mixture of pure silane and nitrous oxide were introduced via mass flow controllers through a toric shaped shower onto the samples. In these experiments, sections of p-type (100) silicon wafers were used and their temperature was maintained between 200 and 300°C. Thermocouple control ensured that, although essentially negligible, the low intensity of the lamp did not increase the surface temperature of the samples during film growth. The shower–substrate and window–substrate distances were kept constant at 1 and 4 cm, respectively. Prior to deposition the samples were cleaned in a propanol solution in ultrasonic bath and the chamber was evacuated to 10^{-6} mbar. The 172 nm emission from the lamp was monitored with a MacPherson VUV monochromator.

The VUV induced reaction scheme between SiH_4 and N_2O has been recently studied by other groups. The absorption coefficient of N_2O at the wavelength used is typically around 2 cm^{-1} atm^{-1} [17,18]. At the window–substrate distance used, and with the pressure around 100 mb, the absorption by N_2O of the radiation entering the processing chamber is about 50%. In the work reported here, mixtures containing between 0.5 to 10% silane in nitrous oxide were introduced into the chamber at a constant flow of 50 sccm. Silane is already known not to be dissociated at these wavelengths and intensities. A simplified reaction scheme can be written as follows:

$$N_2O + h\nu \rightarrow N_2 + O, \quad (1)$$

$$SiH_4 + O \rightarrow SiH_3 + OH, \quad (2)$$

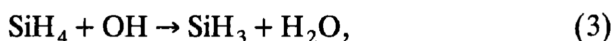

$$SiH_4 + OH \rightarrow SiH_3 + H_2O, \quad (3)$$

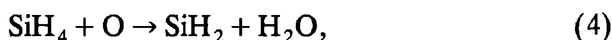

$$SiH_4 + O \rightarrow SiH_2 + H_2O, \quad (4)$$

$$SiH_2 + O \rightarrow SiH_2O, \quad (5)$$

$$SiH_3 + O \rightarrow SiH_2O + H, \quad (6)$$

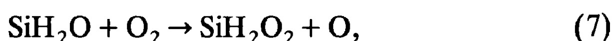

$$SiH_2O + O_2 \rightarrow SiH_2O_2 + O, \quad (7)$$

$$SiH_2O_2 + O_2 \rightarrow SiO_2 + H_2O + O. \quad (8)$$

Basically, nitrous oxide is photo-dissociated (1), leading to the generation of oxygen radicals which

then react with silane, (2)–(4). Branching reactions (5)–(7) subsequently lead to SiO_2 formation (8). A more complete model for this scheme has been recently detailed by Petitjean [13,19]. Film growth proceeds in a continuous manner, like with the laser-initiated layer situation, which by necessity is controlled in a pulsed growth mode.

After continuous irradiation of the silicon for times up to 30 min, the layers grown were characterised using FTIR spectrometry while thickness measurements were carried out with a Rudolf Autoell Ellipsometer. The electrical properties of the films will form the basis of a later paper, but we report here that their characteristics are quite similar to those of conventionally deposited films.

3. Results

For exposure times up to 30 min, film thicknesses of 50 nm were grown at temperatures below 300°C, producing a growth rate of around 0.3 Å/s. Fig. 1a shows the variation of the deposition rate with intensity for the 172 nm radiation used. As expected, it is proportional to the incident flux, and also clearly shows that any thermally controlled deposition of the films was insignificant under these operating conditions. At

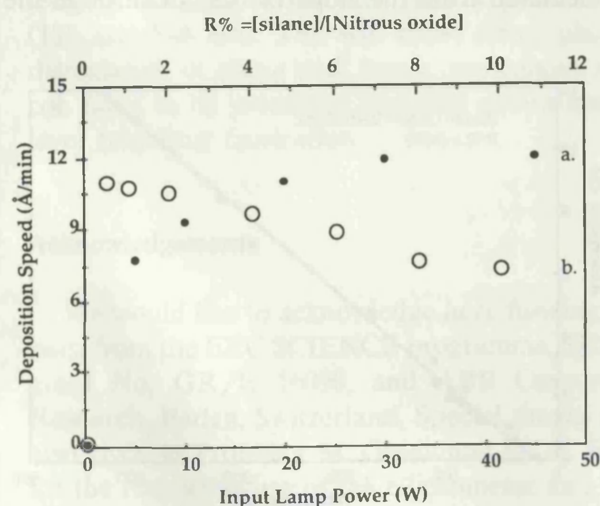

Fig. 1. Deposition speed for silicon dioxide samples deposited at 300°C versus (a) (●): VUV light exposure, and (b) (○) precursor mixture ratio.

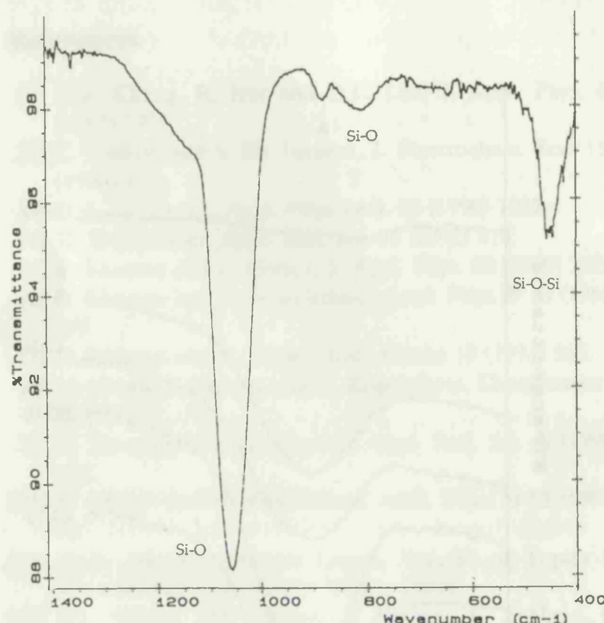

Fig. 2. FTIR absorption spectrum of a 400 Å silicon dioxide layer deposited at 300°C.

total gas pressures exceeding 150 mbar, powder was formed as a consequence of gas phase reactions being stimulated. In contrast, the deposition rate was found to be very low below pressures of about 100 mbar. At intermediate pressures and temperatures between 200 and 300°C, the films formed were scratch resistant and adherent. Typical deposition rates varied from 10 to 15 Å/min. Fig. 1b shows the variation of the deposition rate with R, the SiH_4/N_2O ratio. For $R < 2\%$, the rate is limited by the silane concentration. For $R > 2\%$ gas phase reactions leading to powder formation also limit film deposition. Refractive indices of 1.458 were obtained on optimised samples, values always ranging between 1.4 and 1.5 according to experimental conditions (higher values of 1.6 were obtained for higher ratio R). The structural properties of the oxide films deposited were characterised by their vibrational spectra. Fig. 2 shows a FTIR spectrum of an oxide film photo-deposited at a substrate temperature of 300°C. The spectrum consists of three characteristic absorption peaks at 1065 cm^{-1} (Si–O–Si stretching), 800 cm^{-1} (O–Si–O bending), and 480 cm^{-1} (Si–O–Si rocking) [20,21]. The full width at half maximum (FWHM) for the dominant IR

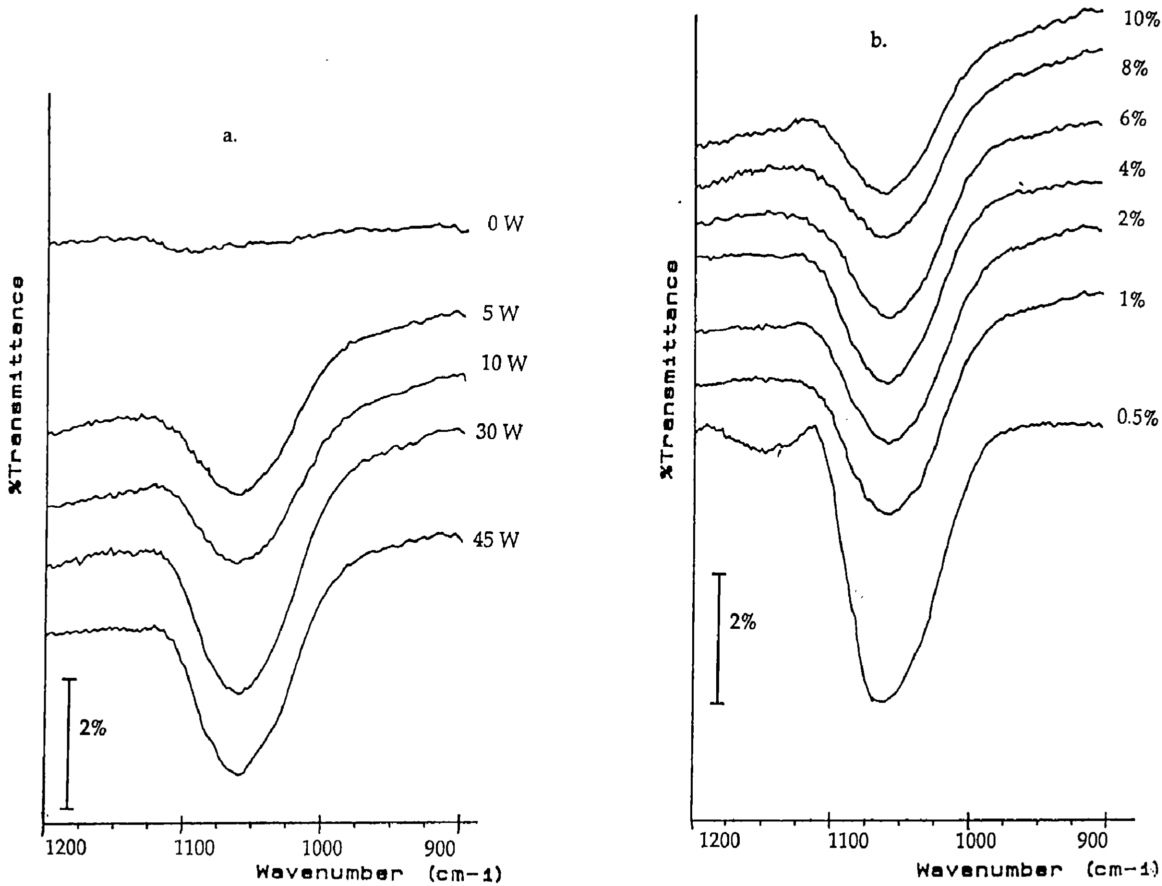

Fig. 3. Sets of FTIR spectra of the 1065 cm^{-1} peak for various (a) input lamp power, (b) precursor mixture ratio R (average thickness: 100 Å).

mode around 1065 cm^{-1} has a value of 70 cm^{-1} and remains essentially the same for all the oxides studied. The small peak centered around 885 cm^{-1} can be attributed either to Si–H, Si–OH, Si_2O_3 or to non-bridging oxygen [26]. However, the presence of Si–H and Si–OH bonds would have led to the presence of other peaks centered around 2270 and 3620 cm^{-1}, which we did not observe. This peak can, therefore, be most likely attributed to a defect state of SiO_2 [27] although further investigations are underway to confirm this point.

The absorption spectra of figs. 3a and 3b show that the quality of the film is not significantly affected by either lamp power or the precursor mixture ratio used. These parameters, however, affect the deposition rate (e.g. 6 Å/min for $R = 10\%$) much more appeciably. A plot of absorbance of the band near 1065 cm^{-1} against film thickness (measured ellipsometrically) is shown in fig. 4 for different samples (Lambert–Bouguer plot). The apparent absorption coefficient α_{app} is calculated from the slope of best fit through the

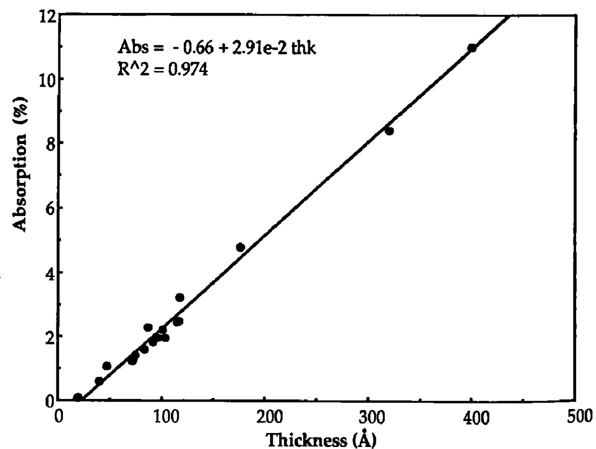

Fig. 4. Lambert–Bouguer plot of absorbance of the Si–O stretching band near 1065 cm^{-1} against film thickness for oxide layers on various silicon substrates.

data points. The intersection with the abscissa indicates the thickness of native oxide on the bare Si sample. This curve gives a native film thickness of 20 Å and and $\alpha_{app} = 2.91 \times 10^4$ cm^{-1} in good agreement with published data for much thicker films obtained from pyrolytic processes [22,23].

4. Conclusion

We have demonstrated the possibility of depositing good quality silicon dioxide films with a photochemical process based on the 172 nm wavelength from the excimer (or second excimer continuum) of xenon in an excimer silent discharge lamp. The deposition rates obtained are comparable to those from similar processes using low pressure mercury lamps [15]. This is very promising considering the fact that our lamp system has not been optimised in terms of the VUV output. This work is thus a proof of principle which can extend the use of excimer lamps to the field of material deposition for semiconductor applications. We are currently studying the application of this technique for the deposition of other material such as silicon nitride and silicon oxynitride and multi-layer dielectrics. We have also recently developed lamps of deeper wavelengths radiating at the Ar_2^* and Kr_2^* continua (126 and 146 nm). This will allow *direct* photodissociation of silane and, hence, amorphous silicon films to be processed enabling in-situ multilayer transistor fabrication.

Acknowledgements

We would like to acknowledge here funding, in part, from the EEC SCIENCE programme, SERC grant No. GR/E 16090, and ABB Corporate Research, Baden, Switzerland. Special thanks are also given to Professor M. Green and Dr. S. Best for the respective use of the ellipsometer and the FTIR spectrometer.

References

[1] R.R. Chang, R. Iyer and D.L. Lile, J. Appl. Phys. 61 (1987) 1995.
[2] C. Vinkier and S. De Jaegere, J. Electrochem. Soc. 137 (1990) 628.
[3] D.A. Buchanan, Appl. Phys. Lett. 56 (1990) 1037.
[4] U. Kogelschatz, Appl. Surf. Sci. 54 (1992) 410.
[5] B. Eliasson and B. Gellert, J. Appl. Phys. 68 (1990) 2026.
[6] B. Eliasson and U. Kogelschatz, Appl. Phys. B 46 (1988) 299.
[7] B. Eliasson and U. Kogelschatz, Ozone 13 (1991) 365.
[8] H. Esrom, J. Demmy and U. Kogelschatz, Chemtronics 4 (1989) 202.
[9] H. Esrom and U. Kogelschatz, Appl. Surf. Sci. 46 (1990) 158.
[10] B. Gellert and U. Kogelschatz, Appl. Phys. B 53 (1991) 14.
[11] Ch.K. Rhodes, Excimer Lasers, Vol. 30 of Topics in Applied Physics (Springer, Berlin, 1984).
[12] Y.I. Nissim, J.M. Moison, F. Houzay, F. Leblanc, C. Licoppe and M. Bensoussan, Appl. Surf. Sci. 46 (1990) 175.
[13] M. Petitjean, N. Proust and J.F. Chapeaublanc, Appl. Surf. Sci. 46 (1990) 189.
[14] P. Patel and I.W. Boyd, Appl. Surf. Sci. 46 (1990) 352.
[15] P.A. Robertson, The Photo-Enhanced Deposition of Amorphous Silicon and Silicon Oxide Thin Films, PhD Thesis, University of Cambridge, 1987.
[16] D.J. Eckstrom, H.N. Nakano, D.C. Lorents, T. Rothem, J.A. Betts, M.E. Lainhart, D.A. Dakin and J.E. Maenchen, J. Appl. Phys. 64 (1988) 1679.
[17] J.G. Calvert and J.N. Pitts, Photochemistry (Wiley, New York, 1966).
[18] D.L. Baulch, R.A. Cox, P.J. Crutzen, R.F. Hampson, J.A. Kerr, J. Troe and R.T. Watson, J. Phys. Chem. Ref. Data 11 (1982) 359.
[19] M. Petitjean, Optimisation des Structures MIS sur InP, Rapport de Thèse, Université Paris 6, 1991.
[20] I.W. Boyd and J.I.B. Wilson, J. Appl. Phys. 53 (1982) 4166.
[21] G. Lucovsky, M.J. Manitini, J.K. Srivastava and E.A. Irene, J. Vac. Sci. Technol. B 5 (1987) 530.
[22] I.W. Boyd and J.I.B. Wilson, J. Appl. Phys. 62 (1987) 3195.
[23] J.E. Dial, R.E. Gong, J.N. Fordemalt, J. Electrochem Soc. 115 (1968) 327.
[24] C.J. Giunta, J.D. Chapple Sokol and R.G. Gordon, J. Electrochem Soc. 137 (1990) 3237.
[25] Y. Tanaka, J. Opt. Soc. Am. 45 (1955) 710.
[26] I.W. Boyd, Laser Processing of Si and the Growth and Structure of Si Oxides, PhD Thesis, Herriot Watt University, 1982.
[27] R.J. Bell, N.F. Bird and P. Dean, J. Phys. C 2 (1968) 229.

Low pressure photodeposition of silicon nitride films using a xenon excimer lamp

P. Bergonzo and Ian W. Boyd
Electronic and Electrical Engineering Department, University College London, London WC1E 7JE, United Kingdom

(Received 17 May 1993; accepted for publication 20 July 1993)

Excimer lamps have recently opened up the field of intense vacuum ultraviolet light generation. The power available from such lamps based on the dielectric barrier discharge generation method can be superior to those of typical low pressure mercury lamps. Additionally, a wide range of shorter and longer wavelengths can be generated as required. Following previous work on silicon dioxide deposition, here we present the use of these lamps for direct photodeposition of silicon nitride from mixtures of silane and ammonia. Optical and physical characterization reveal good film qualities, rendering this new technique promising for low temperature semiconductor and optoelectronic material processing.

Dielectric thin film deposition is an important processing step in semiconductor device fabrication. In silicon very large scale integration (VLSI) fabrication, the deposition of thin dielectric films such as silicon dioxide or silicon nitride is presently quite indispensable in a variety of applications, including multilevel interconnect structures, barrier layers, and final passivation on many types of structures.[1] The necessity to decrease wafer processing temperatures substantially has stimulated research into new possible techniques for the deposition of thin dielectric films. Photolytic chemical vapor deposition (CVD) is one such promising method. Until now, most work in this area has employed high power and costly excimer laser systems or cheaper commercially available low power lamps.[2-4] In recent years there has been interest in developing new types of lamps applicable to this area, which provide higher powers and extended availability of wavelengths.[5,6] We have previously reported the development and use of xenon excimer lamps to directly photodeposit silicon dioxide films at low temperatures.[7] The 172 nm radiation generated was used to enhance the direct photolysis of a nitrous oxide-silane mixture. Here we present for the first time the deposition of silicon nitride layers using these lamps. Ultrathin Si_3N_4 films have superior insulating and masking properties to SiO_2 and are potential candidates to replace thin oxide films in various VLSI applications.[8] Here, after a brief presentation of the experimental apparatus, we will analyze the correlation between the deposition conditions and the physicochemical properties of the Si_3N_4 films obtained. The deposited films were characterized using ellipsometry, Fourier transform infrared spectroscopy (FTIR), and secondary ion mass spectroscopy (SIMS) analysis.

Figure 1 shows a schematic diagram of the photo-CVD reactor designed for this process. The system basically consists of a set of two chambers separated by a MgF_2 window transparent to the vacuum ultraviolet (VUV) radiation. The 7.2 eV photons are generated in the top chamber and irradiate a low pressure gas phase mixture in the bottom chamber. An argon gas purge is used during processing to prevent deposition on the window of material which was opaque to the radiation. The generation of VUV light from excimer lamps has been the subject of several recent articles.[9,10] The principle is based on the radiative decomposition of excimer states created by dielectric barrier discharges in a gaseous environment.[11] Here we use a pure xenon-filled cylindrical-shaped source, which can radiate up to 40 mW/cm^2 at 172 nm. Such excimer lamps are not presently commercially available, and therefore were designed in-house to produce an arbitrary radiation intensity output. Silane and ammonia precursor mixtures were introduced into the processing cell and exposed to the VUV radiation.

The substrates used were (100) orientation *p*-type crystalline silicon, up to 1 in. in diameter. They were located on a vertical stage holder which allowed the window-substrate distance to be adjusted from 1 to 5 cm, and were heated to temperatures between 200 and 300 °C.

Under the 172 nm radiation, the photochemistry of the ammonia involves the following reaction pathways:[12]

$$NH_3 + h\nu \rightarrow NH_2 + H, \quad (1)$$

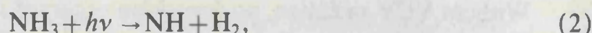

$$NH_3 + h\nu \rightarrow NH + H_2, \quad (2)$$

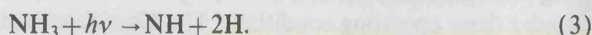

$$NH_3 + h\nu \rightarrow NH + 2H. \quad (3)$$

Of these reactions, Eq. (1) is strongly predominant (95%) at the photon energies involved. The ammonia is dissociated into NH_2 and H radicals that subsequently react with the silane and lead to silicon nitride deposition. Typical

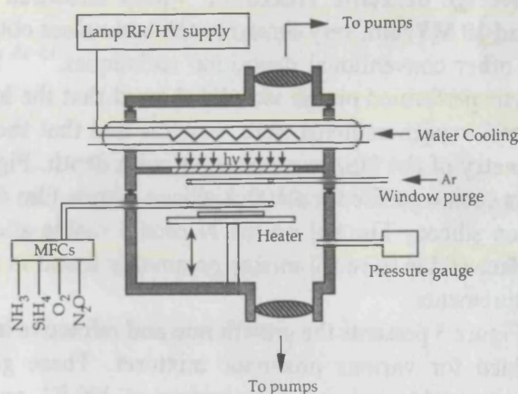

FIG. 1. Excimer lamp photo-CVD system.

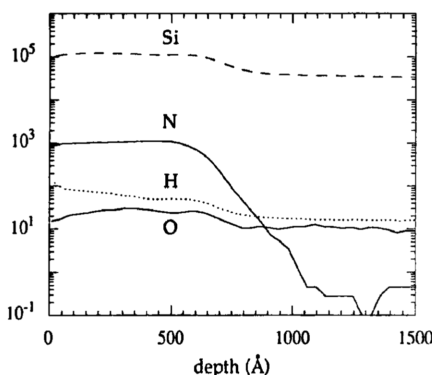

FIG. 2. SIMS profile of a 600 Å silicon nitride film deposited on silicon.

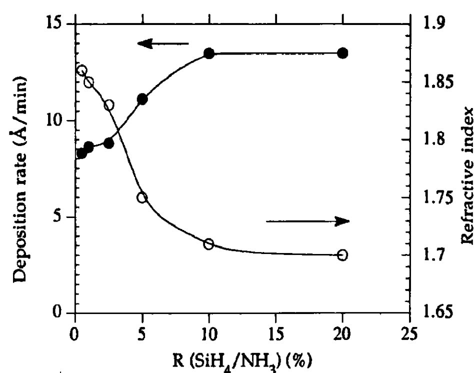

FIG. 3. Deposition rate and refractive index vs SiH_4/NH_3 ratios.

operating conditions used flow rates of SiH_4/NH_3 around 2/20 sccm, respectively, and a total pressure of 5–10 mbar. The initial total absorption of the radiation entering the processing chamber by this concentration of ammonia was calculated to be about 60% after a single pass. However, a large portion of the remaining 40% of the incident radiation was reflected by the silicon ($R \approx 0.7$) and further absorbed to a significant degree after a return pass through the gas. The intensity absorbed by the silicon itself was not sufficient to increase the local surface temperature beyond a few degrees Kelvin.

Preliminary experiments indicated that this process required the use of ultrahigh purity gases. In fact, impurities of only a few 100 ppm (especially O_2, H_2O, and/or CO_2) were sufficient to drastically pollute the deposited film with oxygen, leading to film stoichiometries more closely resembling SiO_2 rather than Si_3N_4. This was due to the higher degree of reactivity of these impurities, rendering them predominant in the deposition photochemistry. Accordingly, the precursor gas purities used were always grade 5.0 level.

Without VUV radiation, no deposition occurred showing that thermally controlled deposition was insignificant under these operating conditions. The films deposited with the VUV lamp were without exception scratch resistant and adherent, nonporous, and chemically stable with respect to exposure to O_2 and H_2O in the atmosphere. The deposited layer thicknesses were uniform within a few percent over the 4 cm^2 of the silicon substrates used. The film etch rate in buffered HF (1:30) was equal to 30 Å/s, and the average dielectric breakdown values measured were around 10 MV/cm, very similar to the best values obtained with other conventional deposition techniques.[13–15] SIMS analysis performed on the samples showed that the hydrogen and oxygen contents were very low and that the stoichiometry of the films were constant with depth. Figure 2 shows such a profile for a 600 Å silicon nitride film deposited on silicon. The tail on the N profile visible after the interface is due to recoil mixing commonly found in SIMS measurements.

Figure 3 presents the growth rate and refractive indices obtained for various precursor mixtures. These growth rates were obtained at a temperature of 300 °C, an NH_3 flow of 20 sccm, a window substrate distance of 12 mm, a total pressure of 10 mbar, and a lamp intensity of about 10 mW/cm^2. The growth rates were not significantly affected by the temperature in the 200–300 °C range used, although they were strongly influenced by the level of photon flux. Growth rate values higher than the 10 Å/min rate obtained here should be readily achievable due to the much higher fluxes of photons which can be generated with these excimer lamps.

As can be seen in Fig. 3, refractive indices as high as 1.85 were obtained for low silane/ammonia ratios. Direct photo-CVD rarely leads to values higher than this due to the difficulties of routinely achieving completely oxygen-free processing conditions. However, the O_2 source is mainly due to the precursor gas purity and therefore could be reduced with more elaborate gas handling.

The value of the refractive index is clearly very strongly dependent on the silane concentration within the ammonia. FTIR spectrometry was used to identify the effect of the gas mixture on the stoichiometric content of the films. No dominant peak was observed in the region where the Si-H vibrational modes are located (around 2175 cm^{-1}).[16] This gives an upper limit to the content of bonded hydrogen in our films of a few percent, indicating a much lower concentration to that typically found in plasma enhanced CVD nitride films, where it can vary up to 35%.[17] In Fig. 4 the relationship between the Si-N stretching vibration mode and the SiH_4/NH_3 ratio R is shown. These measurements were obtained for 300-Å-thick Si_3N_4 films deposited at 300 °C at a constant ammonia flow. As can be seen in Fig. 4, the characteristic broad peak centered around 840 cm^{-1} observed for low R ratios is strongly diminished at higher silane concentrations. Therefore, the refractive index decrease observed for high silane concentrations corresponds to a decrease in the concentration of Si—N bonds in the films. This is explained by the fact that when R is increased at a constant NH_3 total flow, the ratio of dissociated active NH and NH_2 species to the number of silane molecules decreases, rendering the complete dissociation of the silane present to be less probable, leading to a poorer Si—N bond concentration in the film. Further, at very high ratios (20%), the Si-N bond concentration is so low that the relative increase in the concentration of Si—O impurities bonds becomes visible by the associated increase in the absorption near 1060 cm^{-1} due to the presence of Si-O units in the film. These

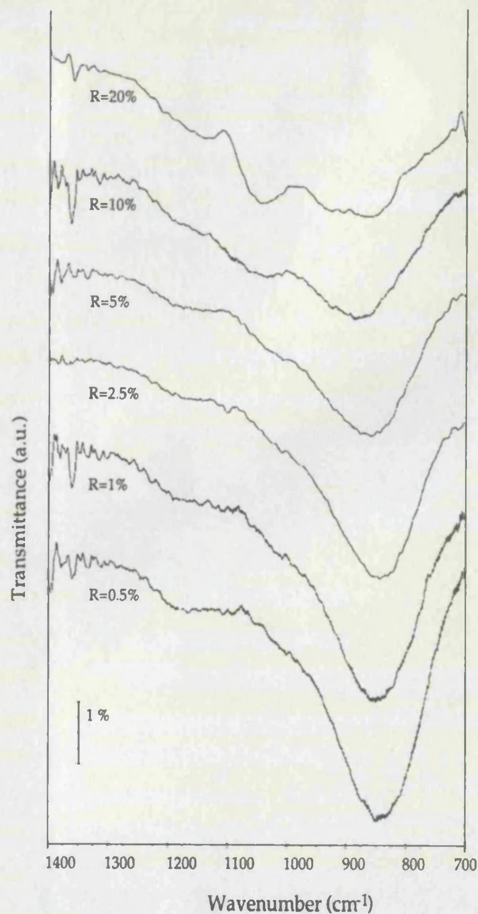

FIG. 4. Evolution of the Si-N vibrational mode with precursor mixture ratio *R*.

observations confirm that it is possible to accurately control the stoichiometry of the deposited films by altering the precursor mixture. This selective precursor excitation feature is therefore an added advantage of this technique over other deposition processes.

In conclusion, we have demonstrated the possibility of depositing good quality silicon nitride films with a photochemical process based on the 172 nm wavelength from the excimer continuum of xenon in a dielectric barrier discharge lamp. Such a deposition process has now been described for both SiO_2 and Si_3N_4 layers and can clearly be applied to a variety of substrates including III-V semiconducting materials, glass, and many heat sensitive compounds. It has been demonstrated that deposition rates comparable to those obtained with mercury lamps can be obtained, with generally higher refractive indexes and better control of the stoichiometry. These observations open a potentially new area for the application of excimer lamps, since the deposition of dielectric films for industrial applications at even higher rates and larger areas may be achieved by scaling up the geometry of the apparatus used.

The authors like to thank Steve Best and Christiane Dubois for the use of the FTIR spectrometer and the SIMS analysis, respectively. Special gratitude is also extended to Dr. Ulrich Kogelschatz for his active participation in the early stages of this project.

[1] Y. Numasawa, K. Yamazaki, and K. Hamano, Jpn. J. Appl. Phys. **22**, L792 (1983).
[2] P. K. Boyer, G. A. Roche, W. H. Ritchie, and G. J. Collins, Appl. Phys. Lett. **40**, 716 (1982).
[3] M. Okuyama, Y. Toyoda, and Y. Hamakawa, Jpn. J. Appl. Phys. **23**, L97 (1984).
[4] Y. Nissim, J. L. Regolini, D. Bensahel, and C. Licoppe, Electron Lett. **8**, 488 (1988).
[5] P. Patel and I. W. Boyd, Appl. Surf. Sci. **46**, 352 (1990).
[6] P. Bergonzo, P. Patel, I. W. Boyd, and U. Kogelschatz, Appl. Surf. Sci. **54**, 424 (1992).
[7] P. Bergonzo, I. W. Boyd, and U. Kogelschatz, Appl. Surf. Sci. **69**, 393 (1993).
[8] E. C. Paloura, S. Logothetidis, S. Boultadakis, and S. Ves, Appl. Phys. Lett. **59**, 280 (1991).
[9] B. Gellert and U. Kogelschatz, Appl. Phys. B **52**, 14 (1991).
[10] U. Kogelschatz, Appl. Surf. Sci. **54**, 410 (1992).
[11] B. Eliasson and U. Kogelschatz, IEEE Trans. Plasma Sci. **PS-19**, 309 (1991).
[12] J. G. Calvert and J. N. Pitts, in *Photochemistry* (Wiley, New York, 1966).
[13] R. Padmanabhan and B. J. Miller, J. Vac. Sci. Technol. A **4**, 363 (1986).
[14] M. Petitjean, Rapport de Thèse, Université Paris 6, 1991.
[15] C. S. Pai, C. P. Chang, F. A. Baiocchi, and J. Swiderski, J. Appl. Phys. **68**, 2442 (1990).
[16] M. Berti, M. Meliga, G. Rovai, S. Stano, and S. Tamagno, Thin Solid Films **165**, 279 (1988).
[17] R. Chou, W. A. Lanford, W. Ke-Ming, and R. S. Rosler, J. Appl. Phys. **53** , 5630 (1982).